Bio-Based Structural Insulated Panel for Buildings

Bio-Based Structural Insulated Panel: Experimental, Analytical, and Parametric Study for Residential Building Applications

CIEM0500: Master Thesis

Katariina Johanna Järvsoo

Delft University of Technology

TU Delft

Bio-Based Structural Insulated Panel for Buildings

Bio-Based Structural Insulated Panel: Experimental, Analytical, and Parametric Study for Residential Building Applications

by

Katariina Johanna Järvsoo

to obtain the degree of Master of Science

at the Delft University of Technology,

to be defended publicly on Thursday January 23, 2025 at 15:00.

Student number:	5623820	
Project duration:	May 16, 2024 – January 23, 2025	
Thesis committee:	Dr. ir. H. Roel Schipper	TU Delft
	Ir. Peter de Vries	TU Delft
	Dr. ir. Michele Mirra	TU Delft
	Dr. ir. Geert J. P. Ravenshorst	TU Delft
	Ing. Johnny van Rie	Kingspan Unidek

Cover: Bing AI

An electronic version of this thesis is available at http://repository.tudelft.nl/.

TU Delft

Preface

This thesis represents the culmination of my Master's program in Civil Engineering at Delft University of Technology. It explores the structural design methods for sandwich panels and shows the difficulties in the design processes. The research was driven by my interest in sustainability and the desire to learn more about parametric design.

Over the course of six months, this work evolved through rigorous modelling, analysis, and countless revisions. The process was as challenging as it was rewarding, offering me valuable insights and skills to analyse, understand and research further, and in the end to trust myself.

I would like to express my heartfelt gratitude to my supervisor, Dr. ir. Roel Schipper, for their unwavering guidance and encouragement. I am very grateful for the support and guidance of Dr. ir. Michele Mirra. I would like to give a special thank you to Dr. ir. Robin Oval for taking the time to help with the Grasshopper model development and thinking along with my modelling work. I am grateful for the support by ir. Peter de Vries, and finally I am thankful for the opportunity provided by Kingspan Unidek with the help of Ing. Johnny van Rie and Dr. ir. Geert Ravenshorst. Lastly, I am deeply indebted to my family who made my master's journey in the Netherlands possible, and to friends here and in Estonia for their support and patience throughout this journey.

It is my hope that the findings presented here will inspire further research and contribute meaningfully to the field of civil engineering. This thesis marks the end of one chapter and the beginning of another.

Katariina Johanna Järvsoo
Delft, January 2025

Summary

Parametric tools could significantly increase efficiency in the design process within the construction industry, especially with prefabricated elements. Efficiency is also searched for in material use. An element that uses its material very effectively is a structural insulated panel (SIP). However, the synthetic polymers used in already existing panels are not very sustainable. The new climate agreements push producers into making more sustainable choices. Due to this, Kingspan Unidek is experimenting with a bio-based insulation material integration into the SIP. A new structural insulated panel with OSB/3 faces and a Steico wood fibre polyurethane resin insulation core is being developed. In this thesis, the panel's behaviour is analysed for construction purposes under axial and transverse loading experimentally, analytically and through modelling. The behaviour of the panel is analysed for residential building applications, and the possibility of using parametric modelling tools in the design process for SIPs is assessed.

The analysis is performed by using four main methods – full-scale experiments under eccentric axial loading by Kingspan, models on Karamba3D and RFEM, and analytical calculations with Timoshenko beam theory, shear beam equations and rod in compression equations. The failure methods are analysed with hand calculations from sandwich panel theory. The Karamba3D model is developed by using shell and beam elements since it is not yet possible to model layered materials. The material is defined by the user and the core is modelled as beams which are scaled to match the Timoshenko beam equation results.

The faces exhibited a separate behaviour during the experiments under low eccentric axial loads suggesting a delamination failure or a core failure. The failure occurred during an eccentric 18 kN/m axial loading which caused the faces to behave separately. The core has very low strength properties compared to other conventionally used SIP insulation materials which are at least twice as strong as the Steico insulation board. Additionally, the analytical calculations showed that the panel has very low transverse loading capacity as a result of core shear failure – a maximum distributed load between 0.1 kN/m to 2.5 kN/m can be applied depending on the analysis method. These findings confirm that the panel could only be used with the application of through-thickness stiffeners. The developed Karamba3D model successfully reproduced the experimental results, but the model should not be used for failure analysis since local failures or interface failure is not described. Timoshenko beam theory and the RFEM model showed a good correspondence for transverse loading, but a bending test should be performed to confirm the results. The RFEM model could not show the SIP behaviour under axial loading but did exhibit a trend in deflection results towards where a local failure could occur. The conventional sandwich panel theory overestimated the panel resistance based on the experimental results and the modelling results.

The panel in this form could only be applied if through-thickness stiffeners are used to strengthen the panel or if the core material is significantly improved. However, there is a possibility that the separate behaviour by the faces could be avoided by avoiding eccentric loading and only applying centric loading. It would be necessary to test the panel for failure to get a better un-

derstanding of the failure modes and to further validate the model values. Additional testing to confirm the failure method would be testing the material properties of the Steico material, and the bond strength of the interface between the faces and the core. The model has the potential to be used for analysing all different sandwich structures, but would need to be further verified with different materials.

Contents

Preface i

Summary ii

1 Introduction 1
- 1.1 Research Context . . . 1
- 1.2 Research Problem . . . 2
- 1.3 Research Objectives . . . 4
- 1.4 Research Scope . . . 4
- 1.5 Research Questions . . . 5
- 1.6 Research Method . . . 5

2 Literature Review 9
- 2.1 Material properties and characteristics of a bio-based SIP . . . 9
- 2.2 Failure modes of SIPs . . . 18
- 2.3 Panel to panel connections . . . 25
- 2.4 Panel to floor beams connections . . . 29
- 2.5 Models and experiments of SIPs . . . 30
- 2.6 Conclusions . . . 33

3 Methodology 35
- 3.1 Karamba model . . . 36
- 3.2 RFEM model . . . 41
- 3.3 Shear Beam equations . . . 43
  - 3.3.1 Kinematic Relations . . . 43
  - 3.3.2 Constitutive Relations . . . 44
  - 3.3.3 Equilibrium Equation . . . 44
  - 3.3.4 Governing Equation . . . 44
  - 3.3.5 Solution for a Cantilever Beam . . . 44
- 3.4 Timoshenko Beam Theory . . . 44
  - 3.4.1 Kinematic Relations . . . 44
  - 3.4.2 Constitutive Relations . . . 45
  - 3.4.3 Equilibrium Equations . . . 45
  - 3.4.4 Governing Equations . . . 45
  - 3.4.5 General Solution for Simply Supported Beam with Uniform Distributed Load q . . . 46
- 3.5 Rod in compression . . . 46
  - 3.5.1 Kinematic Relation . . . 46
  - 3.5.2 Constitutive Relation . . . 46
  - 3.5.3 Equilibrium Equation . . . 46
  - 3.5.4 Governing Equation . . . 47

3.5.5 Boundary Conditions and Solution . . . 47
3.6 Experiments by Kingspan Unidek . . . 47

4 Structural Insulated Panel Analysis 53
4.1 Initial information . . . 53
4.2 Hand calculations . . . 56
4.3 Analytical results . . . 59
4.4 Experiment Results . . . 59
4.4.1 Experiment Results Analysis . . . 64
4.5 Model results . . . 68
4.5.1 Karamba3D model results* . . . 68
4.5.2 RFEM model results . . . 74
4.6 Comparison of experimental, analytical and modelling results . . . 75
4.6.1 Transverse loading . . . 75
4.6.2 Outer face loaded . . . 80
4.6.3 Inner and outer face loaded . . . 89
4.7 Conclusions . . . 93

5 Discussions 95
5.1 Panel material and experiments . . . 95
5.1.1 Creep . . . 98
5.2 Models . . . 99
5.2.1 Karamba3D model . . . 99
5.2.2 RFEM model . . . 101
5.3 Experiments vs modelling . . . 102
5.4 Additional points . . . 103
5.4.1 Openings . . . 103
5.4.2 Connections . . . 103
5.4.3 Fire safety . . . 103
5.4.4 Regulations development . . . 103

6 Conclusions 104

7 Recommendations 107
7.1 For Kingspan . . . 107
7.1.1 Panel development . . . 107
7.1.2 Model development . . . 108
7.2 For further research . . . 108
7.2.1 Panel development . . . 108
7.2.2 Model development . . . 108
7.2.3 Regulated guidelines for design . . . 108

References 110

A Load on the outer face F=6 kN Maple output 115

B Load on the outer face F=129 kN Maple output 120

C Transverse loading q=2.5 kN/m Maple output 125

D Outer face loaded with F=6 kN Maple output 132

E Inner and outer face loaded F=125 kN Maple output - vertical displacements 139

F Additional experiment results 143

G Additional connection type figures 161

H Model of a Residential Building 165
H.1 Karamba3D Model 166
H.2 Dlubal Model 169
H.3 Additional modelling suggestions 169
H.4 How can a residential building out of SIPs be modelled in Grasshopper? . . . 170

1

Introduction

1.1. Research Context

The construction industry is one of the slowest developing industries. All innovations take around 30 years to reach practice in the field. A good example of this is the integration of building information modelling (BIM) into the industry – the idea was first introduced in 1975, but is still not used by all parties in the construction process [1]. One reason for this is the fast pace and growing demand of projects, leaving little time for self-study or research for practising engineers. Additionally, the long duration of projects and the confidence in already tested and known ways [2], results in low interest for exploring possibly more effective methods. Another reason could be the specific demands from clients [2] and a wish to keep prices low, since new products or solutions usually have a low demand resulting in a higher cost and could sometimes also mean longer realisation times. Oftentimes, even if engineering companies have gone over to computer based models, construction companies have not gone through that change and either demand paper based information or need guidance and assistance to get used to the new techniques [3]. This requires time and resources. In order to successfully implement a change or start using a new method, the engineer has to be familiar with it or has to have a deep interest for starting. Only then the best integration into the project can be ensured with the least amount of time while having the support of the client. So, a crucial part for integrating new techniques is the availability of knowledge, and the depth of it.

The construction industry is being pushed into making more sustainable choices to reach the 2030 and 2050 European Union climate targets to reduce emissions [4]. Since this announcement, producers are making their efforts to reduce their CO2 emissions [5]. There are many ways how to reduce the carbon footprint in the industry. One option is to use a more effective way of construction in terms of insulation capabilities, erection time, and material use [2], [6], [7]. All of these could be addressed with structural insulated panels (SIPs). SIPs have been around for almost a hundred years now, and starting from the 1980s oriented strand board (OSB) skins have been used [8]. SIPs are a construction product that combines load bearing and insulation together in one panel. It is lightweight, and easy to produce in the factory under a controlled environment, and then easily assembled on the construction site, conserving time, and lowering the amount of labour, and therefore the possibility of error [2], [5]. Their erection is less labour intensive meaning faster production compared to traditional construction meth-

ods like timber or steel frame buildings [2], [9], [10]. They have better insulation capabilities compared to conventional construction techniques, since they have a reduced amount of thermal bridges in the form of having no frame that pierces through the panel from the inside to the outside [7]. This is well illustrated in figure 1.3 where the timber frame elements run through the wall, whereas in figures 1.2, 1.4, 1.5, and 1.6, there are no elements running from the inside to the outside that would disrupt the insulation layer. This positively influences the amount of material used for the building, and additionally by reducing heat losses, decreases the amount of energy required to heat the building [2], [5], [7]. It is possible to reduce energy costs up to 50% per year [6].

SIPs can be used for walls and roofs. Roofs can range from a flat roof to sloped roofs. An example for a roof cross section can be seen in figure 1.6. Currently, most commonly used SIPs are with a metal skin with an insulation core of either mineral wool, glass wool, extruded polystyrene (XPS), expanded polystyrene (EPS) or polyurethane (PUR). Although, OSB faces have gained popularity in the last decade, it is possible to produce a sandwich panel that is more sustainable, and uses bio-based materials. First step towards that is in addition to the faces, changing the core material to a bio-based material. This is currently explored by Kingspan Unidek, integrating a bio-based insulation material between two OSB skins. However, using hand calculations to analyse the behaviour and failure mechanisms is often not very accurate, and requires a lot of time. Analysing and describing a sandwich panel's behaviour is not an easy task, while testing out new material combinations. There are no universal design standards [6], [11] and a lack of overview on existing panels' behaviour [5]. Thus, a need for an accurate modelling method is necessary, which could further be applied for building applications, and simplify the design with SIPs.

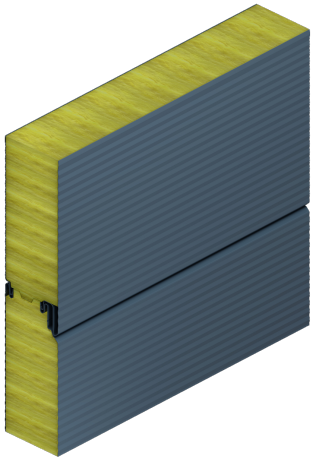

Figure 1.1: Sandwich panel with metal skins and mineral wool insulation. [12]

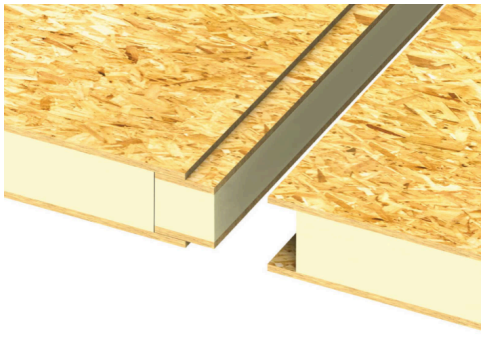

Figure 1.2: TEK panel with OSB skins and PUR foam. [13]

1.2. Research Problem

Kingspan Unidek is interested in exploring the possibility to have a structural insulated panel building model on Grasshopper with the Karamba3D plug-in. Grasshopper provides the possibility to have a parametric model, while performing many different analyses, which include thermal performance, sustainability, structural stability, natural light, and many more. Parametric modelling tools have been available for 20 years now, and their use is now increasingly

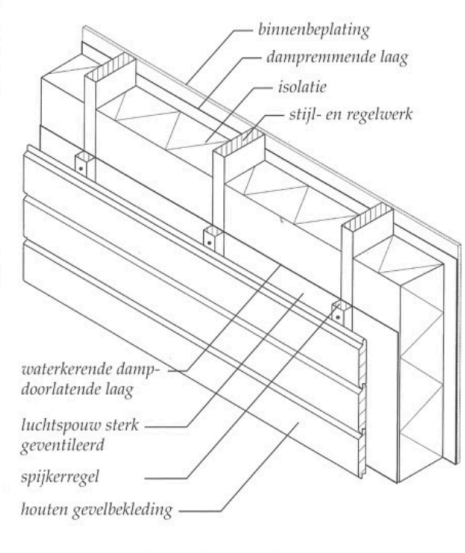

Figure 1.3: Timber frame cross-section with timber cladding. [14]

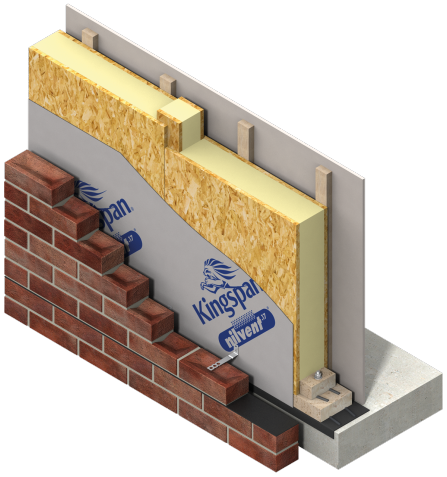

Figure 1.4: Kingspan TEK building system with brick cladding. [13]

Figure 1.5: Sandwich panel system with timber cladding. [15]

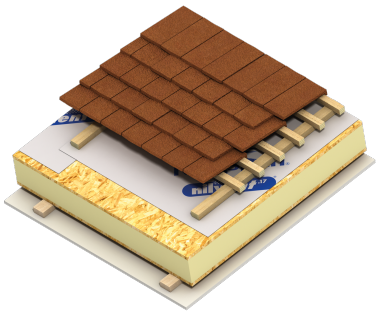

Figure 1.6: TEK system roof cladding. [13]

popular. However, the adoption of the possibilities provided by parametric tools could be much better integrated into the construction industry.

Building with structural insulated panels is one of the fastest ways of construction, and if bio-based insulation materials are used, the transition towards a more sustainable built environment is promoted [5]. There is a need for a new and improved structural insulated panel to address its possible drawback [6]. Incorporating a parametric approach in the design process of a residential building out of SIPs would significantly reduce the time necessary to move from design to construction process [16]. It is first important to verify the accuracy that grasshopper provides to model a sandwich panel, and check if the model can predict real panel behaviour. As far as is establishable, structural insulated panels have not yet been modelled on Grasshopper.

Often, hand calculations predict global failure methods to be governing, but in practice local failure methods occur before global failure loads are achieved [17]. If the model predicts failure and shows accurate behaviour, implementing the panel into a building model could give an effective method to design with SIPs. So far, there are difficulties showing the functionality of structural insulated panels through one specific method [18], since there is no unified method

nor codes to prove the panel's behaviour [7], [19] and there is a lack of info on commonly used sandwich panels' behaviour [5]. Thus, a method to model a SIP that accurately predicts the behaviour of the panel, and be also implemented in a building model, could simplify the design process significantly, and speed up the development of structural insulated panels. This research aims to create a SIP model which successfully describes the behaviour of the panel, and to give a preliminary tool to design a residential building with structural insulated panels to make the design process easier and less time consuming.

1.3. Research Objectives

This thesis will analyse and model the behaviour of a novel bio-based structural insulated panel in development by Kingspan Unidek. The panel will be loaded axially and transversely (wind load), and the out of plane behaviour will be observed. It aims to give a method of designing with SIPs by using a parametric structural model to accurately simulate the real life behaviour of a SIP, and integrating it into a building model. The possibility of using Grasshopper Karamba3D to analyse the panel's behaviour will be explored. Further, two options are investigated to model a SIP building on Grasshopper – one with Karamba3D plug-in, and another with Dlubal plug-in connected to RFEM. The building modelling methods will be brought out in appendix H.

1.4. Research Scope

The research will focus on the analysis and modelling of the novel Kingspan Unidek bio-based structural insulated panel. The investigated panel dimensions are defined by the available tested panel, which are as follows: height - 3200 mm, width - 1020 mm, thickness - 124 mm. The bio-based SIP is made of OSB/3 as the skin material, 12 mm on each side, and the core is Steico medium density fibre board (MDF-board) type M dry (140 kg) 100 mm with a declared thermal conductivity of 0.037 [W/mK]. The panel looks very similar to the existing Kingspan TEK system panel that can be seen in figure 1.2. The panel will be modelled on Grasshopper Karamba3D, validated by hand calculations, and compared to test results and to a model on RFEM to find the most suitable and accurate approach. The material properties are provided by Kingspan Unidek, and the missing core material properties will be assumed based on available test results and literature. The load cases analysed will involve axial loading as floor and construction weight loads, and transverse loading as wind loads perpendicular to the plane of the panel.

In the second part of this thesis, two building model creation methods will be investigated on Grasshopper for SIP applications. First, again a model on Karamba3D, and second a model on Dlubal. To limit complexity for the scope of the thesis project, the building models will not be analysed, but are proposed as possible options for further research. These are presented in appendix H.

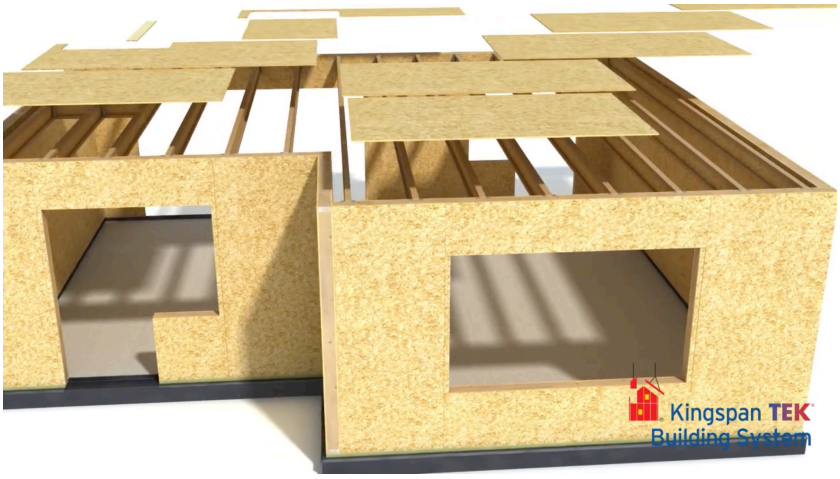

Figure 1.7: TEK building system. [20]

1.5. Research Questions

Main question

> **What is the out of plane behaviour of the novel Kingspan Unidek bio-based panel under axial and transverse loading, and how can analytical and numerical methods be used in the design process?**

Subquestions

1. What is the correspondence between experimental and modelling work?
2. To what extent is analysis possible with parametric tools for SIPs?
3. What is the best method to predict structural insulated panel behaviour?

1.6. Research Method

In this thesis the modelling method will be used. The thesis will consist of two different parts – first, as the main part the panel analysis and modelling, and second, the building modelling. The research begins with a detailed literature review to:

- Understand the structural behaviour of sandwich panels, failure mechanisms, and their applications.
- Gather key material properties for bio-based SIPs, with a specific focus on the Kingspan Unidek panel.
- Investigate existing methods for modelling SIPs in structural design.
- Review experimental test data for sandwich panels to get an understanding of SIP behaviour under different load cases.

The insights from the literature review will provide necessary background knowledge to create and analyse the models.

Next, the panel analysis will follow. A model on Rhino 7 Grasshopper Karamba3D and RFEM

will be created. The novel Kingspan Unidek panel will be modelled on Karamba3D, and validated through analytical calculations and the RFEM panel model. Further, it will be compared to the test results provided by Kingspan Unidek. A panel model in Grasshopper Karamba3D will be created to evaluate the possibility of analysing SIPs with Karamba3D. The independent input parameters for the model will be the material characteristics of the structural insulated panel made of bio-based materials. The novel Kingspan Unidek panel will be compared to the models, to judge the behaviour of the panel in structural applications, and to evaluate if the panel is ready for structural applications. Additionally, the capability of Karamba3D to model SIPs for structural analysis will be assessed.

The next part explores the possibility of modelling a residential building out of structural insulated panels with parametric tools. To limit the scope of the thesis, no analysis is performed, but the modelling options are presented in appendix H. Two building models will be created – one with Karamba3D in Grasshopper Rhino 7, and the other with Dlubal in Grasshopper Rhino 8 connected to RFEM. Both models will include parametric design flexibility to modify spans, openings (e.g., windows and doors), and material configurations. The models will be simple – only one storey, one opening, rectangular geometry, and floor/roof beams. This is brough out in appendix H.

Expected Research Outputs:

- A validated panel model capable of predicting the structural behaviour of the novel Kingspan SIP.
- Insights into the best analysis method of SIPs.
- Recommendations for further development of bio-based SIPs and their modelling methods.

This is illustrated in figure 1.8.

Why Grasshopper and Karamba?
One of the most widely used visual programming languages in architecture, engineering, and construction is Grasshopper. It allows the user to create a design that can be modified and already verified in the matter of minutes [21] [22]. It is very useful for optimisation, and to explore the effect of parameter choices in an early design stage, hence it is a good way to connect the work of an architect and an engineer. Additionally, Grasshopper connects to many other products and has multiple plug-ins to perform different tasks within itself, and can also be linked with python. Karamba allows structural analysis already inside the Grasshopper environment without putting the model into another medium [23]. In addition, visualization of the design has many benefits, including a uniform understanding of the project, and faster optimization [16].

Karamba has developed the possibility to analyse shell structures only recently, so now in addition to beams and trusses it is also possible to analyse shells [24]. Hence, most researches that have been done so far have focused on steel structures [25], since the feature of beams and trusses analysis was present earlier. Additionally, it is possible to create complicated geometries in Grasshopper, thus it is useful for 3D printed structures [26]. Mostly, it has been used to design high-rise buildings with a very repetitive floor plan [27], but also for huge projects with extravagant geometries. Grasshopper can also be used to calculate the life cycle costs [28] or building physics aspects like thermal performance or irradiance values with additional

plug-ins. Karamba is most useful for preliminary design options since it can optimise to find the smallest cross-sections possible to make the most optimal design in terms of material use and resistance. Timber has mostly been analysed as beams and trusses [29], but also as shells of CLT panels [30] [31].

Revit in combination with Dynamo is another widely used parametric tool. Compared to Rhino and Grasshopper, it is more manual creation than editing the design by parameters. Revit allows the user to create families, by changing one element of the family, all of the elements change. However, the insertion of the elements into the design is still manual and can not be defined the way it is possible in Grasshopper (visual coding). Although, by using Dynamo, it is possible to make the design more automatic, which would then work in a similar way to Grasshopper. In addition, Grasshopper allows structural analysis without transferring the project to another program, whereas for Revit, Autodesk Robot needs to be used, where the model can be transferred. This takes time, especially with bigger projects, and load cases can only be defined in Robot. Finally, if the model would need to be modified later on by a final user, then the interface for modification can be created in Grasshopper. However, in the case of Revit, the user would need to know the program well to change the spans and then transfer the model to Robot and define load cases to perform analysis to get preliminary results. Hence, to get first design options, Grasshopper in combination with Karamba3D is faster, and combines multiple outputs in one program making it easier to use.

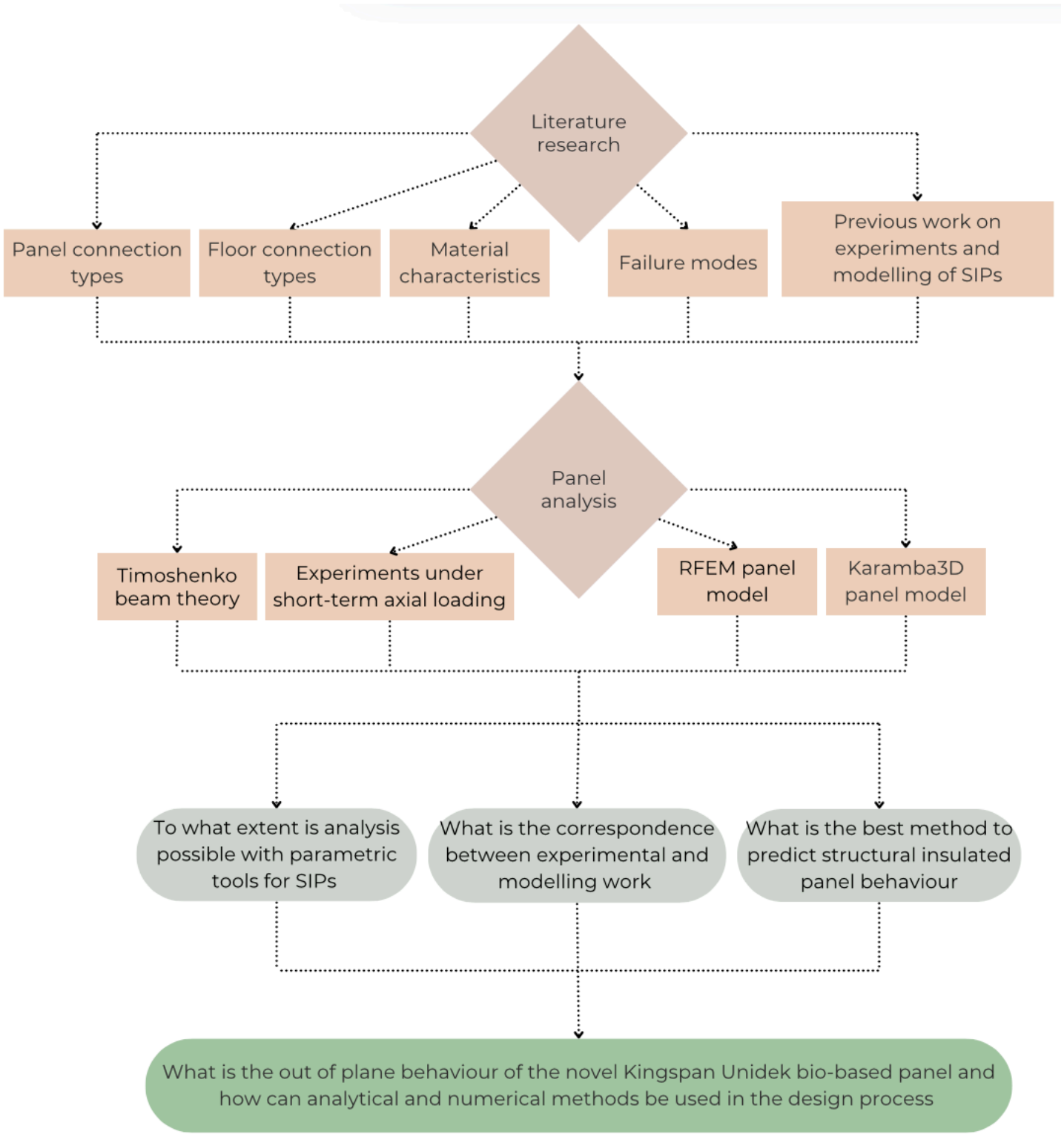

Figure 1.8: Theoretical framework

2

Literature Review

The literature review will give an overview of structural insulated panels, their characteristics, material properties, failure mechanisms, and connections. Previous research on modelling and experiments on structural insulated panels will be looked into. It will provide important background knowledge to create a model in Grasshopper Karamba3D, and to understand its behaviour. The literature review will focus on bringing sufficient background information by answering the following five questions:

- What are the material properties and characteristics of a bio-based SIP?
- What are the failure modes of a SIP?
- What are the connection types used for bio-based SIPs?
- What are the floor connection types used for SIPs?
- How have SIPs been modelled, and how do test results correlate to the analytical and computational results?

2.1. Material properties and characteristics of a bio-based SIP

Structural insulated panels or sandwich panels are a specific combination of materials to efficiently use the resistance, insulation, and stiffness capabilities of a specific material combination. The panel consists of two skins and a core, connecting the two through an interface with an adhesive. The adhesive needs to resist the shear and tensile stresses to transfer the forces to efficiently use the panel materials. The requirements for the core and the faces are different due to serving different purposes in the structure. Zenkert [32] states that the most important parameters for the core of the SIP are: low density, shear modulus, shear strength, stiffness perpendicular to the face, and thermal insulation; and for the faces: stiffness, tensile and compressive resistance, impact resistance, surface finish, environmental resistance, and wear resistance. Davies adds that [33] a structural insulated panel needs to satisfy the following requirements: safety, serviceability, durability, and aesthetics. Safety needs to be addressed during the whole life-cycle, including production, transportation, and construction phases [33]. These requirements have been met in different industries through different material combina-

tions. In construction, the most common combination is a sandwich panel with metal skins (usually aluminium or steel) and a core made of PUR. Nowadays, the integration of bio-based materials is ongoing, thus OSB skins are becoming increasingly popular and the selection for cores is substantial.

OSB faced sandwich panels have their disadvantages. Sah et al. [5] have brought out three negative aspects about OSB faced SIPs. Firstly, they have very low fire resistance, which is exacerbated by synthetic polymer cores. Second, they have durability issues since OSB is bio-based, it is susceptible to environmental factors – mould caused by moisture, and living organisms living from the material. Lastly, they have a low blast resistance, which is important in case winds shoot debris against the OSB sandwich wall. However, all of these downsides can be mitigated by using preventative construction measures. In contrast to the negative sides, OSB faced sandwich panels have many advantages. Sah et al. [5] stated that they have good thermal insulation capabilities, high strength to weight ratio, they are economical, and have low embodied carbon. Additionally, they are easy to install and lightweight.

Generally, two main types of face/skin materials are distinguished: “metallic and non-metallic materials” [32]. For non-metallic skins, especially bio-based ones, extra weather protection is necessary for example by the facade. The more commonly used panels are metallic panels due to their weather resistance, thus they do not require cladding to protect the metallic skin.

The loads are distributed in a SIP in a very specific way. The faces of a structural insulated panel are only in tension and compression due to bending, whereas the core is in shear [32]. The inside skin is usually in compression and the outside skin is mostly in tension [34]. The bearing capacity of a SIP is usually most restricted by the compressed face [35], but there are 8 different failure modes, which will be further elaborated later on.

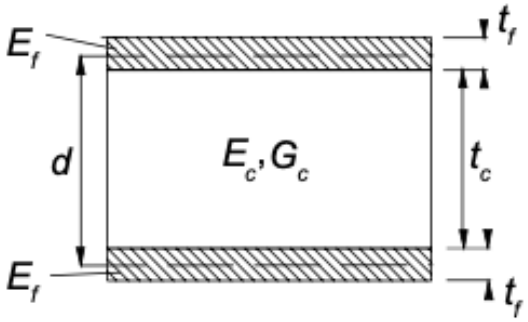

Figure 2.1: Sandwich beam sketch [32].

The main reasons for deflections in bio-based SIPs are climate and loading. Relative humidity influences the deflections of the sandwich panel seasonally, causing extra stresses if one of the skins is exposed to higher relative humidity [34]. It is also mentioned in the NEN-EN 1995-1-1 that an OSB/3 has 0.03% expansion in plane per 1% of material moisture content. Rungthonkit [18] also found that relative humidity negatively influences the creep behaviour, making creep deflections bigger the higher the relative humidity. According to a 24 year long research on TEK panels by Aicher et al. [34] made with particle board skins, the outside skin had 40% of the mean strength value of the inside skin, illustrating that environment is a governing factor in the design. So, relative humidity influences the lifespan of the outside skin and impacts negatively

on the deflections seasonally. In the research mentioned, the inside skin had twice the strength than what was expected according to the Eurocode, which led to a conclusion that the time-dependent deformation factors (k_{def}) in the Eurocode for timber based materials used in SIPs are too big [34]. Therefore, through further knowledge and testing, more economical designs could be made by making material modification factors smaller. Additionally, Aicher et al. [34] concluded that after 24 years, the creep values of the panel did not further increase under floor loads. However, Rungthonkit [18] performed creep tests over three months observing primary and secondary creep effects, and found that the creep deflections doubled over three months after the primary creep stage. Although concludingly, he also agrees that the design creep deflection "values are acceptable but overly conservative" and showed that 86.60% of the creep deflections can recover if given enough time – "70% is recovered after a day unloading; around 87% recovery after 2 months" [18].

The panel that will be used in this research is being developed based on the Kingspan Unidek TEK panel system, which already has OSB/3 skins, but the core is currently made of PUR (polyurethane). The PUR insulation will be replaced by a STEICO low density fibre board in this research. As already described earlier, the panel will have the following specifications:

- Core: Steico low density fibre board type M dry 100 mm (Figure 2.2, Table 2.1)
- Skins: OSB/3 2x12 mm (Table 2.2)
- Total panel thickness: 124 mm

Table 2.1: Steico Low density fibre board technical information [36].

Property	**Unit**	**Test method**	**Board type – M dry**
Nominal board density	$[kg/m^3]$	EN 1602	140
Density variation	$[kg/m^3]$	EN 1602	±20
Declared thermal conductivity λ_D	$[W/(m*K)]$	EN 12667	0.040
Compression strength (at 10 % deformation)	$[kPa]$	EN 826	100
Tensile strength perpendicular to face $\perp$	$[kPa]$	EN 1607	20
Shear strength	$[kPa]$	EN 12090	40
Dimensional stability	-	EN 1604	DS(70,90)3
Class of water absorption	-	EN 1609	1.0
Water vapour diffusion resistance factor μ	-	EN 12086	3
Fire class	-	EN 13501-1	E
Ingredients	-	-	wood fibre, polyurethane resin, paraffin wax
Waste code (EAK)	-	-	030105/170201

The missing values for the insulation panel are a shear modulus and the modulus of elasticity. These will be assumed based on already existing panel insulation values and available test

Table 2.2: OSB skin properties [Kingspan Unidek]

Property		parallel to span direction	perpendicular to span direction	unit
Bending resistance perpendicular to plane	$f_{m,k}(y-y)$	16.4	8.2	N/mm^2
Compression resistance perpendicular to plane	$f_{c,k}$	10.0	10.0	N/mm^2
Shear resistance perpendicular to plane	$f_{v,k}$	1.0	1.0	N/mm^2
Bending resistance in plane	$f_{m,k}(z-z)$	9.4	7.0	N/mm^2
Tension resistance in plane	$f_{t90,k}$	9.4	7.0	N/mm^2
Compression resistance in plane	$f_{c90,k}$	15.4	12.7	N/mm^2
Shear resistance in plane	$f_{v,rol}$	6.8	6.8	N/mm^2
Modulus of elasticity perpendicular to plane	E_{mean}	4930	1980	N/mm^2
Shear modulus perpendicular to plane	G_{mean}	50	50	N/mm^2
Modulus of elasticity in plane	E_{mean}	3800	3000	N/mm^2
	E_{05}	$0.85 * 3800$	$0.85 * 3000$	N/mm^2
Shear modulus in plane	G_{mean}	1080	1080	N/mm^2
	G_{05}	$0.85 * 1080$	$0.85 * 1080$	N/mm^2
Density	ρ_k	580	580	kg/m^2

results. Table 2.4 [18] provides an overview of commonly used core materials' properties. The Steico core material info is obtained from Kingspan Unidek. The obtained E modulus is between 1.5 MPa to 10 MPa. The G modulus is between 2.04 MPa to 7.6 MPa (20 - 24 MPa with fibres perpendicular to the faces). Knowing this, an assumption for an isotropic material with the E modulus as 5 MPa, and G modulus as 2.2 MPa (Table 2.3) was made based on Hooke's law to have a Poisson's ratio similar to materials generally used in sandwich panels seen in Table 2.4.

$$E = 2 * G * (1 + \nu) \tag{2.1}$$

Figure 2.2: Steico low density fibre board. [37]

Table 2.3: Steico low density fibre board properties.

MDF board (core) material info			
Young's modulus	E	5	*MPa*
Shear modulus	G	2.2	*MPa*
Poisson's ratio	v	0.14	

Table 2.4: Existing sandwich panel core material properties [18].

Inner core material	Density (kg/m^3)	Shear Modulus (N/mm^2)	Modulus of Elasticity (N/mm^2)	Shear Strength (N/mm^2)
EPS	14	2.1	1.4	0.14
	18	2.7	2.1	0.17
	22	3.3	2.3	0.20
	29	4.3	3.3	0.24
XPS	26	2.9	9.3	0.10
	29	3.1	12	0.14
	35	5.1	18	0.24
	48	6.2	26	0.28
PUR	48	2.8	2.9	0.29
	64	4.5	5.8	0.43
	80	6.4	10	0.60

Classification of sandwich beams

Allen [38] distinguishes three main types of sandwich beams classified by their skin thicknesses (seen in Table 2.5) which each result in a different set of assumptions for analysis: thick, thin, and very thin. The panels studied in this thesis, according to this classification have thin faces, thus need to be analysed as a Timoshenko beam due to having a shear component as well as a bending component [38]. The flexural rigidity is presented below, however, since the Young's modulus varies along the cross-section, it can not be taken out of the integral, meaning that EI will be marked as D [32]. The equation for the flexural rigidity of a structural insulated panel is as follows:

$$D = \int Ez^2 dz = \frac{E_f * b * t_f^3}{6} + \frac{E_f * b * t_f * d^2}{2} + \frac{E_c * b * t_c^3}{12} = 2D_f + D_0 + D_c \tag{2.2}$$

Where:
- E is the modulus of elasticity of the panel.
- z is the coordinate over the cross-section.
- E_f is the modulus of elasticity of the face.
- E_c is the modulus of elasticity of the core.
- t_f is the thickness of the face.
- t_c is the thickness of the core.
- b is the width of the panel.
- d is the centre to centre length of the faces.
- D_f is the bending stiffness of the faces.
- D_0 is the bending stiffness of the faces with a lever arm.
- D_c is the bending stiffness of the core.

Simplifications for the flexural rigidity

Usually, the second term of the flexural rigidity (see equation 2.2) is dominating [38]. The first term of equation 2.2 can be neglected when the faces of the panel are thin (and very thin) compared to the core, meaning the first term is less than 1% of the second term. This happens

Table 2.5: Classification of sandwich beams [38].

Category	Condition	Analysis method
Very thin	$\frac{d}{t_f} > 100$	Timoshenko
Thin	$100 > \frac{d}{t_f} > 5.77$	Timoshenko
Thick	$\frac{d}{t_f} < 5.77$	Ritz Method

when the following condition is met:

$$3\left(\frac{d}{t_f}\right)^2 > 100 \; or \; \frac{d}{t_f} > 5.77 \tag{2.3}$$

Substituting the values for our panel, this yields:

$$3\left(\frac{112}{12}\right)^2 = 261 > 100 \; or \; \frac{112}{12} = 9.33 > 5.77 \tag{2.4}$$

Hence, the first term can be neglected.

The third term can be neglected when the modulus of elasticity of the core is much lower than the modulus of elasticity of the faces, yielding a third term smaller than 1% of the second term [32]. This occurs when the following condition is met:

$$\frac{6E_f * t_f * d^2}{E_c * t_c^3} > 100 \tag{2.5}$$

Substituting the values for our panel, this yields:

$$\frac{6 * 3800 * 12 * 112^2}{E_c * 100^3} > 100 \Rightarrow E_c \leq 34 N/mm^2 \tag{2.6}$$

In this case, the modulus of elasticity of the core needs to be less than 34 N/mm^2 to use this simplification. Previously, the E modulus of the core was assumed to be 5 N/mm^2, therefore the assumption is made that both of these conditions are met, so it is a sandwich panel with thin faces and a weak core, and corresponds to the simplification seen on the far right in figure 2.3. Therefore, the flexural rigidity can be simplified into the following [38]:

$$D = \frac{E_f * b * t_f * d^2}{2} \tag{2.7}$$

Substituting the values for our panel, this yields:

$$D = \frac{3800 * 12 * 112^2}{2} = 286.00 kNm^2 \tag{2.8}$$

Important relations for the sandwich panel analysis

"The stresses vary linearly within each material constituent, but there is a jump at the face/core interface" [32]. This can be seen in figure 2.3, where the left side represents the real situation for axial and shear stresses, and the middle and right side sketches represent two different simplifications. First, for when the core is much weaker than the skins, and second, where the skins are very thin, so there is no increase in stresses within the skins themselves. The stresses

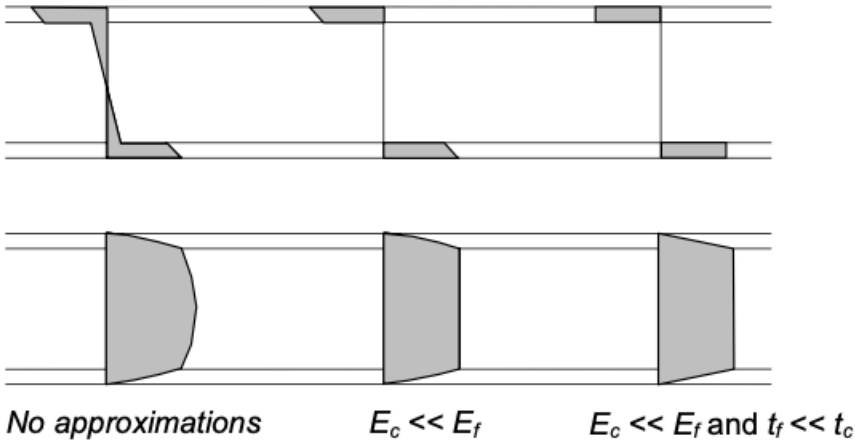

Figure 2.3: Direct and shear stresses. Two approximations. [32]

in the sandwich beam can be calculated with the following formulas [32] for the faces:

$$\sigma_f = \frac{M_x z E_f}{D} \; for \; \frac{t_c}{2} < |z| < \frac{t_c}{2} + t_f \tag{2.9}$$

For the core:

$$\sigma_c = \frac{M_x z E_c}{D} \approx 0 \; for \; |z| < \frac{t_c}{2} \tag{2.10}$$

Where:
- M_x is the bending moment.
- z is the coordinate over the cross-section.
- E_f is the modulus of elasticity of the face.
- E_c is the modulus of elasticity of the core.
- t_f is the thickness of the face.
- t_c is the thickness of the core.
- D is the bending stiffness of the panel.

General stress strain relation [32]:

$$\varepsilon_{x0} = \frac{N_x}{E_1 t_1 + E_2 t_2 + E_c t_c} = \frac{N_x}{A_x} \Rightarrow \sigma_f = \varepsilon_{x0} E_f \; and \; \sigma_c = \varepsilon_{x0} E_c \tag{2.11}$$

Where:
- ε_{x0} is the strain at the neutral axis.
- N_x is the normal force.
- A_x is the area where the force is applied.
- E_f is the modulus of elasticity of the face.
- E_c is the modulus of elasticity of the core.

- t_1 is the thickness of the face.
- t_2 is the thickness of the face.
- t_c is the thickness of the core.

Shear stress in the core can be found with the following formula [32]:

$$\tau_c(z) = \frac{T_x}{D}\left[\frac{E_f t_f d}{2} + \frac{E_c}{2}\left(\frac{t_c^2}{4} - z^2\right)\right] \tag{2.12}$$

Where:
- T_x is the shear force.
- D is the bending stiffness of the panel.
- E_f is the modulus of elasticity of the face.
- E_c is the modulus of elasticity of the core.
- t_f is the thickness of the face.
- t_c is the thickness of the core.
- z is the coordinate over the cross-section.
- d is the centre to centre distance of the faces.

Shear stress in the faces [32]:

$$\tau_f(z) = \frac{T_x E_f}{2D}\left(\frac{t_c^2}{4} + t_c t_f + t_f^2 - z^2\right) \tag{2.13}$$

Maximum shear stress at the neutral axis (z=0) can be found [32]:

$$\tau_{c,max}(z=0) = \frac{T_x}{D}\left(\frac{E_f t_f d}{2} + \frac{E_c t_c^2}{8}\right) \tag{2.14}$$

Shear stress on the interface of the two materials [32]:

$$\tau_{c,min}\left(\frac{t_c}{2}\right) = \tau_{f,max} = \frac{T_x}{D}\left(\frac{E_f t_f d}{2}\right) \tag{2.15}$$

Approximation to the shear stress in the core can be made, which was also seen above for the flexural stiffness formula simplification at equation 2.5. The difference between the maximum and minimum shear in the core will be less than 1% if [32]:

$$\frac{E_f t_f d}{E_c t_c^2} > 100 \tag{2.16}$$

If the core is weak $E_c << E_f$ (figure 2.3 in the middle) then the shear stress will be constant in the core and there will be no axial stresses in the core [32].
Face stress

$$\sigma_f(z) = \frac{M_x z E_f}{D_0 + 2D_f} \tag{2.17}$$

Core stress

$$\sigma_c(z) = 0 \tag{2.18}$$

Face shear stress

$$\tau_f(z) = \frac{T_x E_f}{2(D_0 + 2D_f)} \left(\frac{t_c^2}{4} + t_c t_f + t_f^2 - z^2 \right) \tag{2.19}$$

Core shear stress

$$\tau_c(z) = \frac{T_x E_f t_f d}{2(D_0 + 2D_f)} \tag{2.20}$$

If the core is weak $E_c << E_f$ and the faces are thin $t_f << t_c$ (figure 2.3 on the right) then the core will have constant shear stress and there is also no change in axial stresses in the skins, meaning a constant compression and tensions in the skins [32].
Core stress

$$\sigma_c(z) = 0 \tag{2.21}$$

Face stress

$$\sigma_f(z) = \frac{M_x}{t_f d} \tag{2.22}$$

Core shear stress

$$\tau_c(z) = \frac{T_x}{d} \tag{2.23}$$

Face shear stress

$$\tau_f(z) = 0 \tag{2.24}$$

A conclusion can be made by saying that faces carry tensile and compressive stresses from bending, and the core takes the transverse forces as shear stresses [32]. The sandwich panel utilises the material to the most of its bending strength and flexural rigidity by having a lever arm between the faces due to the core and thus increasing the moment of inertia and creating a stronger material. Sandwich panels with asymmetrical face thicknesses follow similar equations. The neutral axis will have a different position and therefore the equations for stresses will differ. However, this will not be focused on in this thesis, but has been brought out in [32].

Transverse shear deformations
Deformations always occur from two types of deformations: due to bending moments and due to shear forces (as seen in figure 2.5), hence shear deformation is composed of transverse and in-plane deformations seen in figure 2.4 [32]. The assumption is made, that only the core deforms in shear, since the core takes all the shear forces.

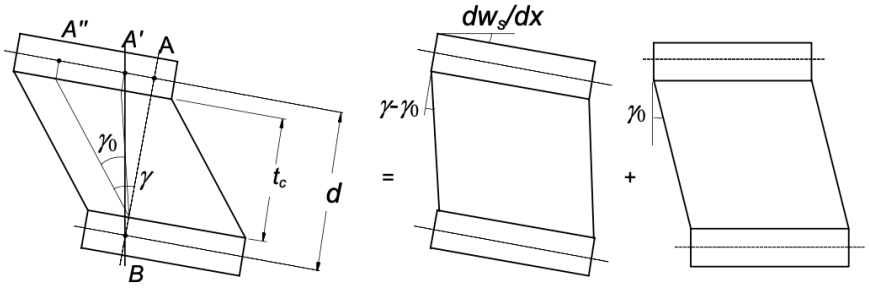

Figure 2.4: Shear deformation of a SIP – total deformation; transverse deformations; in-plane deformations [32].

Shear stiffness
The shear stiffness for thin faces and weak core is the following [32]:

$$S = \frac{G_c d^2}{t_c} \tag{2.25}$$

Where:
- G_c is the shear modulus of the core.
- d is the centre to centre distance of the faces.
- t_c is the core thickness.

Total deformation
In the considered model of sandwich panels, the total deformation of a structural insulated panel consists of two parts: the bending deformation, and shear deformation. This can also be seen in figure 2.5. The total deformation [32]:

$$w = w_b + w_s \tag{2.26}$$

Where:
- w_b is the bending deformation.
- w is the total deformation.
- w_s is the shear deformation.

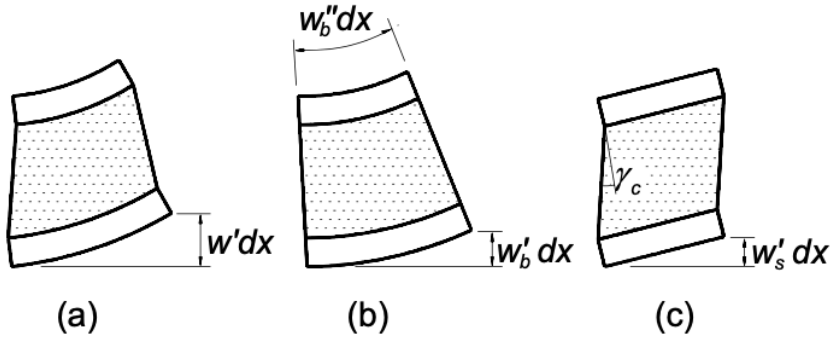

Figure 2.5: SIP deformations: a) total deformation; b) bending deformation; c) shear deformation [32].

2.2. Failure modes of SIPs

There are many failure modes for structural insulated panels. Failure can occur with only one failure mode, but it can also be a combination of multiple [33]. The different cases a structural insulated panel can fail are presented in figure 2.6 [32]. Under transverse loads, the panel can fail in “face failure, inner core shear failure, debonding and indentation at the loading point” [18]. Under axial loads, the failure may occur due to “buckling, end bearing and debonding” [18]. Rake [39] stated that “analytical calculations of individual geometric instabilities are insufficient to determine the sandwich panel behaviour of coupled instabilities”. Therefore, the analytical calculations can give very important insights, but coupled failure mechanisms should be considered as well.

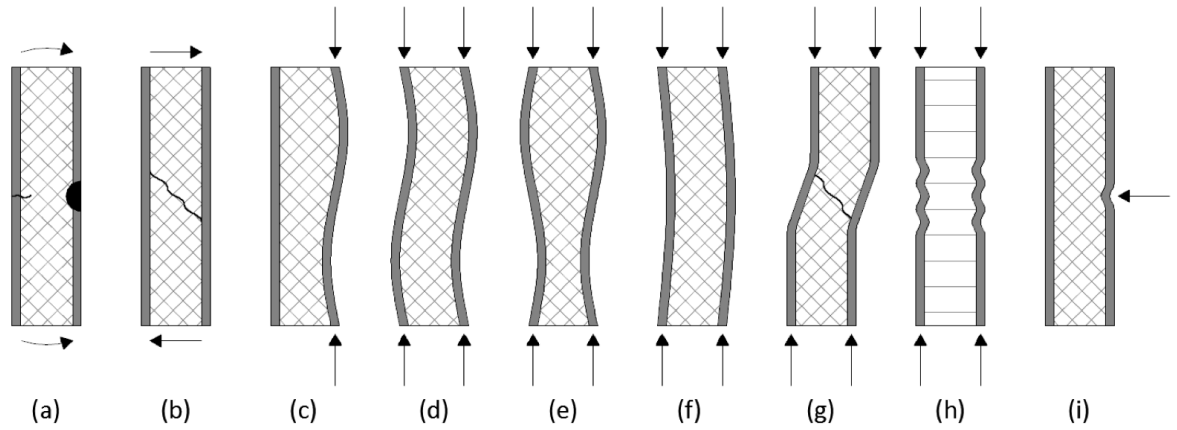

Figure 2.6: Sandwich panel failure modes. a) Face yielding/fracture; b) core shear failure; c) face wrinkling - local buckling - delamination; d) face wrinkling - local buckling - delamination; e) face wrinkling - local buckling - delamination; f) general buckling; g) shear crimping; h) face dimpling - only for honeycomb; i) local indentation. [39]

There is a set of assumptions for classical sandwich panel theory by Davies [33] listed by Rungthonkit [18]:

- The faces and the inner core are linearly elastic.
- The deflections are small.
- The shear stress in the core is constant across its thickness.
- There is no slip between the core and the faces.
- There is no deformation of the inner core in a direction perpendicular to the faces (i.e. the inner core is not crushed).

These conditions have to be fulfilled to use the equations following for the panel analysis.

a) Face yielding/fracture
In the case of a bio-based skin, the tensile failure is a brittle failure mechanism. For that the normal tensile failure equations can be used for OSB. The compressive and tensile stresses can be calculated with the following formula:

$$\sigma_c = \frac{F}{A} \tag{2.27}$$

- σ_c is the compressive stress.
- F is the axial force applied over the cross-section.
- A is the area where the force is applied.

Bending of the panel attributes to the compression and tensile forces of the skins, so the compression from the bending and the direct force need to be added to do the compression and tension check. The bending stress can be calculated according to equation 2.9.

The compression and tension checks are performed according to the Eurocodes:

$$\frac{\sigma_{c,d}}{f_{c,d}} \leq 1 \tag{2.28}$$

$$\frac{\sigma_{t,d}}{f_{t,d}} \leq 1 \tag{2.29}$$

where

$$f_{c,d} = \frac{f_{c,k}}{\gamma_M} k_{mod} \tag{2.30}$$

$$f_{t,d} = \frac{f_{t,k}}{\gamma_M} k_{mod} \tag{2.31}$$

Where:
- $\sigma_{c,d}$ is the design compressive stress.
- $\sigma_{t,d}$ is the design tensile stress.
- $f_{c,d}$ is the design compressive resistance.
- $f_{t,d}$ is the design tensile resistance.
- $f_{c,k}$ is the characteristic compressive resistance.
- $f_{t,k}$ is the characteristic tensile resistance.
- γ_M is the material safety factor.
- k_{mod} is the modification factor to account for load duration and environmental conditions.

The material safety factor from Eurocode NEN-EN 1995-1-1 for OSB/3 is: $\gamma_M = 1.2$, and the k_{mod} values for OSB/3 are brought out in the coming chapter. The service class for the panels discussed in this thesis will be service class 2, because they are in outside conditions, but with the assumption of having a cladding that protects the panel from direct rain, and will allow the panel to dry.

b) Core shear failure
The critical spots for shear failure are usually in the middle of the core or at the face/core interface [33]. The shear resistance needs to be compared to the shear stress in the panel, which can be found with the following equation [33]:

$$\tau_{cr} = \frac{V(\sum E_i S_i)_{max}}{(\sum E_i S_i)B} = \frac{V(\frac{E_F t e}{2} + \frac{E_C d_C^2}{8})}{(\frac{E_F t e^2}{2} + \frac{E_C d_C^3}{12})B} \approx \frac{V(1 + \frac{E_C e}{8E_F t})}{(1 + \frac{E_C e}{6E_F t})eB} \tag{2.32}$$

Where:
- $d_C \approx e$
- S is the shear stiffness.
- E_f is the modulus of elasticity of the face.
- E_c is the modulus of elasticity of the core.
- B is the width of the panel.
- V is the shear force.
- t is the thickness of the panel.
- e is the eccentricity of the centre of the panel and the centre of the face.
- d_c is the thickness of the core.

The critical shear force [33]:

$$V_{cr} = eBf_{Cv} \tag{2.33}$$

Where:
- B is the width of the panel.

- f_{Cv} is the shear resistance of the core.
- e is the eccentricity of the centre of the panel and the centre of the face.

c) d) e) Face wrinkling
Face wrinkling, which is a form of buckling in short waves, can occur in three ways: rigid base, symmetrical and anti-symmetrical [32]. These can be seen in Figure 2.7.

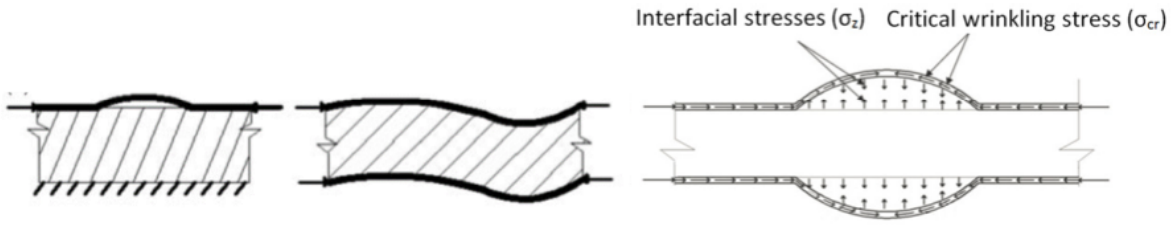

Figure 2.7: Three wrinkling modes – Rigid base; Asymmetrical; Symmetrical [39].

"Thin steel faces supported by a thick foam core can be considered as a plate on elastic foundation. Mathematically the problem can be modelled as shown in Figure 2.8. A simply supported rectangular plate is subjected to an applied stress p along the two transverse edges. The buckled shape can be represented by a double sine series as given by (Davies and Hakmi 1990)" [40].

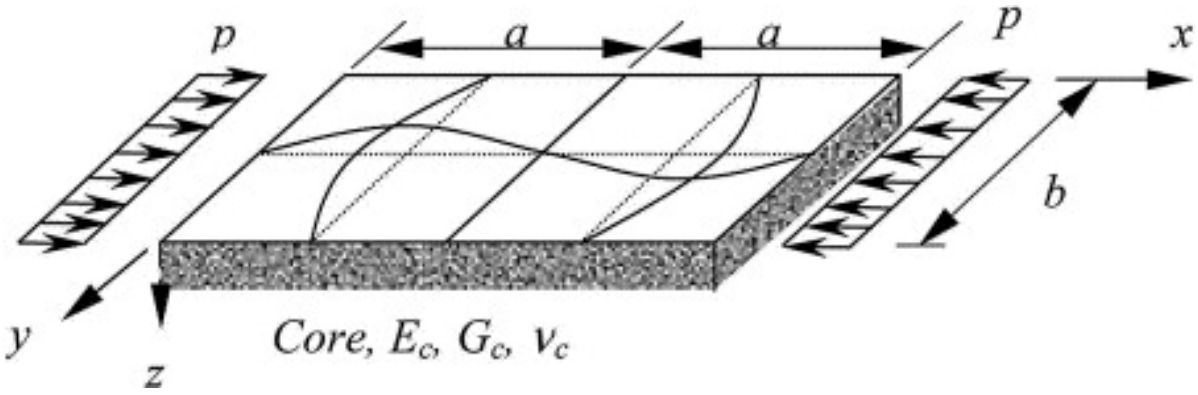

Figure 2.8: A plate on elastic foundation buckling shape [40].

The condition for anti-symmetrical buckling is $t_c/t_f < 17$. If that ratio is above 17, then the buckling of the faces is symmetrical [32]. In the case of the panel discussed in this thesis, the face wrinkling will happen in an anti-symmetrical way. To find a solution, the Winkler Foundation approach is suggested, which would model the core as a set of springs [32]. However, in the case of anti-symmetrical buckling, the springs remain unloaded, meaning that no solution can be found, since there will be no tension and compression in the core, but only shear, which that method does not describe [32]. Hence, another method needs to be used. The critical face wrinkling force can be found with the following formula suggested by Hoff, which corresponds well with analytical and test results [32]:

$$\sigma_{f,cr} = 0.5\sqrt[3]{E_f E_c G_c} \tag{2.34}$$

Where:
- E_f is the modulus of elasticity of the face.

- E_c is the modulus of elasticity of the core.
- G_c is the shear modulus of the core.

A second method to solve the face wrinkling problem is Hoff's method, where the shear stress is included, and modelled by a linear decay function [32]. It assumes that the core is minimally influenced, with a depth h [32]. The anti-symmetrical case for thick cores ($h < t_c/2$) equation with the Hoff's method reads [32]:

$$\sigma_{f,cr} = 0.51\sqrt[3]{E_f E_c G_c} + 0.33 G_c \left(\frac{t_c}{t_f}\right) \tag{2.35}$$

There are many more similar equations from different sources which are presented in Table 2.6 which follow the shape:

$$\sigma_{f,cr} = k_m \sqrt[3]{E_f E_c G_c} \tag{2.36}$$

The face can buckle into the core and out of the core as seen in figure 2.6 c) d) and e). This depends on the strength of the core and the adhesive joint [32]. In general, the wrinkling stress should be determined through tests with the specific panel [35]. "To prevent coupled instabilities the compression stresses in the face sheets have to be lower than the wrinkling load of wrinkling case I – rigid base" [39].

Table 2.6: Face wrinkling critical forces equations.

$\sigma_{f,cr} = 0.5\sqrt[3]{E_f E_c G_c}$	Hoff's conservative suggestion (Eurocode suggestion) [32]
$\sigma_{f,cr} = 0.91\sqrt[3]{E_f E_c G_c}$	Hoff's method - symmetrical buckling [32]
$\sigma_{f,cr} = 0.51\sqrt[3]{E_f E_c G_c} + 0.33 G_c \left(\frac{t_c}{t_f}\right)$	Hoff's method - anti-symmetrical buckling [32]
$\sigma_{f,cr} = 0.65\sqrt[3]{E_f E_c G_c} + 0.33 G_c \left(\frac{t_c}{t_f}\right)$	ECCS recommendation [33]

f) General buckling

According to the assumptions of the linear sandwich theory, three models can be described to determine the global buckling load of sandwich panels [39]:

- Allen's formula for thin faces.
- High-order sandwich panel theory – only for weak cores.
- Extended high-order sandwich panel theory – core can behave linearly or non-linearly in the axial direction; core shear stiffness, transverse stiffness, and axial stiffness taken into account – for weak and strong cores.

There is a difference between thin face, and thick face panel global buckling calculations. In the case of thin faces, the stiffness of the faces is so small, it can be neglected, and the core stiffness plays a larger role than in the case of thick skins [41]. "Sandwich panels with cores that have a very low shear modulus will be dominated by the term of the core shear buckling

load [...]. If the core shear modulus is very high (e.g., a honeycomb core), the global buckling load approaches the Euler buckling load" [39].

Euler critical load for axially loaded elements [38]:

$$F_{cr,Euler} = \frac{\pi^2 D}{L^2} \tag{2.37}$$

Where:
- D is the bending stiffness of the panel.
- L is the height of the panel.

The critical load in sandwich structures is smaller than the Euler load due to shear deformations in the core, which reduces the stiffness of the whole panel [38]. Hence, a critical load for a sandwich panel needs to be derived, which takes into account the reduction by the core. This was done by Davies [33] and presented below.

Critical load for thick skins [33]:

$$F_{cr,thick} = \frac{F_E F_{EF} - F_{EF}^2 + F_E F_C}{F_E - F_{EF} + F_C} \tag{2.38}$$

where $F_E = F_{cr,Euler}$ is the Euler critical buckling load of the whole panel;
F_{EF} is the Euler critical buckling load of the faces only

$$F_{EF} = \frac{\pi^2 E_f I_f}{L^2} \tag{2.39}$$

F_C is the shear critical load:

$$F_C = A_C G_{eff} = \frac{G_c d^2 b}{t_c} \tag{2.40}$$

Critical load for thin skins [41]:

$$F_{cr,thin} = \frac{F_E}{1 + \frac{F_E}{F_C}} \tag{2.41}$$

g) Shear crimping
Shear crimping is most likely to happen after large buckling has occurred [32]. Shear crimping is a shear instability failure which can be calculated with the following formula [32]:

$$\sigma_f = \frac{S}{2t_f} \tag{2.42}$$

Where:
- S is the shear stiffness.
- t_f is the thickness of the face.

h) Face dimpling
Face dimpling can happen only in panels with honeycomb or corrugated cores [32]. Since this is not the case in the panel discussed in this thesis, it will not be further elaborated.

i) Local indentation
Sandwich panels are very sensitive to high localised lateral loads [32]. These cause indentations in the skins, which are supported by the core, and if the core is compressed, the panel can fail. This can be seen in figure 2.9. The minimum area of the skin that can be under a concentrated load, can be calculated with the following formula [32]:

$$A = \frac{P}{\sigma_{cz}} \tag{2.43}$$

Where:
- σ_{cz} is the compressive strength of the core material.
- P is the concentrated force.

This failure mode can be a problem especially in connections. It is influenced most by the ratio of the Young's modulus of the face and the core, and by the thickness of the face [32]. To solve the likelihood of this failure mode, two methods are proposed, which include the two parameter model and the Winkler foundation model [32]. It is recommended that the Winkler model be used for wave-lengths that are less than 60 mm, and for above both of the methods give similar results [32]. In general, the failure method is not thoroughly researched, so no direct failure can be assumed according to Zenkert [32].

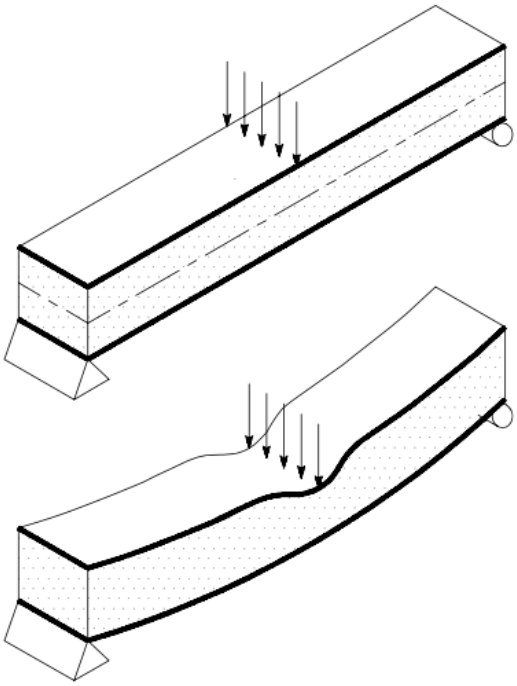

Figure 2.9: localised loads result [32].

j) Vibration
Vibrations cause problems usually in moving structures, this means that the natural frequency should be smaller than the vibration frequency of the loads that it is subjected to [32]. This will most likely not be the governing failure mechanism, since there will not be vibrational loads subjected to a residential building, unless an earthquake occurs.

2.3. Panel to panel connections

Connections are a crucial part of any construction. In SIP systems, they provide structural integrity and air tightness [18]. “Improperly constructed joints present the potential for water penetration” [11]. In all connections in this chapter, timber-to-timber connection equations from the Eurocode can be used.

Sandwich panels are connected with conventional connecting elements like screws or nails. Fasteners are usually loaded in tension and shear [33]. Primary requirements for connections in external walls are [33]:

- strength of the connection;
- hygrothermal performance;
- avoidance of air leakage;
- fire performance;
- appearance.

As discussed previously, the skins of the panel will be in compression and tension from bending and axial forces, and the core will be under shear loading. However, there are a few connections where these assumptions are not true [32]. These forces are shown in figure 2.10, and the corresponding connections can be seen in Figures 2.13, and G.9. The first connection seen in figure 2.10 is a T-connection and it is not very likely to exist in a residential building, only in a very large building that would need structural shear walls inside the building. Otherwise, for non-load-bearing walls the forces will not be high enough to cause problems.

The failure of a connection through a combined case of face buckling and pull through can occur most likely in two different connections seen on the following figure 2.10 as the T-connection and the L-connection [33]. However, there are no evaluation methods available to calculate the failure of the combined case [33]. The rotational stiffness of a connection depends on four criteria: width of the flange of the purlin (connecting column) profile; number and location of screws in the flange; bending stiffness of the lower face; compressive stiffness of the core [33].

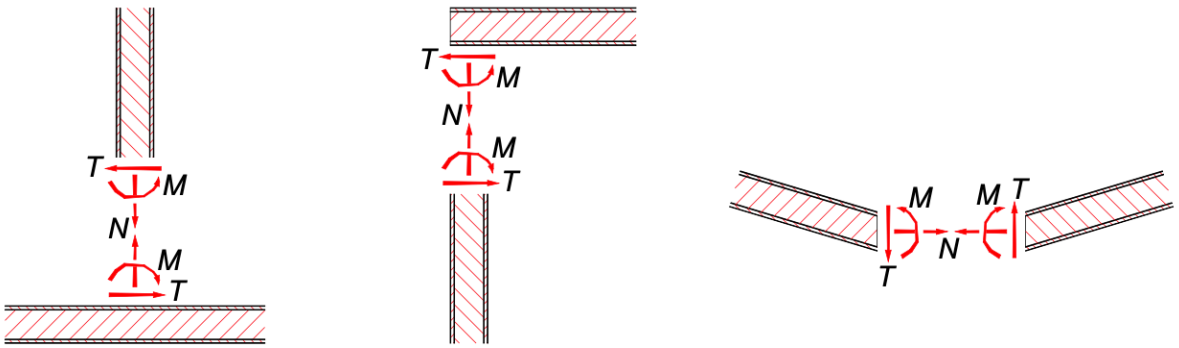

Figure 2.10: Forces acting in the joints [32].

The connections presented here are all commonly used connections for residential buildings built with sandwich panels, these also include connections from the Kingspan TEK system. In figure 2.13 a corner connection can be seen. The connection has been fixed by nails or screws which go completely through one of the panels and embed into the second panel. This connection would be subjected to axial, shear and limited bending forces.

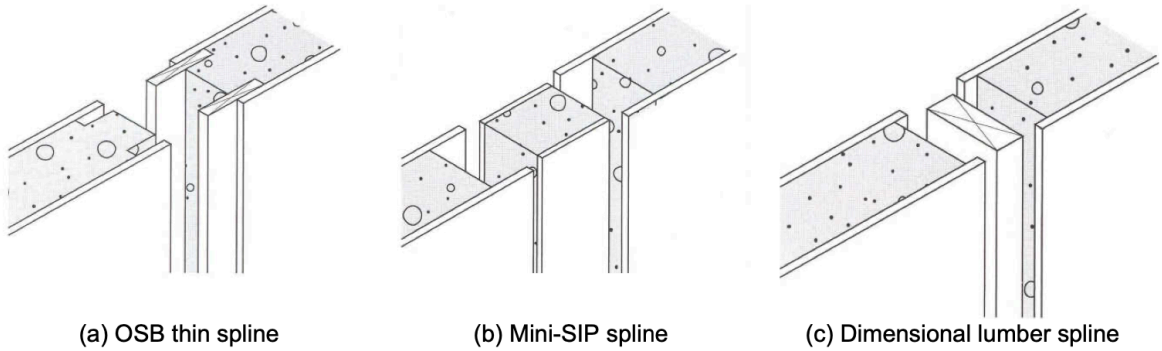

Figure 2.11: Panel to panel connection types [42].

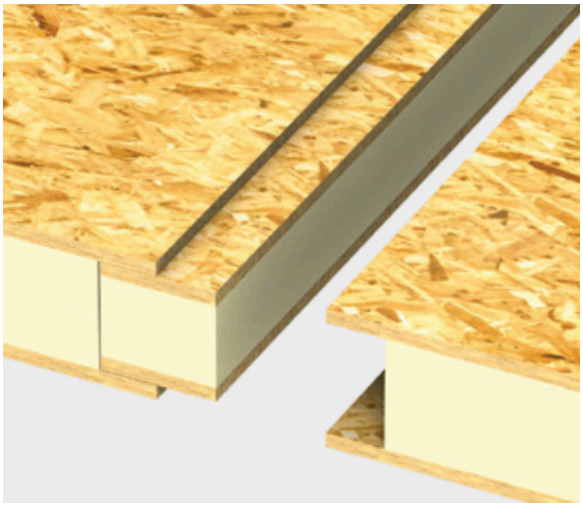

Figure 2.12: Wall continuous connection TEK system 1 – mini-SIP connection. [43]

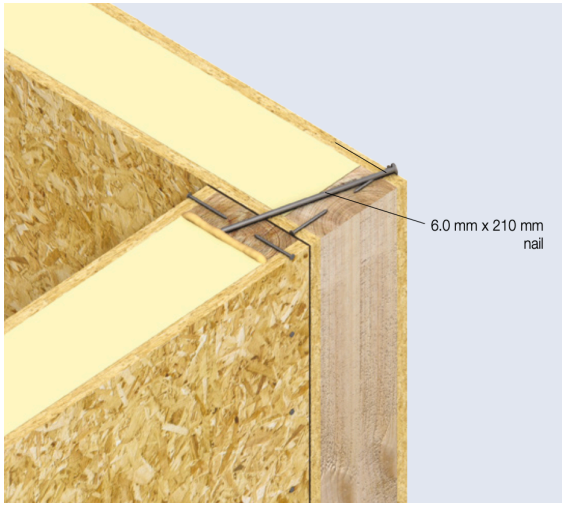

Figure 2.13: Wall corner connection TEK system. [43]

In figures 2.12, 2.14, 2.15, and 2.11 panel continuations can be seen. These connections all follow a similar solution by having a connecting element between them, and transferring minimal axial and shear forces. From a building physics aspect, connections seen in figures 2.12, and G.3 should be preferred, because there is no thermal bridge and the thickness of insulation material is bigger than in all similar connections, limiting the effect of a thermal bridge. These are called a spline and mini-SIP spline. However, the dimensional lumber spline gives more stiffness in the panel. The stiffness can be increased up to 23% [10]. The type of connection changes the amount of deflection seen in tests by Kermani [10]. The biggest change in the amount of deflections compared to a normal panel was for a dimensional lumber spline connection whereas for a mini-SIP spline the effect was the smallest. Additionally, header and footer boards of the panel added stiffness and reduced the amount of deflections.

Openings reduce the strength of the panel by reducing the flexural, shear, and torsional rigidity [33]. Thus, large openings usually need to be reinforced by adding beams around it or by locally making the faces thicker. This can be seen in figures 2.17, and G.5. Additional reinforcements can be placed inside the sandwich panels if the loads get too big, and the panel is not able

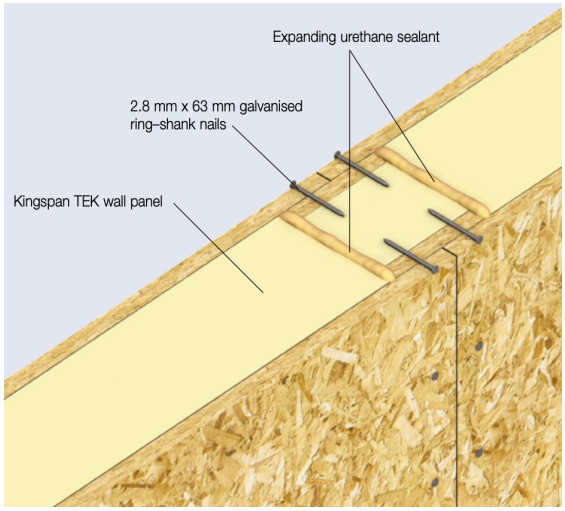

Figure 2.14: Wall continuous connection TEK system 2 – thin spline connection [43].

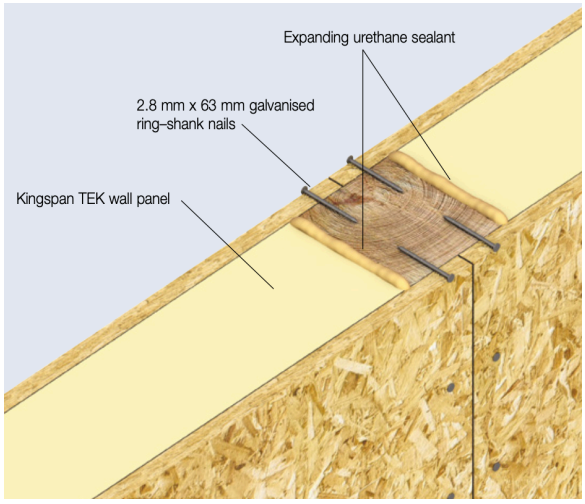

Figure 2.15: Wall continuous connection TEK system 3 – dimensional lumber spline [43].

to resist the forces. The panel with an opening will transfer the load to adjacent panels, while resisting a smaller load [33]. Stress concentrations from small openings and the corners of large openings may cause the panel to prematurely fail [33], [18]. The average ultimate strength of panels with a single outlet (276.0 kN) was 17% lower than those without (331.8 kN) [11]. A study by Jacques et al. [11] showed that the panels with outlet penetrations failed by the face-sheet crushing over the entire width of the OSB at the location of the outlet, likely due to local damage induced by the process of cutting and removing the OSB and foam at the outlet. Panels with outlets exhibited reduced stiffness due to the net reduction in face-sheet area on the compression face. It is anticipated that increasing the number of outlet penetrations would lead to further decreases in load-carrying capacity and panel stiffness, which should be accounted for in practice [11]. Given that the structural behaviour of the wall panels with and without penetrations was largely unaffected when loads were within the design service range, strengthening the panels at the locations of the outlets will likely not achieve a greater level of performance [11].

Roof edge details are usually under high lifting wind loads [33], therefore they require good connections to the wall elements and the roofing elements. Everything will be connected to the panels through fasteners. Fasteners on external walls should be made from durable materials to avoid corrosion lines on the facade [33]. Connecting elements (called inserts) change the stiffness of the panel, making it locally stiffer [32]. A suitable connecting method needs to be used to transfer the loads from one element to another. Some connecting methods can be seen in Figure 2.18, and in Table 2.7 with their performance to different forces. Figure 2.18 [32] shows four different insert types: 1) self-tapping, 2) through-thickness, 3) partial, and 4) flared top inserts. Each insert serves its own purpose. Self-tapping inserts do not take bending moments, and should in general be used where there are no significant forces involved. Thus, to connect small elements. Through-thickness connectors transfer all forces very well, especially shear forces. These should be preferred for transferring high loads. Partial inserts are similar to self-tapping connectors, which do not transfer bending forces nor can they transfer high shear

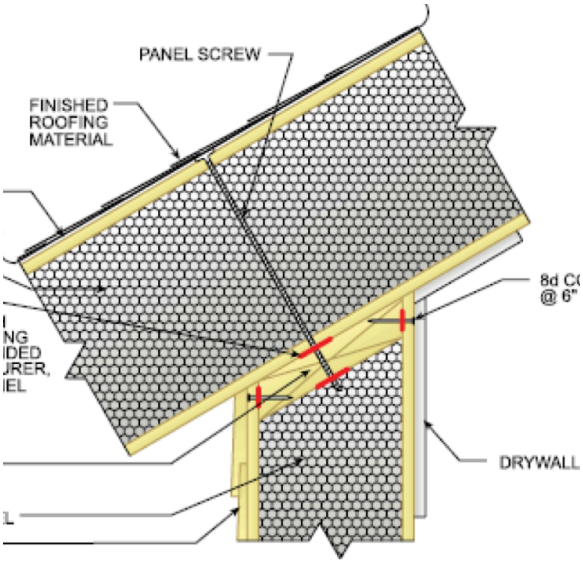

Figure 2.16: Roof wall connection 1. [44]

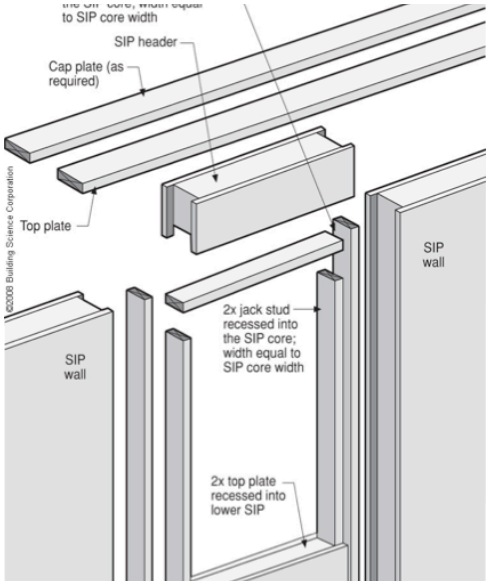

Figure 2.17: Window opening detail. [44]

loads, but can be preferred over through-thickness connectors to avoid damaging both skins of the panel. The flared top is connected with an adhesive making it a good solution to not pierce the core, however, the adhesive needs to be reliable to transfer all the loads. Another addition to the insert can be a flared top to more evenly distribute stresses, however there will still be stress concentrations under the flared edges.

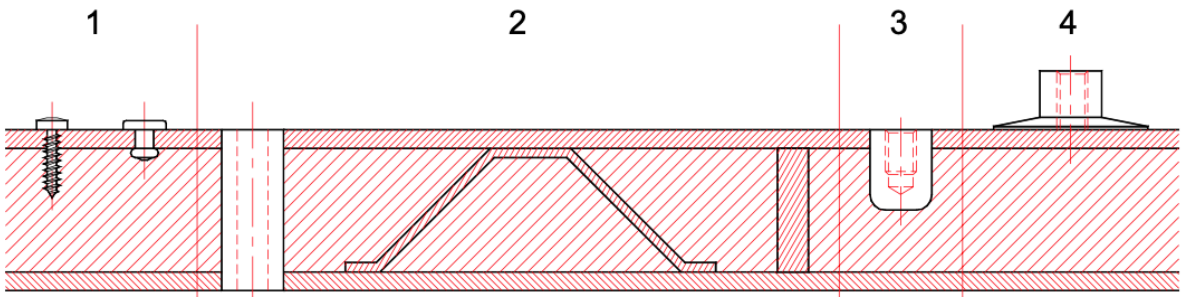

Figure 2.18: Connecting insert types – 1) self-tapping, 2) through-thickness, 3) partial, and 4) flared top inserts [32].

Table 2.7: Connecting inserts performance [32].

	Transverse force 	In-plane force 	Bending moment 	Comments
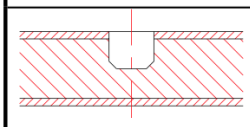 Partial	+	+	÷ ÷	Use where one face sheet must be kept intact Avoid bending moments Do not use in panels subjected to much shear Beware of stress concentration in core
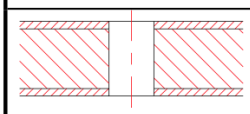 Through-thickness	+ +	+ + +	+ +	Use for heavy loads Note stress-concentrations in core and in core/face-sheet interface
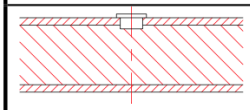 Rivet / screw	÷	+	÷ ÷ ÷	Use for attaching light equipment Use mainly in thick face-sheets Avoid bending moments and transverse forces Beware of stress-concentration in core, in particular when using long screws.
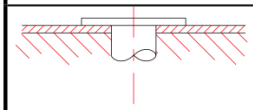 Flared top	+	+ +	+	Use for improved stiffness and pull-out strength Beware of bending stress in face sheets and peel-stresses underneath flared edge

2.4. Panel to floor beams connections

In general, a floor on beams is common for residential buildings made of SIPs. This floor type does not provide a lot of sound insulation, and can also have vibration issues, unless an additional damping layer is constructed. Two different types of connections for floors are commonly used for SIP buildings. First, a floor beam supported directly on the wall, which can be seen in figures G.13, 2.20, G.16, and G.17. This connection causes axial loads for the sandwich panel, but creates a thermal bridge with the rim board and the connecting elements. Second, a floor beam which is connected by a joist hanger, which can be seen in figures 2.19, G.15, and G.14. This connection causes very big eccentricities for the panels, but the effect of a thermal bridge is reduced. In the case of the floor to wall connections, the hanger joist needs to be calculated with timber to steel equations from the Eurocode.

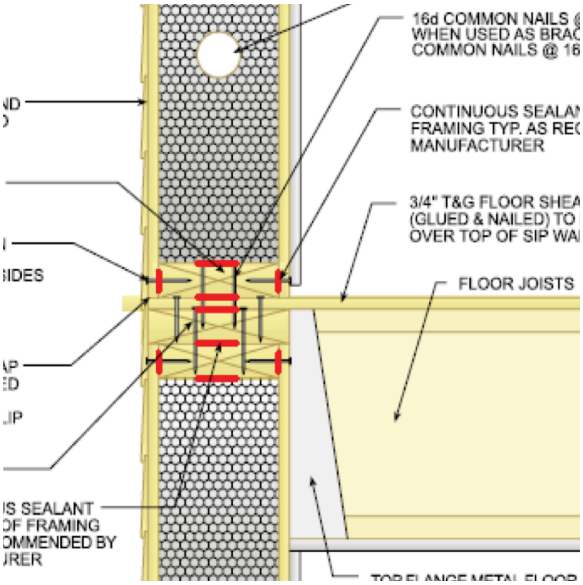

Figure 2.19: Floor beam with a joist hanger [44].

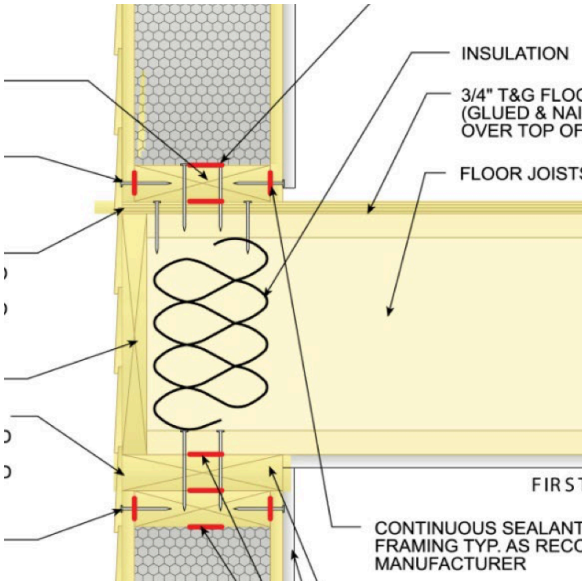

Figure 2.20: Floor beam directly on the panel [44].

2.5. Models and experiments of SIPs

The main loading cases for a sandwich panel are axial, bending, racking, and accidental wind debris collision loads. There is constant research going on to establish the behaviour of new sandwich panel configurations, and to fill missing gaps in the design process. There has been a sufficient amount of research into single loading cases, but only little research into loading combinations [18], [45]. The main software successfully used to analyse sandwich panels has been ABAQUS [17], [46], [47], [18], although, many other finite element modelling (FEM) tools have also been successfully used to model sandwich structures e.g. ANSYS, LS-DYNA, DIANA, and COMSOL [5]. All previously mentioned FEM softwares were able to model the failure modes of the analysed panels, some more successfully [17], [46], [47], [18], [48] than others [39]. The most promising seemed to be the model developed in the process of Smakosz' [47] research for analysing flexural behaviour for all SIPs if small modifications are made to account for material differences, and Santos et al. [46] found only a 12% difference in his ABAQUS model compared to Timoshenko beam equations. Mousa et al. [45] also confirmed the agreement between FEM and analytical results, and proposed the use of the model to reduce the amount of tests necessary to show the panel's agreement to construction requirements. In general, there are options to model the failure behaviour of sandwich panels that give reliable results.

It is possible to use analytical, computational and experimental ways to design with structural insulated panels. However, in general using only one method does not give sufficient reliability, thus Ni et al. [49] recommended using multiple methods to accurately predict a panel behaviour since analytical methods are only accurate to show the linear behaviour of the panel [50], but once the panel reaches failure there are inaccuracies. In general, analytical calculations predicted a higher buckling resistance and overestimated the strength of the panel [51], [47], whereas in some cases, FEM gave a similar result to analytical calculations [17] overestimating the resistance of the panel. Fathi [17] found, that the analytical Euler critical buckling load was never reached, because local panel failure happened earlier – the analytical load was 434 kN, but the failure load in experiments was 96 kN/m. The failure mode was accredited to

wrinkling at the top of the panel. This was also confirmed by Jacques et al. [11] and Kermani et al. [10] who found that linear elastic analysis overestimates the resistance capacity of the panel – panel of OSB faces and PUR foam of 3 m high buckled under 68 kN/m. This is also supported by Rake [39] who states that Timoshenko beam theory and Euler theory are not able to predict the bending behaviour of a sandwich panel, and analytical methods alone do not suffice in predicting the behaviour of the panel if multiple failure methods occur at the same time. In his experiments, he observed that a very sudden and brittle wrinkling and delamination failure occurred for steel faced sandwich panel with a XPS core. It was a combination of multiple failure modes, namely flexural-shear, delamination, buckling, core shear, and faces compression. In general, the failure was often described as sudden and brittle [11], [9]. The failure of a normal timber frame wall is much more ductile than the failure of a SIP wall [9].

The Euler critical buckling equation modified for sandwich panel applications assumes that the load is concentric and divided equally between the two faces, however this is not the case [52]. As Jacques et al. [11] proved, eccentric axial resistance is usually 15% less than concentric resistance of the panels. Vaidya et al. [52] found that the resistance was 35% less in eccentric loading. The variance comes from the different panels tested – in the first case it is OSB faced panels [11], but in the second case the tested panels are E-glass fibres impregnated with polypropylene matrix as the faces [52]. For the latter, the analytical failure load was 40% bigger than the experimental results and failure occurred due to the delamination of the facesheets and the core. The small scale tests which were also performed within that research showed that failure was predicted by the Euler buckling equation for the small scale samples, but on real size panels, delamination occurred which is not represented in the Euler buckling equation [52]. This was strongly supported by the findings of Mousa et al. [48] who tested for axial concentric and eccentric loading and found a buckling failure without debonding during concentric testing [48] whereas a facesheet-core debonding failure during eccentric loading [45]. He showed that the eccentrically loaded panels failed under a load that was 35% lower than the concentric load for composite faces [48] which supports the findings of Jacques et al. [11] and Vaidya et al. [52].

The most common failure mode for OSB or plywood faced panels under axial loading was end bearing failure – core materials: styrofoam [53]; PUR [18]; EPS [9]; styrofoam [54]; EPS, PUR, PI [11]. The core material had an influence on the failure mechanism – the governing failure method for EPS board stock was OSB failure (end bearing and middle failure), but for blown in foam cores the failure mode was shear failure of the core [11]. The end bearing failure consequently caused delamination, and close to the failure the linear behaviour changed to non-linear behaviour [53], [9]. The Euler buckling mode never occurred, but local buckling caused the failure earlier [9]. Jacques et al. [11] eccentric and concentric tests concluded that “the strength of SIPs and their corresponding failure modes were primarily influenced by the panel slenderness and the type of foam core”.

For bending, the failure occurred due to debonding of the compressed sheet which can also be called wrinkling or local buckling of the face, and caused very big shear deformations in the core [53], [18]. When a combination of axial loading and transverse loading was applied, the bending resistance of the panel decreased by 2-7% [18]. However, when openings were made into the panel and tested, the failure mode changed to flexural-shear [18]. Mousa et al. [55] tested composite panels under bending and also found debonding as the failure mechanism where “the out-of-plane tensile stress at the facesheet/core interface exceeded the tensile

strength of the core" and proved that "the interfacial stress [...] only depends on the core properties". Santos et al. [46] presented an analysis on cross-insulated timber panels which is an idea experimented to reduce the amount of timber used in a CLT panel and to improve its insulation capabilities by replacing the middle layer with PUR foam insulation. The failure was governed by core shear for transverse loading. The panels exhibited linear behaviour up until shortly before failure when non-linear behaviour was observed [46] as for all other structural insulated panels analysed [52], [39], [56], [45], [11], [53], [57], [54], [55]. However, with thicker cores the behaviour was linear, then turned non-linear, but continued with a different curve as linear again until failure [46] . Before failure, the foam core deformed significantly. Thicker cores and faces had better shear resistance than thinner cores and faces [46]. However, Pokharel [51] found in previous research that foam thickness does not play a significant role on the buckling strength of the panel. Jacques et al. [50] "showed that the ultimate shear resistance of SIPs is proportional to the mechanical properties of the core, and inversely proportional to the thickness of the core" [50]. Smakosz et al. [56] stated that "the flexural stiffness of panels in large-scale tests depends mostly on the core properties" and Rungthonkit [18] confirmed that the deflection is more dependent on the shear modulus of the core rather than the outer OSB faces or the core's modulus of elasticity. To compare to analytical calculations, Santos' et al. [46] test results showed a higher shear resistance than analytical calculations showed due to the non-linear behaviour of the core which was caused by the densification of the material under compression and bending. The capacity of the core is also observed by Mousa [45] who stated that "in case of global buckling, the core may exhibit a substantial shearing deformation whereas in case of local buckling the core acts as an elastic foundation for the facesheets in compression [...]". The elastic foundation behaviour of the core can successfully be modelled by the Winkler foundation model [45]. In contrast to Santos' et al. [46] results, the experimental results by Mousa et al. [45] were only half of the expected analytical resistances found for wrinkling, meaning failure occurred much earlier than analytically predicted due to "the out-of-plane interfacial stress [exceeding] the core tensile strength" which was also confirmed by the pull-off tests performed. Thus, the densification did not occur for Mousa's et al. [45] experiment who tested EPS core material whereas Santos et al. [46] tested PUR foam. "The main conclusion of these results is that the core density (or shear rigidity) plays a significant role in the resulting deflection and has very little effect on the strain of the facesheets" [45] and the failure method depends on the core material – PI and EPS blown foam core panels failed in core shear, but EPS board stock and LPU failed in OSB failure such as end bearing failure [11]. Thus, the core and the construction mode of the panel play a role in the failure [11]. Additionally, Jacques et al. [11] observed that the face-core bond has a significant effect on the panel behaviour – the axial load resistance was similar with panels that exceeded a 60% bonding between the faces and the core, however, if it subceeded 60% then the faces started to work separately lowering the axial resistance of the panel.

Yang et al. [42] and Rungthonkit [18] found that serviceability limit state was the governing condition when testing OSB faced sandwich panels for a four point bending test. The panel at the deflection limit was only using 15% of its resistance, which was also the case for a mini-SIP connection. However, when a timber beam is used for the connection, then the utilisation was 20%. To analyse the serviceability limit state, the conventional sandwich panel theory is very reliable [46]. This connects well to earlier research by Pokharel [51] who found that sandwich panels have significant postbuckling strength. Rungthonkit [18] also elaborated that "SIPs have a high degree of capacity reserve since the design load allowance is well below the

onset of failure load". Thus, if the serviceability limit state is taken as the limiting criteria, the analytical design calculations can be reliable.

2.6. Conclusions

The literature review chapter is concluded here with the main important points listed.

- Structural insulated panels have many advantages – good thermal insulation capabilities, economical, fast construction.
- The faces are in tension and compression and the core transfers forces through shear.
- Relative humidity influences the creep deflection of the panel with OSB faces.
- Material modification factors in the Eurocode for timber used for SIPs are too large.
- The core material properties were assumed to be E=5 MPa and G=2.2 MPa.
- Simplifications can be made to the flexural rigidity due to the thin faces and the weak core.
- The panel will be analysed according to Timoshenko beam theory.
- The panel analysed has thin faces and a weak core.
- The total deformation of the panel consists of bending and shear deformation.
- There are many failure mechanisms that can occur alone or as a combination.
- Failure combinations are difficult to predict.
- Connections mainly need to provide forces transfer and be air tight.
- There are three main types of panel to panel connections – thin spline, mini-SIP spline, dimensional lumber spline.
- Openings reduce the stiffness but in serviceability limit state stiffening is usually not necessary.
- Through-thickness connectors can add a significant amount of stiffness to the panel.
- The connections can be calculated using Eurocodes for timber to timber connections or timber to steel connections.
- The more common floor beam to panel connection is the joist hanger connections which causes eccentricities for the panel.
- ABAQUS is the most commonly used FEM tool used which can successfully describe the failure of the analysed panel.
- FEA gives reliable results to use in the design process of SIPs.
- Multiple methods are recommended to get reliable results in design with SIPs.
- Analytical methods only describe the linear behaviour of the panel.
- Analytical calculations overestimate the strength of the panel and failure can not be predicted.
- Euler critical buckling equation does not account for eccentricities and assumes the load to be distributed equally between the two faces.

- Structural insulated panels fail abruptly as a brittle failure – timber frame walls have a more ductile failure mode.
- Eccentric resistance for OSB faces is 15% less than concentric resistance; for composite faces the difference is 35% less.
- OSB faces fail for end bearing under axial loading, but the core material has an effect.
- Blown in foam cores fail for core shear whereas board stock cores fail for end bearing and delamination between the core and the faces.
- The behaviour of the panel is linear until shortly before failure when it changes to non-linear.
- The main failure mode under transverse loading was wrinkling or debonding of the face which depends on the core properties.
- Big shear deformations were observed in the cores.
- Bending resistance decreases with the application of a constant axial force.
- Thicker cores have a better shear resistance than thinner cores, but the thickness does not play a role on the buckling strength.
- Core properties dominate the flexural stiffness, especially the shear modulus.
- Densification of the foam core can increase the shear stiffness of the panel.
- The core acts as a elastic foundation for the faces during local buckling which can be described by the Winkler foundation model.
- If the bond between the faces and the core is less than 60% then the faces start to deform separately.
- Serviceability limit state is the governing criteria in the design with structural insulated panels and sandwich panel theory is very reliable in those cases.
- The connection types have an influence on the stiffness of the panel.

3

Methodology

This chapter will give a detailed overview of the methods used to analyse the novel structural insulated panel. First, a Karamba3D model is created, and validated through Timoshenko beam equations and a RFEM model. Further, experimental results will be presented, after which the models and analytical calculations will be compared to experimental results. Lastly, in appendix H two different methods will be explored to model a residential building out of structural insulated panels on Karamba3D and Dlubal. The panel's dimensions are based on a test rig set up by Kingspan Unidek seen in Figure 3.1.

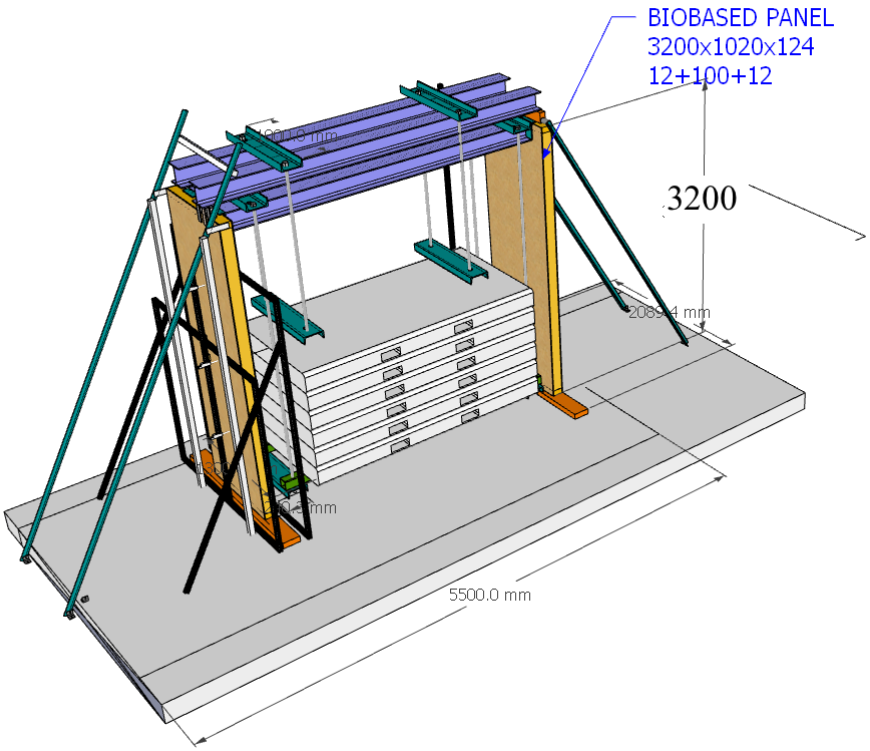

Figure 3.1: Test rig set up by Kingspan Unidek.

3.1. Karamba model

The panel is modelled using two shell-elements as the skins (Figure 3.2) which can transfer axial, shear and bending forces. The core is modelled by beams (Figure 3.2) which in theory are loaded only in shear, and no bending stresses occur in the core. Karamba3D does not allow the user to model a layered material, therefore beams were chosen to represent the core material. These beams were dimensioned so that they would represent the shear behaviour of the core material. In the first version of the panel model, the bending stiffness of the beams is as defined by Karamba3D, but in the next versions, the bending stiffness has been defined by the user to be very low, so the bending stiffness is negligible.

Five different combinations for the beam distribution and dimensions were modelled. They were as follows:

1. Beam distribution of 4x19 with a circular cross section with a diameter of D=21 mm and a significant bending stiffness
2. Beam distribution of 10x32 with a rectangular cross section 100x100 mm without a bending stiffness
3. Beam distribution of 20x64 with a rectangular cross section 50x50 mm without a bending stiffness
4. Beam distribution of 102x320 with a rectangular cross section 10x10 mm without a bending stiffness
5. Beam distribution of 16x49 with a rectangular cross section 65x65 mm without a bending stiffness – final iteration

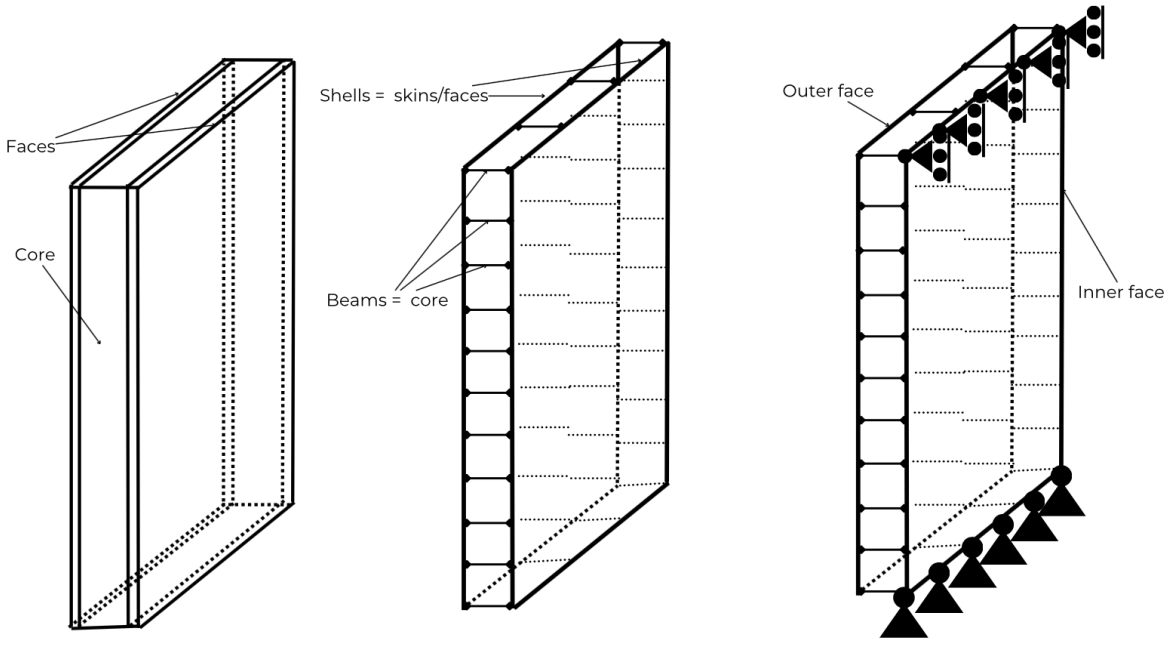

Figure 3.2: Karamba model sketch.

The first option for the beam selection was made based under the wrong assumption that it is not possible for the user to define a material for beams on Karamba3D, thus an existing material was chosen that had a bending stiffness as an E modulus and a predefined G modulus which

could not be removed nor changed (Figure 3.3). The amount of beams was chosen based on the shear stiffness of the core material in vertical direction with the predefined G modulus:

$$A_1 G_1 = A_2 G_2 \tag{3.1}$$

where
-A_1 is the area of the Steico core material $A_1 = 1020 * 3200\ mm^2$
- G_1 is the shear modulus of the Steico core material $G_1 = 2.2$ MPa
-A_2 is the area of the beams representing the core material in Karamba3D
- G_2 is the shear modulus of the beams representing the core material on Karamba3D, chosen as Family: wood, and Name: (VH)III, $G_2 = 270$ MPa

Therefore, the area of the beams was chosen as follows:

$$A_2 = \frac{A_1 G_1}{G_2} = \frac{1020 * 3200 * 2.2}{270} = 26596 mm^2 \tag{3.2}$$

The beam distribution was 19 in vertical direction, and 4 in horizontal directions with the beams having a circular cross-section with a diameter of 21 mm, and a length of 100 mm. This showed to be a not so accurate approach, but not due to the bending stiffness of the beams, but instead due to the small amount of beams and the lack of interaction between each other to provide stiffness for the faces. Thus, the next models were modelled with a user defined material where the E modulus was defined as $E = 0.0001$ MPa (Figure 3.4) to minimize the bending stiffness of the beams to model the core behaviour. The shear modulus was defined as is chosen for the core $G = 2.2\ kN/cm^2$ [1]. This resulted in the choices for combinations 2-5, where the area of the beams was chosen based on the same equation:

$$A_1 G_1 = A_2 G_1 \tag{3.3}$$

where
-A_1 is the area of the Steico core material $A_1 = 1020 * 3200\ mm^2$
- G_1 is the shear modulus of the Steico core material $G_1 = 2.2$ MPa
-A_2 is the area of the beams representing the core material in Karamba3D

Therefore, the area of the beams was chosen equal to the real area of the core:

$$A_2 = \frac{A_1 G_1}{G_1} = 1020 * 3200 = 3264000 mm^2 \tag{3.4}$$

Thus, combinations 2-5 have a beam area close to the real core area: 3264000 mm^2.

Based on the results of combinations 2-4, and comparison between analytical results and RFEM model results, the final combination of beams 16x49 with a rectangular cross section 65x65 mm seemed to most accurately model the behaviour of the panel (Figures 3.7, 3.9, 3.11, 3.13).

[1]Due to the units, an error was made. Instead of 2.2 MPa for the shear modulus, it is 22 MPa. This was changed for only one chapter, which is the Karamba3D model analysis alone.

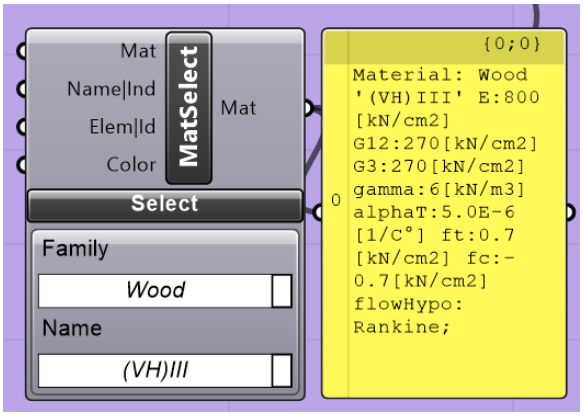

Figure 3.3: Predefined Karamba3D material for the beams. E – modulus of elasticity [kN/cm2]; G12 and G3 – shear moduli in different directions [kN/cm2]; gamma – specific weight [kN/m3]; alphaT – heat conductivity [1/C]; ft – tensile strength [kN/cm2]; fc – compressive strength [kN/cm2]

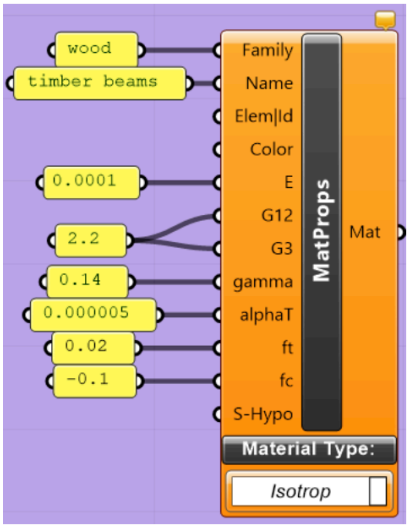

Figure 3.4: User-defined material for the beams. E – modulus of elasticity [kN/cm2]; G12 and G3 – shear moduli in different directions [kN/cm2]; gamma – specific weight [kN/m3]; alphaT – heat conductivity [1/C]; ft – tensile strength [kN/cm2]; fc – compressive strength [kN/cm2]

The panel is supported on the bottom on the inner face by restricting all translations and one rotation in the in-plane direction. This choice was made based on the assumption that the inner face takes on most of the load and the outer face is to provide support for the inner face. The green arrows represent translational constraint directions at the supports. The purple circles represent the rotational constraint location and direction of the constraint. This can be seen in Figures 3.6 to 3.11. Due to the shape of the panel, the assumption is made that in-plane rotation is restricted (around the y-axis) visible in Figure 3.6 represented by the purple circles. On the top of the panel a support has been modelled by restricting translations in x and y direction due to floor beams being connected in those positions, and other panels supporting from the sides in a real building situation. Mesh has been defined as 100 mm for all panels, but for most panels, the mesh got finer due to the beam selection – all beam connections also created a node.

The loads have been added according to a test rig at Kingspan Unidek, and an additional wind load as a distributed load over the panel has been added for comparison with analytical calculations. Loads are applied with an eccentricity, directly on the inside and outside faces as seen in Figure 3.5 and they are distributed loads.

The model will be used to analyse the behaviour of the structural insulated panel under axial and transverse loads – deflections, stresses and strains in the faces. The following points will be analysed:

- Does the model represent experimental results?
- What kind of analysis is possible – SLS and ULS?
- Which kind of failure is the model able to predict?
- Can the model be used in SIPs design process?

- Can the model be used to analyse other SIP material configurations?

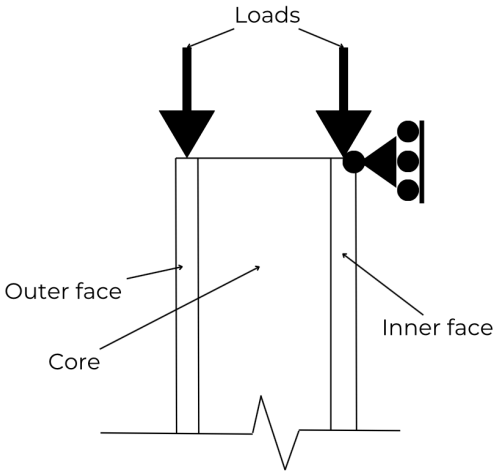

Figure 3.5: Loading schema.

Next, a description of the RFEM model will follow, which was used to verify the transverse behaviour of the Karamba3D model.

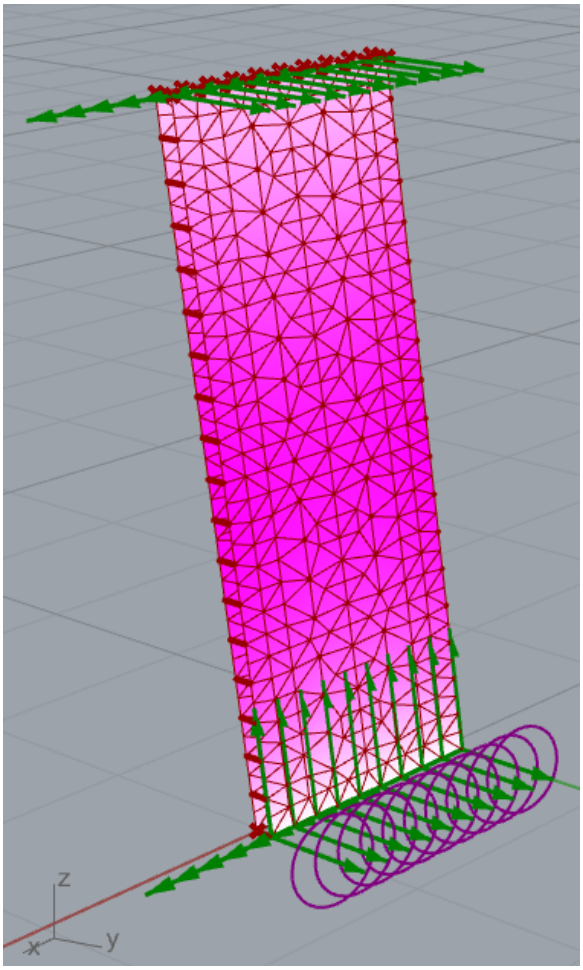

Figure 3.6: SIP panel with D=21 mm beams.

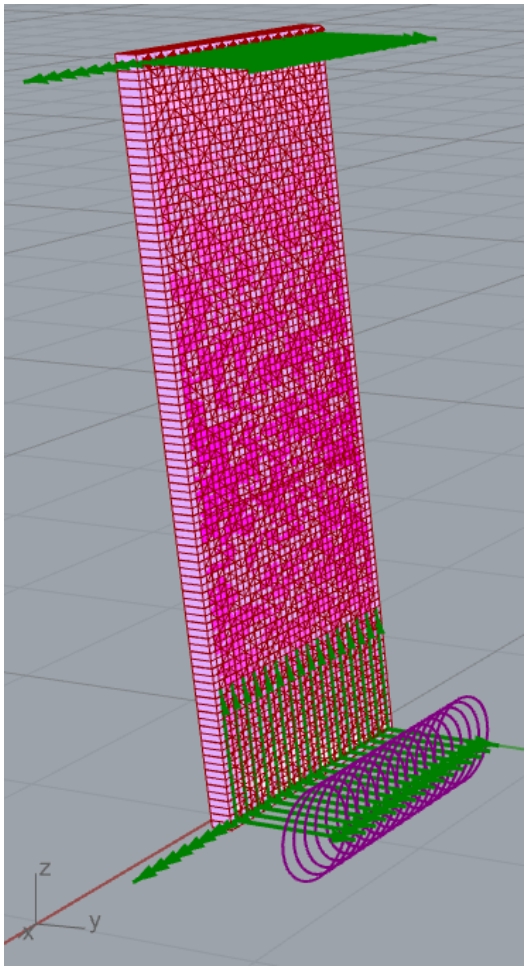

Figure 3.7: SIP panel 65x65 mm isometric view.

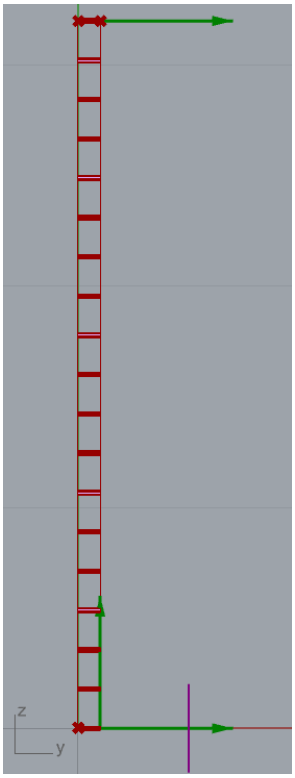

Figure 3.8: SIP panel Karamba3D model D=21 mm beams side view.

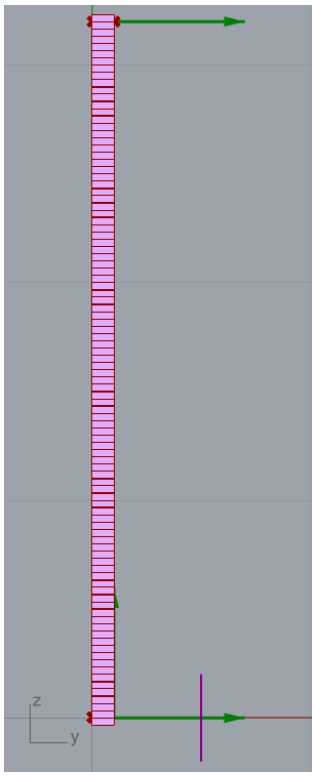

Figure 3.9: SIP panel Karamba3D model 65x65 mm beams side view.

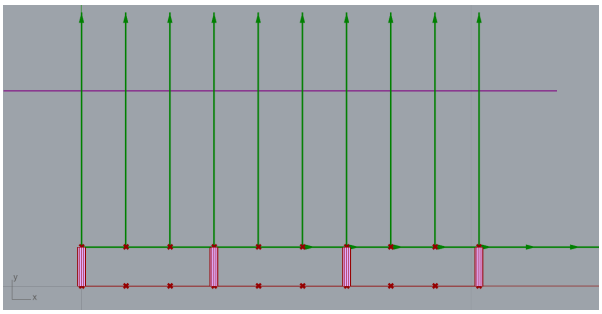

Figure 3.10: SIP panel Karamba3D model D=21 mm beams top view.

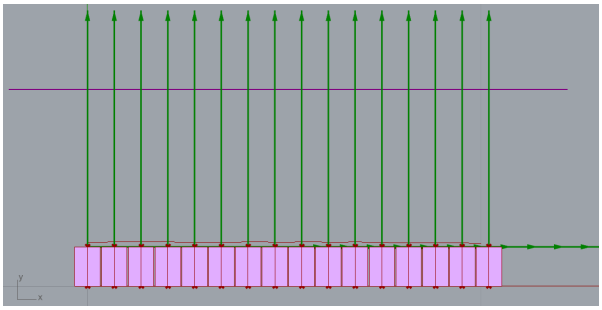

Figure 3.11: SIP panel Karamba3D model 65x65 mm beams top view.

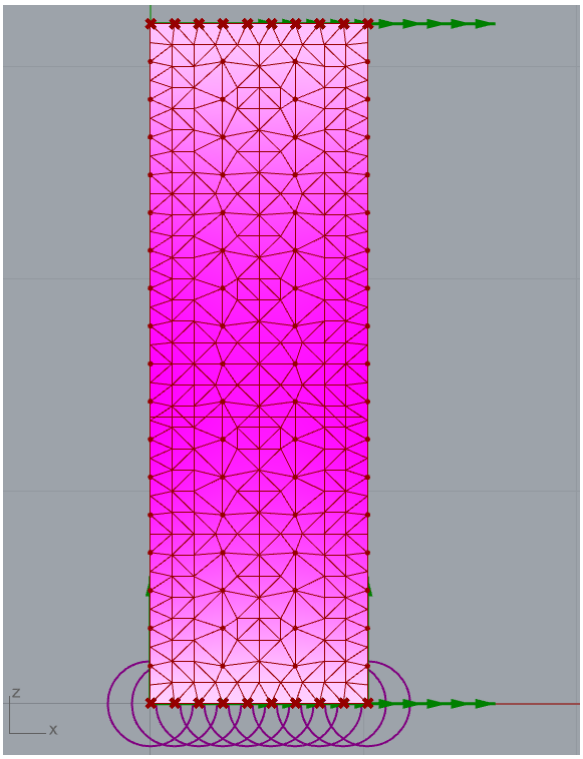

Figure 3.12: SIP panel Karamba3D model D=21 mm beams front view.

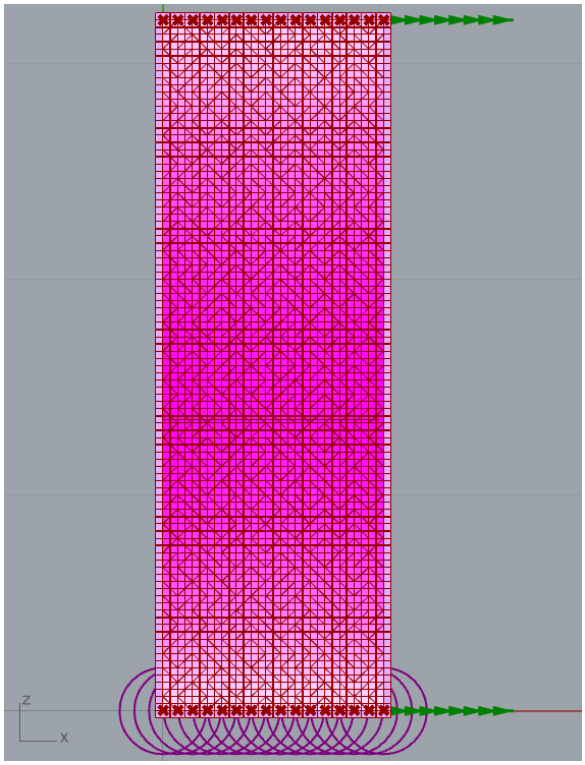

Figure 3.13: SIP panel Karamba3D model 65x65 mm beams front view.

3.2. RFEM model

The RFEM model was created (Figure 3.14) to have a verification possibility for the analytical calculations and the Karamba3D model. RFEM model is based on real material values and modelled as a layered material into one shell-element (Figure 3.16). Additionally, the experimental results are compared to the RFEM model.

A panel model for comparison with Karamba3D was modelled on RFEM. It was modelled as a layered material, while using the existing material "OSB (EN 300), OSB/2 and OSB/3 (>10-18 mm) EN 12369-1:2001-01" as faces of the sandwich panel, and the core material was defined by hand based on "MDF (EN 622-5), MDF.LA (>30 mm) EN 12369-1:2001-01" (Figure 3.15) with material properties brought out earlier in table 2.1, and the E and G moduli are brought out in table 2.2.

The panel dimensions are the same as for the Karamba model, which were based on the test rig set up seen in figure 3.1. At the bottom of the panel all translations and one rotation in the in plane direction of the panel are restricted. At the top, translations in x and y direction are restricted, but the panel can freely move in the z direction. In RFEM it is not possible to apply supports with an eccentricity in normal analysis. A panel with a rigid link between the bottom and the bottom support was modelled to try to model an eccentricity for the support, but it did not show different results due to the definition of the layered material which is one shell within which the different materials are defined. Thus, the rigid link was connecting the whole bottom of the panel, not changing the support conditions. Therefore, the rigid link modelling option was discarded.

The loads are applied with an eccentricity on the inner face and on the outer face in respect to the relevant load case analysed. The mesh size has been defined as 10 mm.

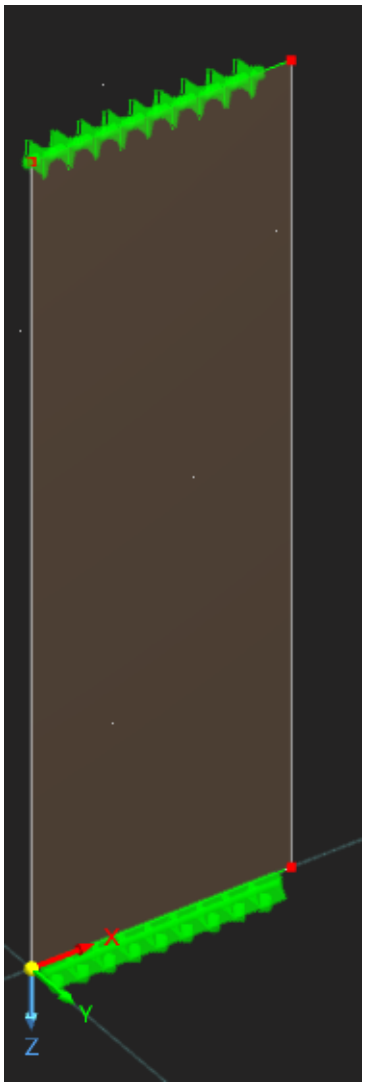

Figure 3.14: RFEM panel model.

The model will be used in the iteration process of the Karamba3D model, and to analyse the behaviour of the structural insulated panel. The same points will be addressed as for the Karamba3D model:

- Does the model represent experimental results?
- What kind of analysis is possible – SLS and ULS?
- Which kind of failure is the model able to predict?
- Can the model be used in SIPs design process?
- Can the model be used to analyse other SIP material configurations?

Further, analytical equations are presented that were used in the panel analysis and model verification processes.

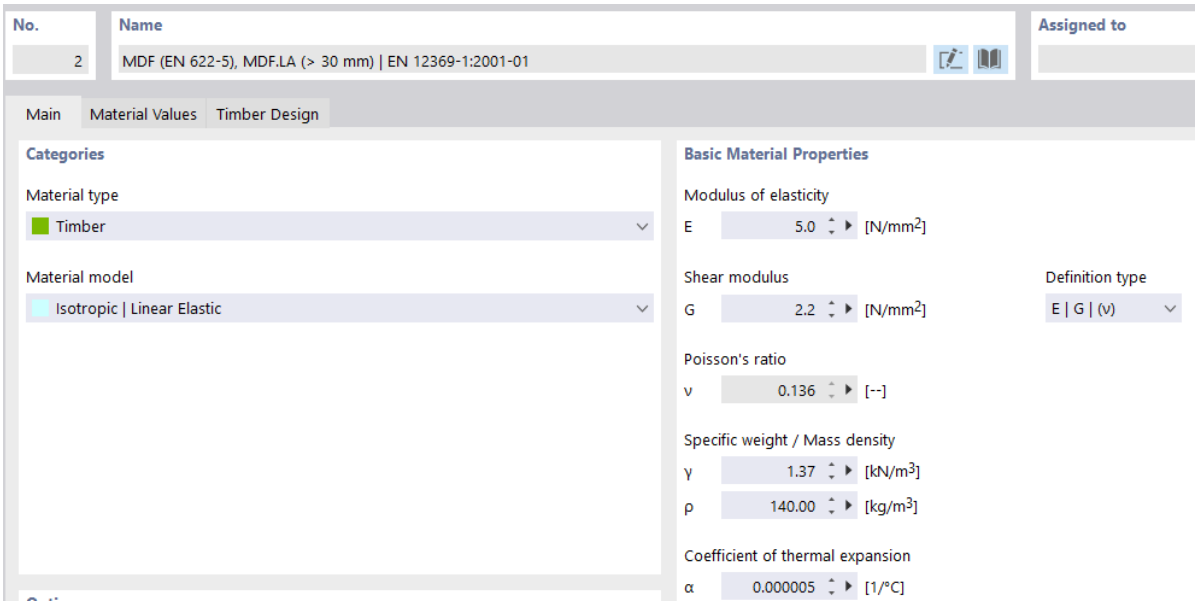

Figure 3.15: Material definition for the core.

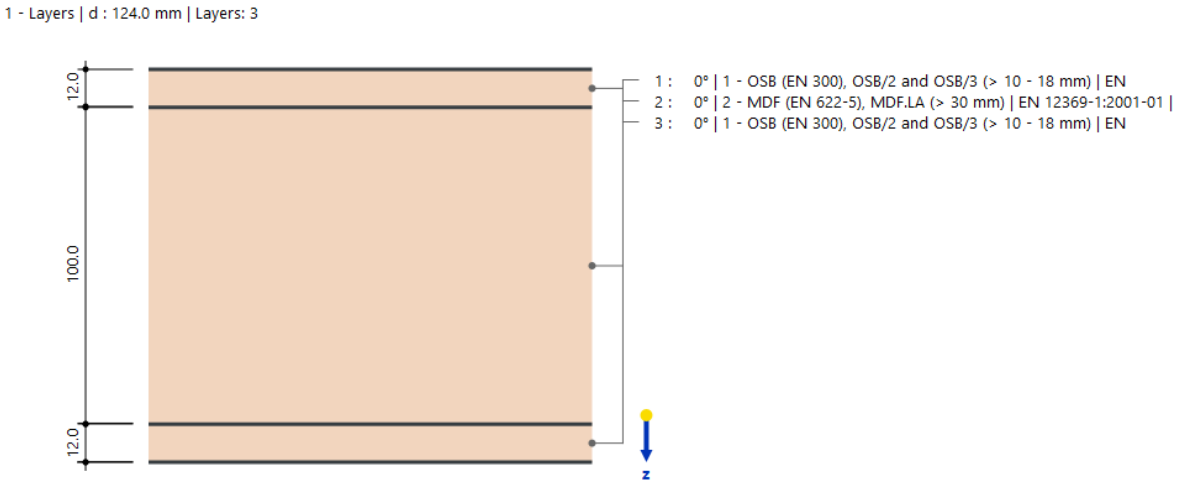

Figure 3.16: Cross section set up on RFEM.

3.3. Shear Beam equations

The shear beam equations have been used to describe the behaviour of the panel when the outer face is not supported, but an axial load has been applied to it. So, the vertical movement of the outer face of the panel since the core only transfers shear loads. This was not experimentally described since in the experiment both of the faces are supported. The equation is used to compare the Karamba3D model results where the outer face is not supported.

3.3.1. Kinematic Relations

For a shear beam, the shear angle $\gamma(x)$ is given by the derivative of the transverse displacement:

$$\gamma(x) = \frac{dw(x)}{dx} \tag{3.5}$$

3.3.2. Constitutive Relations

The shear force $V(x)$ is related to the shear strain $\gamma(x)$ by:

$$V(x) = \kappa G A_s \frac{dw(x)}{dx} \tag{3.6}$$

Where κ is the shear correction factor, G is the shear modulus, and A_s is the shear area.

3.3.3. Equilibrium Equation

The equilibrium equation for the shear force is:

$$\frac{dV(x)}{dx} + q(x) = 0 \tag{3.7}$$

3.3.4. Governing Equation

Substituting the constitutive relation into the equilibrium equation, we get the governing equation:

$$\kappa G A_s \frac{d^2 w(x)}{dx^2} + q(x) = 0 \tag{3.8}$$

3.3.5. Solution for a Cantilever Beam

For a short cantilever beam with a concentrated load F at the free end, the deflection is:

$$w(x) = \frac{-Fx}{\kappa G A_s} \tag{3.9}$$

3.4. Timoshenko Beam Theory

The Timoshenko beam theory has been used to describe the transverse loading situation on the panel. In Timoshenko beam theory, both bending and shear deformations are considered. It is used to verify the transverse behaviour of the Karamba3D model. Additionally, the axial loading was also described with these equations by applying a moment coming from the eccentric loading at the top of the panel. Below are the kinematic relations, constitutive relations, equilibrium equations, and governing equations.

3.4.1. Kinematic Relations

The total rotation of the cross-section is given by the sum of the bending rotation $\theta(x)$ and the shear strain $\gamma(x)$:

$$\phi(x) = \theta(x) + \gamma(x) \tag{3.10}$$

$$\theta(x) = -\frac{dw}{dx} \tag{3.11}$$

$$\gamma(x) = \phi(x) + \frac{dw}{dx} \tag{3.12}$$

Where:
- $w(x)$ is the transverse displacement.
- $\phi(x)$ is the total rotation of the cross-section.
- $\gamma(x)$ is the shear angle.

3.4.2. Constitutive Relations

The constitutive relations for bending and shear stress are:

- The **bending moment** $M(x)$ is related to the curvature:

$$M(x) = EI\frac{d\theta}{dx} = -EI\frac{d^2w}{dx^2} = EI\frac{d\phi}{dx} \tag{3.13}$$

- The **shear force** $V(x)$ is related to the shear strain through the shear modulus G, shear area A_s, and shear correction factor κ:

$$V(x) = \kappa GA_s\gamma(x) = GA_s(\phi(x) + \frac{dw}{dx}) \tag{3.14}$$

Where:
- E is the modulus of elasticity.
- I is the second moment of area.
- κ is the shear correction factor, which in the case of this specific material will be 1.0 since the distribution of the shear stresses is uniform over the cross section.
- G is the shear modulus.

3.4.3. Equilibrium Equations

The equilibrium equations are:

- **Force equilibrium**:

$$V(x) = \frac{dM(x)}{dx} \tag{3.15}$$

- **Moment equilibrium**:

$$\frac{dV(x)}{dx} = q(x) \tag{3.16}$$

Where $q(x)$ is the distributed load.

3.4.4. Governing Equations

The governing equations are derived from combining kinematic relations, constitutive relations, and equilibrium equations:

- **Bending equation**:

$$EI\frac{d^2\phi}{dx^2} = V(x) \tag{3.17}$$

- **Shear equation**:

$$\kappa GA_s\left(\frac{d^2w}{dx^2} + \frac{d\phi}{dx}\right) = -q(x) \tag{3.18}$$

3.4.5. General Solution for Simply Supported Beam with Uniform Distributed Load q

For a simply supported beam of length H, subjected to a uniform distributed load q, the general solution for deflection, shear force, moment, and rotation is:

- **Deflection** $w(x)$**:**

$$w(x) = \frac{qx^4}{24EI} - \frac{qx^3H}{12EI} - \frac{qx^2}{2GA_c} + \frac{qxH}{2GA_c} + \frac{qxH^3}{24EI} \tag{3.19}$$

- **Shear Force** $V(x)$**:**

$$V(x) = q * \left(\frac{H}{2} - x\right) \tag{3.20}$$

- **Moment** $M(x)$**:**

$$M(x) = \frac{q * x}{2} * (H - x) \tag{3.21}$$

- **Rotation** $\phi(x)$**:**

$$\phi(x) = -\frac{qx^3}{6EI} + \frac{qx^2H}{4EI} + \frac{qH}{2GA_c} - \frac{qH}{2GA_c} - \frac{qH^3}{24EI} \tag{3.22}$$

3.5. Rod in compression

Rod in compression equations are used to describe the vertical compression of the panel under axial loads. This will provide a comparison point for the model results.

3.5.1. Kinematic Relation

The strain $\epsilon(x)$ in the rod is given by the derivative of the axial displacement $u(x)$:

$$\epsilon(x) = \frac{du(x)}{dx} \tag{3.23}$$

3.5.2. Constitutive Relation

For a linearly elastic material, the stress $\sigma(x)$ is related to the strain $\epsilon(x)$ through Young's modulus E:

$$\sigma(x) = E \cdot \epsilon(x) = E\frac{du(x)}{dx} \tag{3.24}$$

3.5.3. Equilibrium Equation

The axial force $N(x)$ in the rod is given by the stress $\sigma(x)$ multiplied by the cross-sectional area A:

$$N(x) = \sigma(x) \cdot A = EA\frac{du(x)}{dx} \tag{3.25}$$

In the absence of distributed forces, the equilibrium equation is:

$$\frac{dN(x)}{dx} = 0 \tag{3.26}$$

This implies that the axial force $N(x)$ is constant:

$$N(x) = F \tag{3.27}$$

3.5.4. Governing Equation

From the equilibrium equation and the constitutive relation, the governing equation for the displacement $u(x)$ is:

$$EA\frac{du(x)}{dx} = F \tag{3.28}$$

or

$$\frac{du(x)}{dx} = \frac{F}{EA} \tag{3.29}$$

Integrating this:

$$u(x) = \frac{F}{EA}x + C_1 \tag{3.30}$$

3.5.5. Boundary Conditions and Solution

For a column with a concentrated force F at the top and supported at the bottom:
- At $x = 0$ (the bottom), the displacement is zero: $u(0) = 0$.
- Therefore, $C_1 = 0$, and the displacement becomes:

$$u(x) = \frac{F}{EA}x \tag{3.31}$$

The displacement at the top of the column (at $x = L$) is:

$$u(L) = \frac{FL}{EA} \tag{3.32}$$

All of the previously seen equations will be used in the verification of the models and the analysis of the panel behaviour. Next, an overview of the experiment will be given.

3.6. Experiments by Kingspan Unidek

Five experiments were conducted at Kingspan Unidek, where the panel was tested under axial eccentric loads for multiple load combinations. The tests and the measurements were performed by Kingspan Unidek, but the post-processing and analysis has been carried out within this thesis.

The first test results will be addressed in detail, and the following test results will be provided in Appendix F. The test rig was set up at Kingspan Unidek (Gemert) to measure the horizontal deflections and local strains of the structural insulated panel. The test rig set up can be seen in figure 3.1. The panel was supported at the bottom and top by simple supports (seen in Figures 3.19, and 3.18) with the assumption that the inner face will take most of the loading, and the outer face will only be supporting the inner face. At the top of the panel the two faces were connected by a beam for the final (5th) test, which was unconnected for the previous four

Height	L	3200	mm
Width	W	1020	mm
Thickness	t	124	mm
Core thickness	t_c	100	mm
Face thickness	t_f	12	mm

tests. The top is also able to deflect in the vertical direction. The panel measurements are the following:

The measurements for local strains were taken in the middle of the panel at L = 1600 mm from the inner and outer faces left and right sides seen in figure 3.17 in the middle. For horizontal deflections, the measurements were taken at the following locations with respect to the panel height also from the inside face and the outside face at the following locations (seen in figure 3.17 on the left):

$$L_1 = 800 \text{ mm}$$
$$L_2 = 1600 \text{ mm}$$
$$L_3 = 2400 \text{ mm}$$

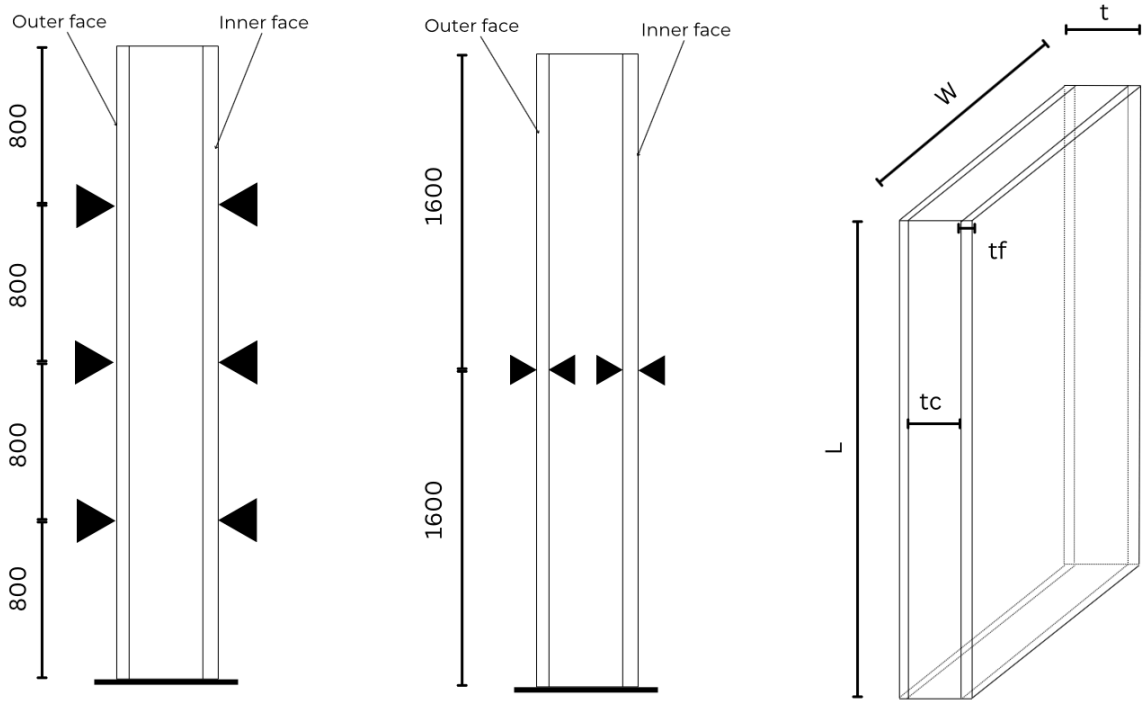

Figure 3.17: a) Horisontal deflection measurements locations; b) Local strains measurements locations; c) Panel sketch.

The deflection results were then interpolated with the thin plate spline radial basis function to get approximate deflection lines over the whole height of the panel. The radial basis function $\phi(r)$ for the thin plate spline is given by:

$$\phi(r) = r^2 \log(r) \tag{3.33}$$

Figure 3.18: Test rig bottom support.

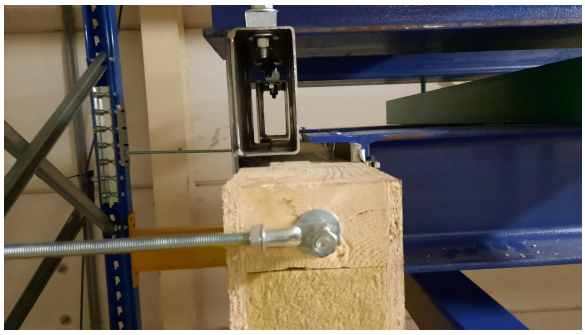

Figure 3.19: Test rig top support.

where $r = \sqrt{(x - x_i)^2 + (y - y_i)^2}$ is the Euclidean distance between the point (x, y) and each interpolation point (x_i, y_i). The function is visualised in Figure 3.20.

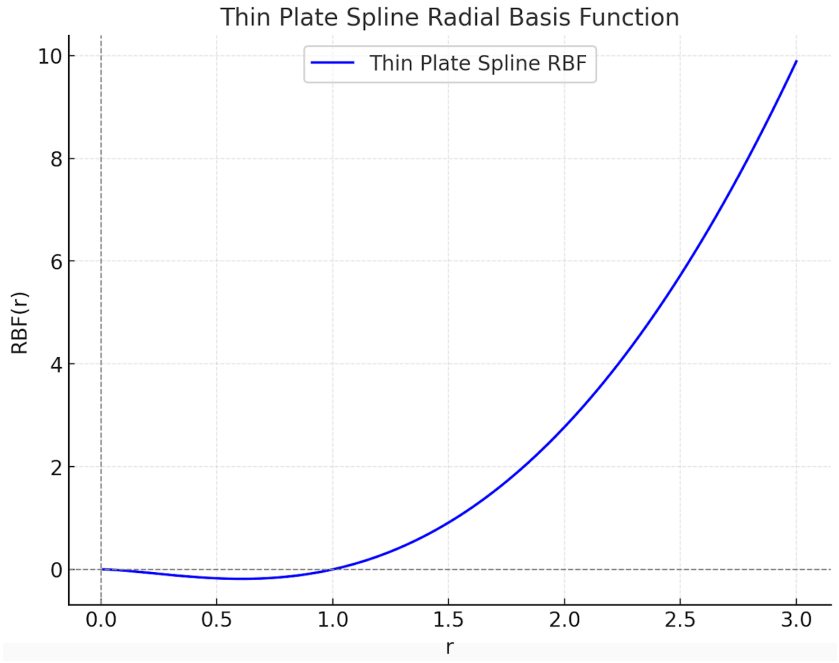

Figure 3.20: Radial basis function of thin plate spline.

The test rig is set up so that the lower row of weights loads the inner face of the panel, and the higher row of weights loads the outer skin. This is best seen in figure 3.21 where 12 kN is on the inner face and 6 kN on the outer face with two weights on the inner face and one weight on the outer face, and also on the schema in figure 3.1. The loads are applied as two point loads for the inner face and for the outer face for the test rig, however a simplification of line loads is assumed while modelling the test on Karamba3D and RFEM.

All five tests had a different loading order which is seen in Figures 3.22, and 3.23 and were as follows:

1. Test 1

    1.1. 6 kN in

1.2. 12 kN in
1.3. 18 kN in
1.4. 12 kN in
1.5. 12 kN in, 6 kN out
1.6. 12 kN in
1.7. 6 kN in

2. Test 2
   2.1. 6 kN in
   2.2. 6 kN in, 6 kN out
   2.3. 6 kN out

3. Test 3
   3.1. 6 kN in
   3.2. 6 kN in, 6 kN out
   3.3. 6 kN in, 12 kN out
   3.4. 6 kN in, 6 kN out
   3.5. 12 kN in, 6 kN out
   3.6. 6 kN in, 6 kN out
   3.7. 6 kN out

4. Test 4
   4.1. 6 kN in
   4.2. 6 kN in, 6 kN out
   4.3. 12 kN in, 6 kN out
   4.4. 12 kN in
   4.5. 6 kN in

5. Test 5
   5.1. 6 kN in
   5.2. 6 kN out
   5.3. 6 kN in, 6 kN out
   5.4. 12 kN in, 6 kN out

Figure 3.21: Test rig set up - load case 3 – 12 kN on the inner face, 6 kN on the outer face.

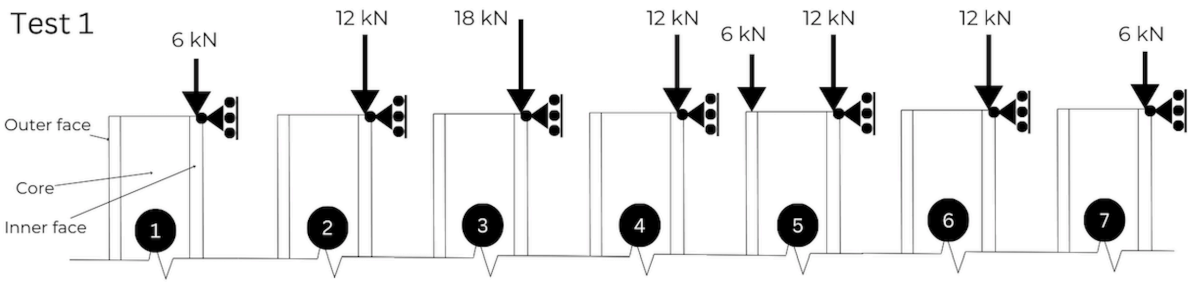

Figure 3.22: Tests loading order.

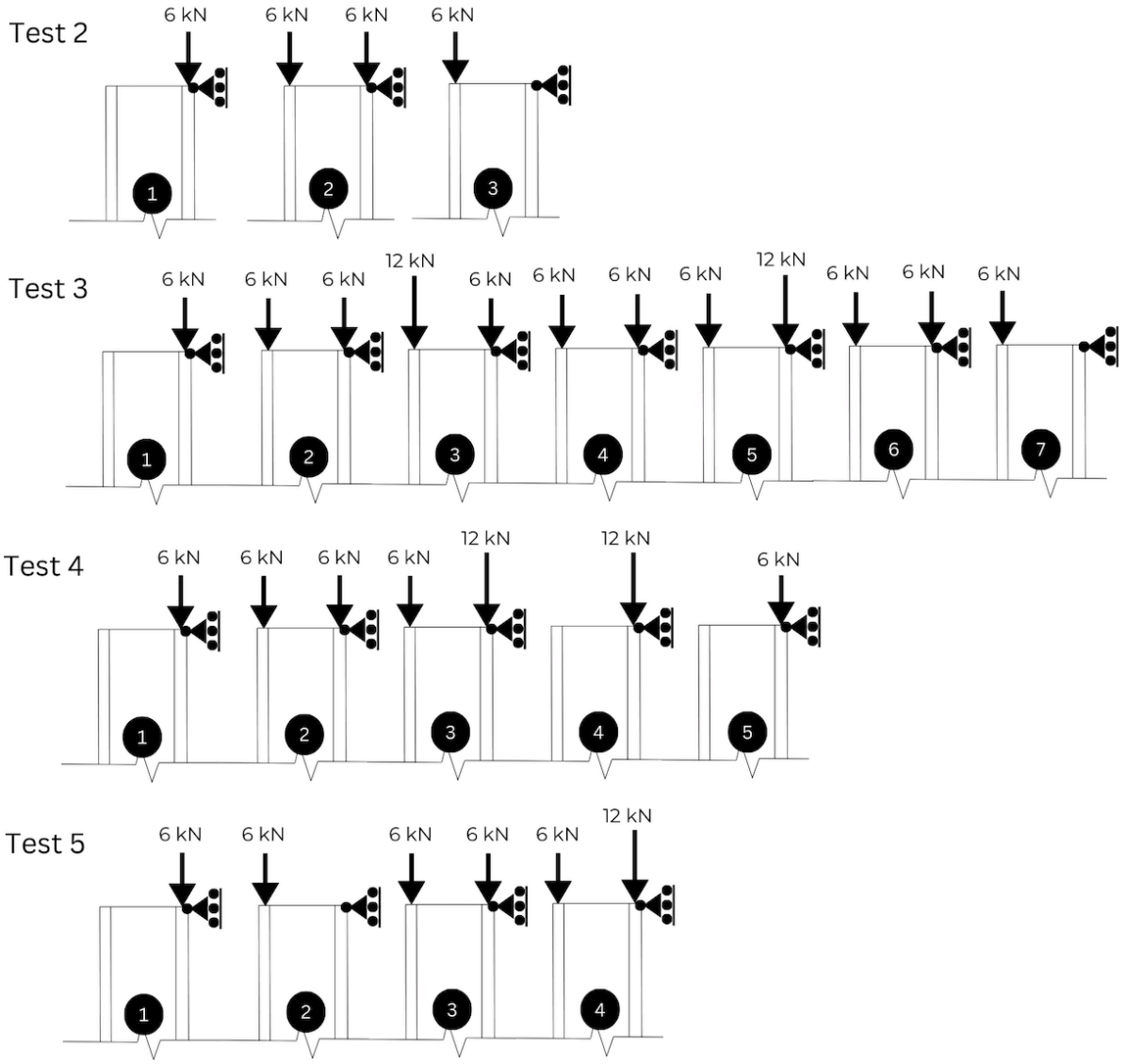

Figure 3.23: Tests loading order.

4

Structural Insulated Panel Analysis

This chapter gives an overview of the bio-based structural insulated panel with OSB/3 boards as faces and the Steico medium density fibre board as the core of the panel while presenting analytical, experimental and modelling results. The initial dimensions are based on a test rig set up in Kingspan Unidek to compare the experimental results with the models. The chapter starts with initial information, next hand calculations from sandwich panel theory will follow which show all the failure stresses. Then, an overview of the Karamba3D and RFEM model findings will be presented, and finally a comparison between the experimental, analytical and numerical results is performed.

4.1. Initial information

The panel calculation sketch is seen in figure 4.1 and 4.2. The panel information is presented in table 4.1.

Table 4.1: Panel information based on test rig set up.

Initial information			
Thickness of the core	t_c	100	*mm*
Thickness of one face	t_f	12	*mm*
Center to center distance (of the faces)	d	112	*mm*
Width of the panel	b	1020	*mm*
Thickness of the panel	t	124	*mm*
Height of the panel	H	3200	*mm*
Eccentricity of forces applied	e	56	*mm*
Force on the inner face	q1	6,12,18	*kN/m*
Force on the outer face	q2	6	*kN/m*

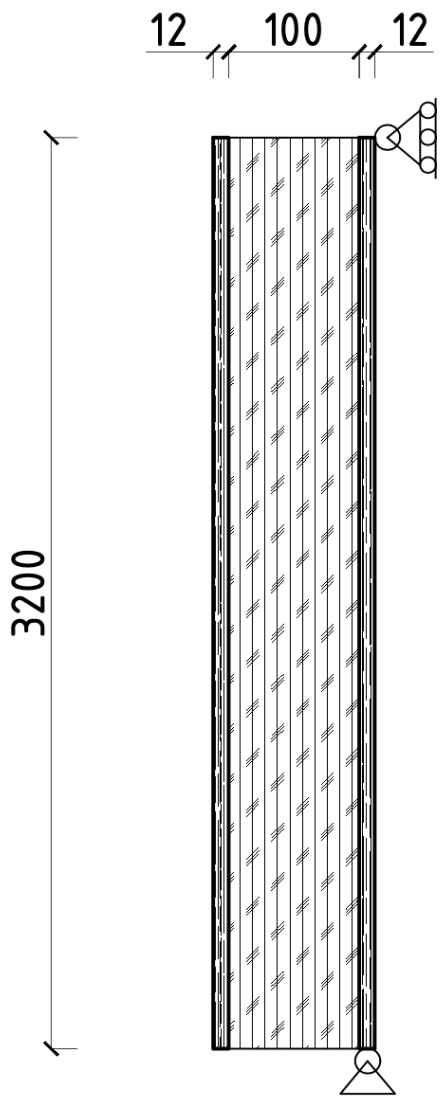

Figure 4.1: Panel sketch side view.

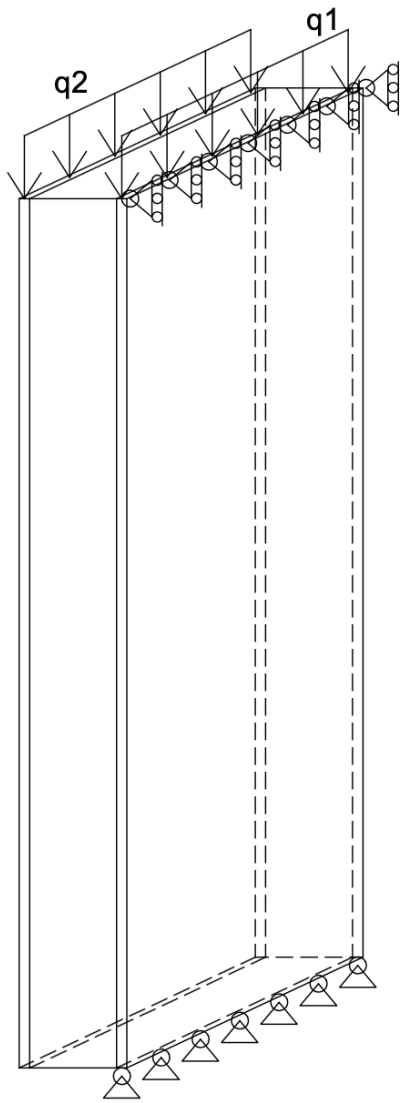

Figure 4.2: Panel sketch isometric.

Linear elastic analysis is performed. The experimental results will be compared to characteristic material values. The failure loads will be evaluated with characteristic values for the material to account for any deviations in the material. Design loads will be found with the help of safety factors, kmod values which account for the load duration, moisture exposure, and the type of material used. The material safety factor from Eurocode NEN-EN 1995-1-1 for medium density fibre board is: $\gamma_M = 1.3$, and the k_{mod} values for MDF are the following:

Table 4.2: MDF (Steico) k_{mod} values for service class 1 (NEN-EN 1995-1-1 table 5.3).

k_{mod} **of medium density fibre board**						
Load duration class		permanent	long	medium	short	instantaneous
Service class	1	0.2	0.4	0.6	0.8	1.1

The material safety factor from Eurocode NEN-EN 1995-1-1 for OSB/3 is: $\gamma_M = 1.2$, and the k_{mod} values for OSB/3 are the following:

Table 4.3: OSB k_{mod} values (NEN-EN 1995-1-1 table 5.3).

k_{mod} **of OSB/3**						
Load duration class		permanent	long	medium	short	instantaneous
Service class	1	0.4	0.5	0.7	0.9	1.1
	2	0.3	0.4	0.55	0.7	0.9

The design resistance values are calculated with the following equations:

$$f_{c,d} = \frac{f_{c,k}}{\gamma_M} k_{mod} \tag{4.1}$$

$$f_{t,d} = \frac{f_{t,k}}{\gamma_M} k_{mod} \tag{4.2}$$

The resistance values for the Steico medium density fibre board for different load durations are presented in table 4.4.

Table 4.4: MDF strength properties based on load duration.

MDF board strength properties based on load duration (eq. 4.1 and 4.2)							
			permanent	long	medium	short	instantaneous
Compression strength at 10% def.	$f_{c,d}$	MPa	0.015	0.031	0.046	0.062	0.085
Tensile strength perpendicular to plane	$f_{t,d}$	MPa	0.0031	0.0062	0.0092	0.49	0.017
Shear strength	$f_{v,d}$	MPa	0.0062	0.012	0.018	0.025	0.034

The design strength properties of the OSB/3 boards are presented in table 4.5. Service class 1 and 2 values are brought out, because for a more precise design, the inner face is in service class 1, because it is in indoor conditions, and the outer face is in service class 2, because it is outside, and exposed to more moisture and temperature variances. The calculated design resistances are important for design situation analysis.

Table 4.5: OSB/3 strength properties based on load duration.

OSB board strength properties based on load duration service class 1 (eq. 4.1 and 4.2)							
			permanent	long	medium	short	instantaneous
Compression resistance perp. to plane	$f_{c90,d}$	MPa	3.33	4.17	5.83	7.50	9.17
Compression resistance in plane	$f_{c,d}$	MPa	5.13	6.42	8.98	11.55	14.21
Tensile resistance in plane	$f_{t,d}$	MPa	3.13	3.92	5.48	7.05	8.62
Shear resistance	$f_{v,d}$	MPa	2.27	2.83	3.97	5.1	6.23
Bending resistance	$f_{m,d}$	MPa	5.47	6.83	9.57	12.3	15.03
OSB board strength properties based on load duration service class 2 (eq. 4.1 and 4.2)							
			permanent	long	medium	short	instantaneous
Compression resistance perp. to plane	$f_{c90,d}$	MPa	2.50	3.33	4.58	5.83	7.50
Compression resistance in plane	$f_{c,d}$	MPa	3.85	5.13	7.06	8.98	11.55
Tensile resistance in plane	$f_{t,d}$	MPa	2.35	3.13	4.31	5.48	7.05
Shear resistance	$f_{v,d}$	MPa	1.7	2.27	3.12	3.97	5.1
Bending resistance	$f_{m,d}$	MPa	4.10	5.47	7.52	9.57	12.30

4.2. Hand calculations

In this chapter, the failure methods are all calculated, based on the panel information in table 4.1 to evaluate which failure method could be governing.

Bending stiffness

$$D = \frac{3800 * 1020 * 12^3}{6} + \frac{3800 * 1020 * 12 * 112^2}{2} + \frac{5 * 1020 * 100^3}{12} = \\ = (1.116 + 291.72 + 0.425) * 10^9 Nmm^2 = 293.26 kNm^2 \tag{4.3}$$

Critical load for **compression in the faces**

$$F_{c,cr} = f_{c90,k} * A_f = 15.4 * 12 * 1020 = 188.50 kN \tag{4.4}$$

Critical load for **tension in the faces**

$$F_{t,cr} = f_{t90,k} * A_f = 9.4 * 12 * 1020 = 115.06 kN \tag{4.5}$$

Shear stress of the panel, load application perpendicular to plane (transverse loading case)

$$\tau = \frac{V(\sum E_i S_i)_{max}}{(\sum E_i S_i) B} = \frac{V(\frac{E_F t e}{2} + \frac{E_C d_C^2}{8})}{(\frac{E_F t e^2}{2} + \frac{E_C d_C^3}{12}) B} \approx \frac{V}{eB} \tag{4.6}$$

where $d_C \approx e$

The critical shear force [33]:

$$V_{cr} = eBf_{v,k} = 56 * 1020 * 0.04 = 2.28kN \tag{4.7}$$

The critical q load on the panel would be

$$q_{cr} = \frac{2V_{cr}}{H} = \frac{2 * 2.28}{3.2} = 1.43kN/m \tag{4.8}$$

Shear stress of the panel, load application in-plane (axial loading)

$$\tau_{cr} = \frac{F}{A_c} \Rightarrow F_{cr} = \tau_{cr} * A_c = 0.04 * 1020 * 3200 = 130.56kN \tag{4.9}$$

Maximum shear angle for the core based on the characteristic shear strength of the core material:

$$\tau_{cr} = G_c\phi_{cr} \Rightarrow \phi_{cr} = \frac{\tau_{cr}}{G_c} = \frac{0.04}{2.2} = 0.018 \tag{4.10}$$

The shear angle of the core material will be one of the governing design criteria in the case of this panel.

Face wrinkling for anti-symmetric wrinkling

$$\sigma_{f,cr} = 0.51\sqrt[3]{E_f E_c G_c} + 0.33 G_c (t_c/t_f) = 0.51\sqrt[3]{3800 * 5 * 2.2} + 0.33 * 2.2 * (100/12) = 23.75N/mm^2 \tag{4.11}$$

Hence, the critical force for that to occur would be

$$F_{f,cr} = \sigma_{f,cr} * A = 23.75 * 1020 * 12 = 290.695 * 10^3 N = 290.70kN \tag{4.12}$$

Therefore, face wrinkling is not a governing design criteria for this panel.

Buckling
Euler critical load for axially loaded elements [38]:

$$F_{cr,Euler} = \frac{\pi^2 EI}{L^2} \tag{4.13}$$

$$F_{cr,core} = \frac{\pi^2 * 5 * 1020 * 100^3/12}{3200^2} = 410N \tag{4.14}$$

$$F_{cr,face} = \frac{\pi^2 * 3800 * 1020 * 12^3/12}{3200^2} = 538N \tag{4.15}$$

Euler critical buckling load for panels with thin skins [41]:

$$F_{cr,thin} = \frac{F_E}{1 + \frac{F_E}{F_C}} = \frac{282.7 * 10^3}{1 + \frac{282.7 * 10^3}{224.4 * 10^3}} = 125.09kN \tag{4.16}$$

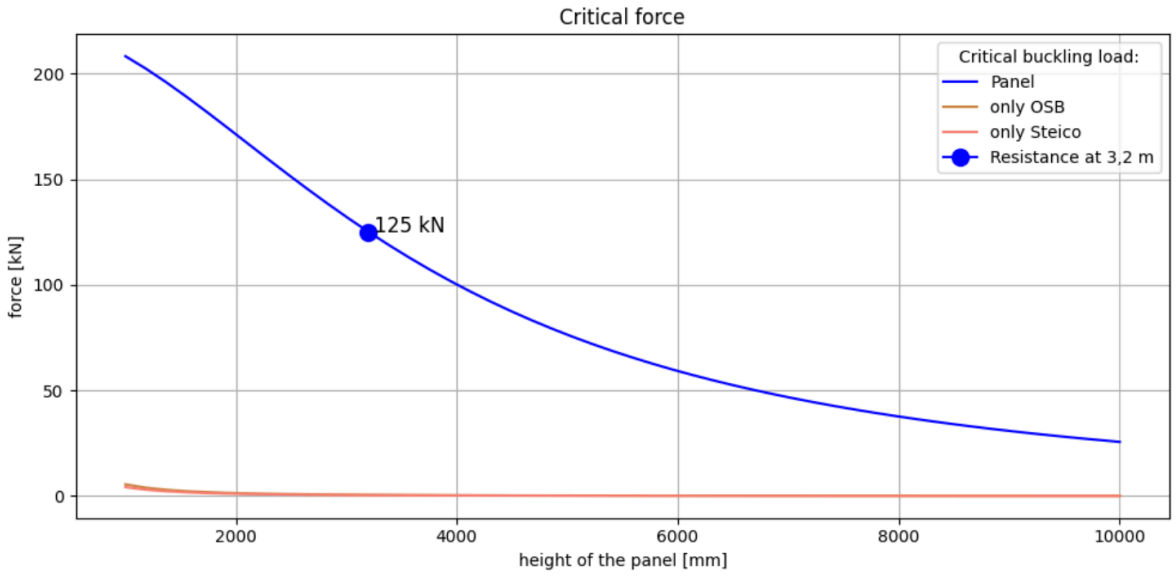

Figure 4.3: Buckling of the panel, and the materials

F_E is the panel critical load without the shear reduction:

$$F_E = \frac{\pi^2 D}{H^2} = \frac{\pi^2 * 293.26 * 10^9}{3200^2} = 282.7 * 10^3 N \tag{4.17}$$

F_C is the shear critical load:

$$F_C = A_C G_C = 100 * 1020 * 2.2 = 224.4 * 10^3 N \tag{4.18}$$

Shear crimping

$$\sigma_f = \frac{S}{2t_f} = \frac{4730.1 * 10^6}{2 * 12} = 197086392 N/mm^2 \tag{4.19}$$

S :

$$S = \frac{2D}{t} = \frac{2 * 293.26 * 10^9}{124} = 4730.1 * 10^6 Nmm \tag{4.20}$$

The critical stress for shear crimping to happen is very high, so it is not a governing criteria for design.

The governing design factors are global buckling, transverse shear failure of the core, and assuming the tensile forces do not get as high as would be critical then tensile failure is unlikely to occur. Global buckling equation does not take eccentricity of the load application into account, thus the critical global buckling load may be even lower. The failure loads have been concluded in Table 4.6.

Table 4.6: Panel failure loads.

Failure method	Failure load	
Face compression	188.50	kN
Face tension	115.06	kN
Core shear transverse	1.43	kN/m
Core shear axial	130.56	kN
Face wrinkling	290.70	kN
Global buckling	125.09	kN

4.3. Analytical results

In order to describe the transverse loading situation Timoshenko beam equations were used. Timoshenko beam equations predicted failure under 2.5 kN/m with the limit criteria of 0.018 shear angle according to equation 3.22. This can be seen in Appendix C.

The serviceability limit state was reached with 2.0 kN/m where the L/150=21.3 mm deflection was reached according to equation 3.19.

Shear beam equations were used to describe the core shear failure under axial loads which occurred at 129.5 kN on the outer face when 0.018 shear angle was reached according to equation 3.9. Maple output has been brought out in Appendix B.

The rod in compression equations were used to describe the vertical displacement of the panel under axial loads. The global buckling failure load 125.09 kN compressed the panel vertically 4.4 mm according to equation 3.31. This can be seen in Appendix E.

4.4. Experiment Results

The experiment performed at Kingspan Unidek consisted of 5 tests. The first test will be addressed in detail within this chapter but the remaining results will be brought out in Appendix F.The loading for test 1 was performed in the following order also seen in Figure 4.4:

1. 1 weight on the inner face - 6 kN
2. 2 weights on the inner face - 12 kN
3. 3 weights on the inner face - 18 kN
4. 2 weights on the inner face - 12 kN
5. 2 weights on the inner face and 1 on the outer face - 12 kN + 6 kN
6. 2 weights on the inner face - 12 kN
7. 1 weight on the inner face - 6 kN

The whole test duration was 13 minutes. The results are presented in the order of appearance, but the same load combinations are presented in the same graphs with the first time that this load appeared.

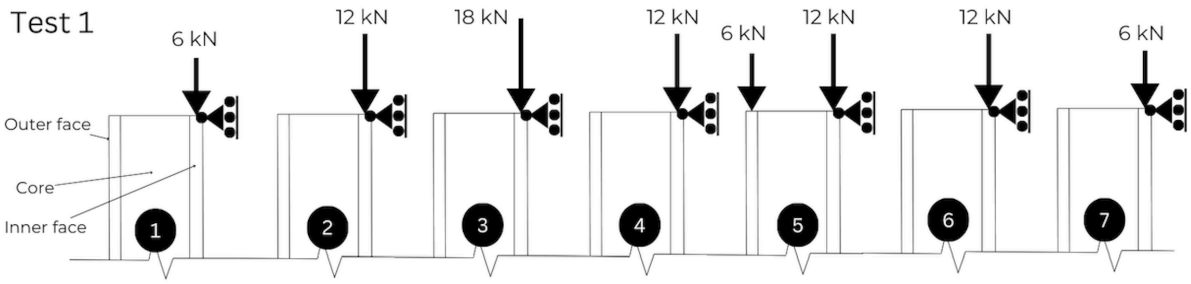

Figure 4.4: Loading order of test 1 (also seen in Figure 3.22.

In figure 4.5 the deflections of the inner and outer faces are presented when the inner face is loaded with 6 kN. The beginning (blue) lines represent when the weights are first applied, and the red lines represent the moment where all additional weights were removed. These deflection results should be of the same magnitude, but a 73% increase is seen. This also applies to measured local strain results seen in Figure 4.6 where an increase of 36% is shown.

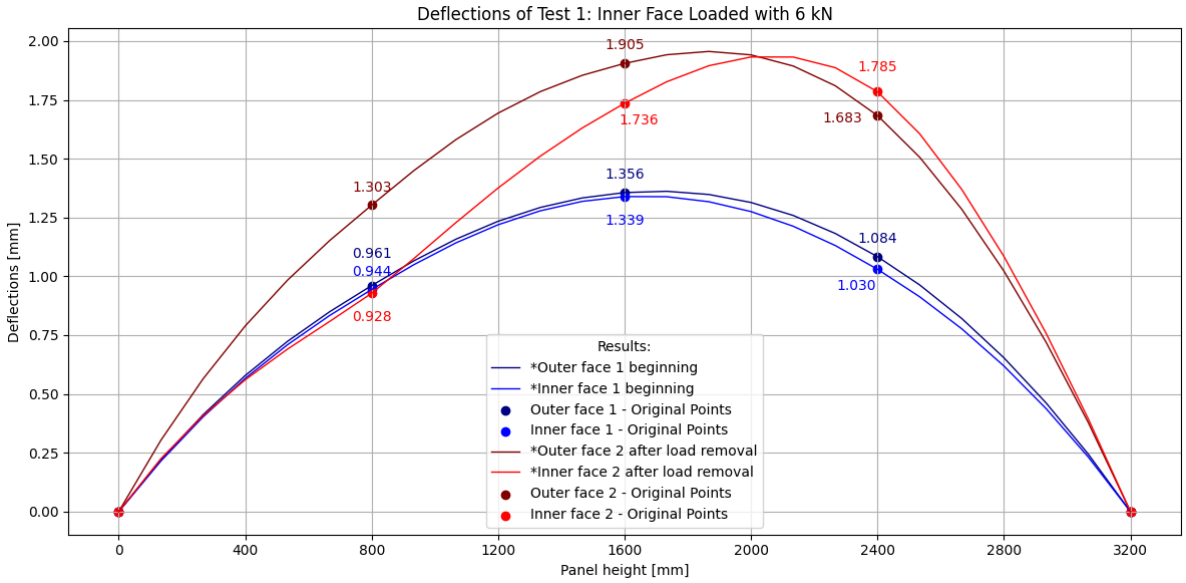

Figure 4.5: Deflections of Test 1 inner face loaded with 6 kN.

After loading the inner face with 6 kN, another weight was added, so the inner face was loaded with 12 kN. This loading case was measured three times which can be seen in Figure 4.7. The beginning inner and outer face deflections already start to show some discrepancies between each other (blue lines) – outer face has bigger deflections than the inner face. However, measurements two (red lines) and three (green lines) show a big difference between the inner and outer face behaviour. This suggests that after the first loading of 12 kN on the inner face, the panel went through a change. Presumably in the core or the interface, since the faces do not deform parallelly anymore, nor do they have the same deformed shape to further confirm separate behaviour. This can be seen for the previous loading case, where similar behaviour occurs, that the upper part of the panel core is under compression and the lower part of the panel core is under tension coming from the faces' behaviour. The increase of strains can be seen in Figure 4.8 where the final loading (green line) of 12 kN shows the biggest strains eventhough the same load is applied. The increase in strains is 26% whereas the increase in deflections is 16%.

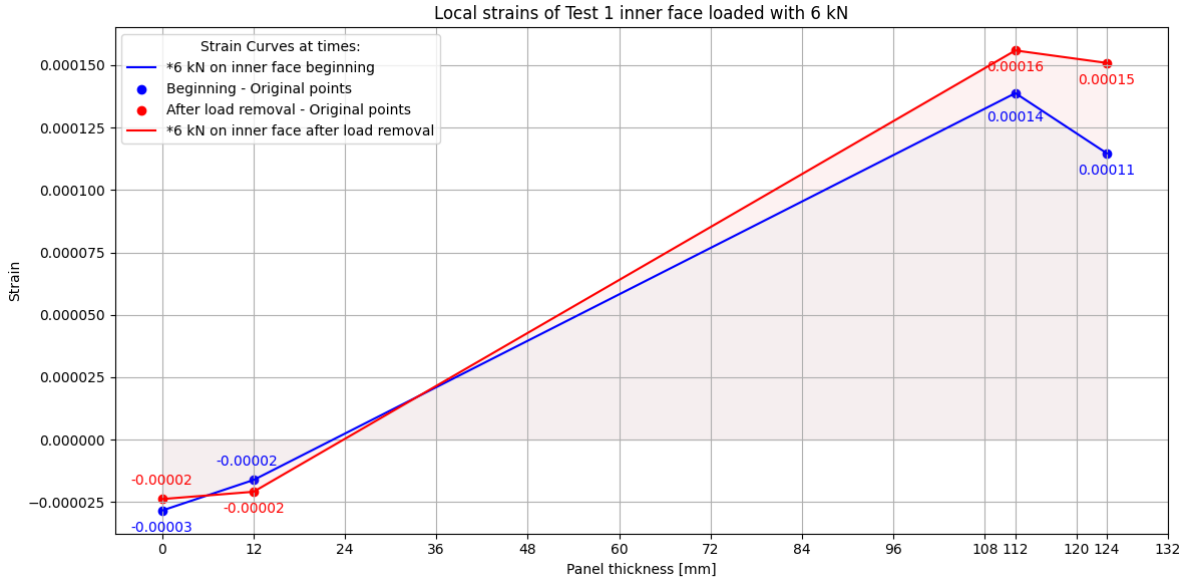

Figure 4.6: Strains of Test 1 inner face loaded with 6 kN.

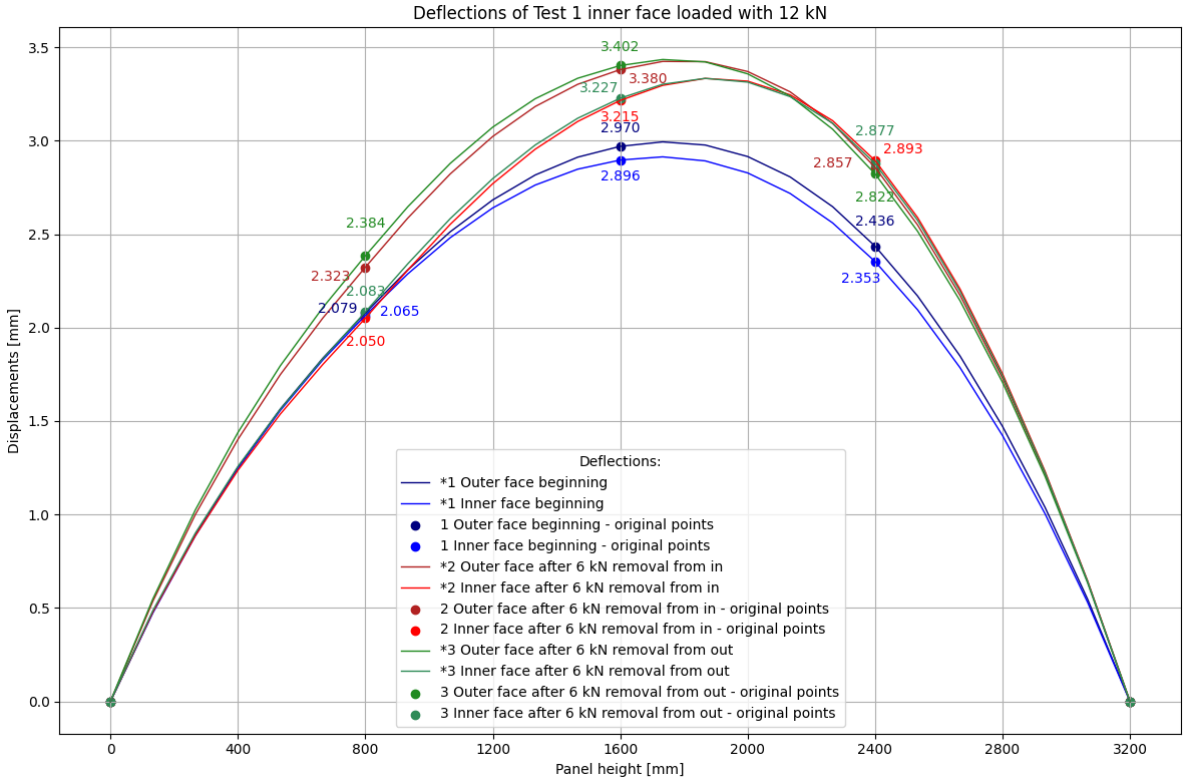

Figure 4.7: Deflections of Test 1 inner face loaded with 12 kN.

The third loading case was 18 kN on the inner face as seen in Figure 4.9. The deflected shape has a stronger deflection concentration slightly towards the top of the panel. This could signify some local damage in the faces since the loads applied are small. The strains can be seen in Figure 4.10. This is most likely the loading situation where the possible damage occurred, since after this the faces started to behave separately.

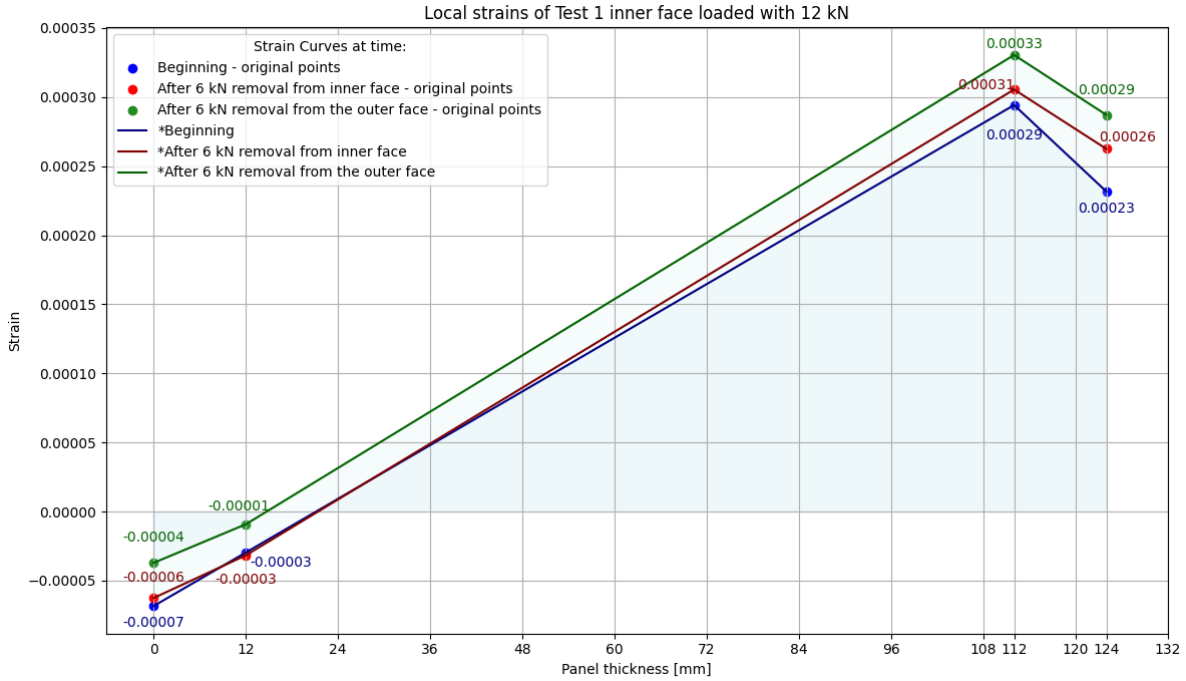

Figure 4.8: Strains of Test 1 inner face loaded with 12 kN.

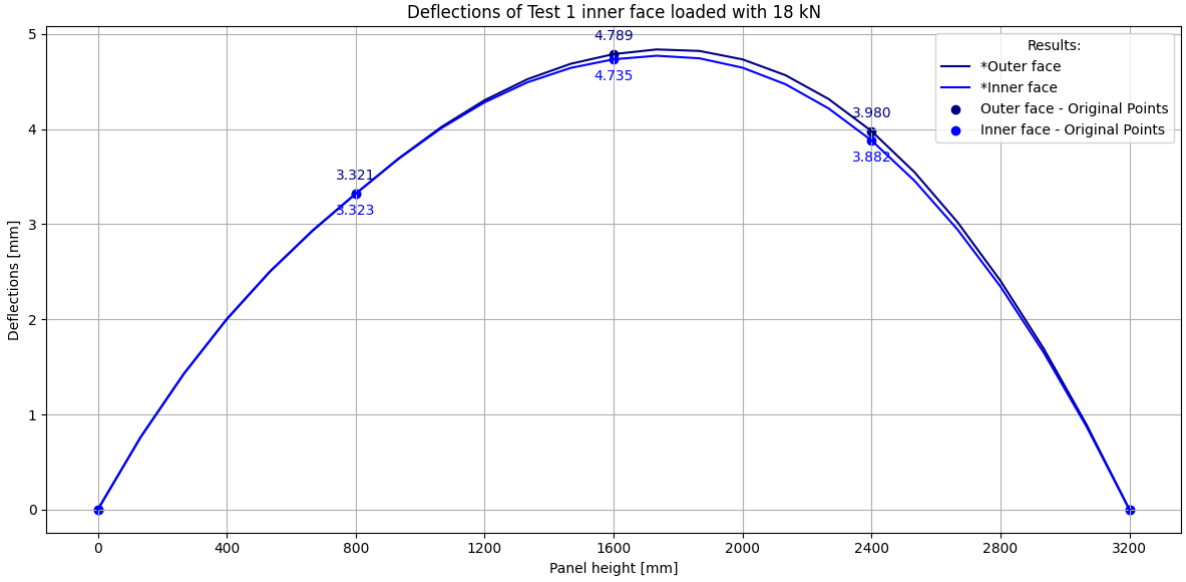

Figure 4.9: Deflections of Test 1 inner face loaded with 18 kN.

Loading 5, where 12 kN were applied on the inner face and 6 kN on the outer face shows a clear difference in the two faces' deflections seen in Figure 4.11. Thus, a change or a possible failure in the core or interface may have happened or the core might be unable to support the faces of the panel to behave as a fully composite material. Alternatively, it could be related to the face/core interface bonding percentage. The core is in compression at 2400 mm and in tension at 800 mm. The strains can be seen in Figure 4.12 where a linear distribution should be seen where the inner face is in compression and outer face in tension, but instead there is bending in the outer face and compression in the inner face. There is no linear behaviour in

the strains in any of the measurements, suggesting a lack of composite action already in the beginning.

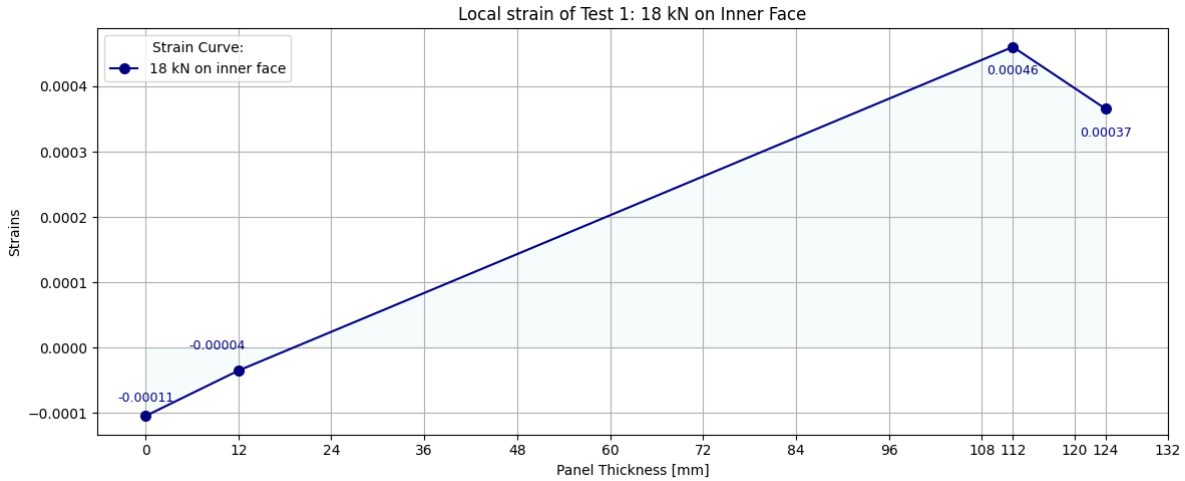

Figure 4.10: Strains of Test 1 inner face loaded with 18 kN.

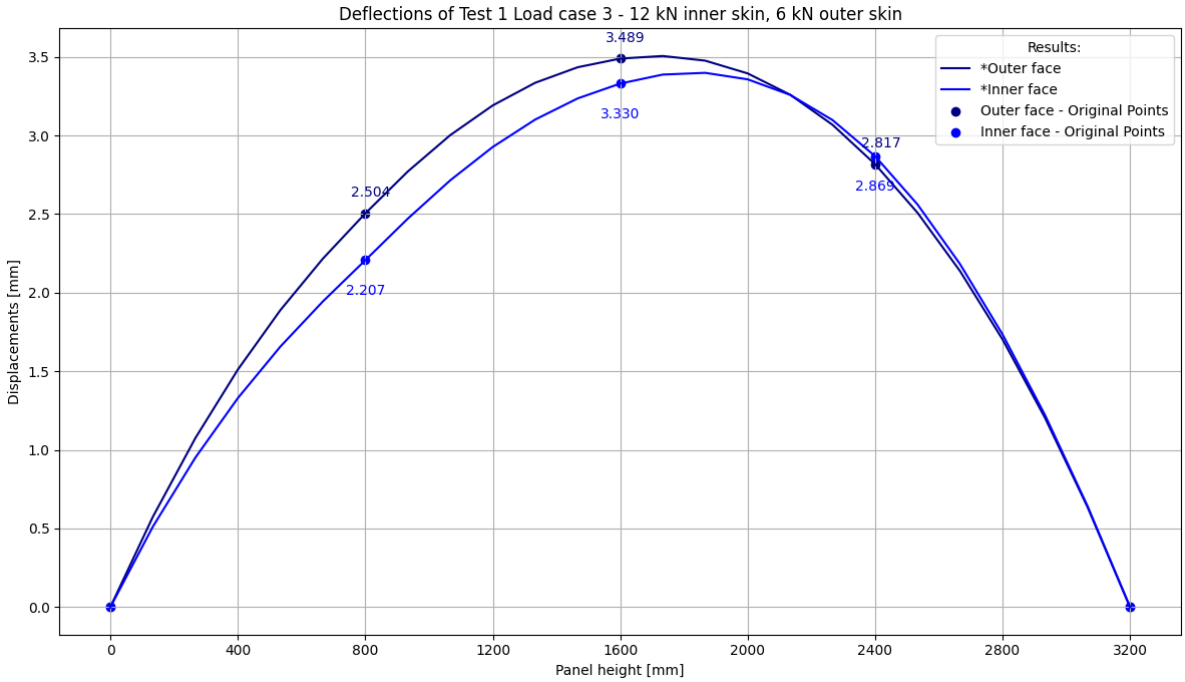

Figure 4.11: Deflections of Test 1 inner face loaded with 12 kN and outer face loaded with 6 kN.

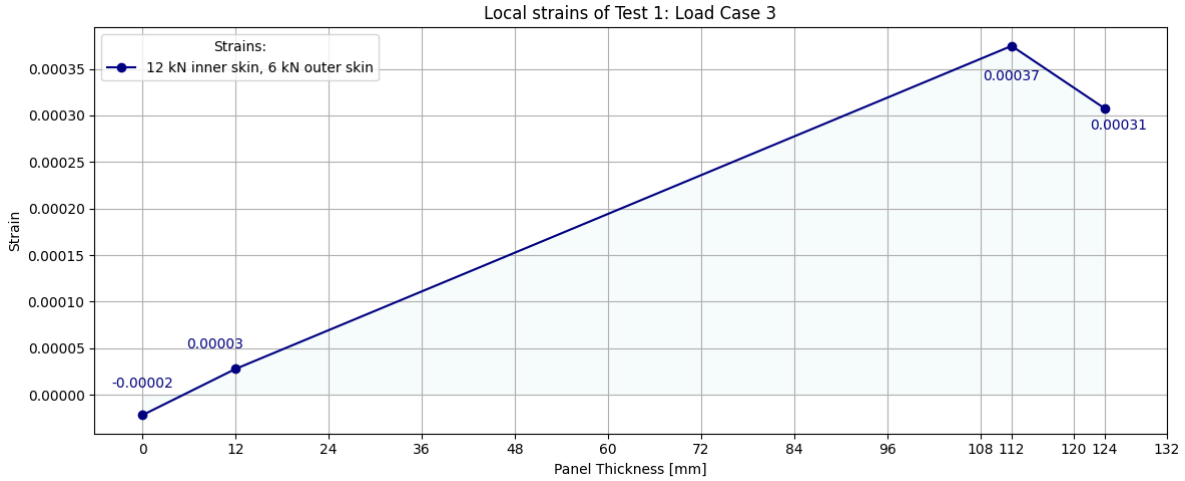

Figure 4.12: Strains of Test 1 inner face loaded with 12 kN and outer face loaded with 6 kN.

4.4.1. Experiment Results Analysis

The experiment results will be further analysed and the stress results will be calculated based on the following formula:

$$\sigma = E * \varepsilon \tag{4.21}$$

For the first loading where the inner face was loaded with 6 kN the panel deflections increased up to 73% after the additional loading between the two measurements (Figure 4.5). This may be caused by the low mechanical properties of the core or could suggest that an overloading happened for some part of the panel leading to an unexpected behaviour where the two faces do not deform together, suggesting a loss in the core stiffness or a change in the composite action of the core and the faces. The strains in figure 4.6 in the inner face increased by 12 to 33% indicating permanent deformations to the faces, but these do not contribute to the core failure. The additional deflections can be caused by plastic deformation, fatigue, or creep. In this situation, since the loads were very low and not cyclic, fatigue can be excluded. Plastic deformations are also unlikely, since the loads are relatively low and the stresses are not near any failure stress as seen in table 4.5, and figure 4.13. The most probable cause for the additional deflection is creep. Test 1 took 13 minutes in total to perform, meaning that already within this time a 73% increase in deflections could happen. Based on the beginning deflection result, second order theory can be added to calculate the amplification factor for the deflections [35]:

$$\alpha = \frac{1}{1 - \frac{N}{N_{cr}}} = \frac{1}{1 - \frac{6}{125.09}} = 1.05 \tag{4.22}$$

Multiplying the beginning deflection with the amplification factor $\alpha = 1.05$, $1.05 * 1.356 = 1.424mm$ it is still not as large as the deflection at the end of the test ($1.905mm$) seen in figure 4.5. Therefore, it seems likely that creep has occurred but additional mechanisms have also occurred. It could be that the core is not able to support the faces and is too deformable, or perhaps the interface has debonded and is causing the faces to resist the loads separately. This is also supported by the strain results seen in Figure 4.6 where the expected fully linear behaviour is not seen. Showing bigger compressive strains at 112 mm which is the inner face's core side. This could imply that the face is trying to work on its own by having higher compressive stresses

on the inside rather than the expected outside. Although, this result could also be explained by the placement of the load on the test rig and the connecting beam at the top between the two faces, making the load press more on the inner face's core side.

Additional creep factor testing should be performed to determine the long term behaviour of the whole panel. Even though literature review showed that creep from loading is not a problem, in this case the primary creep effect is significant, and should be further investigated.

Between the beginning and end of this test, some permanent deformations occurred and it might be that the core lost its stiffness allowing the faces to deform separately and losing a part of its composite action. The two faces are not working together as a composite material already in the first test, and knowing that 4 more tests were performed on the same panel, it can be assumed that based on these results, the following tests may not be reliable if creep deformation has indeed happened or some other failure mechanism. The deflection graphs after load removal show compression in the core at the top of the panel, and tension in the core in the lower half of the panel. The tensile stresses can be found by looking at the difference in deflections between the inside and outside faces:

$$\Delta L = 1.303 - 0.928 = 0.375mm \tag{4.23}$$

$$\varepsilon = \frac{\Delta L}{L} = \frac{0.375}{100} = 0.00375 \tag{4.24}$$

$$\sigma = E * \varepsilon = 5 * 0.00375 = 0.019MPa < 0.020MPa \tag{4.25}$$

The tensile deformation limit for the core is

$$\varepsilon = \frac{\sigma}{E} = \frac{0.020}{5} = 0.004 \Rightarrow 0.004 * 100 = 0.4mm \tag{4.26}$$

Table 4.7: MDF strength properties and maximum strains and deformations.

Insulation board resistances and maximum strain and deformation (eq. 4.24 and 4.26)			
	Characteristic Resistance	**Max strain**	**Max deformation**
	MPa		*mm*
Tension	0.02	0.004	0.4
Compression	0.10	0.02	2.0
Shear	0.04	0.018	57.6

This suggests that core tensile failure occurs when the faces deformations differ by 0.4 mm. Thus, making previously seen 0.375 mm deformation significant.

The stresses calculated based on the local strain results are in accordance with the theoretical stress value in the inner face, although slightly higher than the analytical values:

$$\sigma = \frac{F}{A} = \frac{6000}{12 * 1020} = 0.5MPa \tag{4.27}$$

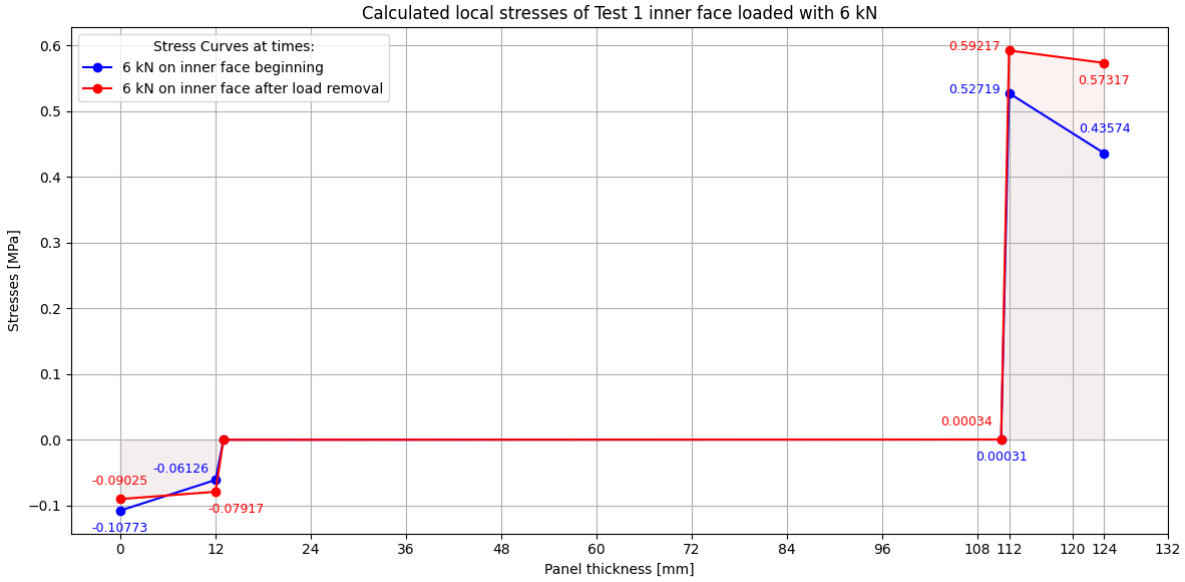

Figure 4.13: Calculated stresses of Test 1 inner face loaded with 6 kN.

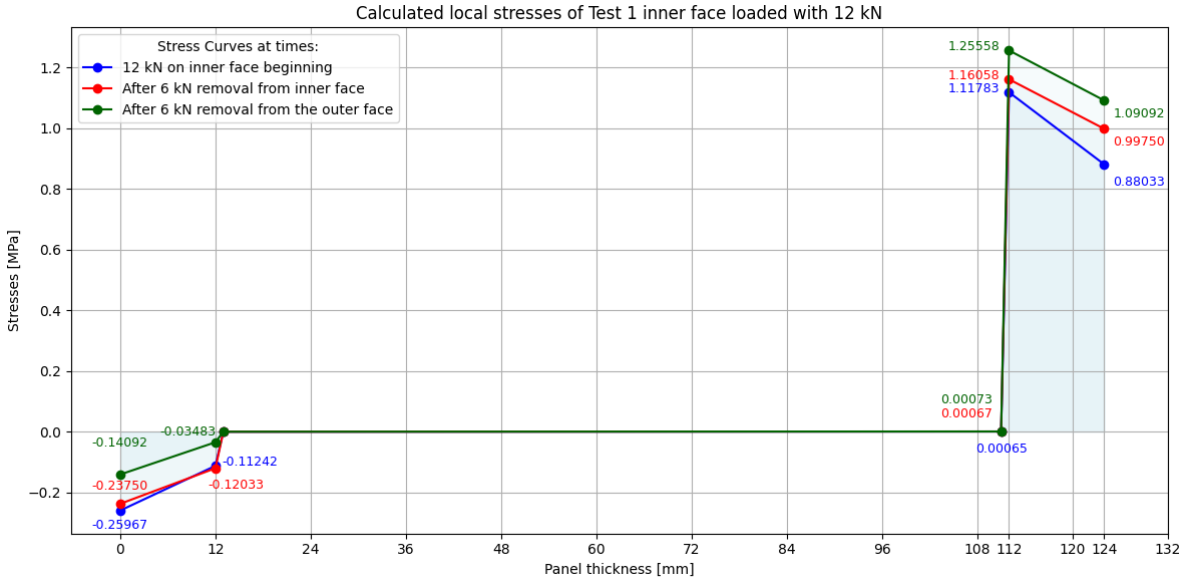

Figure 4.14: Stresses of Test 1 inner face loaded with 12 kN.

This stress distribution supports the assumption for the Karamba3D model where the inner face takes on most of the loads and the outer face is only for providing support and stability. The outside face should be in tenion which can be seen in figures 4.13 to 4.15.

The core compressive failure value is based on 10% deformation failure for an insulation material, meaning that the core could compress for 2 mm and only then analytical failure would occur. However, in the context of a sandwich panel, this deformation could be too big, and the insulation material should be tested as a structural material, to show how easily it will compress or delaminate under tensile and compressive stresses.

For loading 5, 12 kN on the inner face and 6 kN on the outer face, the stresses in the inner

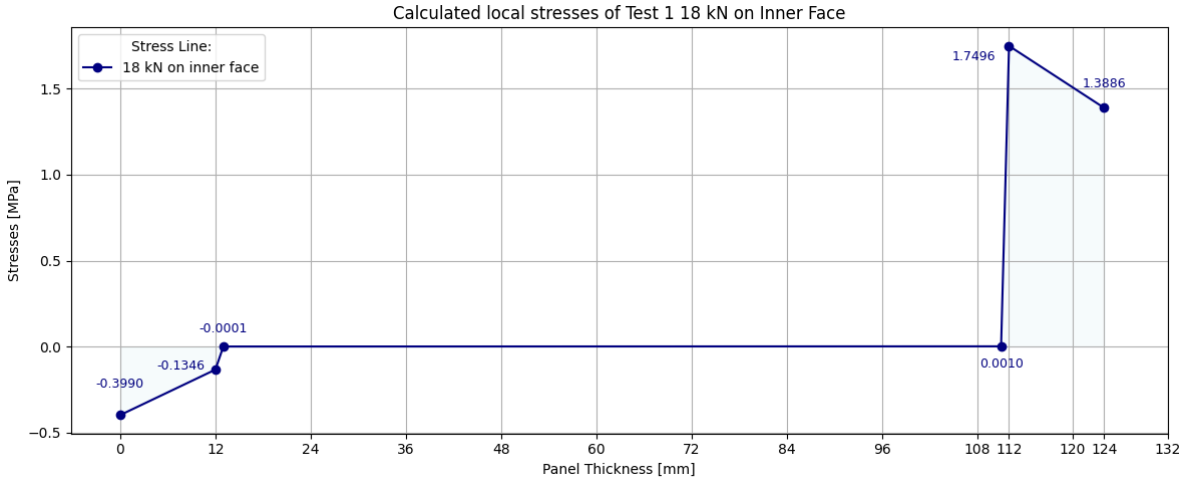

Figure 4.15: Stresses of Test 1 inner face loaded with 18 kN.

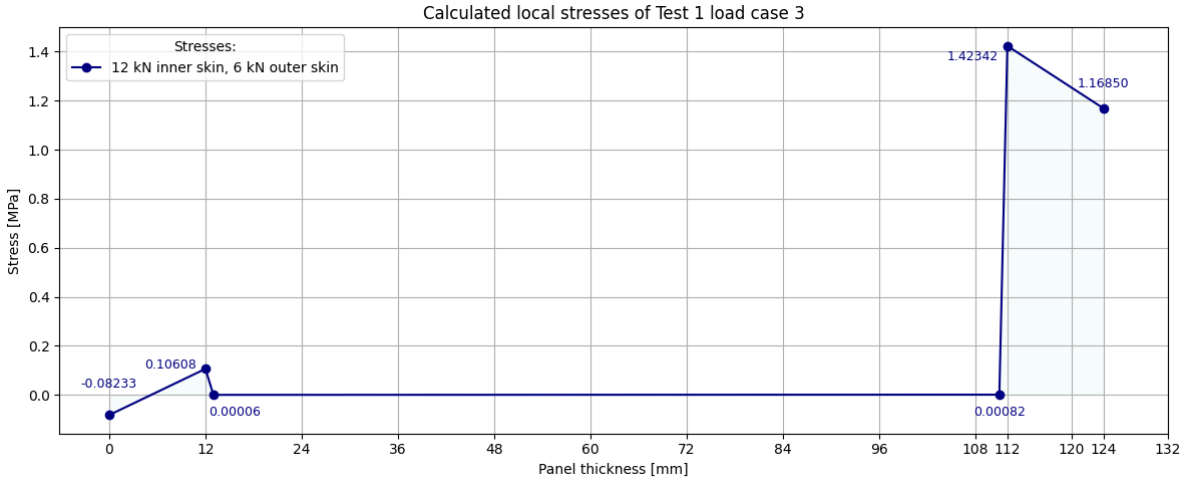

Figure 4.16: Stresses of Test 1 inner face loaded with 12 kN and outer face loaded with 6 kN.

face are 45% ($\sigma = 12000/(12 * 1020) = 0.98MPa \rightarrow (0.98 - 1.423)/0.98 = 45\%$) higher than expected from only the load on the inner face, meaning that the inner face does still resist forces also from the outer face due to the existing composite effect. This could mean that some individual behaviour is allowed for the sandwich panel and should not immediately suggest a failure in the core. This could also be explained by the deformation shape of the whole panel, where the 6 kN load on the outer face will start to push inwards towards the inner face, thus successfully transferring the forces through the core into the inner face. Therefore, the possible failure that has caused separate behaviour of the faces is not a complete failure, but seemingly only partial.

From test 1 it seems that there are three possible options. First is, that the core material fails under compressive or tensile stresses and therefore the faces start to deform separately from each other, and the composite action of a sandwich panel disappears. Second option is, that the core material deforms without failure diminishing composite action which means that it is not suitable for sandwich panel applications. Third option is that the bond between the face and the core delaminated and caused the faces to resist the loads separately. The first two options

give only one possible choice, to use this specific Steico insulation in a SIP a frame needs to be placed inside the panel. This would add significant stiffness to the panel since it would resemble a traditional timber frame building. The third option would require further testing on the developed panel to determine the interface strength and the amount of bonding between the core and the faces. If it would appear that the bond strength is not sufficient then it should be strengthened. If the bond was sufficient, then the first two options are more likely to be accurate.

As seen in test 1 occurrence of creep deformation, and possibly a failure in the core or interface, deems tests 2 to 5 to not be reliable and therefore will not be analysed in depth, but the results are visualised in Appendix F. In order to compare the models to experimental results, some loading cases will still be looked at in the following chapters since it will still give some insight into the accuracy of the modelling results.

4.5. Model results

4.5.1. Karamba3D model results*

**These results were created with a different material definition for the core than the rest of the thesis due to an error in the magnitude of the shear modulus. For the rest of the work it is defined as 2.2 kN/cm^2 which is 22 MPa. The scaling of the panel and the two deflection graphs were created with the 22 MPa but the analysis in this chapter is conducted with the shear modulus of 2.2 MPa so 0.22 kN/cm^2 and the modulus of elasticity is defined as 5 MPa. The beam distribution and dimensions are the same, so the deflection results will be bigger than for the rest of the analysis in this thesis.*

The Karamba3D model described in Chapter 3 was developed to describe the behaviour of the SIP, and to evaluate the possibility of using it in the design process for SIPs. The first iteration had a wood material defined in Karamba3D, which resulted in the beams of the core being very far apart, which caused the interaction between the two skins to be insufficient. The next iterations were scaled based on the Timoshenko beam equation results for deflections under transverse loading according to equation 3.19. This can be seen in figure 4.17.

The deflection difference was minor when only axial loads were applied. The difference between the biggest and the smallest deflection was only 8% and can be seen in figure 4.18. Therefore, the scaling of the final model was based on the transverse loading case, and the final model of 65x65 mm dimension beams will be further analysed.

First, the model was analysed for serviceability limit state. The serviceability limit state is taken as L/150 which is 3200/150=21.3 mm. This is reached in the cases presented in Table 4.8. These results show that the most critical cases are combined loads where there is axial load and transverse load like wind loading. Only the transverse load is already quite small on its own, which means that this panel will deflect quite fast over the SLS limit.

Next, failure was evaluated based on the utilisation percentage of the materials in Karamba3D. The axial failures are presented in Table 4.9, and the transverse loading failures for the face and for the beams are presented in Table 4.10. Axial loading failure depends on where the load is applied – inner face, outer face or both. Axial failure from the model was caused by the failure of the faces (the beam utilisation was not considered in the axial loading cases, but would probably predict failure earlier). If the outer face was loaded, then the failure happened due to

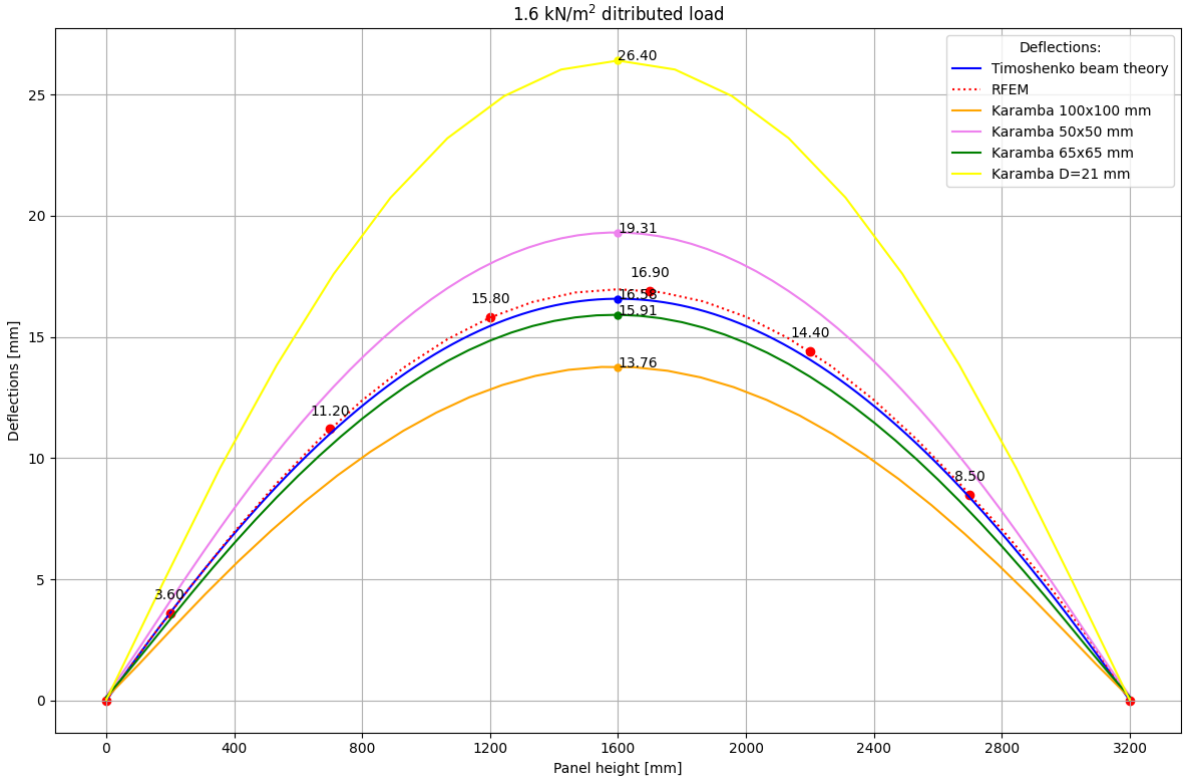

Figure 4.17: Karamba3D model scaling with RFEM and Timoshenko beam equations under 1.6 kN/m^2 transverse loading.

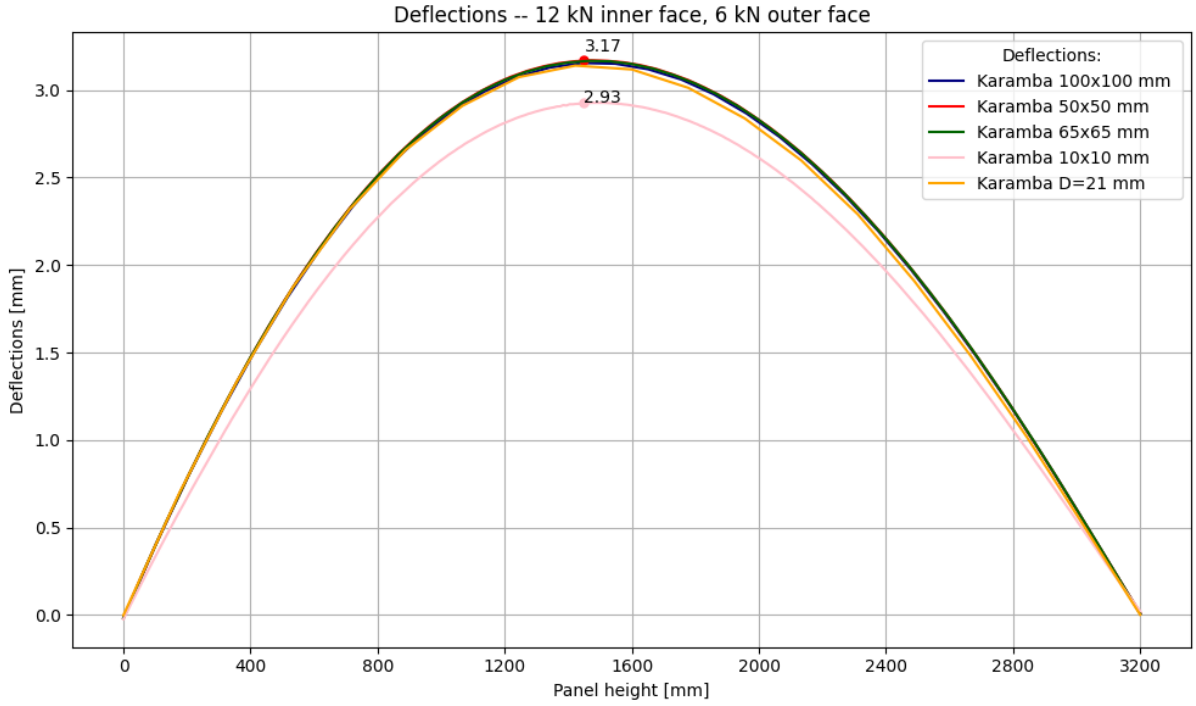

Figure 4.18: Deflections under axial loads.

Table 4.8: SLS limit loads from Karamba3D model.

	inner face kN	outer face kN	transverse kN/m
Axial	75	20	
Axial	74		
Transverse			1.12
Combination	6		1.03
Combination	12		0.94

compressive failure of the outer face as seen in Table 4.9. The lowest OSB failure under axial failure loads according to the Karamba3D model is 87.8 kN when applied only on the outer face. The highest OSB failure load under axial loading is 91.6 kN when applied on the inner face. The shape as which the panel deforms changes – if only inner face is loaded then it deforms according to the first Euler buckling curve, however when a load is applied to the outer core, the deformed shape will be anti-symmetrical wrinkling as seen in Figure 4.21. The critical anti-symmetric wrinkling stress and load has been calculated under Hand Calculations with equation 4.11. The failure shape can be seen in Figures 4.25 and 4.26. In the case of this panel, the critical wrinkling stress is reached at 23.75 MPa which is $23.75 * 1020 * 12 = 290.7kN$. The shape is already seen before the failure mode occurs when load is applied to the outer face. This shows that the failure mode is most probably not face wrinkling. Therefore, according to the model, it can be concluded that the failure method would be end bearing or face crushing, although global buckling can not be disregarded. As seen before, the global buckling failure load is 125 kN, however the axial load that resembled the first Euler buckling shape according to the model only reached 91.6 kN. This is 28% smaller than the analytical calculation predicted. This is probably due to the eccentric loading conditions which are not accounted for in the Euler buckling equation for sandwich panels, and the material characteristics which fail under compression. Also, the core failure was not evaluated for axial loading since it is uncertain whether the results are reliable or not. Additional failure testing should be done to confirm the critical buckling load, and to confirm if the model can predict core failure.

The transverse loading for the faces tensile failure was caused by a distributed force of 6.01 kN/m, whereas the beams had already failed according to the utilisation rate. Tensile failure of the beams already occurred under 2.86 kN/m where the model already deflected 54.3 mm. The change in the shear modulus of the core proved that the core's shear modulus has a significant effect on the bending stiffness of the panel. When a combination of loads was observed then the serviceability limit state was governing for failure. With 12 kN on the inner face and 1 kN/m as wind load, the SLS limit had been reached (22.4 mm), but utilization for the faces was only 19.7% in compression and 17.2% in tension according to the model. Therefore, a SIP that is called a very efficient structure in terms of material use and strength properties, does not even use 50% of the load bearing capacity in serviceability limit state which is the governing design criteria in that case.

The Karamba3D model shows that it is capable to predict OSB crushing failure from the utilisation percentage, and it is able to predict the shape of the panel under different loads. It also predicts failure of the beams that represent the core, but this should be tested on the real panel to confirm the findings. The panel does not describe the interface between the core and

the faces, thus it is unable to predict debonding. The model can successfully show SLS limit states and some failure modes but not all – debonding being the main mode, and core failure should be confirmed by tests. The shear failure of the core is predicted already at 0.29 kN/m which is as low as the panel theory suggests for permanent loading (0.22 kN/m in Table 4.13). Therefore, it is possible that the model can provide similar results to sandwich panel theory.

The stresses and strains seen in figures 4.20 to 4.24 show a linear distribution. This suggests a perfect bond between the faces and the core. In the case of the outer face being loaded as seen in figure 4.24, the inner and outer face both take on the loads and distribute them equally. If the inner face and the outer face is loaded, the deflection shape still remains as if only the outer face is loaded, but the distribution of stresses and strains is different. Both of the faces are still in compression but the most of the loading is taken by the inner face. This is due to the chosen support conditions, where only the inner face is supported. The stress and strain results suggest that Karamba3D is able to predict the correct stress and strain results according to what would be analytically expected. If the outer face is loaded with 91.6 kN, the stress in the inner and outer faces should be $91.6/(2*12*1020) = 3.7MPa$. Figure 4.20 shows that the stresses vary linearly in the OSB faces between 3.7 MPa and 3.8 MPa. Thus, the stress and strain results are reliable. However, the characteristic compression resistance in-plane and parallel to the span direction is 15.4 MPa. This suggests that a failure has not occurred even in the inner face loaded case where a maximum compression stress of 7.9 MPa is shown. Therefore, only half of the characteristic compression resistance is used, but according to the utilisation percentage, the material has failed. These values have been taken in the middle of the panel, but it could be the case that the stress concentrations are very high near the supports, so the stress values here are not representing the failure situation.

Table 4.9: Axial loading failure Karamba3D model.

	inner face kN	outer face kN	utilisation of the inner face %	utilisation of the outer face %	Displacement mm
Axial	91.6		100	6.3	26.2
Axial		91.6	25	105	3.09
Axial		87.8	23.8	100	2.96
Axial	60.4	30.0	7.9	100	15.9

Table 4.10: Transverse loading failure Karamba3D model.

	transverse loading kN/m	utilisation %
Face tensile failure	6.01	100
Beam failure	0.29	100

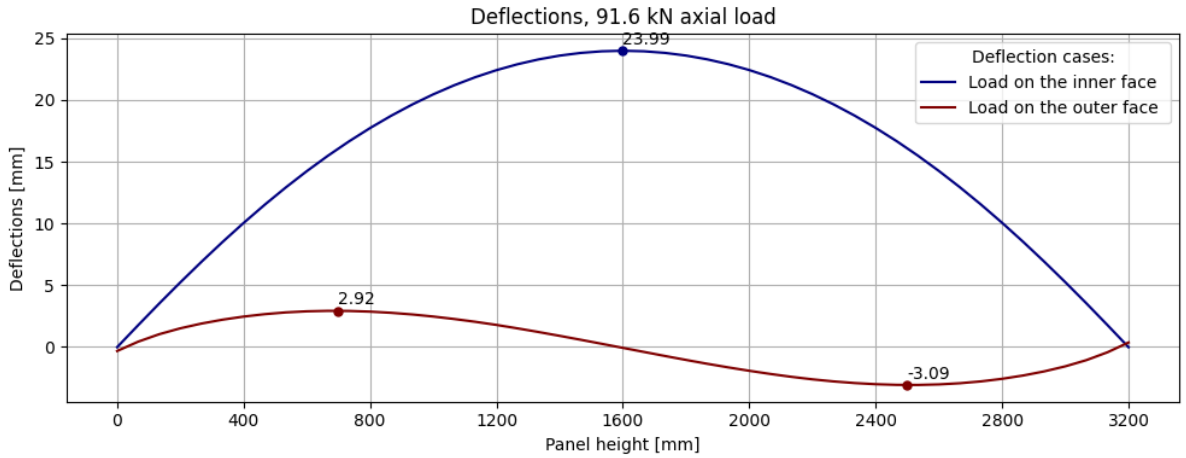

Figure 4.19: Deflections of axial load 91.6 kN.

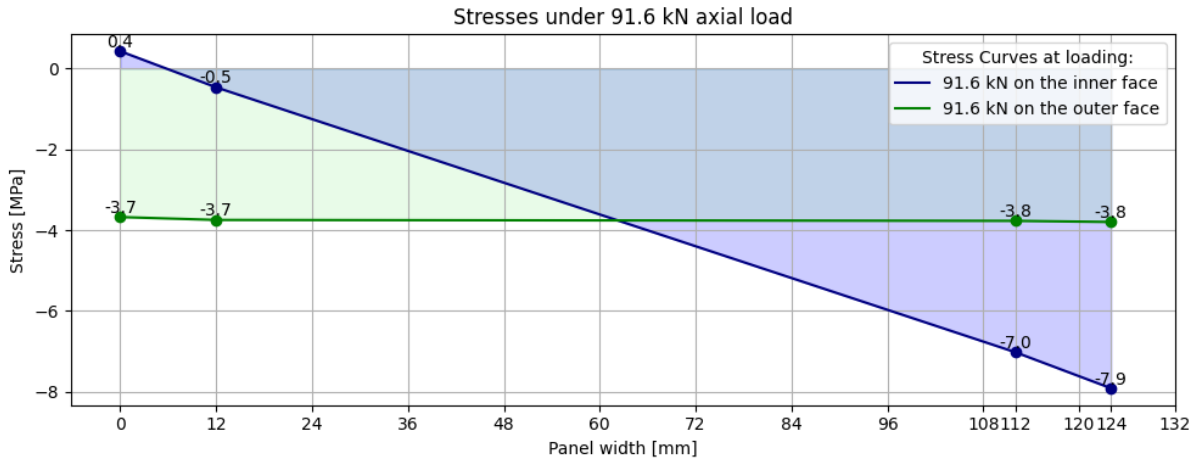

Figure 4.20: Stresses of axial load 91.6 kN (negative is compression and positive is tension).

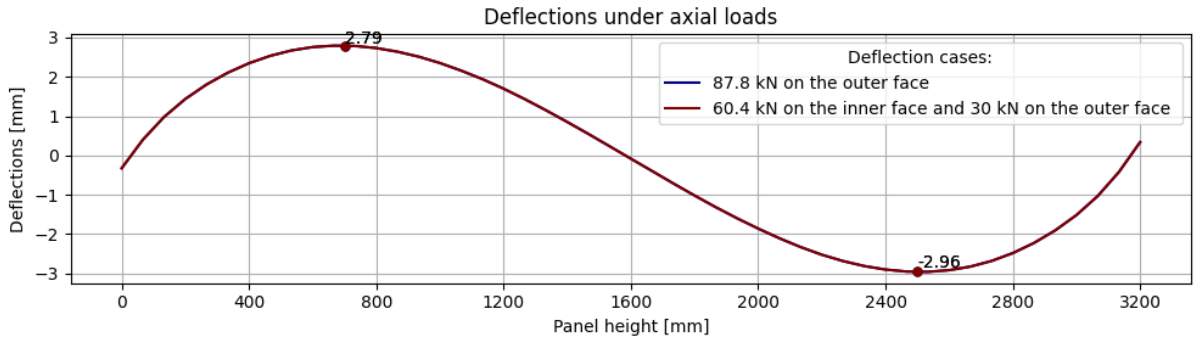

Figure 4.21: Deflections of axial load 87.8 kN and 90.4 kN.

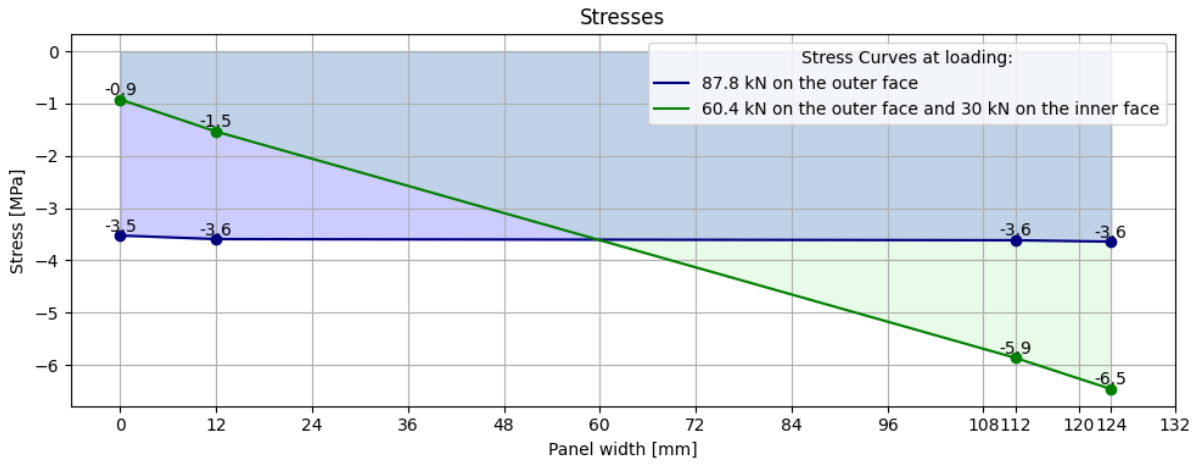

Figure 4.22: Stresses of axial load 87.8 kN and 90.4 kN (negative is compression and positive is tension).

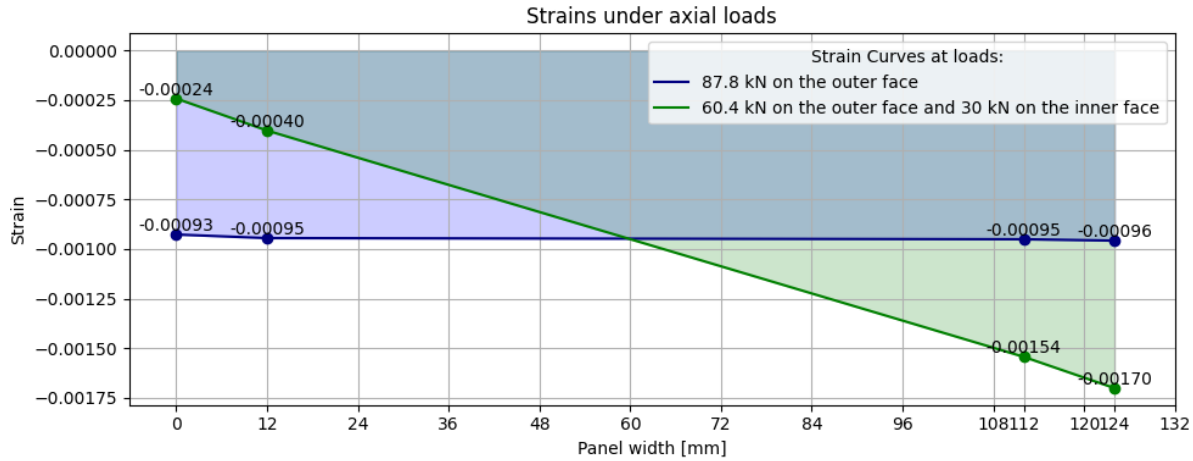

Figure 4.23: Strains of axial load 87.8 kN and 90.4 kN (negative is compression and positive is tension).

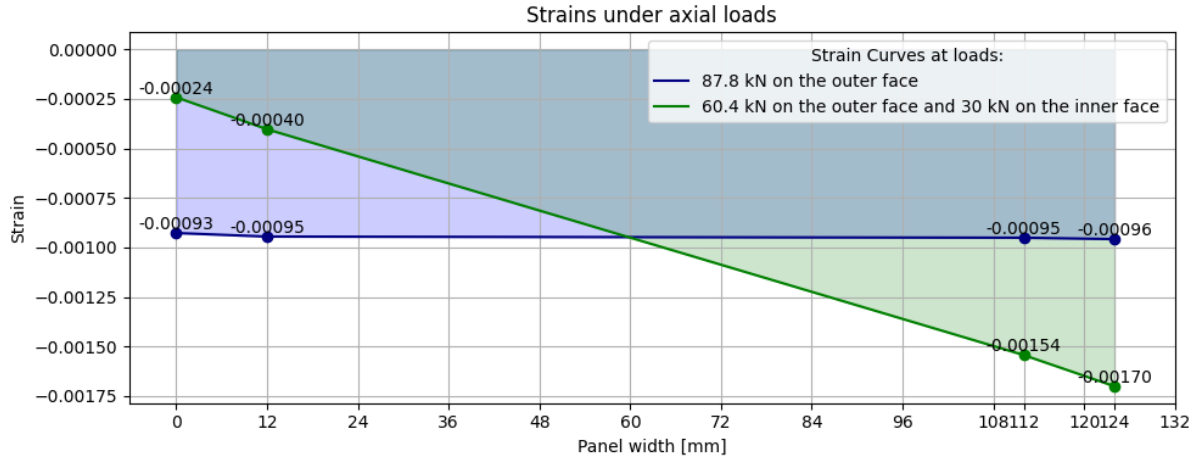

Figure 4.24: Strains of axial load 87.8 kN and 90.4 kN (negative is compression and positive is tension).

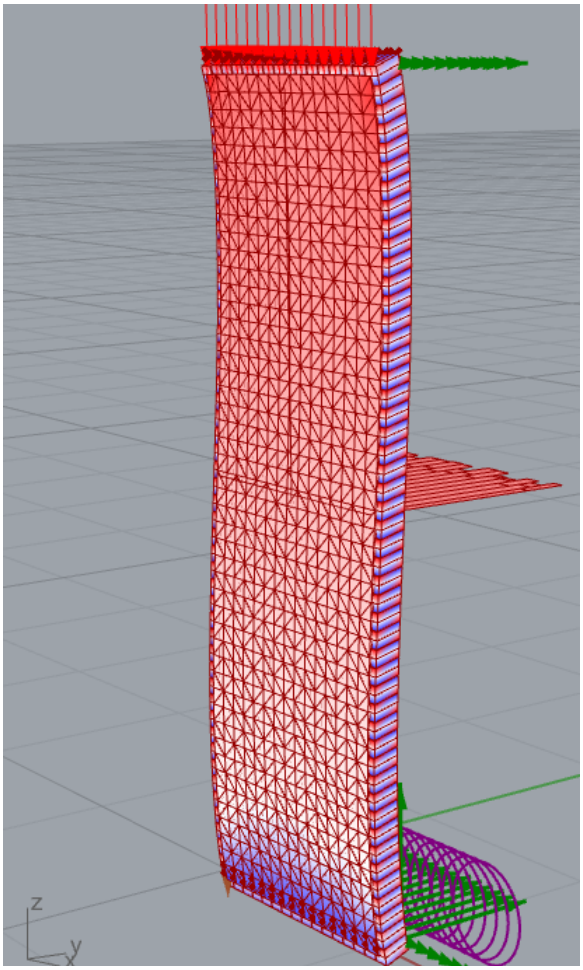

Figure 4.25: Outer face loaded deflected Karamba3D model isometric. Red signifies compression and blue signifies tension.

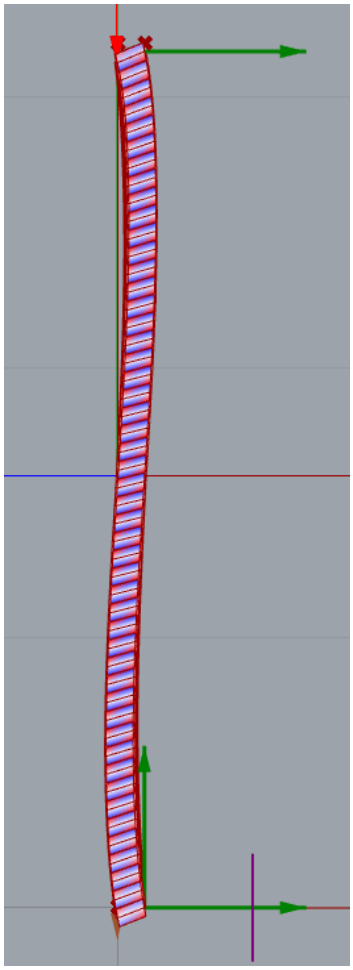

Figure 4.26: Outer face loaded deflected Karamba3D model side view. Red signifies compression and blue signifies tension.

4.5.2. RFEM model results

RFEM model was created to have a comparison point for the Karamba3D model. The RFEM model might be less accurate than the Karamba3D model due to the position of the supports and due to the definition of the panel layers in one shell-element. The model does predict instability at 126 kN axial loading, but it is unable to show the different deformation shapes that would occur in reality. It does give similar results as Timoshenko beam equations and karamba3D model under transverse loading, but axial loading results are not sufficiently accurate to use in design – deflection results are mostly smaller than the experimental results or karamba3D model predicted for axial loads. It does show a trend for a sharper deflection curve towards the top of the panel as happened for test 1 loading 5, 12 kN on the inner and 6 kN on the outer face. The transverse loading capacity according to RFEM is almost 0 – the model states that the structure is unstable already at 0.1 kN/m.

Prediction of stresses and strains was inaccurate under axial loading. This is due to the support conditions. The transverse loading case stresses have a good accordance with the sandwich panel theory.

4.6. Comparison of experimental, analytical and modelling results

This chapter will compare all of the methods used to analyse the SIP behaviour. However, not all methods are used in each loading case comparison. First, transverse loading will be analysed where there are no experimental results to be used. After that, two different loading cases will follow, where all methods are used in the analysis.

4.6.1. Transverse loading

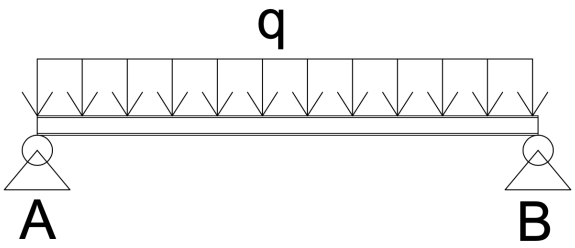

Figure 4.27: Transverse loading schematisation.

Table 4.11: Shear failure of the core.

			unit	*eq.*
Characteristic shear resistance	τ_k	0.04	*MPa*	
Maximum shear angle	$\gamma_{k,max}$	0.018	*rad*	(4.10)
Critical transverse shear load according to panel theory	q_{max}	1.43	*kN/m*	(4.8)
Critical transverse shear load according to Timoshenko	q_{max}	2.5	*kN/m*	(4.8)

Table 4.12: RFEM and Karamba 65x65 mm deflection results.

		Panel theory	Timoshenko	units	
maximum distributed load	q_{max}	1.43	2.5	*kN/m*	
RFEM	w	15.2	26.6	*mm*	*failure warning*
Karamba3D 65x65 mm	w	15.0	28.2	*mm*	

The transverse loading will be analysed with the analytical calculations, Karamba3D model and the RFEM model. The comparison is presented in Table 4.13 where according to the maximum shear angle and the maximum shear resistance, the maximum distributed loads were found with the Timoshenko beam equations and the panel simplification equations seen in table 4.11.

Then, the maximum q loads were taken according to the Timoshenko beam equations and the deflections and shear stresses were found for the RFEM and Karamba3D models seen in table 4.13. The loads were applied with the load duration factors. The shear angle was chosen as the governing failure criteria since it is the weakest failure mode for transverse loading.

Table 4.13 shows that the core will fail earlier than OSB since the permanent maximum distributed load for the OSB is 8.93 kN/m for service class 2, but the permanent maximum distributed load for the core is according to the Timoshenko beam equations 0.35 kN/m, but only 0.22 kN/m according to the panel simplification equations. Therefore, the governing failure method is shear failure of the core under transverse loads. These loads suggest that the panel in this form is not suitable for roofing nor floors, since the maximum permanent load is much lower than usually applicable for floors or roofs – around 2 kN/m^2 permanent load for floors and 0.5 kN/m^2 for roofs. They would need a significant amount of stiffening to prevent shear failure. The solution would be to add through thickness stiffeners.

If we apply the panels as wall panels, then a short-term wind load could be of a maximum magnitude of q=1.5 kN/m according to Timoshenko equations or according to the panel simplification equations q=0.88 kN/m. These loads are without any safety factors, meaning if calculations are made then the loads would be multiplied usually by a safety factor of 1.5. The average wind load expected for a 9 meter tall building in the Netherlands is 1.6 kN/m. Therefore, the panel might not be strong enough to resist those loads. Additionally, the axial loads coming from the building itself will already cause stresses and deflections, resulting in a failure before the 1.6 kN/m average wind load is reached, and causing significant additional deflections meaning second order effects which would lead the situation more critical. Further, creep effects from axial loads would already cause additional deflections, meaning the panel would become unstable earlier than 1.5 kN/m.

The next point of concern would be deflections. Usually, the serviceability limit is between H/150 to H/300. That would mean a deflection between 10-21.3 mm is allowed, but not necessarily wanted. Another concern rises if the movement for other elements connected to the panels is acceptable. Under transverse loading, only the instantaneous load would surpass the serviceability limit state deflection of 21.3 mm. However, if axial loads are applied, the situation declines faster depending on the amount of the axial load and the transverse load meaning that the governing design criteria could be the SLS limit instead of the panel failure.

The panel simplification equations predict failure earlier than the Timoshenko beam theory equations. These values would need to be confirmed by a bending test, to see which method gives a more accurate prediction. The RFEM model only has a 1.4% difference with the Timoshenko beam equations when comparing deflection values seen in figure 4.34. Additionally, the shear stresses from RFEM differ only by 0.004 MPa which is 11.8%. The Karamba model with 65x65 mm beams predicts the deflection result more accurately on higher loads, but for smaller loads the deflection result differs up to 0.66 mm which is 15.5%. The shear stresses seen in figures to show that the 1.43 kN/m load is at the shear resistance limit according to sandwich panel theory, however, the Karamba3D model is exhibiting only half of the failure stresses, whereas the RFEM model has slightly higher shear stresses, but overall falls uner the same magnitude as the Karamba3D model. The load distribution of 2.5 kN/m shows that for both the Karamba3D model and RFEM model the maximum shear stresses have been reached, but the sandwich panel theory shows almost twice the maximum shear resistance. These dif-

Table 4.13: Shear failure under q loads from Timoshenko beam equations.

Medium density fibre board (Steico) shear failure								
		permanent	**long**	**medium**	**short**	**instant**	units	ref
shear resistance	τ_{max}	0.006	0.012	0.018	0.025	0.034	MPa	(4.2)
max shear angle	γ_{max}	0.003	0.006	0.008	0.011	0.015	rad	(4.10)
Timoshenko	w	3.6	8.3	11.4	15.5	21.8	mm	(3.19)
	ϕ	0.0016	0.0035	0.005	0.007	0.01	rad	(3.22)
	M	0.45	1.02	1.41	1.92	2.69	kNm	(3.21)
	V_{max}	0.56	1.28	1.76	2.40	3.36	kN	(3.20)
	q_{max}	0.35	0.8	1.1	1.5	2.1	kN/m	
Panel simplification	V_{max}	0.35	0.70	1.05	1.41	1.93	kN	(4.7)
	q_{max}	0.22	0.44	0.66	0.88	1.21	kN/m	(4.8)
RFEM model	τ	0.005	0.011	0.016	0.021	0.03	MPa	
	w	3.7	8.4	11.6	15.8	22.1	mm	
Karamba3D	w	4.26	8.77	11.8	15.8	21.8	mm	
	τ	0.0019	0.0044	0.0061	0.0083	0.012	MPa	
OSB/3 shear failure								
Shear resistance	sc1 τ_{max}	0.33	0.42	0.58	0.75	0.92	MPa	(4.2)
	sc2 τ_{max}	0.25	0.33	0.46	0.58	0.75	MPa	(4.2)
Shear angle	sc1 γ_{max}	0.007	0.008	0.012	0.015	0.018	rad	(4.10)
	sc2 γ_{max}	0.005	0.007	0.009	0.012	0.015	rad	(4.10)
Max shear force	sc1 V_{max}	19.04	23.80	33.32	42.84	52.36	kN	(4.7)
	sc2 V_{max}	14.28	19.04	26.18	33.32	42.84	kN	(4.7)
Max distributed load	sc1 q_{max}	11.90	14.88	20.83	26.78	32.73	kN/m	(4.8)
	sc2 q_{max}	8.93	11.90	16.36	20.83	26.78	kN/m	(4.8)

ferences are most likely due to the fact that sandwich panel theory underestimates in this case the panel resistance and the RFEM and Karamba3D models have good correspondence with the Timoshenko beam equations.

The bending stress in the cross section of the panel seen in figures 4.28 and 4.29 is found with the analytical formula for sandwich panels, Karamba3D model and the RFEM model. The core does not take any bending due to its low strength properties. The inner face is in compression and the outer face is in tension, analytically anti-symmetric force distribution. The RFEM model has very good correspondence with the sandwich panel theory, showing only minor differences. The Karamba3D model is showing significantly larger distribution of stresses in the faces. The maximum stress is 44% larger than the analytical stress in the face. These results would need to be confirmed by a bending test.

The panel models are presented in figures 4.32 and 4.33. The deflections from the Timoshenko beam equations, Karamba3D model and RFEM can be seen in figure 4.34 which all have a good correspondence with each other.

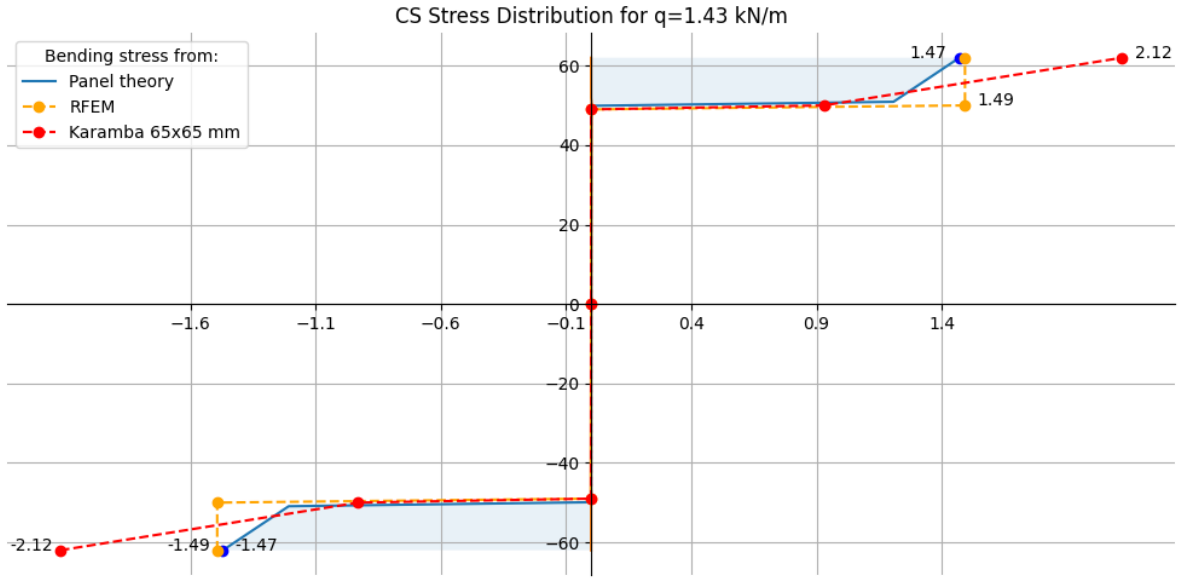

Figure 4.28: Cross section bending stress distribution under q=1.43 kN/m.

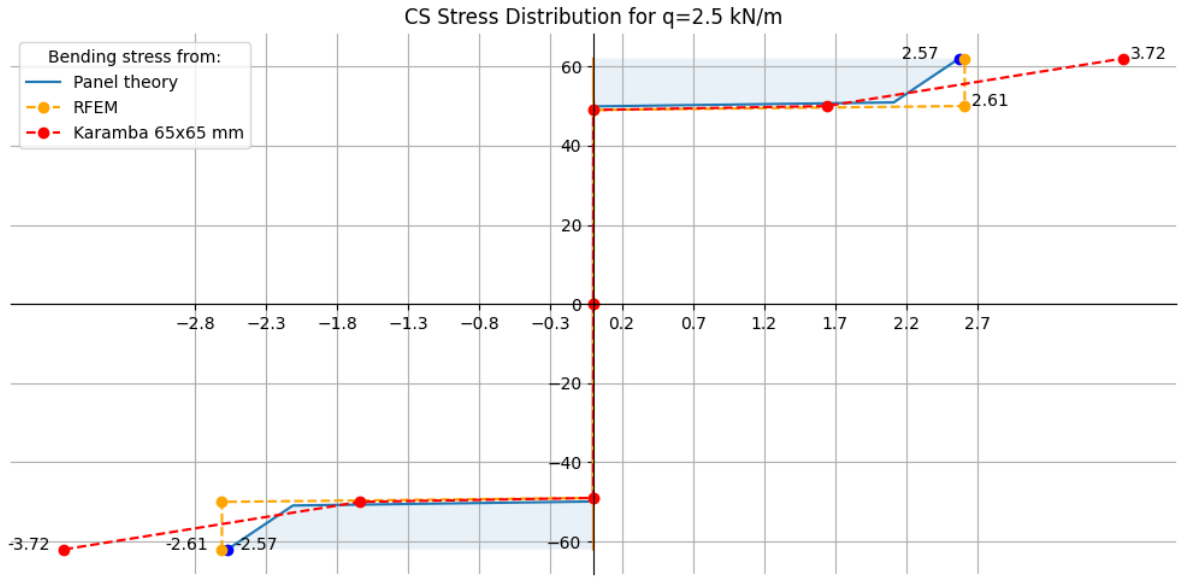

Figure 4.29: Cross section bending stress distribution under q=2.5 kN/m.

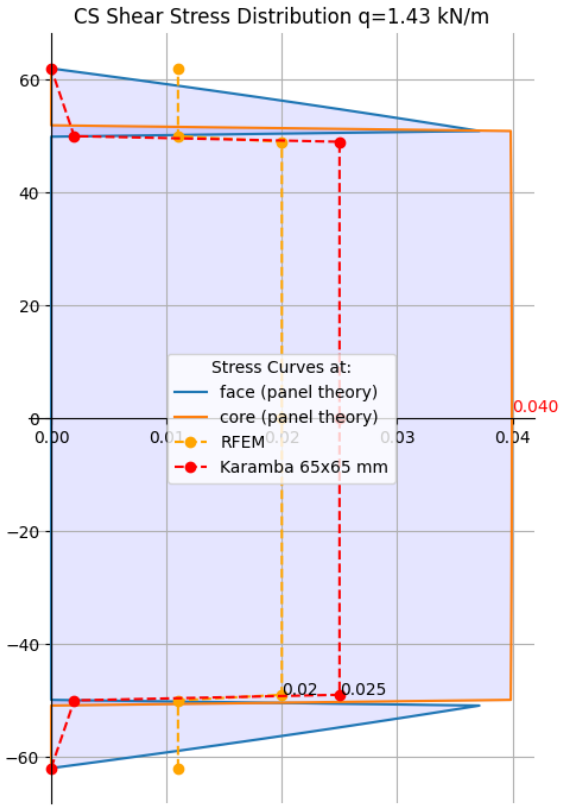

Figure 4.30: Cross section shear stress distribution for q=1.43 kN/m.

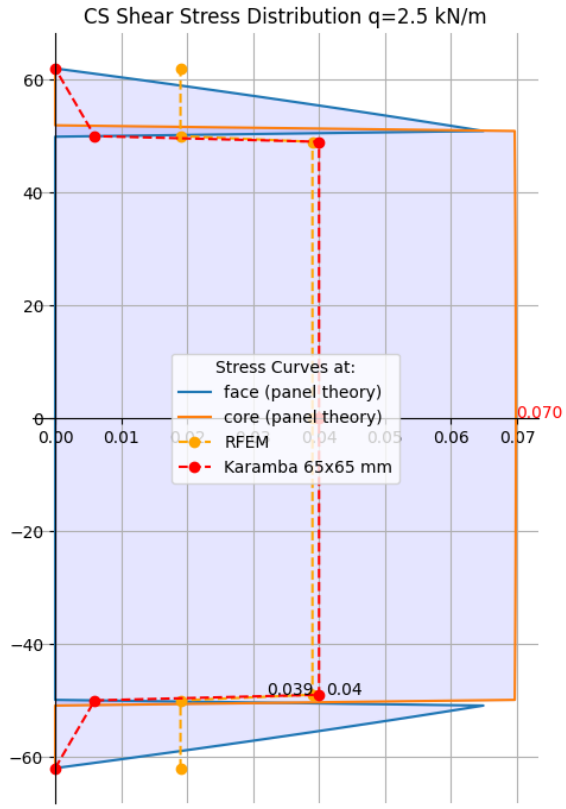

Figure 4.31: Cross section shear stress distribution for q=2.5 kN/m.

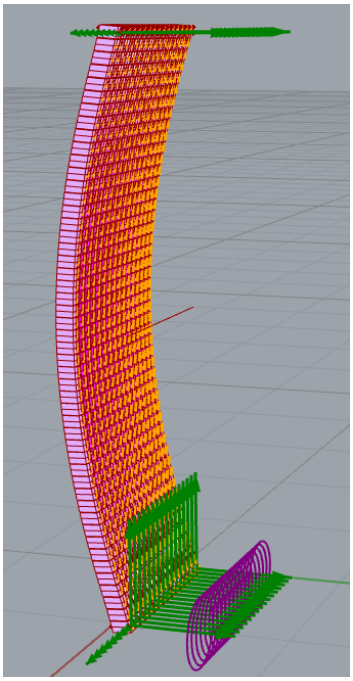

Figure 4.32: Karamba3D model under transverse loading.

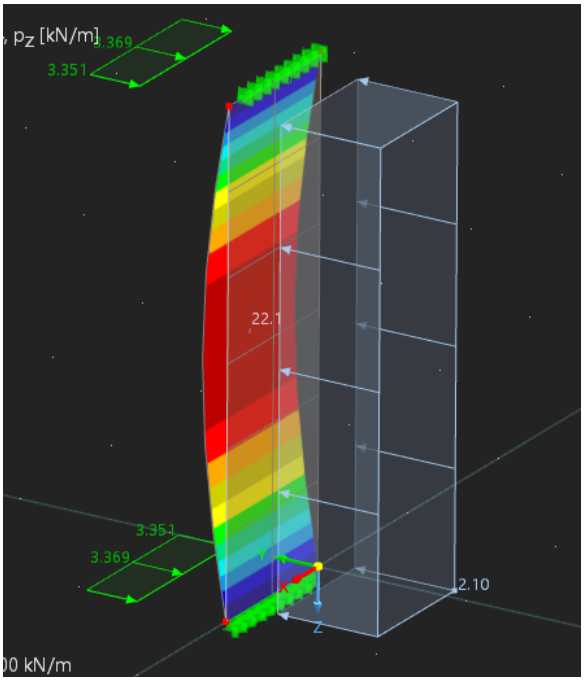

Figure 4.33: RFEM model under transverse loading.

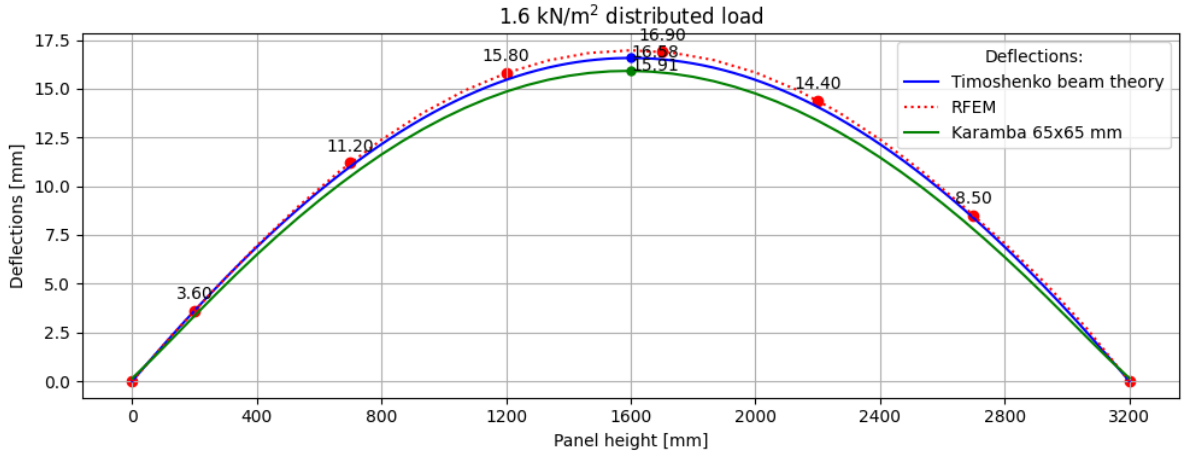

Figure 4.34: Deflections of transverse loading under 1.6 kN/m^2.

4.6.2. Outer face loaded

This load case is compared with all methods used – shear beam equations, experiment results, Karamba3D model results and RFEM results. The outer face is loaded with 6 kN. In the experiment it is two point loads which equal 6 kN but in the models it is assumed to be a distributed load, so F2=6 kN/m. The RFEM model has centric support conditions instead of eccentric, therefore the results differ from the other methods used.

The critical angle in the core under which failure occurs assuming permanent loads.

$$\tau_{cr} = G * \gamma \tag{4.28}$$

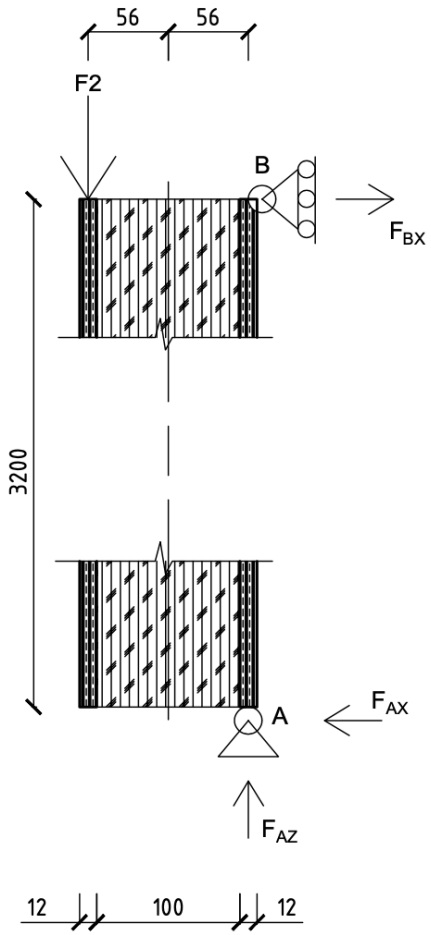

Figure 4.35: Calculation with 6 kN loaded on the outer face

$$\gamma_{max} = \frac{\tau_{cr}}{G} \tag{4.29}$$

$$\gamma_{max} = \frac{0.04}{2.2} = 0.018 rad \tag{4.30}$$

Finding the support reactions.

$$\sum M_A = 0 \qquad \sum M_B = 0 \qquad \sum Z = 0 \tag{4.31}$$

$$F_2 \cdot d - F_{BX} \cdot H = 0 \qquad F_2 \cdot d - F_{AX} \cdot H = 0 \qquad F_{AZ} - 6 = 0 \tag{4.32}$$

$$F_{BX} = \frac{6 \cdot 0.112}{3.2} = 0.21\,\text{kN} \qquad F_{AX} = \frac{6 \cdot 0.112}{3.2} = 0.21\,\text{kN} \qquad F_{AZ} = 6\,\text{kN} \tag{4.33}$$

The support reactions for the RFEM panel are exactly half of what they are supposed to be due to the location of the supports, which is in the middle of the panel instead of the inner face. The support reactions of the Karamba model match the hand calculations.

Largest allowable vertical movement of the outer skin, in regards to the failure of the core in shear.

$$\gamma_{max} = \frac{z_{max}}{t_c} \tag{4.34}$$

$$z_{max} = \gamma_{max} * t_c \tag{4.35}$$

$$z_{max} = 0.018 * 100 = 1.8mm \tag{4.36}$$

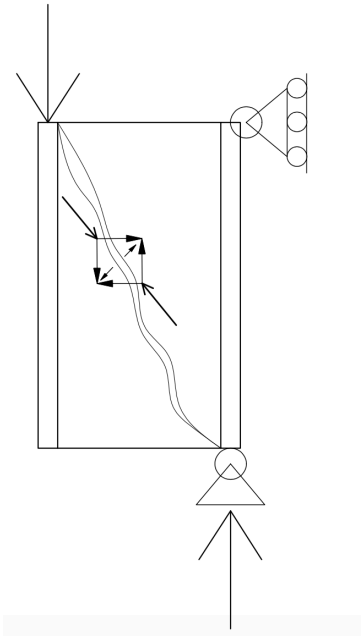

Figure 4.36: Loading case 6 kN on the outer face crack formation/failure

Actual shear stress in the core from the load.

$$\tau = \frac{F}{A} \tag{4.37}$$

$$\tau = \frac{6000}{1020 * 3200} = 0.0018MPa \tag{4.38}$$

Actual vertical movement from the 6 kN load.

$$\varphi = \frac{\tau}{G} \tag{4.39}$$

$$\varphi = \frac{0.0018}{2.2} = 0.0008rad \tag{4.40}$$

$$z = \varphi * t_c \tag{4.41}$$

$$z = 0.0008 * 100 = 0.084mm \tag{4.42}$$

Critical shear force on the outer skin of the panel for core shear failure.

$$F_{cr} = \tau_{cr} * A \tag{4.43}$$

$$F_{cr} = 0.04 * 1020 * 3200 = 130.6kN \tag{4.44}$$

The maximum load bearing capacity of the core under axial loading is 130.6 kN. The applied load is not close to the critical load, so failure should not happen in the core this way. However, the deformed shape under the 6 kN on the outer face is anti-symmetric buckling also discussed earlier under the experiment results analysis. This buckling causes compression and tension perpendicular to the plane in the core material by the faces of the panel. The experimental results, which are presented from tests 2, 3 and 5 (Appendix F) in figure 4.41 show an unusual behaviour after test 2 – test 2 shows the anti-symmetrical wrinkling deformation shape, but 3 and 5 start to resemble more buckling shape 3 of Euler buckling. This suggests a failure, debonding or stiffness loss in the core which causes the OSB faces to resist the loads separately. This is supported by the Euler critical buckling loads for only the OSB faces. It is indeed not a clear third buckling shape, but that could be caused by the composite effect of the sandwich panel acting partly together. The faces resembling a third deformation in the third buckling shape suggest that they are resisting the loads as single standing materials. The third buckling shape load for a single OSB face is the following:

$$F_{cr_3,OSB} = \frac{n\pi^2 EI}{L^2} = \frac{3 * \pi^2 * 3800 * \frac{1020*12^3}{12}}{3200^2} = 4.8kN \tag{4.45}$$

The load that is applied to the outer face is 6 kN, and the critical buckling load for the third shape is 4.8 kN and for the fourth shape is 8.6 kN. Thus it supports the conclusion that the faces could deform in the third buckling shape and might be taking on the loads as single standing material. Therefore, there is a loss in the composite effect. If the gamma method were to be used as for mechanically jointed beams, the gamma factor would then go from 1 to maybe almost to 0, resisting the loads as separate materials.

As mentioned previously, the core is being compressed and is under tension from the OSB faces. Therefore, a check for the maximum and minimum area to resist the loads is done.

Tension check for the core material

$$f_{t,cr} = \frac{F_{BX}}{A_{min}} \tag{4.46}$$

$$A_{min} = \frac{F_{BX}}{f_{t,cr}} \tag{4.47}$$

$$A_{min} = \frac{210}{0.02} = 10500mm^2 \tag{4.48}$$

Compression check for the core material

$$f_{c,cr} = \frac{F_{AX}}{A_{min}} \tag{4.49}$$

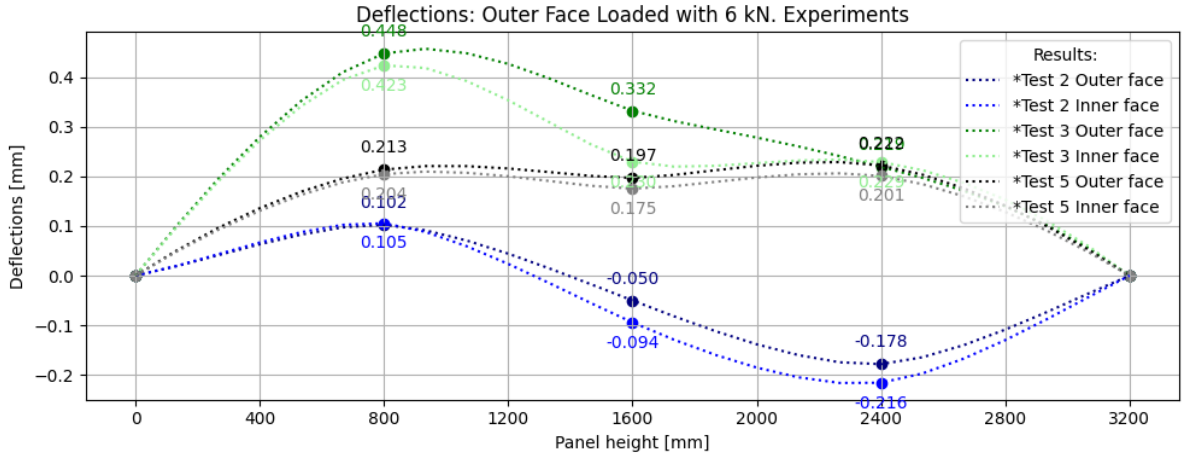

Figure 4.37: Deflections of 6 kN on the outer face experimental results.

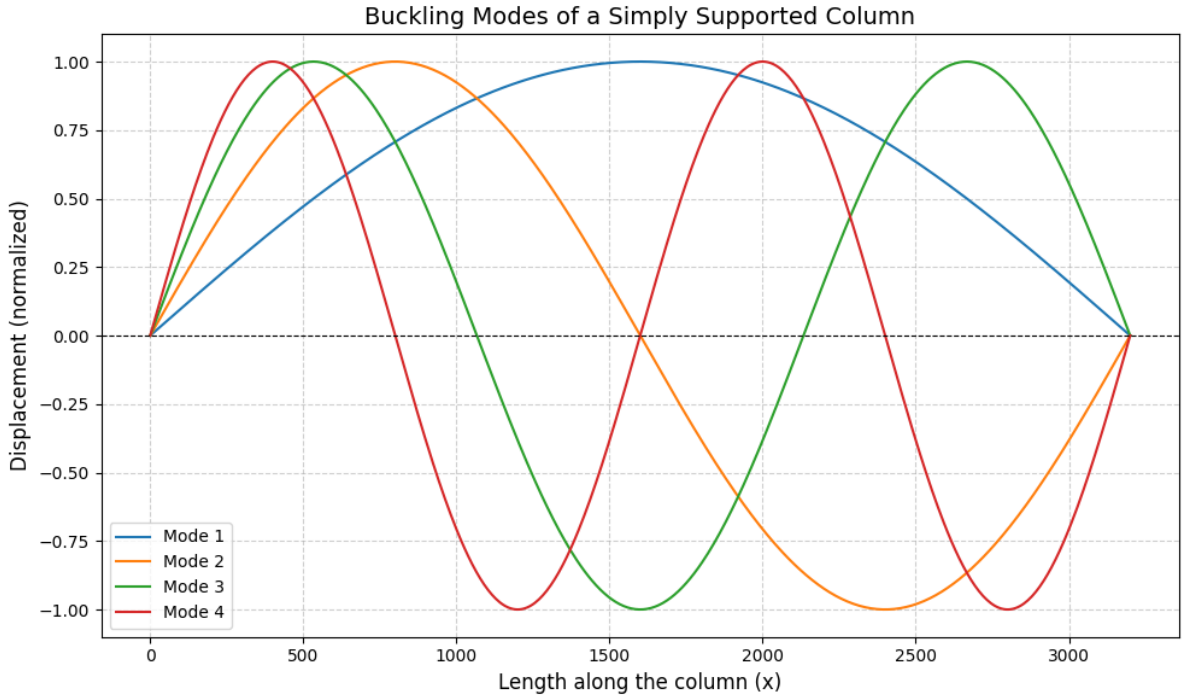

Figure 4.38: Buckling modes 1 to 4.

$$A_{min} = \frac{F_{AX}}{\sigma_{cr}} \tag{4.50}$$

$$A_{min} = \frac{210}{0.1} = 2100mm^2 \tag{4.51}$$

The tension and compression checks were conducted, to see how big should the connecting area be to support the tensile and compressive loads appearing. So, the more critical case is the tension, where a minimum area of 10500 mm^2 is necessary. This means, that over the 1020 mm wide panel a height of at least 10 mm is necessary to distribute the load without failing in tension for the core.

Table 4.14: Outer face loaded concluded results.

	x_{max}	z_{max}	V	gamma
	mm	mm	N	rad
Shear beam		0.094	6000	0.00084
Karamba	0.188	0.144	6000	0.00144
RFEM	1.0	0.3		
Test rig	0.178			

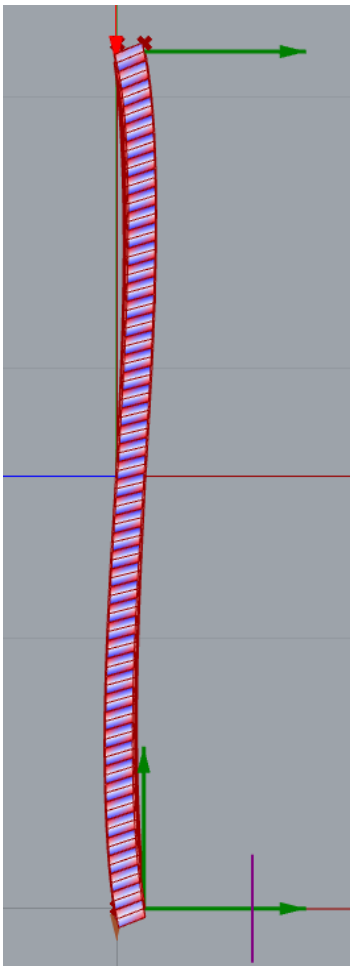

Figure 4.39: Outer face loaded Karamba3D model deformed shape.

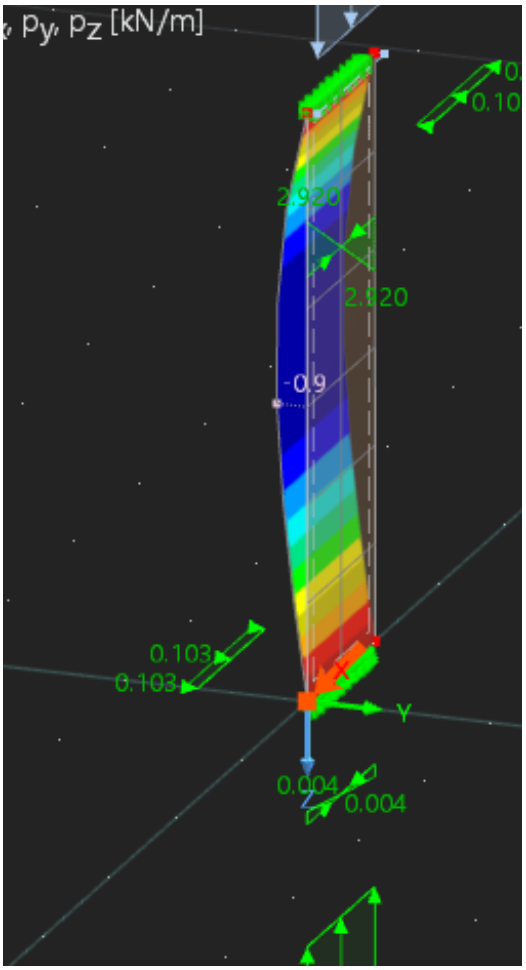

Figure 4.40: Outer face loaded RFEM model deformed shape.

The vertical movement for the experiment was not measured. Also, the panel was supported fully from underneath, so realistically, the modelled situation did not exist in the experiment.

However, the Karamba3D model did predict the shape of the deformed panel for test 2 with $(0.177 - 0.105)/0.105 =)$ 69% difference for the 65x65 mm beams model seen in figure 4.44. The top side of the panel was closer in result with $(0.188 - 0.178)/0.105 =)$ 6% difference in the deflection result. The RFEM model could not predict the deformed shape due to the supports placement seen in figure 4.42. By hand, this shape can only be predicted by the wrinkling equation conditions, but the wrinkling failure will not be the governing case.

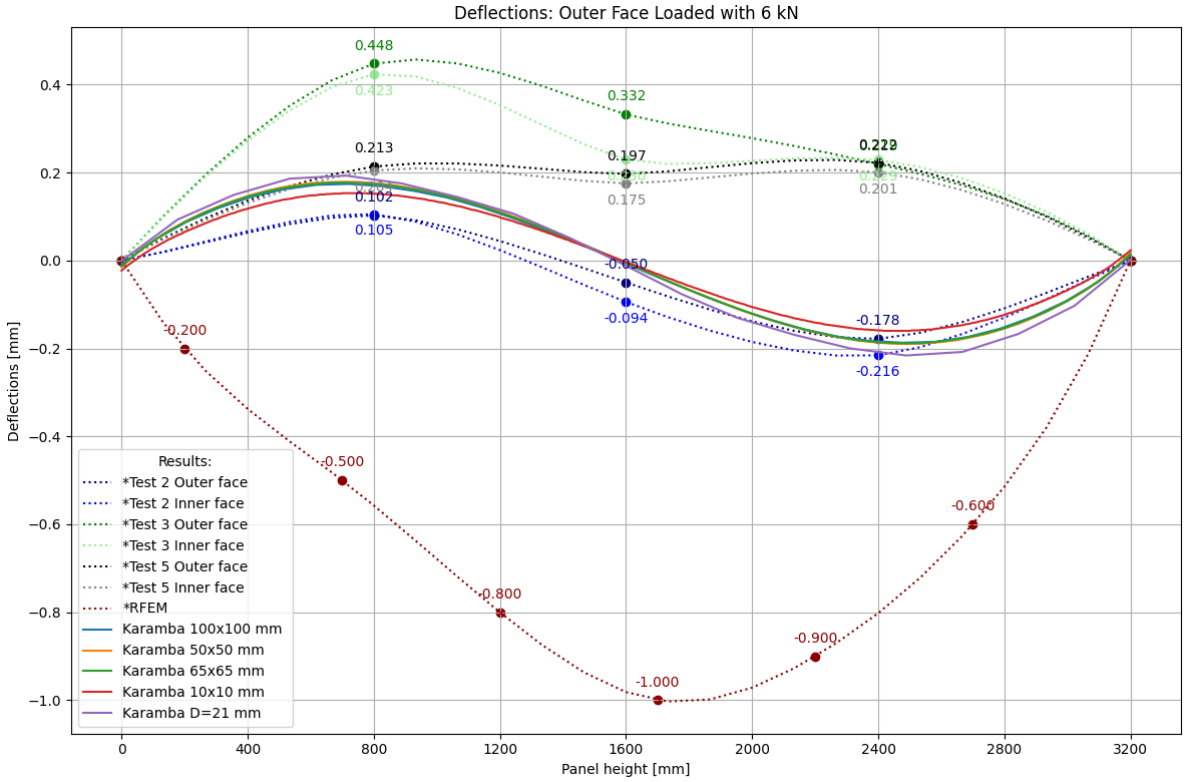

Figure 4.41: Deflections of 6 kN on the outer face.

The strains seen in figure 4.45 show that in the experiment the faces deformed separately, because the strain distribution is not linear over the cross-section. The RFEM model predicts very high strains which are almost twice the experimental results. The Karamba3D and RFEM model outer face strains are very similar to each other, but Karamba3D model also matches with the inner face inner experimental reading of 0.00006 mm/mm. The outer reading follows a linear distribution due to the ideal composite action in the model.

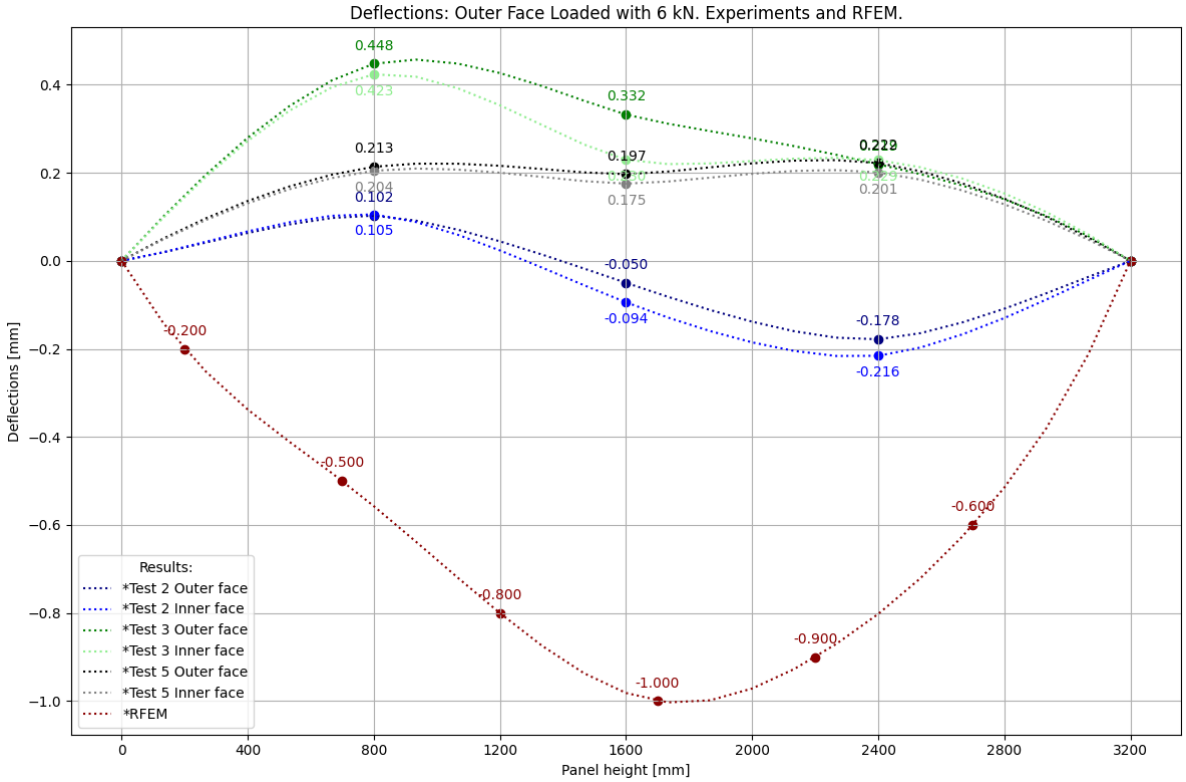

Figure 4.42: Deflections of 6 kN on the outer face - experiments and RFEM.

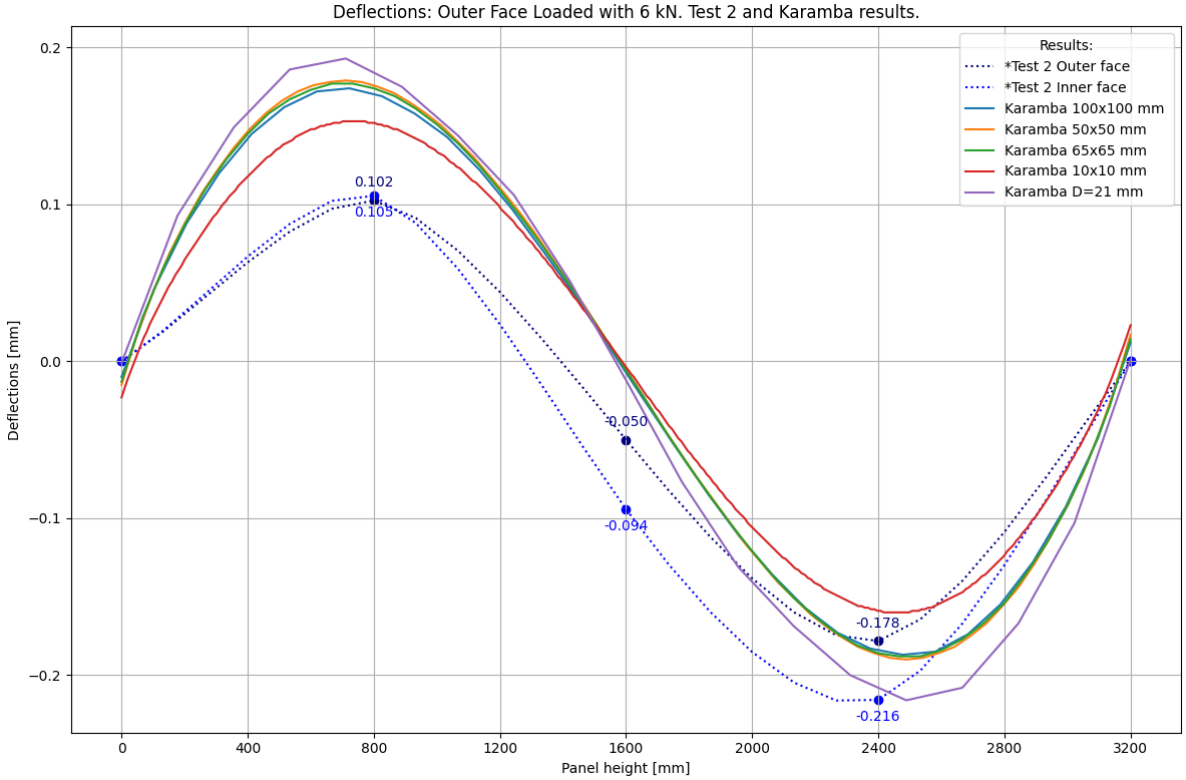

Figure 4.43: Deflections of 6 kN on the outer face - Karamba results and test 2.

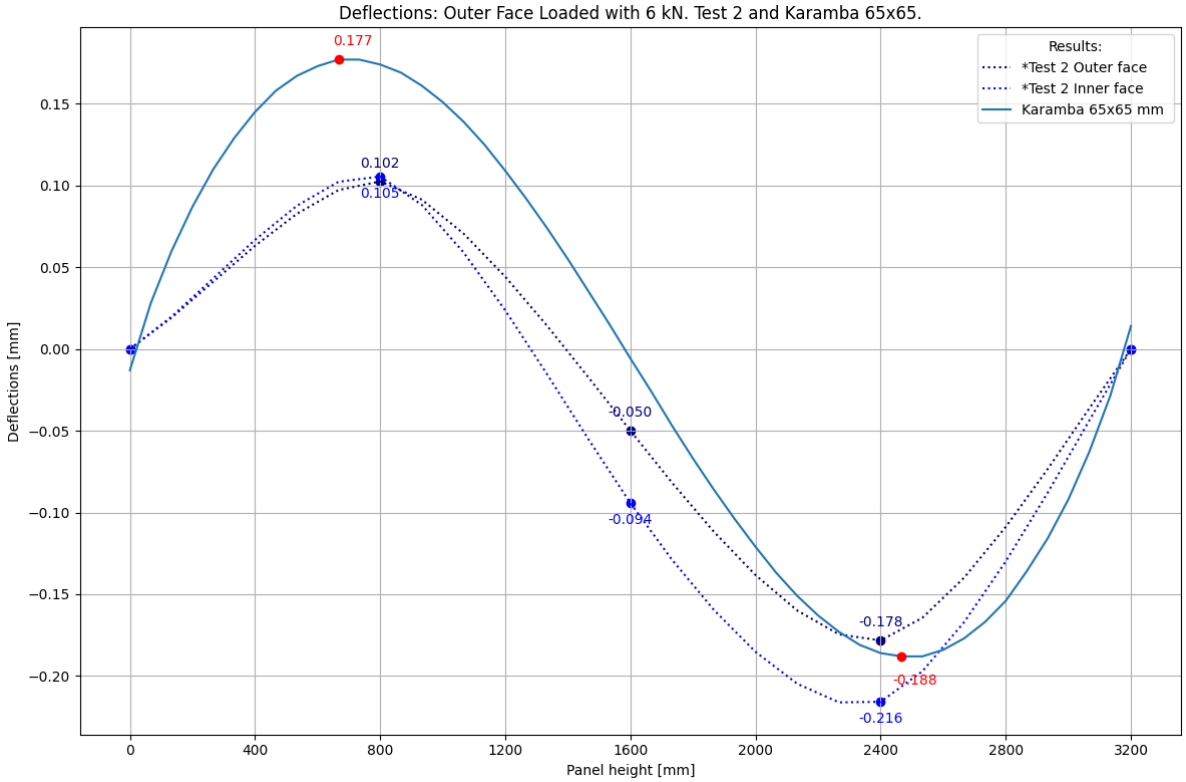

Figure 4.44: Deflections of 6 kN on the outer face - Karamba 65x65 results and test 2.

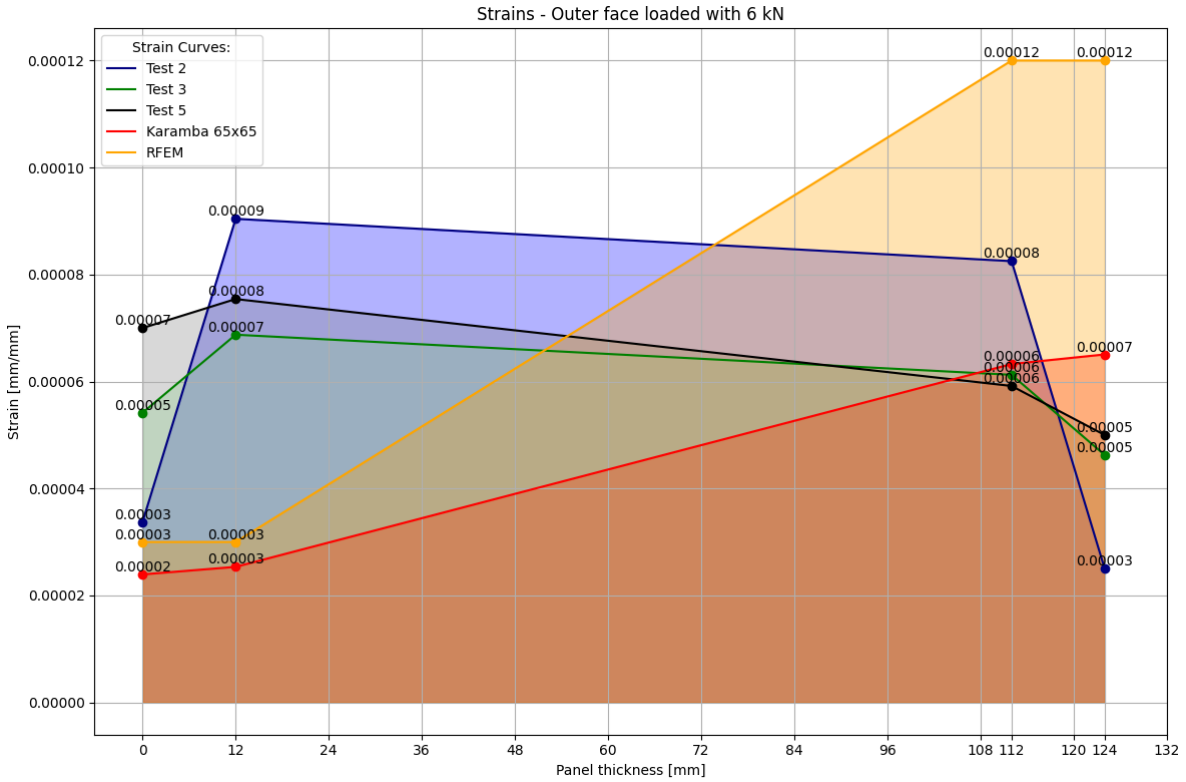

Figure 4.45: Strains of 6 kN on the outer face

4.6.3. Inner and outer face loaded

For the inner and outer face loaded case, two different loads were observed. First, F1=12 kN/m on the inner face and F2=6 kN/m on the outer face, and second, F1=F2=6 kN/m on both the inner and outer face which is presented in appendix F. The first loading case is described by a combination of Timoshenko beam equations and a rod in compression equations with experimental results and also results from both models. The calculation schematisation is seen in figure 4.46.

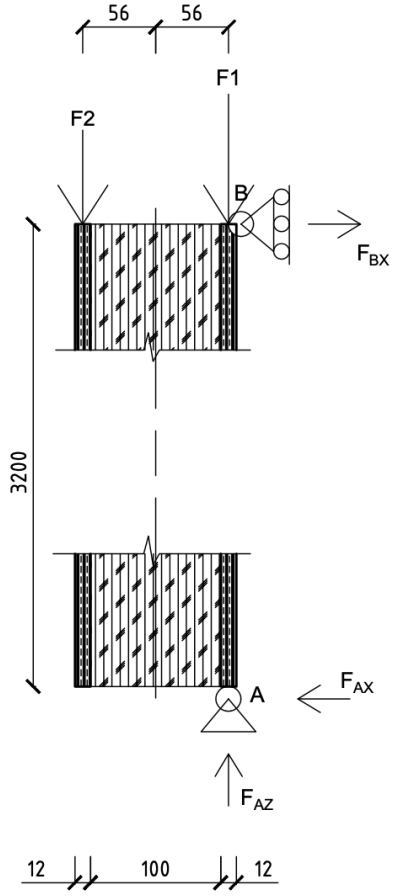

Figure 4.46: Loading on the inner and outer face.

The test results varied a lot for all of the experiment loading cases seen in figure 4.50, even though the same panel was tested and no failure was supposed to occur. Nevertheless, the difference between test 1 and test 5 deflections of 12 kN on the inner and 6 kN on the outer face vary by 44%. The first test deflections being much higher than the last test deflections which are the lowest. This can also be caused by the addition of top and bottom beam to connect the two faces, which would add a significant amount of stiffness to the panel and could explain the change in deflection results. The peak of the deflection results leans towards the top of the panel which could indicate a possible local failure position if higher loads are applied. This is also seen in the RFEM model results and Timoshenko beam equation results seen in figure 4.52. This would suggest that the RFEM model could possibly predict also the local failure spot on the panel if it were to occur as predicted visually. However, if the final (5th) test deflections are observed then the peak leans towards the bottom which can also be seen

Table 4.15: Inner face loaded with 12 kN and outer face loaded with 6 kN displacements.

	x	z
	mm	mm
timoshenko/rod	1.51	0.9
karamba	3.16	0.452
RFEM	2.2	1.2
test rig	3.489	

by the Karamba3D results. The Karamba3D model result or peak formation could suggest that maybe a more accurate prediction can be done for panels with top and bottom beam/plates. The Timoshenko beam equations do not reach the experimental deflections due to the boundary conditions. It is not possible to describe behaviour under axial loads, but in this case the load was applied with an eccentricity into the boundary condition, but should be multiplied by two to get similar results as the experiment or Karamba3D model. The RFEM model does show the deflection shape, but does not reach the measured deflections, presumably due to the support conditions definition. Therefore, if two faces are loaded, an experiment or the Karamba3D model could predict the deflection results most accurately.

The Karamba3D model iterations had minor differences in the deflection results seen in figure 4.51. The smallest deflection value was predicted by the 10x10 mm beams model. The rest of the models all showed a 3.15 mm deflection result. This shows that the axial loading case is not influenced that much by the beam size. The Karamba3D 65x65 mm model corresponded well with the average experimental result. A comparison is shown in figure 4.53 where the maximum deflection differs only by 0.12 mm which is 4%. Therefore, the Karamba3D model has good correspondence with the experimental results.

The strain results seen in figure 4.49 showed a separate behaviour from the faces as for the previous loading case. The RFEM and Karamba3D model showed a linear distribution, but the RFEM model suggested a higher strain result than the Karamba3D model. The RFEM model result was similar to the first test result where a possible creep behaviour might have occurred, but the Karamba3D model showed a more similar result to all the other experimental results, especially the inner face strains matched well.

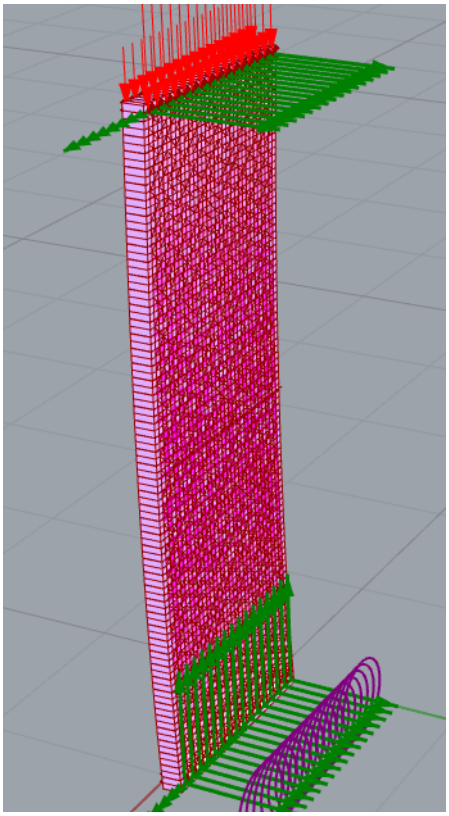

Figure 4.47: Case 3 Karamba panel.

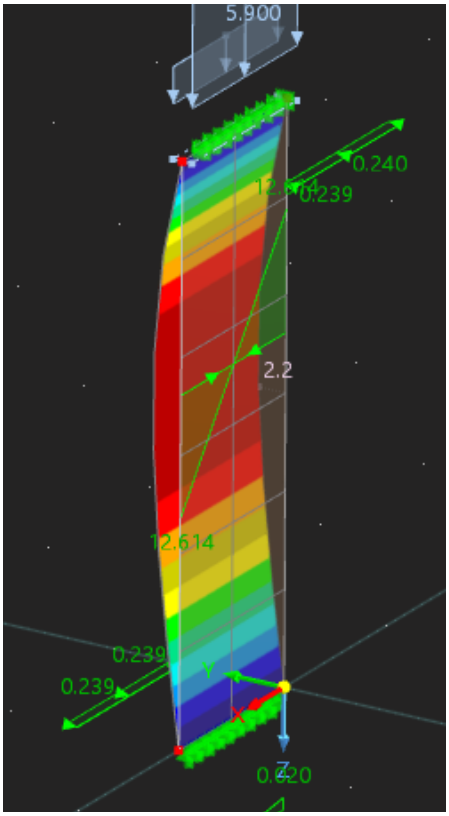

Figure 4.48: Case 3 RFEM model.

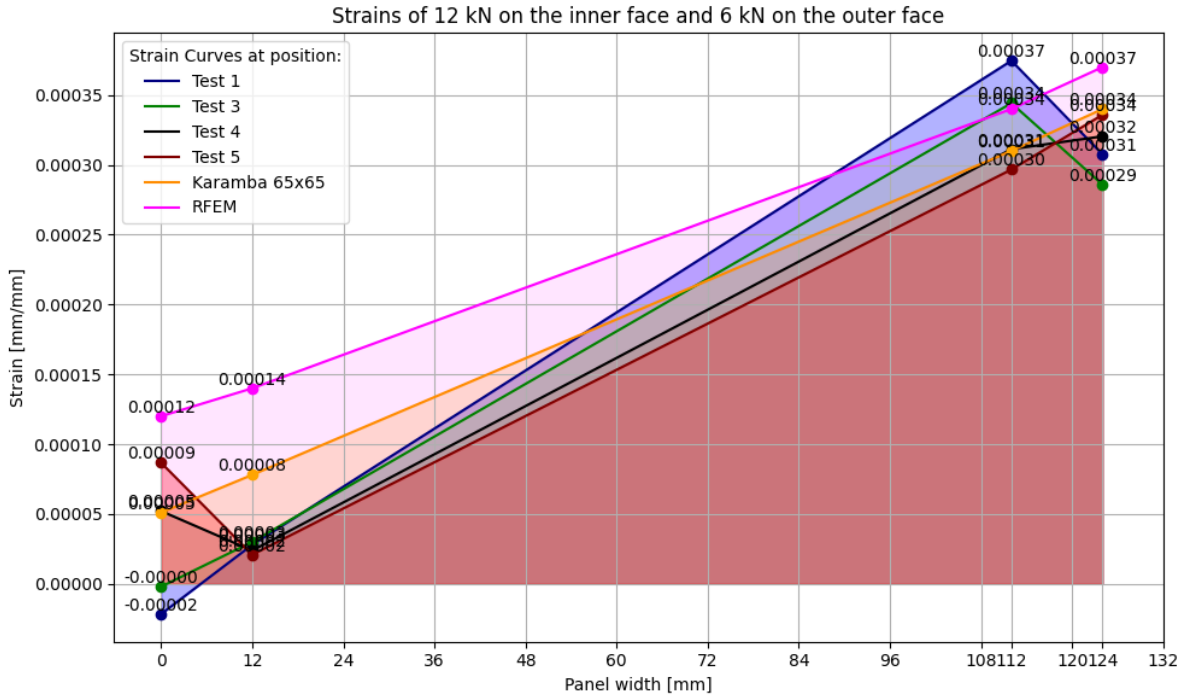

Figure 4.49: Strains of 12 kN on the inner face and 6 kN on the outer face (compression is positive and tension is negative).

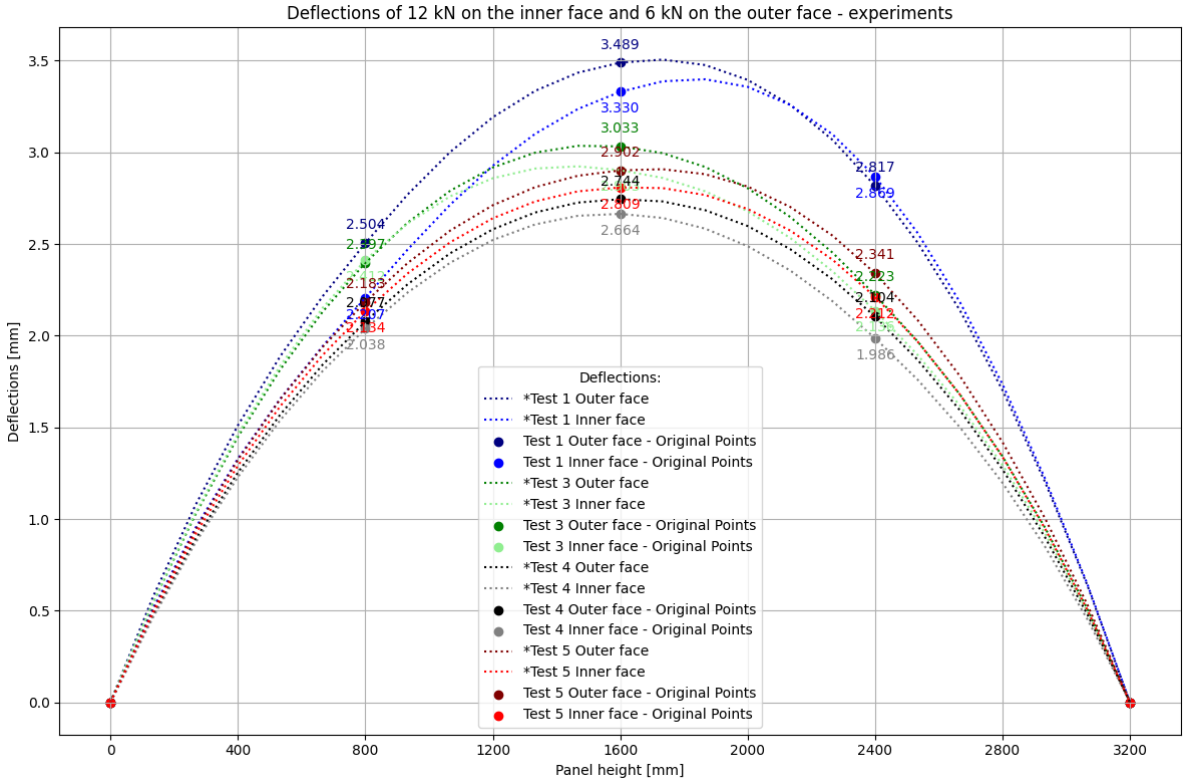

Figure 4.50: Experiments deflections of 12 kN on the inner face and 6 kN on the outer face.

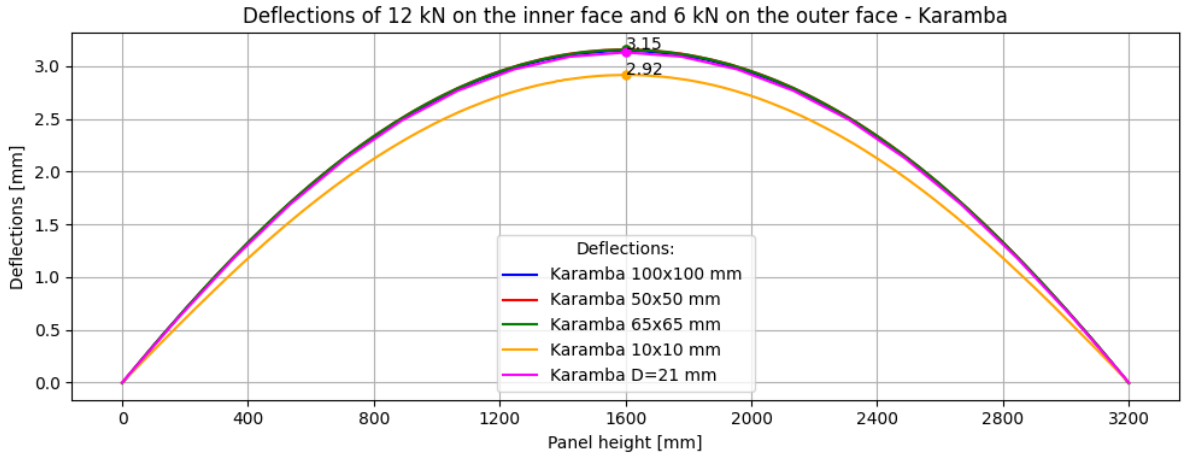

Figure 4.51: Karamba deflections of 12 kN on the inner face and 6 kN on the outer face.

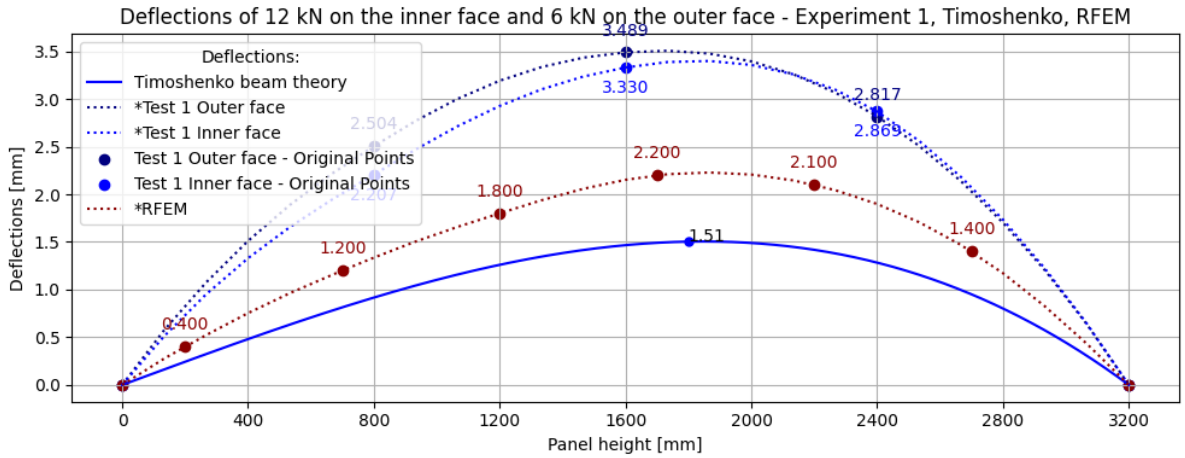

Figure 4.52: Experiment 3, Timoshenko and RFEM deflections of 12 kN on the inner face and 6 kN on the outer face.

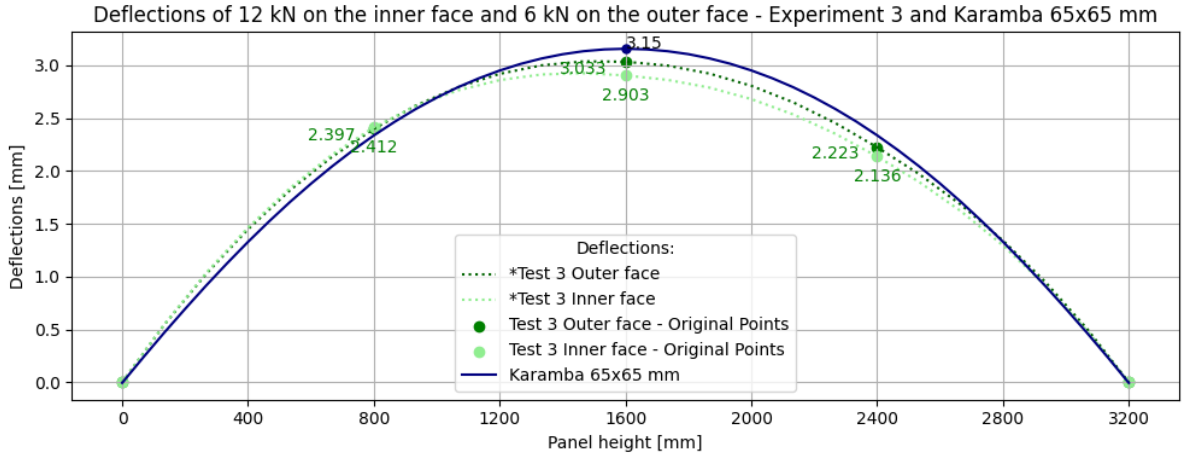

Figure 4.53: Experiment 3 and Karamba 65x65 mm deflections of 12 kN on the inner face and 6 kN on the outer face.

4.7. Conclusions

Based on the tests, models from Karamba3D, RFEM, and analytical results, it can be concluded that this panel with the combination of the given materials might not be a suitable option for construction applications. Firstly, looking at the test results, the core is unable to sufficiently support the faces making them resist the loads as single standing materials (for example when only the outer face is loaded). Secondly, the shear capacity of this panel is very low due to the core material properties, which makes it unsuitable for both floor panel or wall panel applications without significant additional stiffening. The only option to use this combination of materials in a structural insulated panel would be to add stiffeners which would have to be through the whole core. However, this would result in a traditional timber frame prefabricated panel. Therefore, based on the test results, it can be concluded that the Steico medium density fibre board is not suitable for sandwich panel applications due to its deformability and tensile/compressive strength properties. If this behaviour did not occur, then a possible option to increase the shear resistance of the panel could be to make the panel thicker, which would

give a larger shear area in the transversal direction, and would increase the lever arm between the two faces resulting in a higher bending stiffness.

The modelling methods could somewhat accurately predict the behaviour of the sandwich panel. RFEM model provides very good accuracy with transverse loads such as wind loads on the panel, but does not describe sufficiently the panel behaviour under axial loads. The developed Karamba3D model accurately predicts the panel faces behaviour under axial and transverse loading. If the core material behaviour is known through test results, then the core can be modelled as beams which need to be scaled first and can be used for future panel verifications. However, the governing situation to know the number of beams accurately is the transverse loading case, since for the other load cases all models showed a very similar result. The final version of the Karamba model has 16 beams in the horizontal direction and 49 beams in the vertical direction with the dimensions of 65x65 mm to represent the Steico medium density fibre board. The model should be further tested to verify its behaviour when the panel dimensions are changed, but could be used for further research on sandwich panels.

The experiment results had a lot of variance in them and suggested failure of the core or some delamination which resulted in the faces to have some composite interaction but mostly the faces were resisting the loads separately. The experimental results outcome could be improved by using a regulated testing method for SIPs. Additionally, the lack of knowledge about the core material properties cause a lot of uncertainty while interpreting the experimental results.

5

Discussions

5.1. Panel material and experiments

The panel core's Young's and shear moduli were unknown and were thus assumed based on other sandwich panel's insulation materials. The insulation material has lower strength properties than other commonly used core materials – tensile strength 0.1 MPa, compressive strength 0.02 MPa, and shear strength 0.04 MPa. The assumed Young's modulus and shear modulus fell in the range of other commonly used materials like EPS and PUR – for Steico insulation board the assumed values were E = 5 MPa and G = 2.2 MPa. However, the behaviour of a bio-based fibre panel compared to a foam is completely different, suggesting that maybe the assumptions should have been done based on a different material, but there were also some tested values for Steico insulation which gave an idea on where the range should be and the lower end of that range was chosen. There have been studies which tested first the core material which gives an insight on whether the Steico insulation could be considered for sandwich panel applications. For example, Santos et al. [46] tested PUR foam properties and found that the E modulus in tension and compression ranged from 7 to 15 MPa, and the shear modulus G was 3 MPa. Therefore, the shear modulus is very close to the Steico insulation material, but the modulus of elasticity is in some cases three times higher. The shear strength for PUR is 0.12 MPa [46] which is also three times higher than the shear strength of the Steico insulation board. Similarly, Yang et al. [53] tested styrofoam under compression which showed 0.35 MPa for the compression strength under 10% deformation which is 3.5 times higher than Steico, for tensile strength they measured 0.46 MPa which is 23 times higher than Steico, and for shear strength 0.13 MPa was measured, which is also 3 times higher as well as the previously discussed PUR foam. The shear modulus for styrofoam was measured as 4 MPa, and the Young's modulus was in the range of 20 to 24 MPa. Therefore, the shear modulus is almost twice as high as for Steico, and the modulus of elasticity is already 4 to 5 times higher. Rungthonkit [18] tested EPS, XPS and PUR insualtion materials (Table 2.4), which showed that EPS shear and Young's moduli are smaller than the Steico insulation panel values, although with a density of 29 kg/m^3 the shear modulus is higher than the shear modulus of Steico insulation panel. For XPS all shear and Young's moduli were higher – G modulus between 2.9 MPa and 6.2 MPa, and E modulus between 9.3 MPa and 26 MPa depending on the density of the product. PUR foam lower density insulation material has very similar properties to the Steico panel – E = 2.9 MPa and G = 2.8 MPa. Higher densities have higher moduli values. However, the biggest

difference with all of the materials is that the shear strength is at least twice as high as for the Steico insulation material. The highest case is for PUR foam which has a shear strength 15 times higher than the Steico insulation board. Additionally, foams exhibited densification under loads which increased the shear strength of the panel [46]. The discussed strength values show that the insulation materials commonly used are at least twice as strong as the applied Steico insulation material. Therefore, the E and G moduli are not as important in this case, but the strength properties should be improved. The large difference in the strength properties is most likely due to the fibres used in the Steico insulation material and how they are bonded together. They seem to be brittle and therefore have low strength properties. The material could be improved by either changing the polyurethane resin used to see if other resins provide a better bond, longer wood fibres could be used to increase the bonding ability of the material itself, or a more random direction for the fibres could be chosen to homogenise the material better. All in all, the material needs to be at least twice as strong in tension, compression and shear. Especially since the flexural stiffness "depends mostly on the core properties" [56].

The core material or the interface bond were the most likely causes for the separate behaviour of the faces during experiments. When the outer face is loaded, the faces want to behave separately – the trend is seen even if the inner face is also loaded in addition to the outer face. However, the separate behaviour occurred already during the first experiment after the inner face was loaded with 18 kN and no load had been applied to the outer face. This suggests that the panel was overloaded, but 18 kN is still a very low load considering that the critical global Euler buckling load is 125 kN. This situation was also observed by Vaidya et al. [52] where the theoretical Euler critical buckling load was around 3000 kN, but then delamination occurred at 18 kN. The delamination was also described by Abbasi et al. [9] and Mousa et al. [45]. This could suggest that a similar phenomenon occurred during the analysed experiment which was not expected. Vaidya et al. [52] concluded that the delamination occurred due to the eccentric loading which caused higher shear stresses at the interface. This could suggest that centric loading could avoid the delamination from occurring, but would need to be further verified through testing. Mousa et al. [45] elaborates that the delamination occurred "because the out-of-plane interfacial stress exceeded the core tensile strength", and in a previous study Mousa et al. [55] found that delamination occurs with soft core materials under transverse loading. Therefore, this might still be the failure mode under transverse loading, even if the delamination is avoided with centric axial loading.

The delamination or lack of bond theory is supported by the loading case where the outer face is loaded with 6 kN (Figure 4.35). In experiment 2 the expected sinusoidal wrinkling shape is seen, but for experiments 3 and 5 the faces start to deform in the third Euler buckling mode which suggests the faces working on their own. This could be caused either by failure in the core, the core's deformability and inability to sufficiently support the face or a low bond between the faces and the core (either delamination or lack of bond from the beginning). The failure of the core could be suggested based on deflections of experiment 1 where the inner face was loaded with 6 kN (Figure F.3) in the beginning and end of the experiment. The deflection results are significantly different from each other. The first measured case shows how the faces deflect together and with a normal first Euler buckling shape. However, the second measurement shows how the faces do not deform together, they have an almost 0.4 mm difference which suggests core tensile failure according to the characteristic strength value of the core. Showing a significant decrease in the composite action of the panel. However, the

mean value would be attained if the characteristic value is multiplied by 1.65, yielding the limit to 0.66 mm. Therefore, it can be argued that it is not failure but just the deformable nature of the core, but in that case the first measurement should have also showed different behaviour of the faces compared to each other. The last possibilities for the separate behaviour of the faces could be the delamination discussed earlier or the lack of bond between the faces and the core from the manufacturing process. This was studied by Jacques et al. [11] where they found that a bond percentage of less than 60% resulted in a separate behaviour from the faces which significantly reduced the axial resistance of the panel. Therefore, it could be a possible cause for the behaviour of the panel, especially when considering the brittleness of the material and the fibre surface characteristics. If this is the case, a change in the application of the glue should be made or different glues should be tested to compare the bonding strength and percentage. Lastly, it could be argued that maybe it is normal for structural insulated panels to have such a difference in the two faces' behaviour since insulation materials are deformable, but Pokharel et al. [51] reported that "there was no relative movement between the core and the faces under the loading". Suggesting that the assumption that maybe the movement is normal is not likely. Thus, the bonding percentage should be investigated.

The adhesive is another unknown factor that was not considered in this research. The assumption was that the adhesive is strong enough that debonding failure could not occur. However, the test results now suggest otherwise. It has also been suggested in earlier studies that the adhesive plays an important role when the panel is buckling, and a comment for moisture resistance was made with an addition for the durability over the service life of the panel [18]. Additionally, in some cases, the insulation in the SIP is made up of multiple boards within the panel, but these disconnected boards should also be glued together, because if not, the panel strength could be reduced up to 20% [10]. This was not an issue in the panel analysed here, but should be taken into consideration when larger production quantities are made, and these kind of situations could occur.

The type of the insulation material also influences the failure mode. Jacques et al. [11] described that if the insulation material was a board then the failure was due to the face sheet of the panel, but if the insulation was blown foam the failure mode was due to core shear. This could suggest that since the analysed panel has a board insulation that the main failure method under axial loading would be face crushing. Even though failure tests were not performed, the experiment results so far would indicate a delamination failure. For quite a few OSB faced panels, end bearing was the main failure method which was followed by delamination [54]. Additionally, the core density influences the panel's deflections, but will not affect strains in the panel's faces [45]. This could suggest that the delamination occurs together with the end bearing failure, since it is possible for multiple failure methods to occur together. Rake [39] stated that "to prevent coupled instabilities, the compression stresses in the face sheets have to be lower than the wrinkling load of wrinkling case I – rigid base." Additionally, the strains in the face sheets also create higher stresses at the interface resulting in delamination [45].Therefore, to rule out a double failure mechanism, the wrinkling for rigid base should be calculated.

The deflection graphs started to show a trend where the deflection curve peak tilted to the bottom or to the top of the panel. This also seems logical if the deflection graphs for the outer loaded face are investigated which show that there is compression and tension occurring in the core at the top half and at the bottom half. These results suggest that a local failure might occur at those spots. Delamination at the top half of the panel was also observed by Vaidya et al. [52].

Therefore, it is highly likely that if the panel were to be tested for failure, a delamination would occur at the top half of the panel with a possible OSB bearing failure as dicussed earlier.

An unknown factor in the test set up could also be a possible cause for the separate behaviour of the faces. Firstly, the same panel was tested multiple times since the loads applied were far from failure loads and it was not expected to have any form of failure. Second, there were no regulated test instructions followed, which makes it difficult to know the reliability of the tests following the first one. Thirdly, the end plates for the panel were applied between the fourth and the fifth test, which could explain the lower deflection results, since end plates increase the strength of the panel according to Jacques et al. [11], and additionally cause delamination between the core and the faces while the end plates were applied. These could also cause additional human errors which could influence the experiment results. Fourth, the eccentric loading could have caused the faces to presumably delaminate from the core. Therefore, assuming no eccentric loading is applied, the separate behaviour of the faces might not occur. This theory should have to be confirmed through experiments, since there were no failure experiments conducted, and the RFEM and Karamba3D models do not describe the interface delamination. In order to model that failure mechanism DIANA or ABAQUS could possibly be used. If the separate behaviour of the faces still occurs with centric loading, then only through-thickness stiffeners can be used to make the panel suitable for construction. However, in that case the insulation material will not carry nor transfer any loads, and the panel would not be considered a sandwich panel anymore, but rather a prefabricated timber frame panel. Fifth, there could also be an effect from the initial slack which could mean that the whole panel has to still shift into place. Jacques et al. [11] observed that the initial slack was overcome only after 50 kN loads were exceeded. Lastly, relative humidity could have had a significant effect on the experiments. OSB is very susceptible to moisture effects, the insulation material is made of wood fibres making it also susceptible to any moisture, and finally the adhesive needs to be durable for moisture effects. The moisture content in the air was not measured, and can not be determined anymore, but the test set up was in a warehouse which was not heated. All of the points mentioned here can be accounted under uncertainty in the experiment which could have caused the delamination or the core failure.

The panel in this form is not suitable for use in construction. If the separate behaviour of the faces is disregarded, then the shear strength of the core will be governing in transverse loading cases – for the panel simplification equations the distributed transverse load can be maximum 1.43 kN/m, the Karamba3D model predicts maximum utilisation at 2.8 kN/m, RFEM at less than 0.1 kN/m, and Timoshenko beam equations at 2.5 kN/m. These are too low to take on any wind loads, hence the shear strength would need to be improved. One method for that would be increasing the core thickness to add more shear area in transverse direction. This is also supported by Santos et al. [46] and Jacques et al. [50]. However, this can only be done if the previously discussed delamination or core deformability is disregarded or does not occur.

5.1.1. Creep

The strain measurements in the experiments suggest that there could be creep occurring. In these tests, only primary creep could be happening since the experiments are relatively short (maximum 17 minutes). The strains increased under the same loads within the same experiments. However, the creep coefficient was not big enough to explain the whole increase in deflections and strains. This suggests that permanent deformations could have occurred in the

faces, although the loads were not as high as to cause any failure. Creep behaviour for sandwich panels has been described by multiple earlier researches. Rungthonkit et al. [18] and Yang et al. [42] all concluded that creep deformations are continuing at a constant rate. Yang et al. [42] saw a doubling in creep deflections over three months. Mousa et al. [45] and Vaidya et al. [52] said that there was a permanent deformation of the panel after unloading. However, Kremani et al. [10] and Rungthonkit et al. [18] stated that the permanent set recovered over some time, where Rungthonkit [18] stated that the speed of recovery is slower than the speed of creep, but only a 87% recovery was measured at the end of the experiment. Additionally, OSB creep depends on relative humidity and its moisture content [18], and since the insulation material in this case is also bio-based, there are high chances that this also has a correlation between relative humidity and creep. The creep should be measured for the whole panel to extract creep coefficients that would be useful for further design. Rungthonkit [18] found that the design creep deflections were much higher than the actual creep deflections measured for a test spanning three months. Therefore, creep does not have a high significance in this thesis, but should be investigated for long-term load applications.

5.2. Models

5.2.1. Karamba3D model

Now, in addition to ABAQUS, DIANA and many other FEA tools, it can be concluded that Karamba3D can be "tricked" into successfully predicting the behaviour of a structural insulated panel. Karamba is a very effective way of modelling and analysing the behaviour of a structural insulated panel. Eventhough the modelling of layered materials is not possible on Karamba, the method of using equivalent beams to model the core proved to be relatively accurate in predicting the global behaviour of the panel if normal core behaviour would have occurred in the tests (so no separate behaviour by the faces). The Karamba3D model was scaled based on the Timoshenko beam equations and RFEM panel model. The deflection values for transverse loading differed from the analytical Timoshenko beam equations by 2 % under higher loads, but under lower loads the difference increased to 18%, but still showed a larger deflection result than analytical results, so the design would be on the safer side if the model would be used. There were some differences where the Karamba3D predicted deflection was smaller than what was experimentally measured, but this is most likely due to the "ideal" conditions in the model and the uncertainties in the experiment. It could be argued that the Karamba3D model is not accurate due to the way the core is defined, and there are no failure tests done to actually prove the failure results. Additionally, the Timoshenko beam equations used to scale the model might not be accurately describing the panel, leading to a too low of a deflection result which would yield the model unfit for use in transverse loading cases. In addition, the RFEM model which was also used for scaling does not describe the interface between the two materials, thus can not accurately predict failure, which would make the transverse loading case even less trustworthy. However, for the axial loading cases the experimental results are used for comparison. Therefore, it can only be said that the axial load cases can be analysed with the Karamba3D model with complete certainty, but precision could be added to the model by testing the panel for transverse loading.

The model's calculation time increased with the increase of the number of beams used to model the core. The final version of 65x65 mm beams has a reasonable amount of elements, limiting the calculation time to a few seconds if changes are made.

The model could be improved by further trying to scale the beams of the core material. As seen previously during the calibration process, a bigger beam dimension resulted in a stiffer panel showing smaller deflections, and a larger width between the beams resulted in a less stiff panel. In order to additionally adjust the deflection results, maybe a smaller beam dimension could be used or a smaller mesh size. Presumably, a finer mesh could possibly result in a better match between the experimental results and the Karamba3D results due to having more calculation points in the FEA model.

The core material was defined incorrectly for the panel analysis by defining the shear modulus as 22 MPa due to the units defined by Karamba3D. This material was used for the scaling process for the main analysis part of this thesis. The magnitude of the shear modulus was changed for the Karamba3D analysis chapter, but the beam dimensions were kept the same. This error resulted in showing that the shear modulus has a significant effect on the deflections, and the modulus of elasticity has a smaller influence on the deflections. This was also stated by Rungthonkit [18] with an addition that the shear modulus of the core has an even higher influence on the deflections than the OSB faces. Due to the error in the magnitude of the shear modulus, the deflection results are larger when the material is defined correctly. Therefore, an additional scaling should be performed to again describe the behaviour of the panel and to compare to the experimental results. Although, the method still remains valid and can be used for further research. Additionally, the correct definition of the core material allowed the model to also predict core shear failure through the utilisation percentage of the beams representing the core, but this would need to be confirmed by bending tests.

To accurately describe the failure modes of a SIP, a non-linear analysis should be performed using another modelling method since karamba3D is not suitable for that purpose. The analysis that was performed was linear elastic analysis. It can not show any additional densification of the core material or a local failure in the faces. Smakosz et al. [56] agreed that a linear elastic approach is not sufficient to describe the failure of a SIP. However, SIPs follow a linear elastic behaviour up until shortly before failure where a non-linear behaviour is observed which is fast followed by an abrupt failure [53], [11], [45], [57], [39], [9].

The Karamba3D model could show strain results which matched with the experimentally measured strain results. However, the biggest difference is that the strain results from the model were linear, but the strain results for the experiments were often not linear and showed a separate behaviour by the faces. The interface definition of the Karamba model is the limitation where a perfect connection is assumed. The connection can transfer all forces – shear, axial, bending. Although, the connection could be defined as a spring to possibly more accurately describe the interface conditions. This is worth looking into.

The face's failure can be predicted since the strain results measured on the test rig matched with the strain results of the Karamba model. Additionally, the stress results for the faces were equivalent for what was expected analytically. Thus, it is a very effective method to model sandwich structures if the core behaviour can be modelled accurately, which in this case was achieved thanks to test results. Even if test results are not available, then the correct amount and size of the beams had a significant effect only on the transverse loading cases, making axially loaded analysis results still valid.

The support conditions were chosen to analytically model the panel. The assumption of the inner face mainly supporting the full panel and the outer face supporting the inner face was

made. Therefore only the inner face was supported. The top supporting condition was based on the real construction situation where the panel has loads coming from the top floor beams which are applied with an eccentricity since the joist hanger is the more common floor beam connection system. The floor beams would then provide support in the transverse direction of the panel. The panels next to the single observed panel would then support the panel from the sides, restricting any translations and rotations towards the sides. However, the vertical translations were unrestricted. The bottom had similar conditions with the addition that vertical movement is restricted due to the foundation. This was only applied to the inner face whereas in reality the outer face is also supported. This could also be a point where the results could become even more precise if the outer face was also supported.

The failure load according to the material utilisation for the Karamba3D model was lower than the Euler buckling load calculated analytically. The more critical case was when the outer face was loaded. The model would suggest an end bearing failure – OSB bearing failure. End bearing failure is very common for OSB faced panels [18], [53]. End bearing failure is usually shortly followed by delamination. The model suggested lower failure value could be due to the eccentric application of the load. Mousa et al. [48] found that the eccentric failure load was 35% smaller than the Euler buckling load due to eccentricity. In this case the axial failure load is 30% smaller than the Euler buckling load. This is only according to the model and should be further tested on the real panel. The panel can also fail by a combination of failure modes, but the model is not able to predict that.

Load combinations lower the load bearing capacity of the panel. The rate of decline for the transverse loading capacity was 8% according to the karamba3D model when an axial load of 6 kN and 12 kN was applied and then the transverse load was analysed for the serviceability limit state. Rungthonkit [18] observed a similar trend. The bending capacity reduces as an axial load is applied [57]. Kermani et al. [10] stated that if bending is the dominant loading case, in combination of axial loads, the panel resistance is overestimated. However, in most cases the governing factor is the serviceability limit state [18].

Yang et al. [42] found that serviceability limit state was the governing condition when testing OSB faced sandwich panels for a four point bending test. The panel at the deflection limit was only using 15% of its resistance, which was also the case for a mini-SIP connection. However, when a timber connection beam is used, then the utilisation was 20%. This is also the case with the Karamba3D model. Before a failure can occur, the 21.3 mm serviceability limit is reached, where the faces use only 19% of their resistance. The axial load for SLS is 74 kN, and the transverse load for SLS is 1.12 kN/m. These are significantly lower than the failure loads. Therefore, in general design, if failure modes do not need to be accurately described, the model can be successfully used in the design process.

5.2.2. RFEM model

As well as the Karamba3D model, the RFEM model can not describe the interface between the faces and the core. The RFEM model has additional limitations. First is the fact that the panel is defined by one single shell element and the material is defined within that shell. This assumes a perfect material as the core which does not describe the faces movement as the experiments show nor as the karamba3D model exhibits. Additionally, the supports can not be defined eccentrically as was modelled for the Karamba3D model. this however, should not be an issue since in the real experiment the whole bottom is supported. Nevertheless, the model is

not able to show the sinusoidal anti-symmetrical wrinkling shape when the outer face is loaded. This is most likely due to the top support which is also supporting the whole top part instead of the inner face only. However, there is a slight trend that the RFEM model shows, which is where the local failure of the panel could occur in real life due to the eccentric loading. This is most likely realised due to the eccentric load application.

The axial failure loads were very similar to what the sandwich panel theory predicted – 125 kN. The transverse loading failure case was predicting failure already at 0.1 kN/m. This is most likely due to the safety factors used in the programme. For the loads, it is still possible to see how far the actual load value is, but for the material failure it is not possible to see the characteristic failure values. The model can predict failure through instability warnings but it does not specify in which material the failure occurred. Similarly to the Karamba3D model, the RFEM model can not predict local failures nor interface delamination.

5.3. Experiments vs modelling

In the scope of this thesis no failure testing was conducted, therefore it is difficult to conclusively state if the modelling methods predict a higher resistance than the panel actually would have experimentally. However, it can be stated that analytical methods did predict a higher resistance than the models showed. Therefore, it can be said that analytical methods do predict a higher resistance for this bio-based structural insulated panel than FEM tools predict. This could suggest that analytical methods do predict higher resistance for SIPs than experimentally occurs. This was also found by multiple studies by Fathi et al. [17], Smakosz et al. [47], Pokharel et al. [51] and Kermani et al. [10]. There is a high possibility for coupled instabilities to occur, but this would also need to be experimentally tested, and multiple analysis methods should be used [39], [49].

The wrinkling sinusoidal shape is only seen when the outer face is loaded due to the top support conditions of the karamba3D model and in the case of the experiment, the top inner face was also supported by the loading beams – holding the inner face in place and not allowing it to deform outwards or inwards. It would be interesting to change the inner face's constraints and then perform tests.

The effect of eccentric and concentric loading should be investigated – how much should the Euler buckling load be decreased. According to the Karamba3D model, the load bearing capability is 30% smaller than analytically calculated. Vaidya et al. [52] found that it is 40% smaller in eccentric loading, and Mousa et al. [48] found it to be 35% lower. Therefore, failure tests would bring more insights into the topic.

The models can predict the panel behaviour as long as it stays in the linear behaviour. Timoshenko beam theory has been found accurate in some cases as well [46] which gives reasonable credibility to the results, especially considering that the axial loading deflections had a good correspondence between the Karamba3D model and the experiments.

Rungthonkit [18] had an interesting statement saying "that SIPs have a high degree of capacity reserve since the design load allowance is well below the onset of failure load". This probably is not the case with the panel analysed here. It does seem that the design loads are quite near to the failure loads, if the behaviour of the panel is observed within this thesis.

5.4. Additional points

5.4.1. Openings

Openings were not under investigation within this thesis, but they do have an important place in residential building design. Starting from small openings for outlets and ending with big window openings. A small outlet can already cause the panel to lose 17% of its resistance capabilities [11]. The stiffness of the panel reduces and the effective area working in compression and tension is decreased with any opening leading to an increase in stresses. Therefore, it is very likely that a face bearing failure occurs on the same line as the opening, although the design service range is not really affected by the opening [11]. Therefore, it is probably not necessary to strengthen the small openings locally. However, the failure mode might change due to the presence of an opening – debonding without openings and flexure-shear with openings [18].

5.4.2. Connections

Connections were also not under investigation in this thesis, but they can have a big influence on the panel behaviour. There are multiple ways how to construct a panel to panel connection – mini SIP, small dimensional timber connection and a big dimensional timber connection. The joint could be a weak point in the structure where water could penetrate through [11]. Additionally, depending on the joint type, it can significantly improve the deflection result – dimensional timber connections have the best improvement in results [18].

5.4.3. Fire safety

This panel does make a step towards a more sustainable future, however as is the problem with most bio-based materials, they are very flammable. This issue should be addressed for this panel. Very often timber is impregnated with fire proof substances, but these make it very hard to reuse or recycle the same timber material. Therefore, another option could be to cover the panel from inside and outside, but that would not stop the spread of the fire once it has breached the fire proof layer.

5.4.4. Regulations development

There are some guidelines on how to design with SIPs. Most commonly used is the Easie guidelines [35]. There is a big variance in the behaviour of the panel depending on the material and the difficulty in creating one big code is evident. In some cases the sandwich panel theory equations are more or less accurate, but mostly for OSB faced panels the equations overestimate the resistance. Already assigning right creep coefficients should be done depending on the material combinations. Additionally, having multiple failure methods which exhibit non-linear behaviour make the analysis difficult [56].

There are some norms on how to find creep coefficients or how to test sandwich panels materials. BS EN 14509 - Cl. A.6.5 for creep coefficients [18]; BS EN 14509 – tension tests and BS EN 12090 – double shear tests [54];

A modelling tool would significantly simplify the design of SIPs [45]. A combination of loads can not be analysed with the available methods yet [18]. This has been an obstacle in the design of SIPs where it is difficult to prove the reliability of a product [18], [11].

6

Conclusions

This thesis analysed and modelled the novel Kingspan Unidek panel behaviour with four different methods. The research questions of interest are brought out below and will be answered in this conclusions chapter.

Main question

> **What is the out-of-plane behaviour of the novel Kingspan Unidek bio-based panel under axial and transverse loading, and how can analytical and numerical methods be used in the design process?**

Subquestions

1. What is the correspondence between experimental and modelling work?
2. To what extent is analysis possible with parametric tools for SIPs?
3. What is the best method to predict structural insulated panel behaviour?

What is the out-of-plane behaviour of the novel Kingspan Unidek bio-based panel under axial and transverse loading?

The panel exhibits a failure under the experimented axial loads which can most likely be attributed to delamination or a failure of the core. This was unexpected since the global buckling load was supposed to be governing under axial loading, and no failure was expected to occur. The analytical global buckling load was 125 kN, which was also confirmed by the RFEM model results. However, the Karamba3D model only allowed 87.8 kN on the outer face as an axial load, and 91.6 kN on the inner face while predicting OSB/3 compressive failure. The experimented axial load under which a probable delamination or core failure occurred was 18 kN on the inner face. This could have been caused by the eccentric load application. This was concluded based on the observed separate behaviour of the panel faces.

The panel's deformed shapes are different depending on the application of the axial load – load on the inner face causes a normal first Euler buckling shape, but if there is already 6 kN applied to the outer face, the buckling shape turns into an anti-symmetric sinusoidal curve. This is due to the top support conditions for the experiment.

Additionally to the experimented axial loads, the analytical calculations showed that the transverse loading case would cause shear failure of the core very early, yielding the panel unsuitable for use even for wind loads – panel theory 1.43 kN/m; Timoshenko beam theory 2.5 kN/m; Karamba3D model 0.29 kN/m; RFEM model <0.1 kN/m. Therefore, the panel is not suitable for construction purposes due to the core material and the possible delamination. The only possibility to use this panel would be to significantly improve the core material or to use full-thickness timber stiffeners that connect the inner and outer faces which would allow the loads to be transferred without loading the Steico insulation board to avoid damage.

How can analytical and numerical methods be used in the design process?

The Timoshenko beam equations proved useful to describe the transverse loading situation, and had a good accordance with the RFEM model. The Karamba3D model which was scaled based on the Timoshenko beam equations successfully described the experimental results albeit with minor differences. None of the methods describe the delamination failure since none of them model the interface between core and skin, assuming a perfect bond.

The stresses, strains and deflections can be accurately predicted with the Karamba3D model. All of the methods describe the linear behaviour and do not show non-linear behaviour nor failure situations, but they do predict failures based on the utilisation percentage, setting a constraint, or through instability warnings. The Karamba3D model was most successful in describing the behaviour of the panel, and could be used for design purposes where mostly serviceability limit state is governing. The RFEM model is best for transverse loading cases, but can not predict the behaviour under axial loading. Local failures can not be predicted with any of the methods.

What is the correspondence between experimental and modelling work?

The developed Karamba3D model successfully described the behaviour of the panel under both axial and transverse loads compared to the experimental results. This is considering the experimental results where no big deviations from the mean were observed. The RFEM model could only show good agreement under transverse loading, and could not predict axial loading behaviour. Although, it did show some trends towards where a local failure might occur. The analytical calculations most likely overestimated the load bearing capacity of the panel compared to modelling results, and could not predict local failures. The separate behaviour of the faces in the experiments was not predicted by any of the methods.

To what extent is analysis possible with Karamba for SIPs?

Karamba3D can successfully describe the structural insulated panel behaviour under axial and transverse loading. It can predict global failure for both the faces and the core based on the utilisation percentage of the material. It can show the correct deformed shape and give stress results which were analytically predicted. It can not predict local failure, nor can it describe the interface between the faces and the core. Therefore, delamination can not be analysed with this model. So, this model should be used when the general failure mode is known and preferably not for failure analysis, but for design purposes on limited stress and strain levels in SLS load combinations.

What is the best method to predict structural insulated panel behaviour?

The work seen previously suggests that the most accurate panel behaviour prediction can only

be achieved through experimental results. Experimental work should be carried out at different scale levels (material characteristics of the separate layers, interface experiments to investigate the bond, full-scale in- and out-of-plane global behaviour). However, if testing is not possible, then a good understanding can be given by the Karamba3D model and analytical sandwich panel theory calculations. Overall, a combination of multiple methods can give a thorough understanding of the panel behaviour.

7

Recommendations

7.1. For Kingspan

7.1.1. Panel development

Compared to conventional polymer-based structural insulated panels' core materials' strength properties, the Steico insulation material is quite weak. The panel's core material should be improved for tension, compression and shear. The fibres could be made longer to increase the material strength, the fibre orientation could be made more random to increase material homogeneity or another resin could be used for the binding agent. In the case that the material is not improved, only through-thickness stiffeners could be used to use this panel in construction applications. Alternatively, the stiffeners could be made discrete to reduce the thermal bridge effect.

A delamination test should be performed. If delamination was the reason for faces' separate behaviour then centric loading experiments should be preformed to possibly avoid the delamination. However, it is difficult to control in real situations to completely avoid eccentric loading.

The panel should be tested for failure to confirm if the analytical calculations accurately predict the correct failure method for this specific panel, and to further validate the model results. Additionally, four point bending tests should be performed to observe the shear failure of the core. If indeed the core does fail under low shear loads, then a thicker core material could be used to increase the shear resistance of the panel.

Regulated test methods should be used while testing a new panel. Also, two panels were under the loads, but only one panel was measured – if the second panel were measured as well, there would be a comparison for the results to confirm whether there was a defect in the panel that was observed or if similar mechanisms occurred as for the already measured panel.

Second order effects should be tested by conducting a bending test under an axial load, to see how much the panel load bearing capacity decreases.

Creep tests should be conducted for the whole panel. Additionally to creep, the relative humidity effects on the insulation material as well as for the whole panel's creep results should be evaluated.

Racking loading should be tested only if the panel will not be stiffened with through thickness stiffeners.

7.1.2. Model development

The Karamba3D panel model can be effectively used to describe the behaviour of the panel. The panel model should be further scaled with the correct core material, and tested if a smaller or a larger panel can be successfully described with the same model. Also, if other panels can be analysed with the same model when dimensions and material properties are changed.

The Karamba3D model should not be used for failure analysis since it does not describe the interface. For failure analysis, DIANA or other available FEA methods can be used which can describe local failures, interface strength and eccentric support conditions.

7.2. For further research

7.2.1. Panel development

The effect of the bond percentage (area which is fully glued) between the core and the faces should be analysed, since it has a significant effect on the load bearing capacity of a SIP. The bond percentage influences the composite behaviour – if it is low, the faces start to behave separately.

The delamination effect under eccentric loading should be further explored to have a good understanding of the mechanism and to have an analytical description.

The effect of load combinations, openings, vibration analysis, and second order analysis should be further explored - how much does the core influence the results.

7.2.2. Model development

The Karamba3D model showed promising results to use the method to design and analyse other sandwich panels - easy to build a model, but results visualization and results retrieval can be a bit difficult. The trickiest part is modelling the core, but if analytical calculations are preformed then based on them the core can be already modelled within a reasonable error margin. If the iterations made in this thesis are observed then for axial loading the amount of beams did not influence the results too much, only in transverse loading, so for wind loads, the amount of beams is more governing and could cause a big error.

The panel model should be further analysed to see if other SIPs can be analysed and described by the same model. Additionally, the height and thickness should be changed in the model and the effect should be investigated to see if scaling the panel would still give accurate results and still be in correspondence with experimental results.

7.2.3. Regulated guidelines for design

It is difficult to develop a unified code for a composite structure when the range of materials is wide. There are some patterns for materials that usually bring about the same failure method – for example blown foam cores or board insulation materials. These patterns would need to be recognised and grouped. Additionally, the Euler critical buckling load equation should be modified for eccentric loading or a reduction factor suggested for different panel compositions. In general, the analytical sandwich panel theory equations overestimated the panel strength,

and should be reevaluated. This is based on the experimental results and the model results.

References

1. Eastman, C. The Use of Computers Instead of Drawings in Building Design. *AIA Journal* **63** (Jan. 1975).
2. Mullens, M. A. & Arif, M. Structural Insulated Panels: Impact on the Residential Construction Process. *Journal of Construction Engineering and Management* **132.** https://ascelibrary.org/doi/full/10.1061/%28ASCE%290733-9364%282006%29132%3A7%28786%29#tab-citations (2006).
3. LetsBuild. *Why the slow uptake of technology in construction is holding the industry back* https://www.letsbuild.com/blog/why-the-slow-uptake-of-technology-in-construction-is-holding-the-industry-back (2023).
4. Directorate-General for Climate Action. *2030 climate targets* https://climate.ec.europa.eu/eu-action/climate-strategies-targets/2030-climate-targets_en (2024).
5. Sah, T. P., Lacey, A. W., Hao, H. & Chen, W. Prefabricated concrete sandwich and other lightweight wall panels for sustainable building construction: State-of-the-art review. *Journal of Building Engineering* **89,** 109391. ISSN: 2352-7102. https://www.sciencedirect.com/science/article/pii/S2352710224009598 (2024).
6. Panjehpour, M., Ali, A. & Voo, Y. Structural Insulated Panels: Past, Present, and Future. *Journal of Engineering Project and Production Management* **3,** 2–8 (Jan. 2013).
7. The Federation of American Scientists. Expanding the Scope and Market of SIP Technologies: A History of SIPs and CSIP Manufacturing, Construction, and Market Issues. *Building Technologies Program.* https://programs.fas.org/energy/btech/about/Expanding%20the%20Scope%20and%20Market%20of%20SIP%20Technologies.pdf (2009).
8. SIP Build UK. *The history of Structurally Insulated Panels* https://sipbuilduk.co.uk/news/the-history-of-structurally-insulated-panels/ (2024).
9. Abbasi, H., Hojatkashani, A., Sennah, K. & Nematianjelodar, H. Compressive loading of structural insulated panels and conventional stud walls: a study. *Proceedings of the Institution of Civil Engineers - Structures and Buildings* **176,** 833–844. ISSN: 0965-0911. https://www.sciencedirect.com/science/article/pii/S0965091121000937 (2021).
10. Kermani, A. Performance of structural insulated panels. *Proceedings of the Institution of Civil Engineers - Structures and Buildings* **159,** 13–19. https://doi.org/10.1680/stbu.2006.159.1.13 (2006).
11. Eric Jacques, M. & Makar, J. Behavior of Structural Insulated Panels Subjected to Short-Term Axial Loads. *Journal of Structural Engineering* **145.** https://ascelibrary.org/doi/full/10.1061/%28ASCE%29ST.1943-541X.0002393#tab-citations (2019).

12. Kingspan. *K-Roc KS1000 RH gevelpaneel* https://www.kingspan.com/nl/nl/producten/geisoleerde-sandwichpanelen/gevelpanelen/ks1000-rh-gevelpaneel/.

13. Kingspan. *TEK Building System* https://www.kingspan.com/gb/en/products/structural-insulated-panels/tek-building-system/.

14. De Graaf, P. & Banga, J. Nederlands. in *Handboek houtskeletbouw : ontwerp, techniek, uitvoering* (SBR, 2000). ISBN: 90-5367-305-9.

15. SBS Limited. *SIP Building Systems* https://www.sipbuildingsystems.co.uk.

16. Bouchlaghem, D., Shang, H., Whyte, J. & Ganah, A. Visualisation in architecture, engineering and construction (AEC). *Automation in Construction* **14.** International Conference for Construction Information Technology 2004, 287–295. ISSN: 0926-5805. https://www.sciencedirect.com/science/article/pii/S0926580504001025 (2005).

17. Fathi, N. *Study of an axially loaded sandwich panel : Study based on finite element analysis and experimentation of a 1 mm flat profiled steel plate* 2017.

18. Rungthonkit, P. *Structural behaviour of structural insulated panels (SIPS)* PhD thesis (University of Birmingham, 2012).

19. Yeh, B., Williamson, T. & Keith, E. Development of Structural Insulated Panel Standards. *Structures Congress 2008: Crossing Borders*. https://ascelibrary.org/doi/abs/10.1061/41016(314)232#tab-citations (2012).

20. Kingspan, N. T. *Kingspan TEK animatie* Youtube. https://www.youtube.com/watch?v=A0sPHIu3jL8.

21. Trimble. *Breaking down the benefits of Grasshopper and Tekla products Interoperability* https://www.tekla.com/resources/articles/breaking-down-the-benefits-of-grasshopper-and-tekla-products-interoperability#:~:text=With%20Grasshopper%2C%20users%20can%20quickly,to%20improve%20design%20and%20analysis. (2023).

22. BackofficePro. *Why was Grasshopper architecture created?* https://www.backofficepro.com/engineering/grasshopper-in-architecture.php (2023).

23. Cvetković, D. *Grasshopper 3D – Your Guide to Parametric Modeling* https://howtorhino.com/blog/software-for-architects/grasshopper-3d/ (2023).

24. Preisinger, C. & Heimrath, M. Karamba—A Toolkit for Parametric Structural Design. *Structural Engineering International* **24,** 217–221. eprint: https://doi.org/10.2749/101686614X13830790993483. https://doi.org/10.2749/101686614X13830790993483 (2014).

25. Dzwierzynska, J. Shaping of Spatial Steel Rod Structures Based on a Hyperbolic Paraboloid. *Archives of Civil Engineering* **64,** 309–320 (Dec. 2018).

26. Golkar, N., Sadeghpour, A. H. & Divandari, J. Drawing inspiration from the spine, designing a pedestrian bridge [spine-inspired design of a pedestrian bridge]. *JOURNAL OF ARCHITECTURE AND URBANISM* **45,** 119–130 (Aug. 2021).

27. Jongenotten, J. *Parametric comparison of stability systems: Development of a parametric tool for the comparison and optimisation of four concrete stability systems for high-rise buildings between 100 m and 250 m in an early design phase* Master's thesis. Available at http://resolver.tudelft.nl/uuid:b55c53f9-df45-4629-afd6-073bae268f2b. The Netherlands, 2021.

28. Van der Linden, T. *Embodied carbon optimization for gridshells* Master's thesis. Available at http://resolver.tudelft.nl/uuid:f143eaa1-1a72-4d32-a0d7-358997258112. The Netherlands, 2023.

29. Jacobsson, N. A. & Bohman, S. *A Generative Design of TimberStructures According to Eurocode : Development of a Parametric Model in Grasshopper* MA thesis (KTH, Structural Engineering and Bridges, 2019).

30. Cheng, A. A. H. *Parametric design of timber shell structures* PhD thesis (University of British Columbia, 2015). https://open.library.ubc.ca/collections/ubctheses/24/items/1.0216008.

31. Hamelijnck, M. *Parametric hybrid modular timber construction* Master's thesis. Available at https://repository.tudelft.nl/islandora/object/uuid:63fd5c41-77a6-44ca-8a73-4dd5449a2f22?collection=education. The Netherlands, Aug. 2021.

32. Zenkert, D. *An Introduction to Sandwich Construction* ISBN: 9780947817770. https://books.google.nl/books?id=zc-GQgAACAAJ (Engineering Materials Advisory Services, 1995).

33. Davies, M. in *Lightweight Sandwich Construction* (John Wiley Sons, Ltd, 2001). ISBN: 9780470690253. eprint: https://onlinelibrary.wiley.com/doi/pdf/10.1002/9780470690253.ch1. https://onlinelibrary.wiley.com/doi/abs/10.1002/9780470690253.ch1.

34. Aicher, S., Simon, K. & van Rie, J. Full-scale axial compression loading of sanwich panels (SIPS) with wood based skins and a PUR-foam core – first results of a 24 years experiment with highly ecentric loads (2023).

35. Käpplein, S. & Misiek, T. *EASIE - Axially loaded sandwich panels* June 2011.

36. STEICO. *STEICO Special dry* https://www.steico.com/en/products/insulation/ventilated-facade-insulation-systems/closed-facade-timber-frame-construction/steicospecial-dry (2024).

37. STEICO. *How STEICO wood fibre insulation materials are manufactured* https://www.steico.com/en/solutions/product-advantages/steico-insulation-materials (2024).

38. ALLEN, H. G. in *Analysis and Design of Structural Sandwich Panels* (ed ALLEN, H. G.) (Pergamon, 1969). ISBN: 978-0-08-012870-2. https://www.sciencedirect.com/science/article/pii/B9780080128702500055.

39. Rake, F. *Stability of axially loaded GFRP sandwich wall panels* MA thesis (Eindhoven University of Technology, 2016).

40. Pokharel, N. & Mahendran, M. Experimental investigation and design of sandwich panels subject to local buckling effects. *JOURNAL OF CONSTRUCTIONAL STEEL RESEARCH* **59,** 1533–1552. ISSN: 0143-974X (Dec. 2003).

41. Derks, A. *Axial load-bearing capacity of sandwich panel walls in residential buildings* Master's thesis. Available at https://research.tue.nl/en/studentTheses/axial-load-bearing-capacity-of-sandwich-panel-walls-in-residentia. The Netherlands, 2023.

42. Yang, J. & Rungthonkit, P. *Behaviour of Structural Insulated Panels (SIPs) under both short-term and long-term loadings* English. in *11th International Conferenced for Non-conventional Materials and Technologies Materials for Sustainable and Affordable Construction* (Sept. 2009).

43. Kingspan. *Kingspan TEK Bouwsysteem* https://www.kingspan.com/nl/nl/producten/sips-structural-insulated-panel-system/kingspan-tek/?s=d (2024).

44. Cobb, A. *BEST Building Education with SIPs Training – Basic SIP Design and Engineering* https://www.sips.org/resources/bestprogram (2024).

45. Mousa, M. A. & Uddin, N. Structural behavior and modeling of full-scale composite structural insulated wall panels. *Engineering Structures* **41,** 320–334. ISSN: 0141-0296. https://www.sciencedirect.com/science/article/pii/S0141029612001460 (2012).

46. Santos, P., Correia, J. R., Godinho, L., Dias, A. & Craveiro, H. Experimental and numerical assessment of a cross-insulated timber panel solution. *Engineering Structures* **235,** 112061. ISSN: 0141-0296. https://www.sciencedirect.com/science/article/pii/S014102962100211X (2021).

47. Smakosz, Ł., Kreja, I. & Pozorski, Z. Flexural behavior of composite structural insulated panels with magnesium oxide board facings. *Archives of Civil and Mechanical Engineering* **20** (2020).

48. Mousa, M. A. & Uddin, N. Global buckling of composite structural insulated wall panels. *Materials Design* **32,** 766–772. ISSN: 0261-3069. https://www.sciencedirect.com/science/article/pii/S0261306910004619 (2011).

49. Ni, X., Prusty, G. & Hellier, A. BUCKLING AND POST-BUCKLING OF ISOTROPIC AND COMPOSITE STIFFENED PANELS: A REVIEW ON ANALYSIS AND EXPERIMENT (2000-2012). *Transactions of the Royal Institution of Naval Architects Part A1: International Journal of Maritime Engineering* **157,** A–9 (Jan. 2015).

50. Jacques, E. & Makar, J. Behaviour of structural insulated panels (SIPs) subjected to short-term out-of-plane transverse loads. *Canadian Journal of Civil Engineering* (2019).

51. Pokharel, N. & Mahendran, M. Finite element analysis and design of sandwich panels subject to local buckling effects. *Thin-Walled Structures* **42,** 589–611. ISSN: 0263-8231. https://www.sciencedirect.com/science/article/pii/S0263823103001472 (2004).

52. Vaidya, A., Uddin, N., F.ASCE & Vaidya, U. Structural Characterization of Composite Structural Insulated Panels for Exterior Wall Applications. *Journal of Composites for Construction* **14.** https://ascelibrary.org/doi/full/10.1061/%28ASCE%29CC.1943-5614.0000037#tab-citations (2010).

53. Yang, J., Li, Z. & Du, Q. *An Experimental Study on Material and Structural Properties of Structural Insulated Panels (SIPs)* in *Computational Mechanics, Materials and Engineering Applications* **147** (Trans Tech Publications Ltd, Feb. 2012), 127–131.

54. Yang, J., Li, Z. & Du, Q. An Experimental Study on Material and Structural Properties of Structural Insulated Panels (SIPs). *Applied Mechanics and Materials* **147,** 127–131 (Dec. 2011).

55. Mousa, M. A. & Uddin, N. Flexural Behavior of Full-Scale Composite Structural Insulated Floor Panels. *Advanced Composite Materials* **20,** 547–567. eprint: https://doi.org/10.1163/156855111X610208. https://doi.org/10.1163/156855111X610208 (2011).

56. Smakosz, Ł. & Tejchman, J. Evaluation of strength, deformability and failure mode of composite structural insulated panels. *Materials Design (1980-2015)* **54,** 1068–1082. ISSN: 0261-3069. https://www.sciencedirect.com/science/article/pii/S0261306913008844 (2014).

57. Imjai, T. *et al.* Performance of a novel structural insulated panel in tropical climates: Experimental and numerical studies. *Construction and Building Materials* **421,** 135568. ISSN: 0950-0618. https://www.sciencedirect.com/science/article/pii/S0950061824007098 (2024).

A

Load on the outer face F=6 kN Maple output

```
> restart;
shear beam
[units N and mm]
> with (plots):

> ODE:=-GAeff*diff(w(x),x$2)=0;
```

$$ODE := -GAeff\left(\frac{d^2}{dx^2}\, w(x)\right) = 0 \tag{1}$$

```
> assign(dsolve({ODE},{w(x)}));
>
>  w:=w(x):
>  V:=GAeff*diff(w,x):
> w;
```

$$\_C1\, x + \_C2 \tag{2}$$

```
> V;
```

$$GAeff\_C1 \tag{3}$$

```
> Gamma;
```

$$\Gamma \tag{4}$$

```
> x:=0: eq1:=w=0:

> x:=L: eq2:=V=F:
>
> Gamma := diff(w, x) :
>
> assign(solve({eq1,eq2},{_C1,_C2})); x:='x':
> w;
```

$$\frac{F\, x}{GAeff} \tag{5}$$

```
> _C1;
```

$$\frac{F}{GAeff} \tag{6}$$

```
> _C2;
```

$$0 \tag{7}$$

```
                                                                    (8)
> V;
```

$$6.000000000 \tag{9}$$

```
Panel info:
> GAeff:=7180800: L:=112: F:=6000: h:=3200:
```

```
> plot( −w, x = 0 ..L, title = "Deflection w(x)" );
```

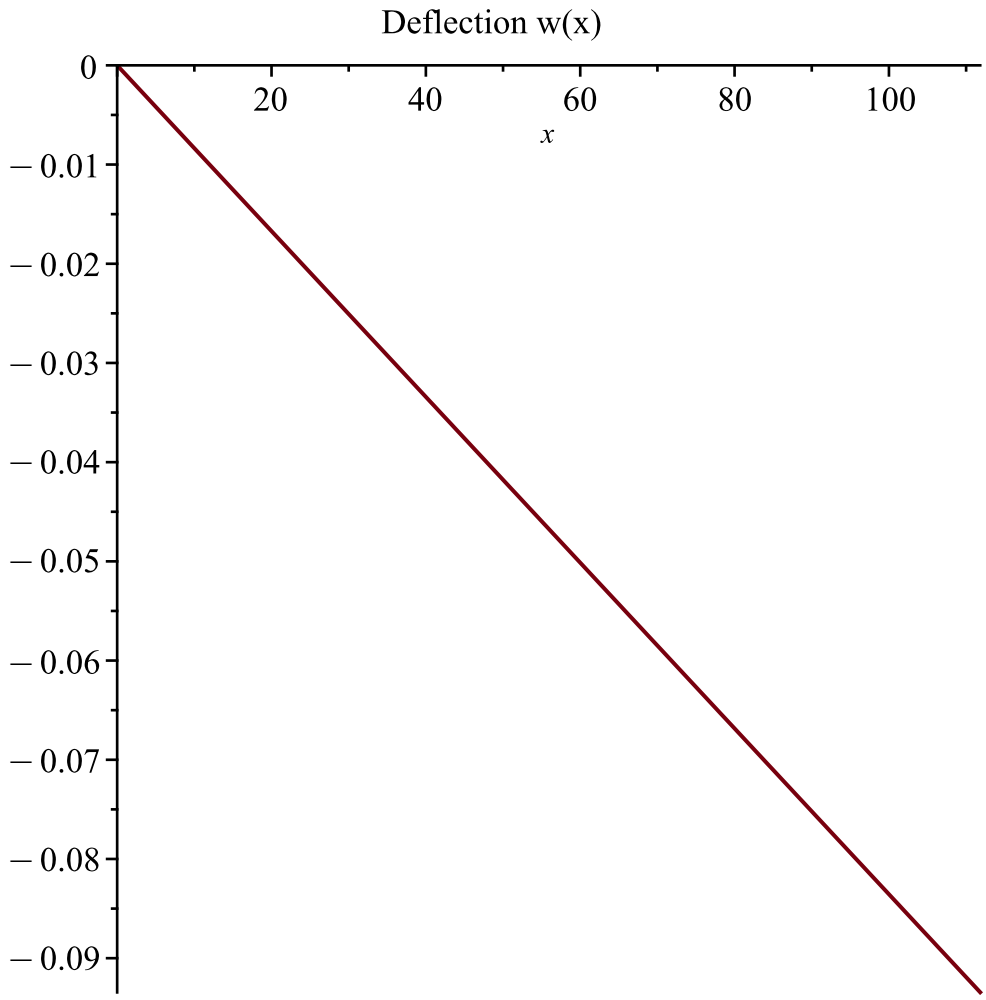


```
> plot( −V, x = 0 ..L, title = "Shear force distribution V(x)" );
```

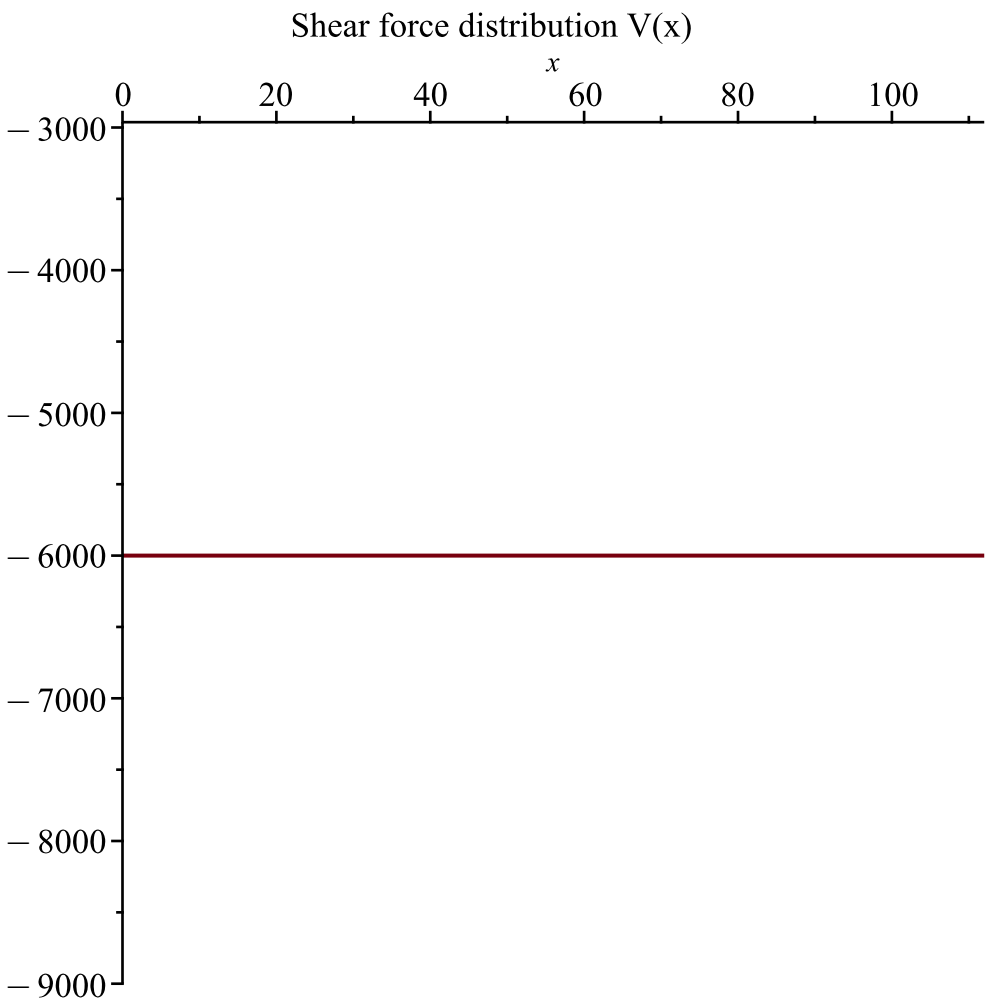


```
> plot( -Gamma, x = 0 ..L, title = "Shear angle Gamma(x)" );
```

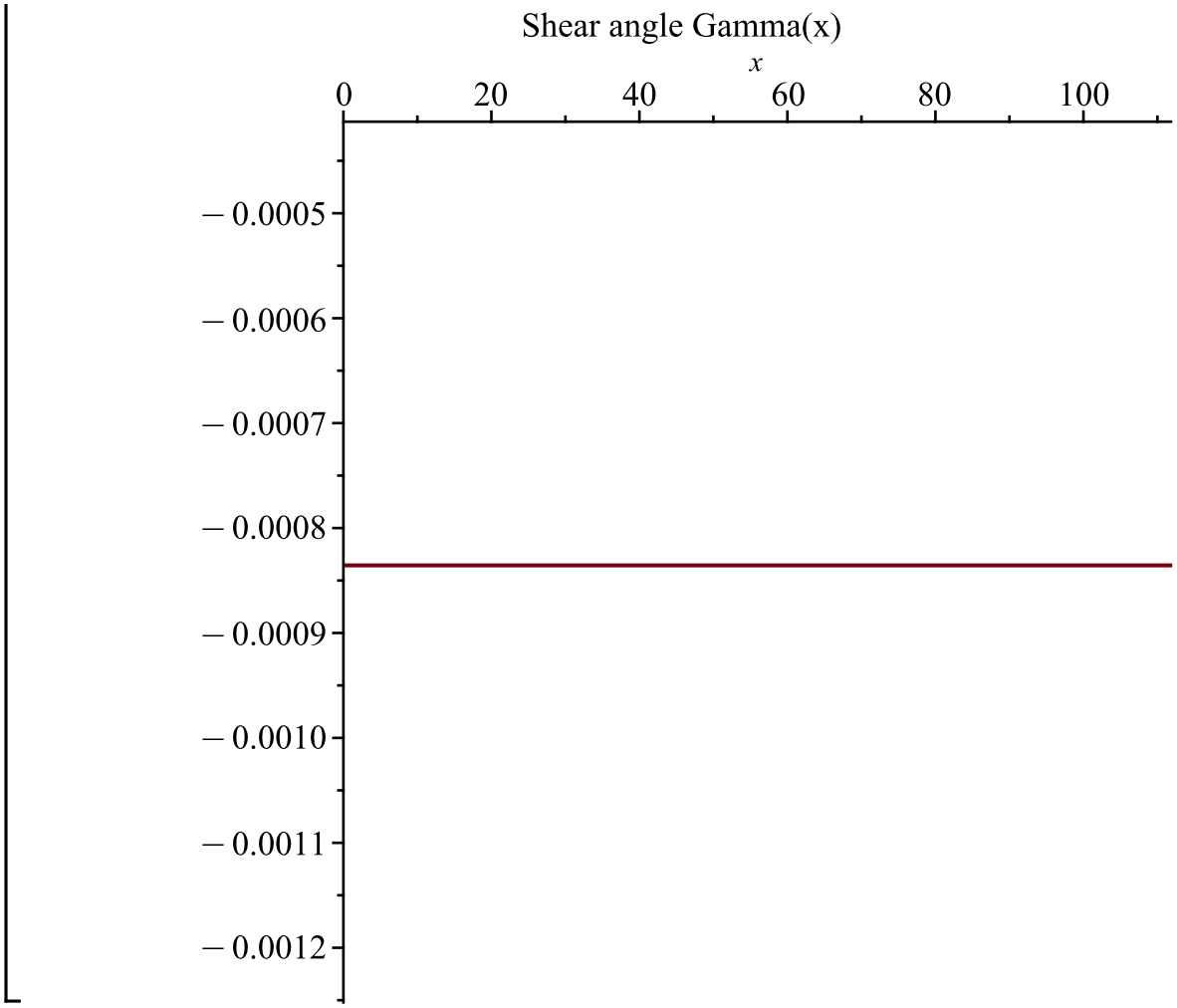
Shear angle Gamma(x)
x
0
20
40
60
80
100
– 0.0005
– 0.0006
– 0.0007
– 0.0008
– 0.0009
– 0.0010
– 0.0011
– 0.0012

>
>
>
>
>
>

B

Load on the outer face F=129 kN Maple output

```
> restart;
shear beam
[units N and mm]
> with (plots):

> ODE:=-GAeff*diff(w(x),x$2)=0;
```

$$ODE := -GAeff\left(\frac{d^2}{dx^2}\, w(x)\right) = 0 \tag{1}$$

```
> assign(dsolve({ODE},{w(x)}));
>
>  w:=w(x):
>  V:=GAeff*diff(w,x):
> w;
```

$$\_C1\, x + \_C2 \tag{2}$$

```
> V;
```

$$GAeff\_C1 \tag{3}$$

```
> Gamma;
```

$$\Gamma \tag{4}$$

```
> x:=0: eq1:=w=0:

> x:=L: eq2:=V=F:
>
> Gamma := diff(w, x) :
>
> assign(solve({eq1,eq2},{_C1,_C2})); x:='x':
> w;
```

$$\frac{F\, x}{GAeff} \tag{5}$$

```
> _C1;
```

$$\frac{F}{GAeff} \tag{6}$$

```
> _C2;
```

$$0 \tag{7}$$

```
                                                                    (8)
> V;
```

$$6.000000000 \tag{9}$$

```
Panel info:
> GAeff:=7180800: L:=112: F:=6000: h:=3200:
```

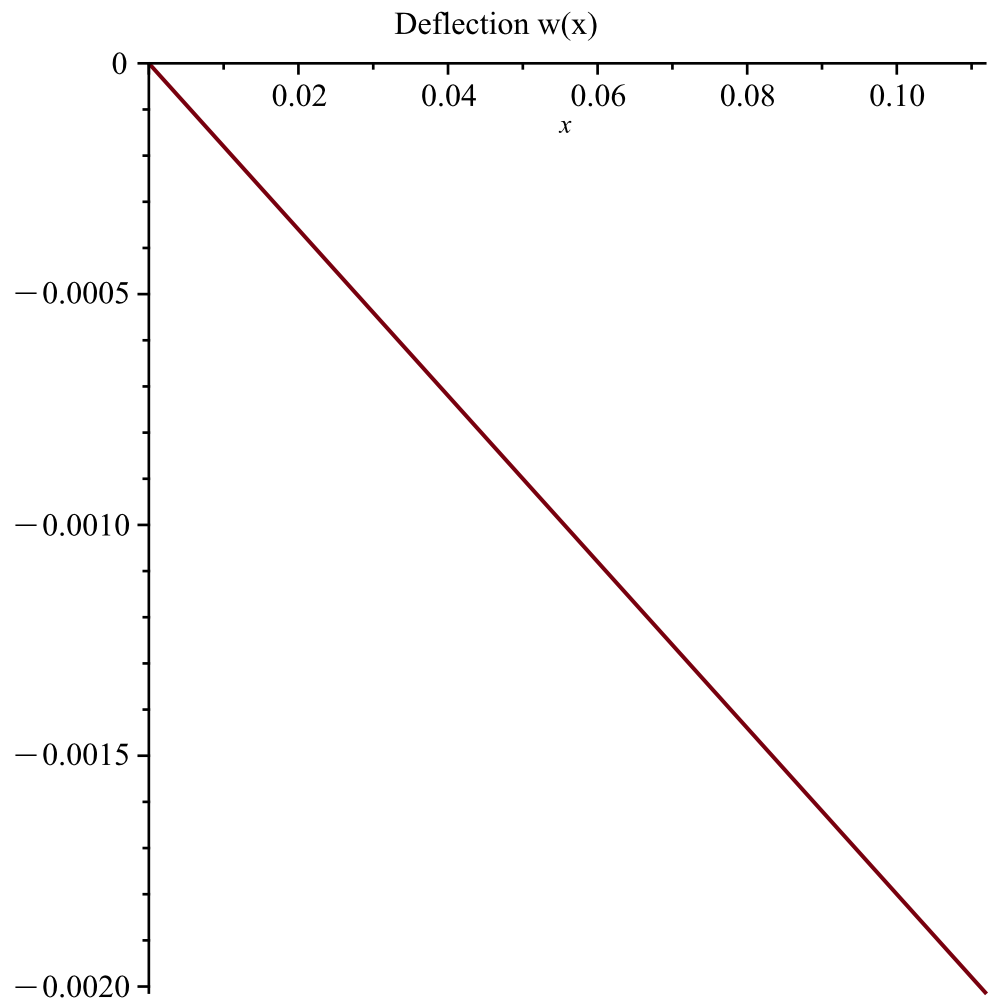


```
> plot(-V, x = 0 ..L, title = "Shear force distribution V(x)");
```

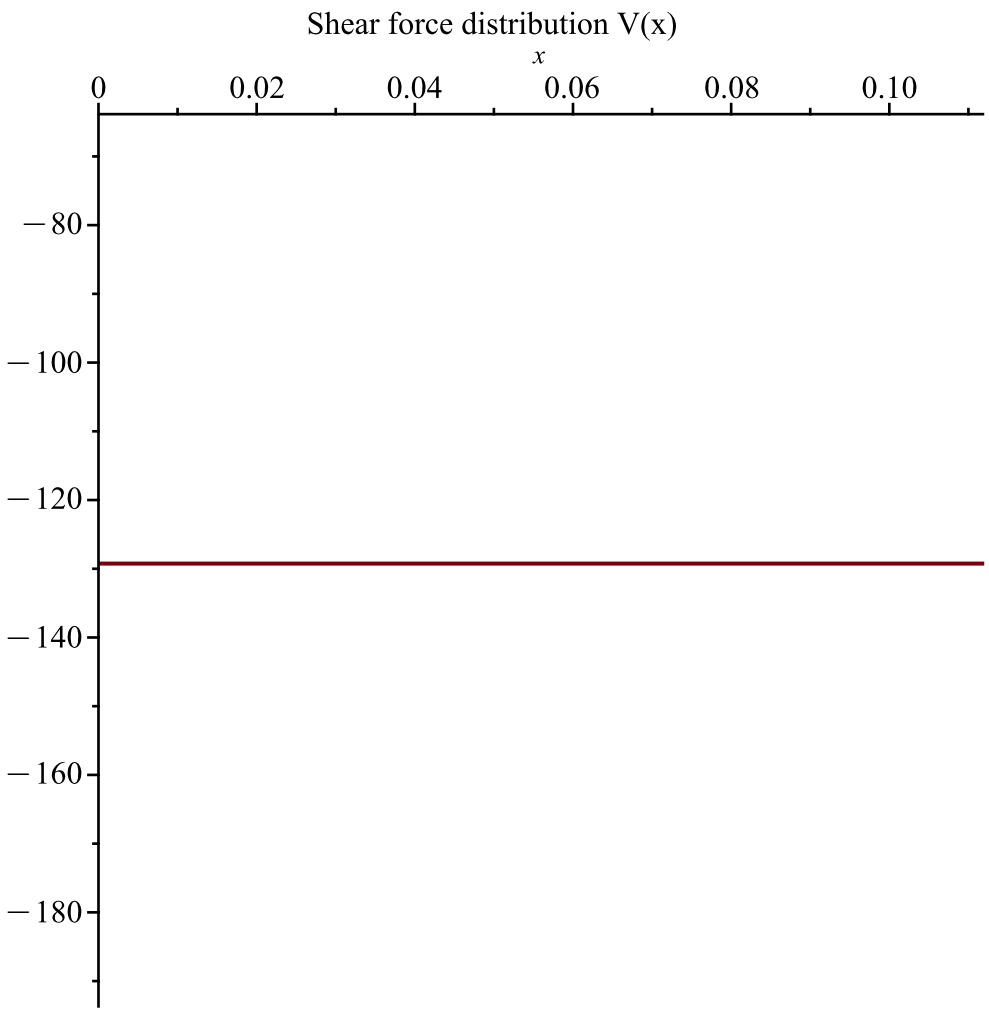


```
> plot( −Gamma, x = 0 ..L, title = "Shear angle Gamma(x)" );
```

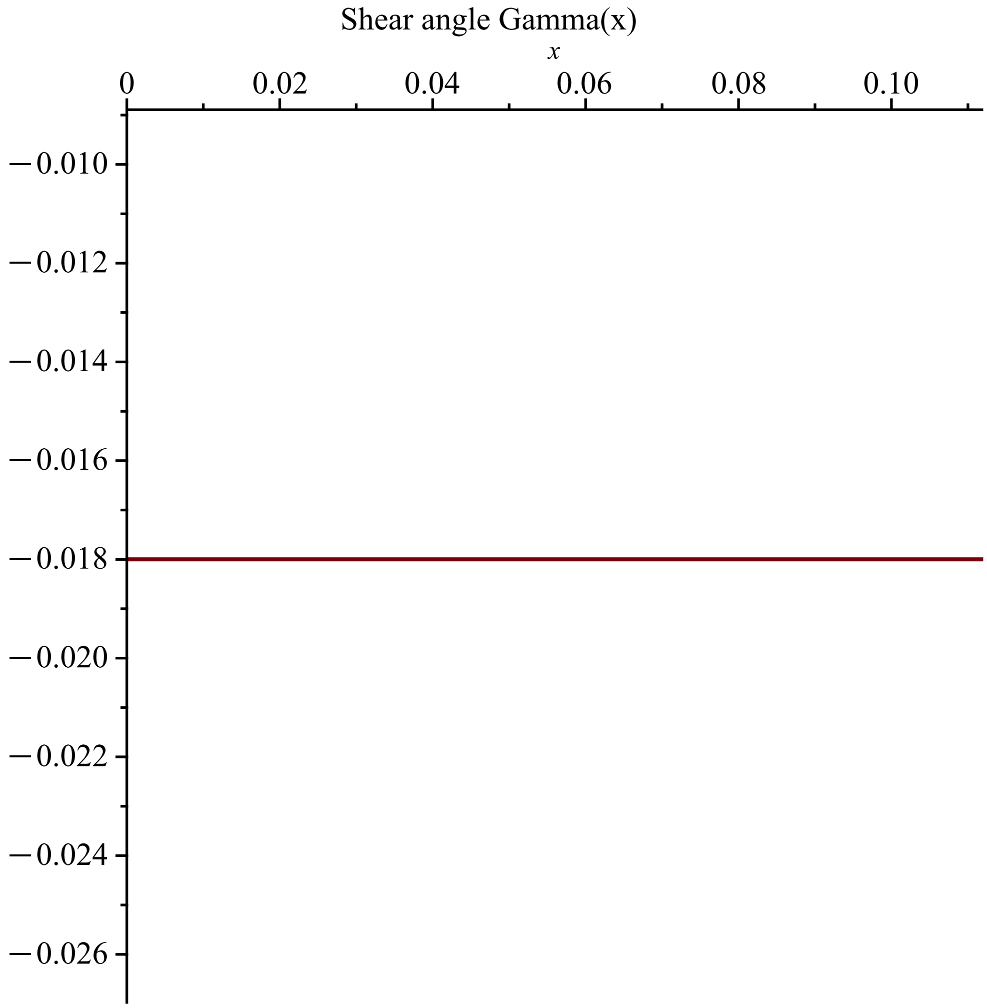
Shear angle Gamma(x)
x
0
0.02
0.04
0.06
0.08
0.10
−0.010
−0.012
−0.014
−0.016
−0.018
−0.020
−0.022
−0.024
−0.026

>
>
>
>
>
>

C

Transverse loading q=2.5 kN/m Maple output

```
> restart;

Timoshenko beam
[units N and mm]
>
> DV1 := EI*diff(phi(x), x$2) - GA*(diff(w(x), x) + phi(x)) = 0;
```

$$DV1 := EI\left(\frac{d^2}{dx^2}\,\phi(x)\right) - GA\left(\frac{d}{dx}\,w(x) + \phi(x)\right) = 0 \tag{1}$$

```
> DV2 := GA*(diff(w(x), x$2) + diff(phi(x), x)) = -q;
```

$$DV2 := GA\left(\frac{d^2}{dx^2}\,w(x) + \frac{d}{dx}\,\phi(x)\right) = -q \tag{2}$$

```
> sol1 := dsolve({DV1, DV2}, {w(x), phi(x)}) : assign(sol1) :
> w := (w(x)); phi := (phi(x));
```

$$w := \frac{\_C1\,x^3}{6} + \frac{q\,x^4}{24\,EI} + \frac{\_C2\,x^2}{2} + \_C3\,x + \_C4$$

$$\phi := -\frac{\_C1\,x^2}{2} - \frac{q\,x^3}{6\,EI} - \_C2\,x - \frac{EI\,\_C1}{GA} - \_C3 - \frac{q\,x}{GA} \tag{3}$$

```
> Gamma := diff(w, x) + phi : kappa := diff(phi, x) :
> alpha_bending := phi : alpha_shear := diff(w, x) :
> V := GA*Gamma : M := EI*kappa :
> x := 0 : eq1 := w = 0 : eq2 := M = 0 :
  x := L : eq3 := w = 0 : eq4 := M = 0 :
> sol2 := solve({eq1, eq2, eq3, eq4}, {_C1, _C2, _C3, _C4}) : assign(sol2); x := 'x':
>
> _C1;
```

$$-\frac{q\,L}{2\,EI} \tag{4}$$

```
> _C2;
```

$$-\frac{q}{GA} \tag{5}$$

```
> _C3;
```

$$\frac{q\,L\left(GA\,L^2 + 12\,EI\right)}{24\,EI\,GA} \tag{6}$$

```
> _C4;
```

$$0 \tag{7}$$

```
> w;
```

$$-\frac{q\,L\,x^3}{12\,EI} + \frac{q\,x^4}{24\,EI} - \frac{q\,x^2}{2\,GA} + \frac{q\,L\left(GA\,L^2 + 12\,EI\right)x}{24\,EI\,GA} \tag{8}$$

```
>
```

```
>
> phi;
```

$$\frac{q\,L\,x^2}{4\,EI} - \frac{q\,x^3}{6\,EI} + \frac{q\,L}{2\,GA} - \frac{q\,L\,\left(GA\,L^2 + 12\,EI\right)}{24\,EI\,GA} \tag{9}$$

```
> M;
```

$$EI\left(\frac{q\,L\,x}{2\,EI} - \frac{q\,x^2}{2\,EI}\right) \tag{10}$$

```
> V;
```

$$GA\left(\frac{q\,L}{2\,GA} - \frac{q\,x}{GA}\right) \tag{11}$$

```
> L := 3.2·1000 : q := 2.5 : EI := 293.26·10^9 : GA := 224.4·10^3;
```

$$GA := 224400.0 \tag{12}$$

```
> plot( -w, x = 0 ..L, title = "Deflection w(x)" );
```

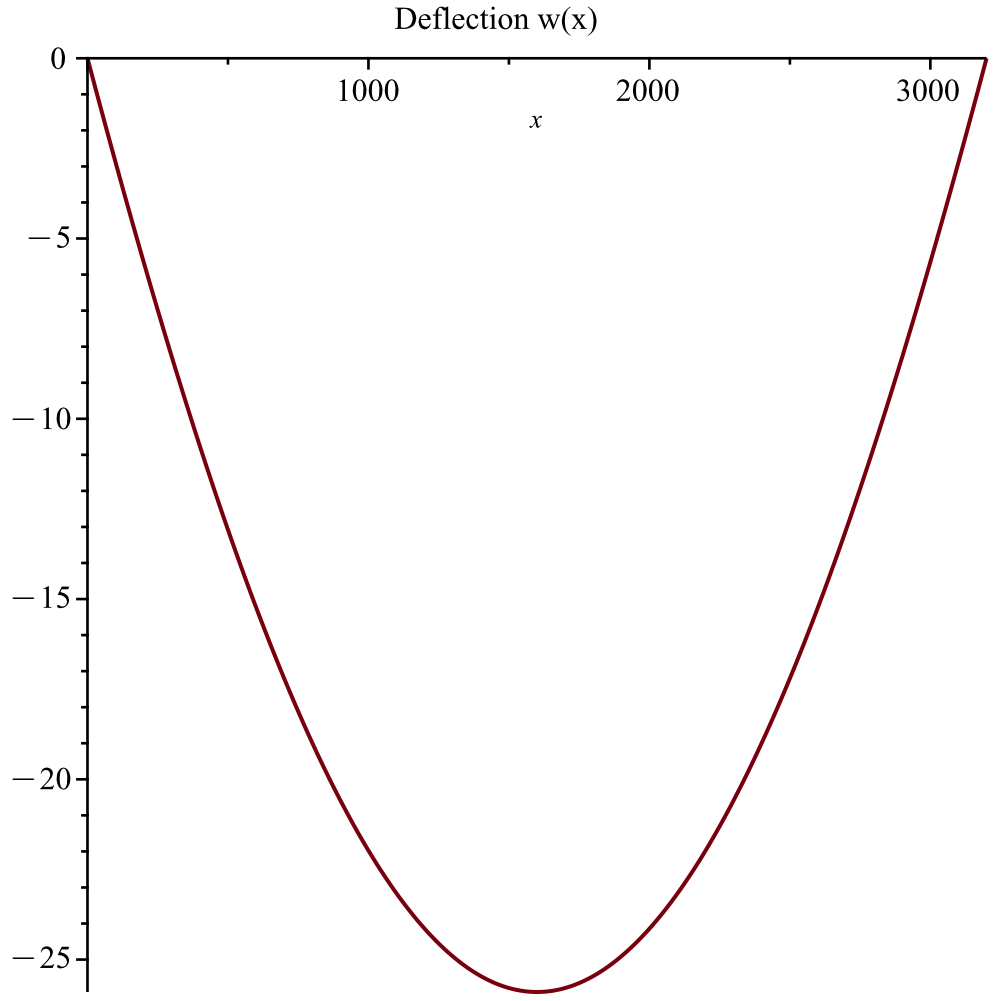


```
> plot( -phi, x = 0 ..L, title = "Bending rotation phi(x)" );
```

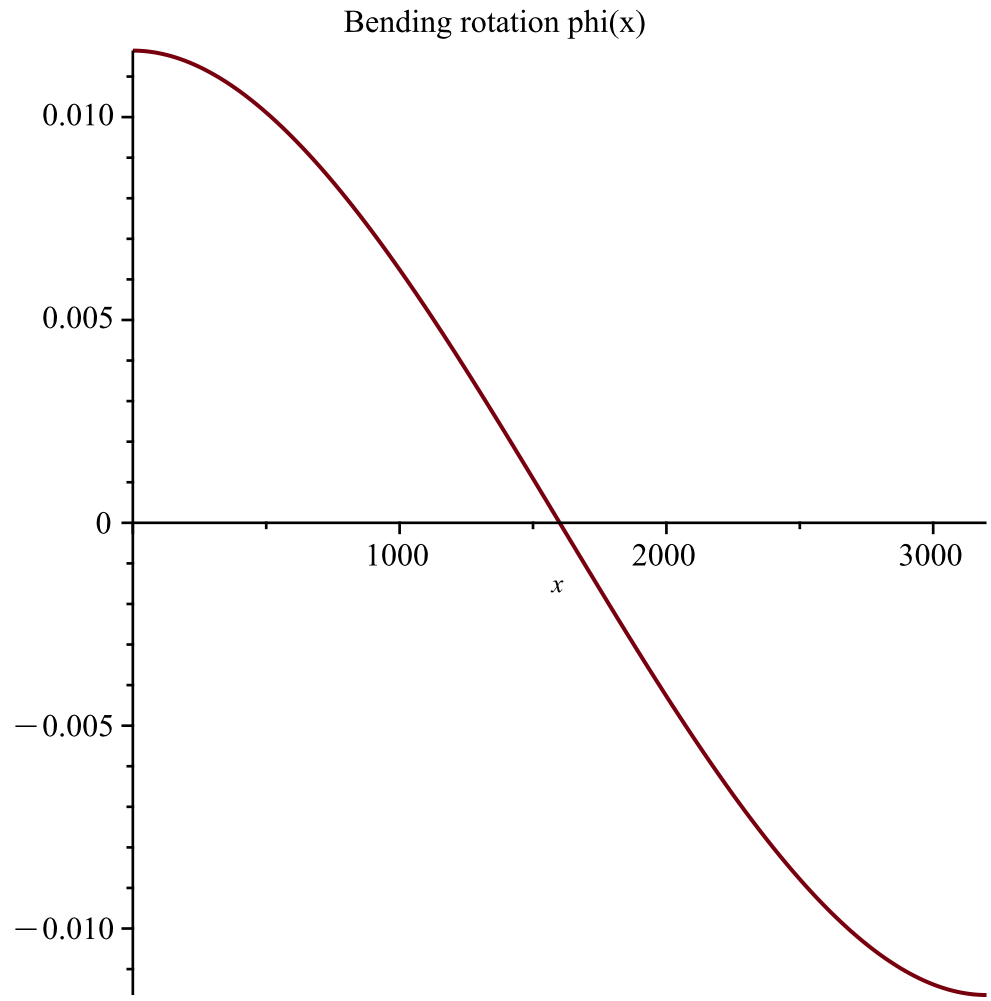


```
> plot(-M, x = 0..L, title = "Moment distribution M(x)");
```

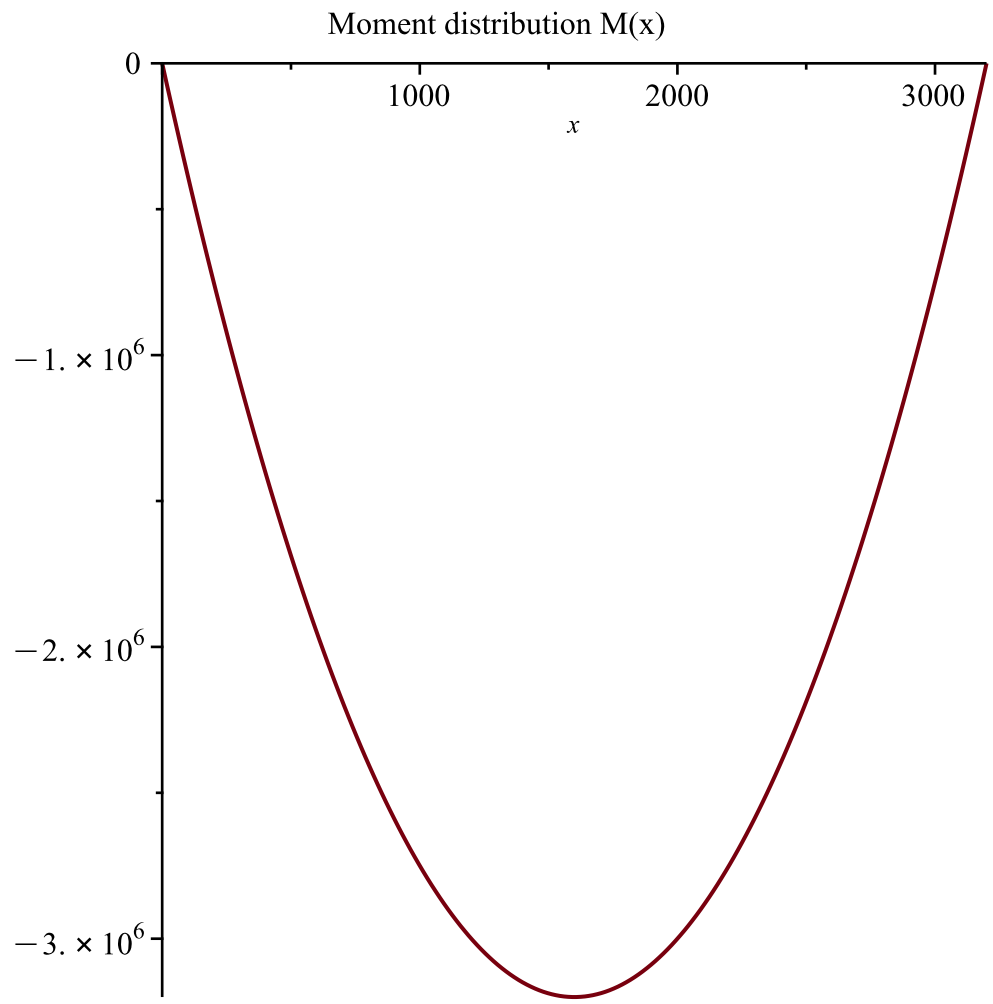


```
> plot( −V, x = 0 ..L, title = "Shear force distribution V(x)");
```

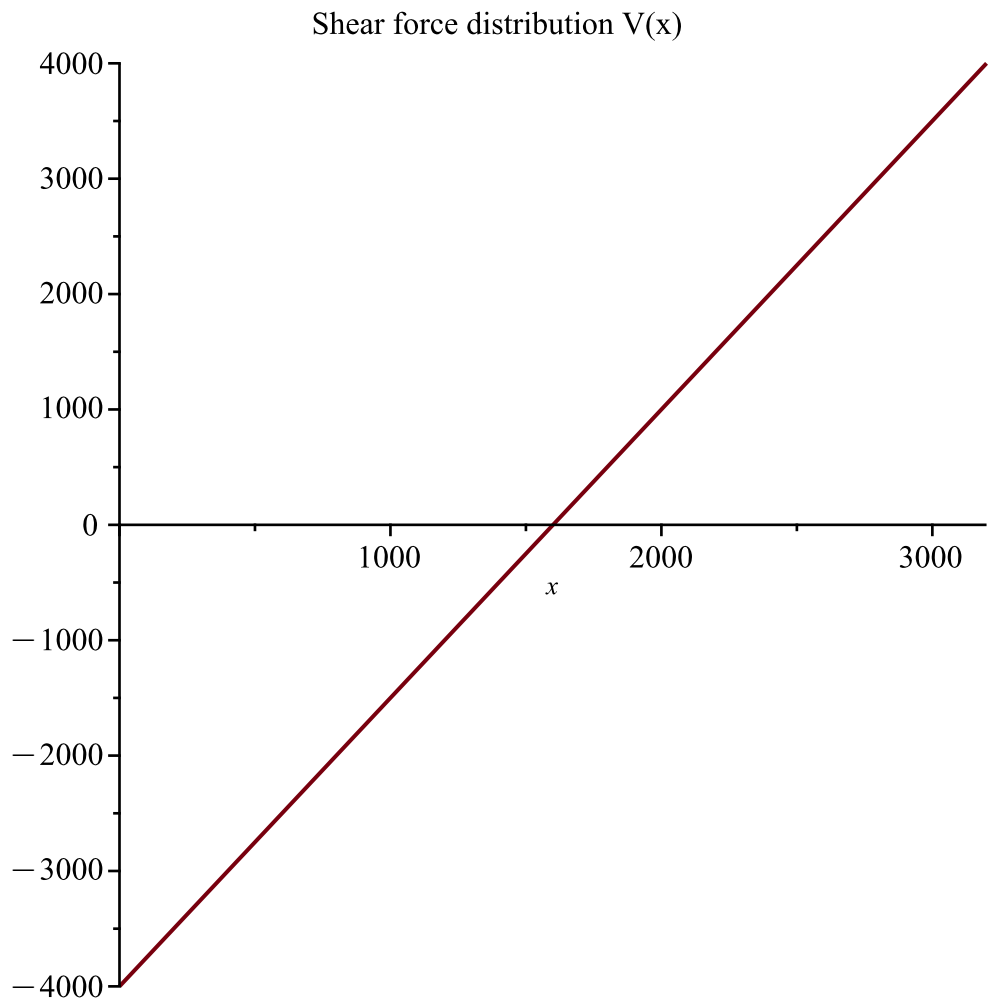


```
> plot( −Gamma, x = 0 ..L, title = "Shear angle Gamma(x)" );
```

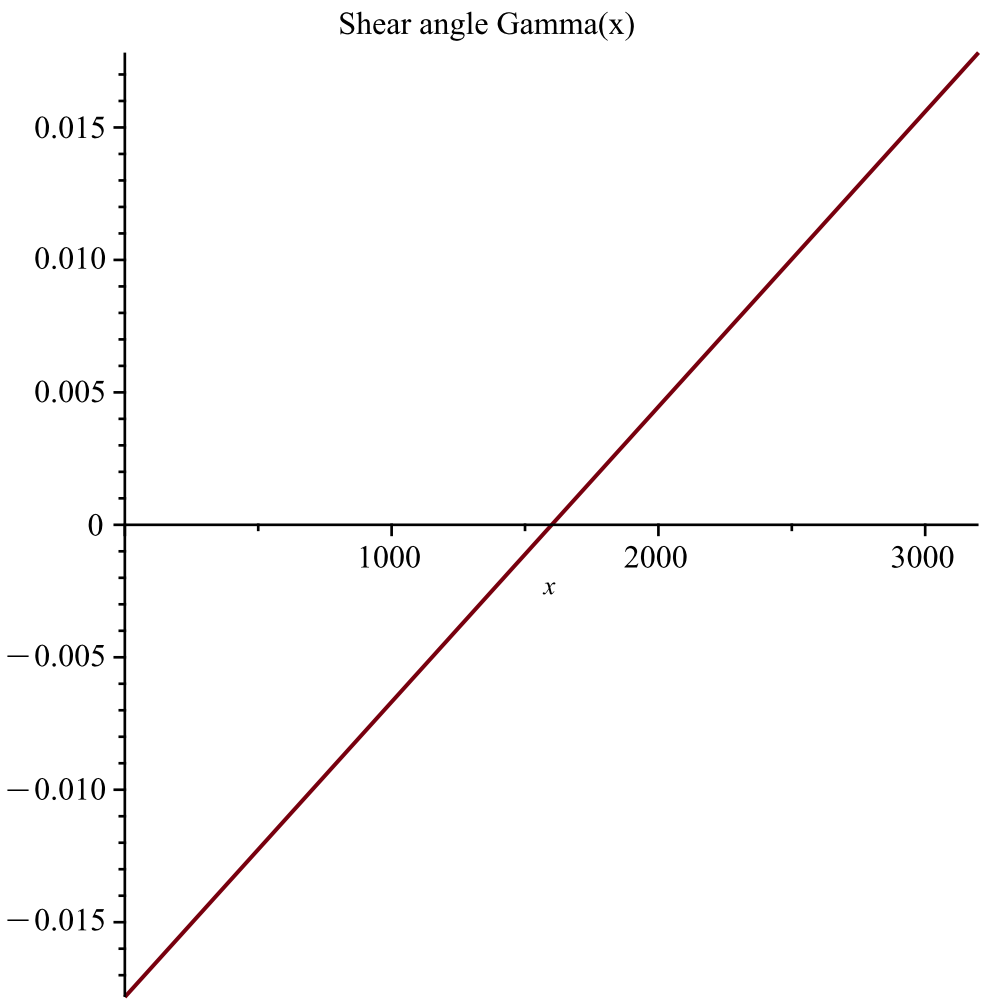
Shear angle Gamma(x)
0.015
0.010
0.005
0
−0.005
−0.010
−0.015
1000
2000
3000
x

D

Outer face loaded with F=6 kN Maple output

```
> restart;

  Timoshenko beam
  [units N and mm]
>
> DV1 := EI*diff(phi(x), x$2) - GA*(diff(w(x), x) + phi(x)) = 0;
```

$$DV1 := EI\left(\frac{d^2}{dx^2}\,\phi(x)\right) - GA\left(\frac{d}{dx}\,w(x) + \phi(x)\right) = 0 \tag{1}$$

```
> DV2 := GA*(diff(w(x), x$2) + diff(phi(x), x)) = 0;
```

$$DV2 := GA\left(\frac{d^2}{dx^2}\,w(x) + \frac{d}{dx}\,\phi(x)\right) = 0 \tag{2}$$

```
> sol1 := dsolve({DV1, DV2}, {w(x), phi(x)}) : assign(sol1) :
> w := (w(x)); phi := (phi(x));
```

$$w := \frac{1}{6}\,\_C1\,x^3 + \frac{1}{2}\,\_C2\,x^2 + \_C3\,x + \_C4$$

$$\phi := -\frac{\_C1\,x^2}{2} - \_C2\,x - \frac{EI\,\_C1}{GA} - \_C3 \tag{3}$$

```
> Gamma := diff(w, x) + phi : kappa := diff(phi, x) :
> alpha_bending := phi : alpha_shear := diff(w, x) :
> V := GA*Gamma : M := EI*kappa :
> x := 0 : eq1 := w = 0 : eq2 := M = Fe :
  x := L : eq3 := w = 0 : eq4 := M = 0 :
> sol2 := solve({eq1, eq2, eq3, eq4}, {_C1, _C2, _C3, _C4}) : assign(sol2); x := 'x':
>
> _C1;
```

$$\frac{Fe}{EI\,L} \tag{4}$$

```
> _C2;
```

$$-\frac{Fe}{EI} \tag{5}$$

```
> _C3;
```

$$\frac{L\,Fe}{3\,EI} \tag{6}$$

```
> _C4;
```

$$0 \tag{7}$$

```
> w;
```

$$\frac{Fe\,x^3}{6\,EI\,L} - \frac{Fe\,x^2}{2\,EI} + \frac{L\,Fe\,x}{3\,EI} \tag{8}$$

```
>

>
```

> phi;

$$-\frac{Fe\,x^2}{2\,EI\,L}+\frac{Fe\,x}{EI}-\frac{Fe}{GA\,L}-\frac{L\,Fe}{3\,EI} \tag{9}$$

> M;

$$EI\left(-\frac{Fe\,x}{EI\,L}+\frac{Fe}{EI}\right) \tag{10}$$

> V;

$$-\frac{Fe}{L} \tag{11}$$

> $L := 3.2\cdot 1000 : Fe := 112\cdot 6000 : EI := 293.26\cdot 10^9 : GA := 224.4\cdot 10^3;$

$$GA := 224400.0 \tag{12}$$

> plot(−w, x = 0 ..L, title = "Deflection w(x)");

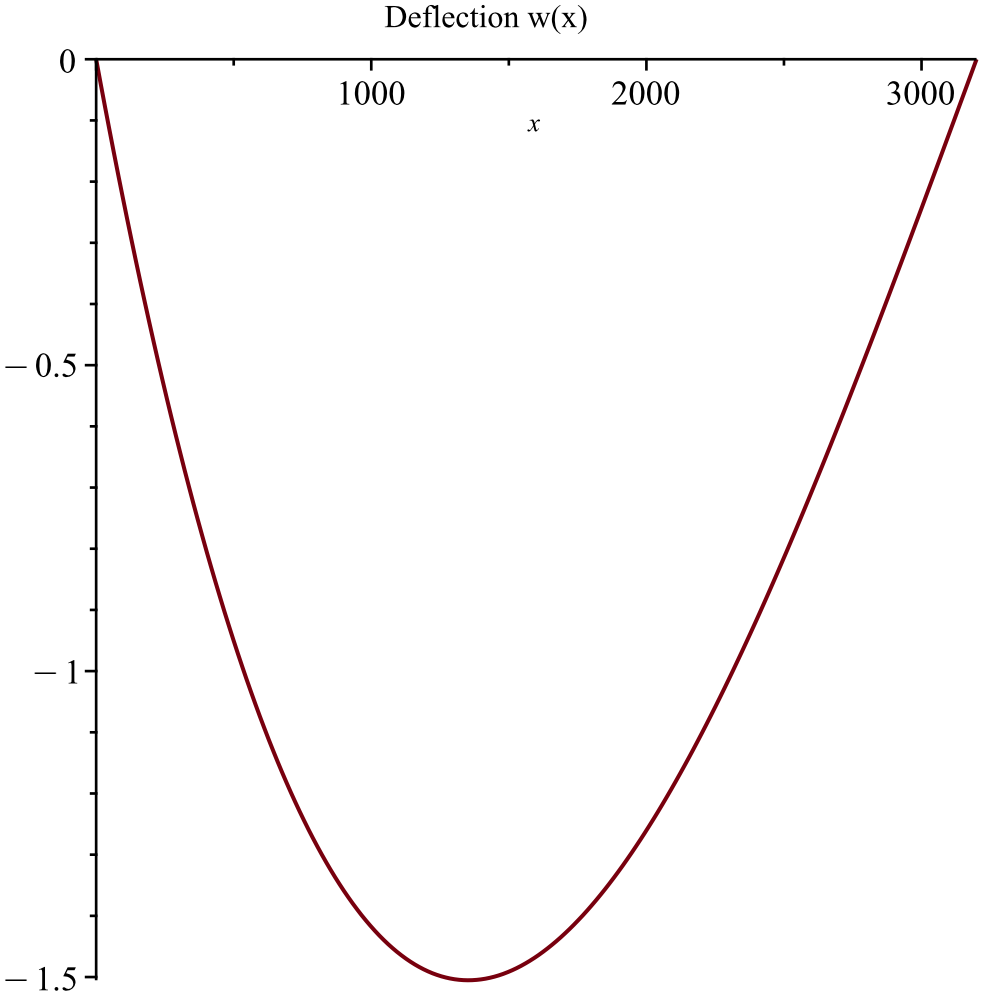

> plot(−phi, x = 0 ..L, title = "Bending rotation phi(x)");

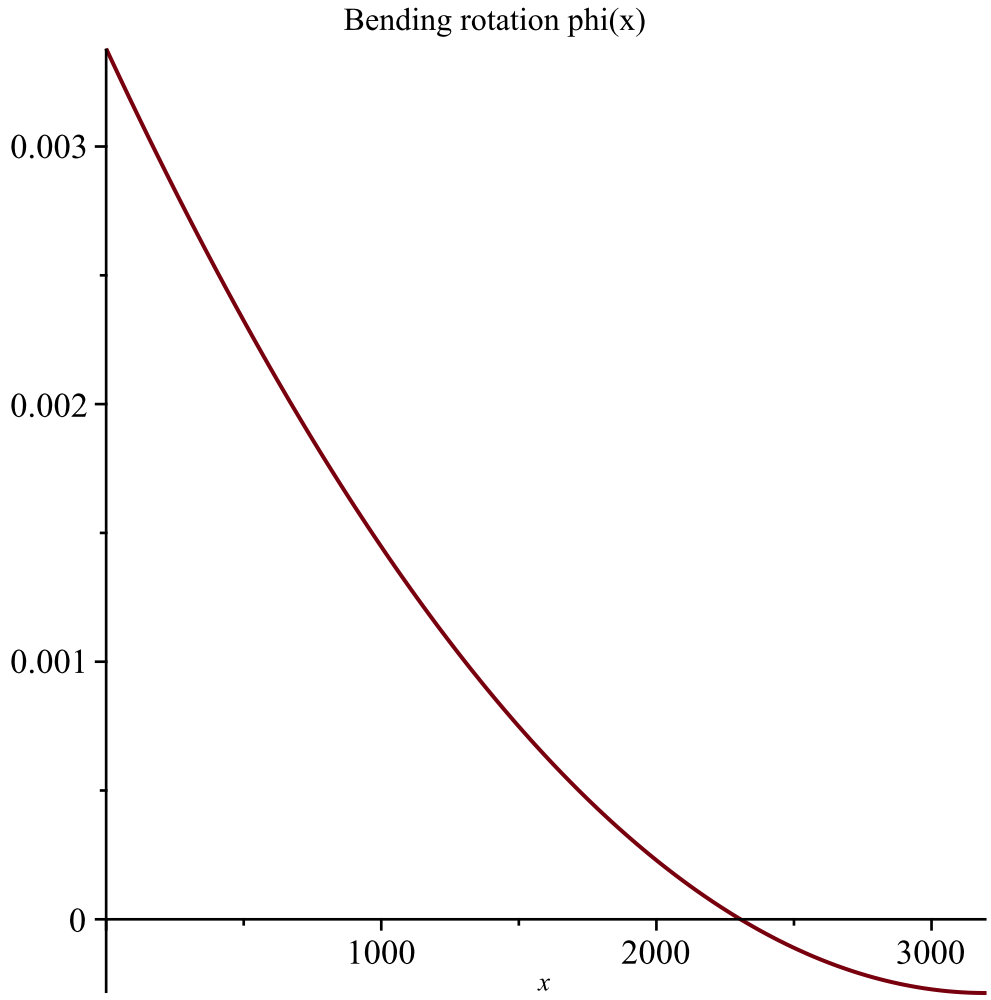


```
> plot(-M, x = 0..L, title = "Moment distribution M(x)");
```

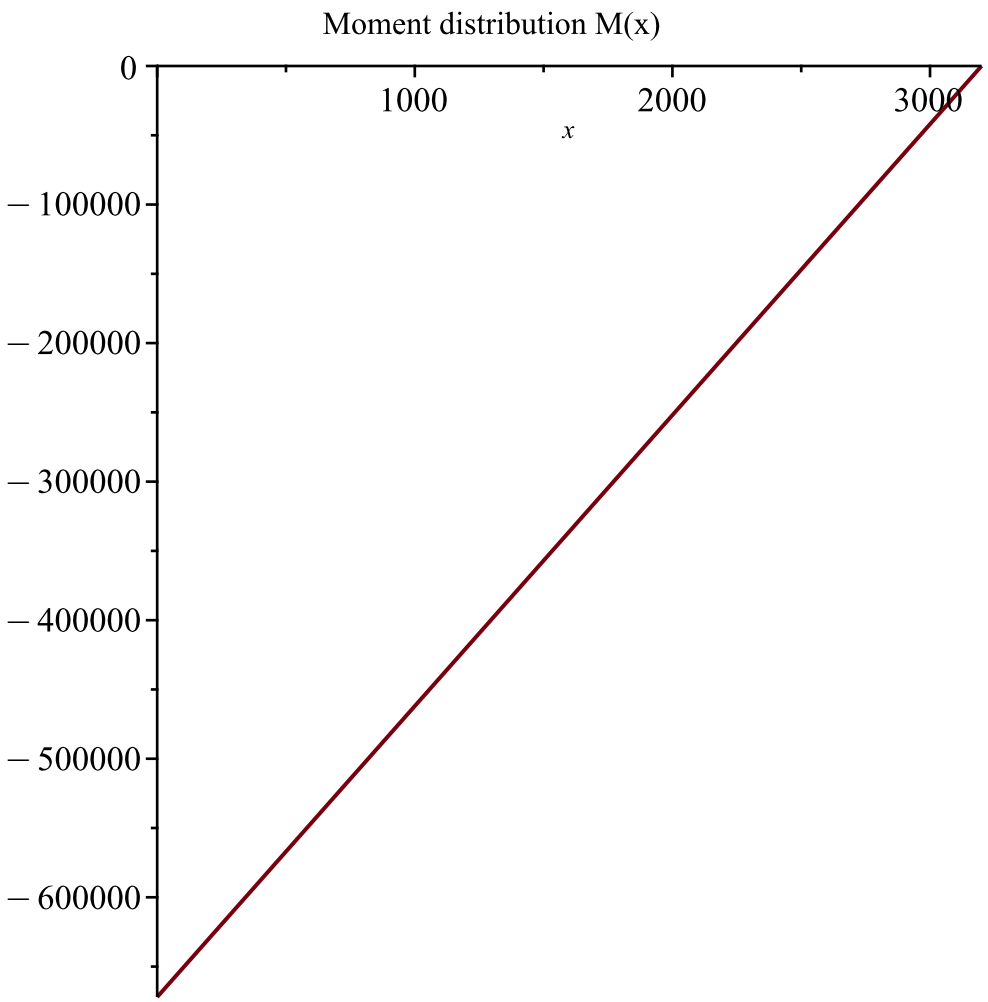


```
> plot( −V, x = 0 ..L, title = "Shear force distribution V(x)");
```

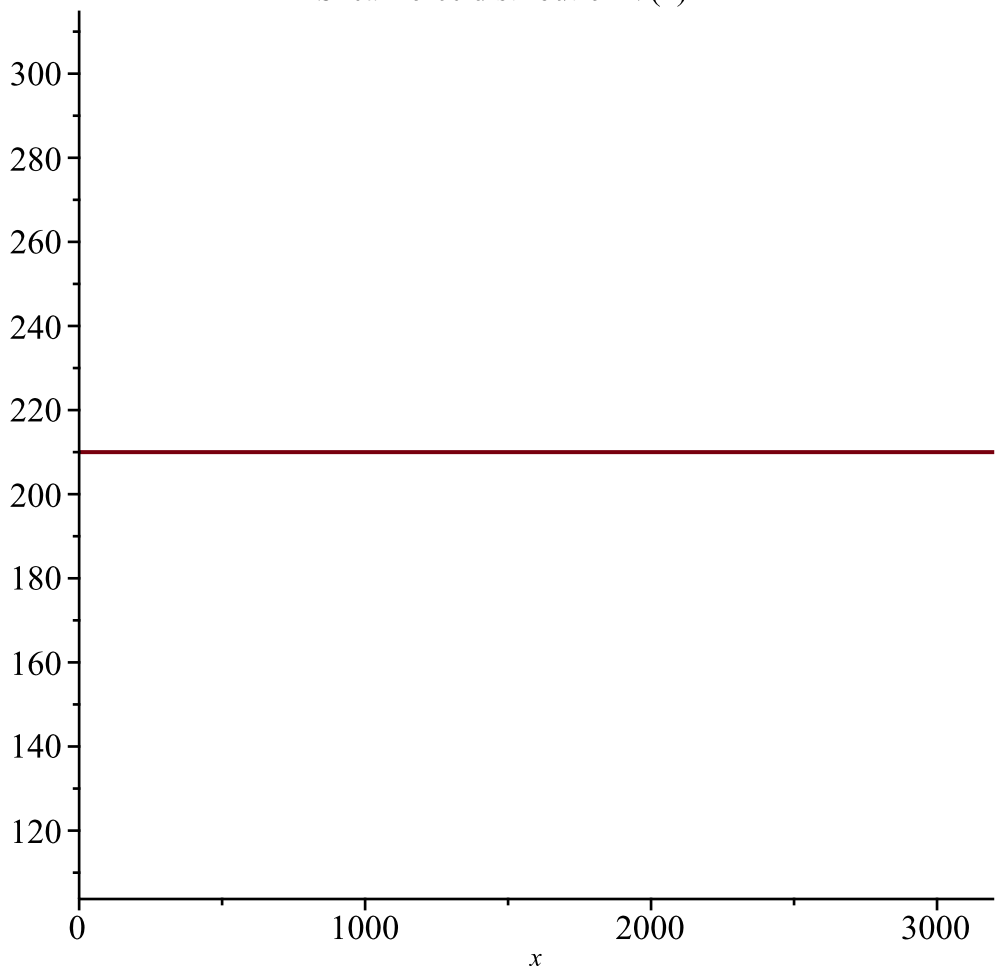


```
> plot( -Gamma, x = 0 ..L, title = "Shear angle Gamma(x)" );
```

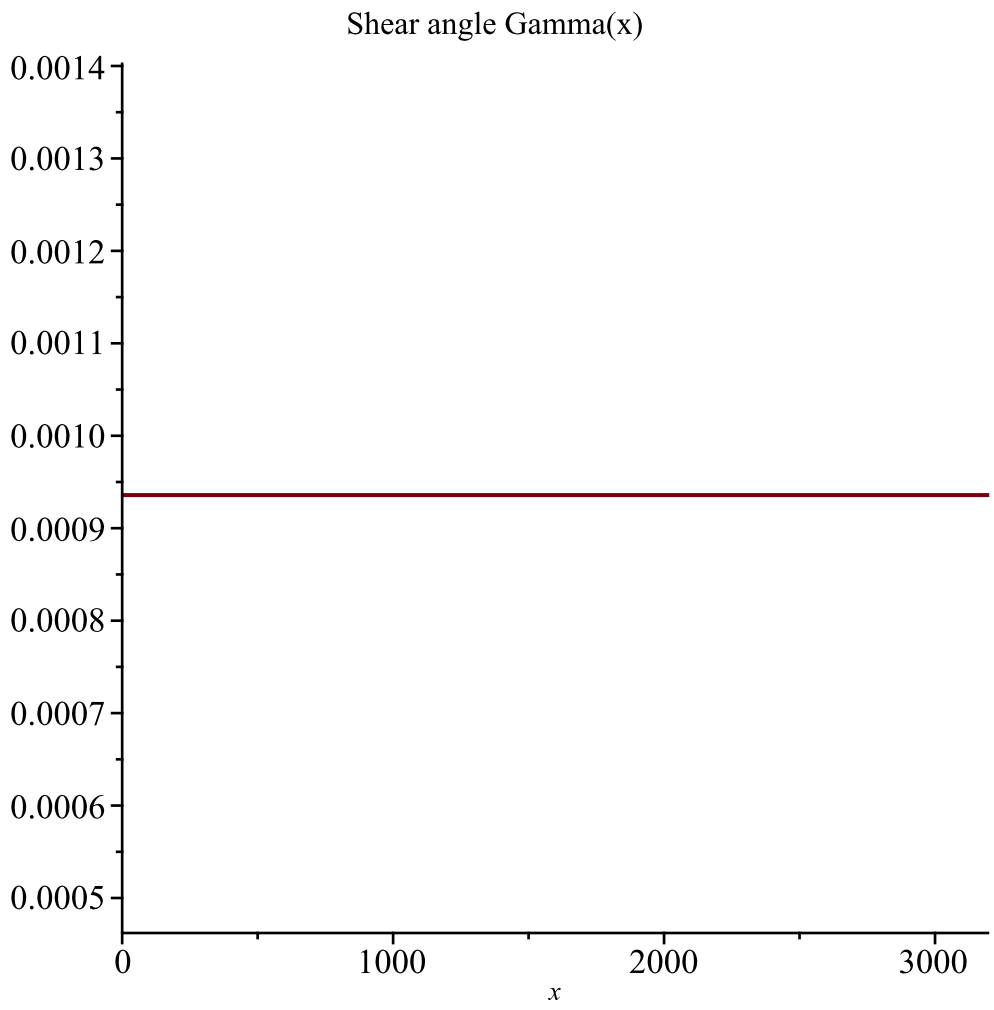
Shear angle Gamma(x)
0.0014
0.0013
0.0012
0.0011
0.0010
0.0009
0.0008
0.0007
0.0006
0.0005
0
1000
2000
3000
x

>

>

E

Inner and outer face loaded F=125 kN Maple output - vertical displacements

```
> restart;

Rod in compression
[units N and mm]
>
> DV := EA*diff(u(x), x$2) = 0;
```

$$DV := EA\left(\frac{d^2}{dx^2}\,u(x)\right) = 0 \tag{1}$$

```
>
> sol1 := dsolve({DV}, {u(x)}) : assign(sol1) :
> u := (u(x));
```

$$u := \_C1\,x + \_C2 \tag{2}$$

```
> N := EA·diff(u, x) :
>
>
> x := 0 : eq1 := u = 0 :
  x := L : eq2 := N = −F :
> sol2 := solve({eq1, eq2}, {_C1, _C2}) : assign(sol2); x := 'x':
>
> _C1;
```

$$-\frac{F}{EA} \tag{3}$$

```
> _C2;
```

$$0 \tag{4}$$

```
>
```

$$\_C4 \tag{5}$$

```
> u;
```

$$-\frac{F\,x}{EA} \tag{6}$$

```
> N;
```

$$-F \tag{7}$$

```
```

(8)

```
> L := 3.2·1000 : F := 1.02·(125090) : EA := 5·100·1020 + 3800·24·1020 :
> plot(u, x = 0..L, title = "Deflection u(x)");
```

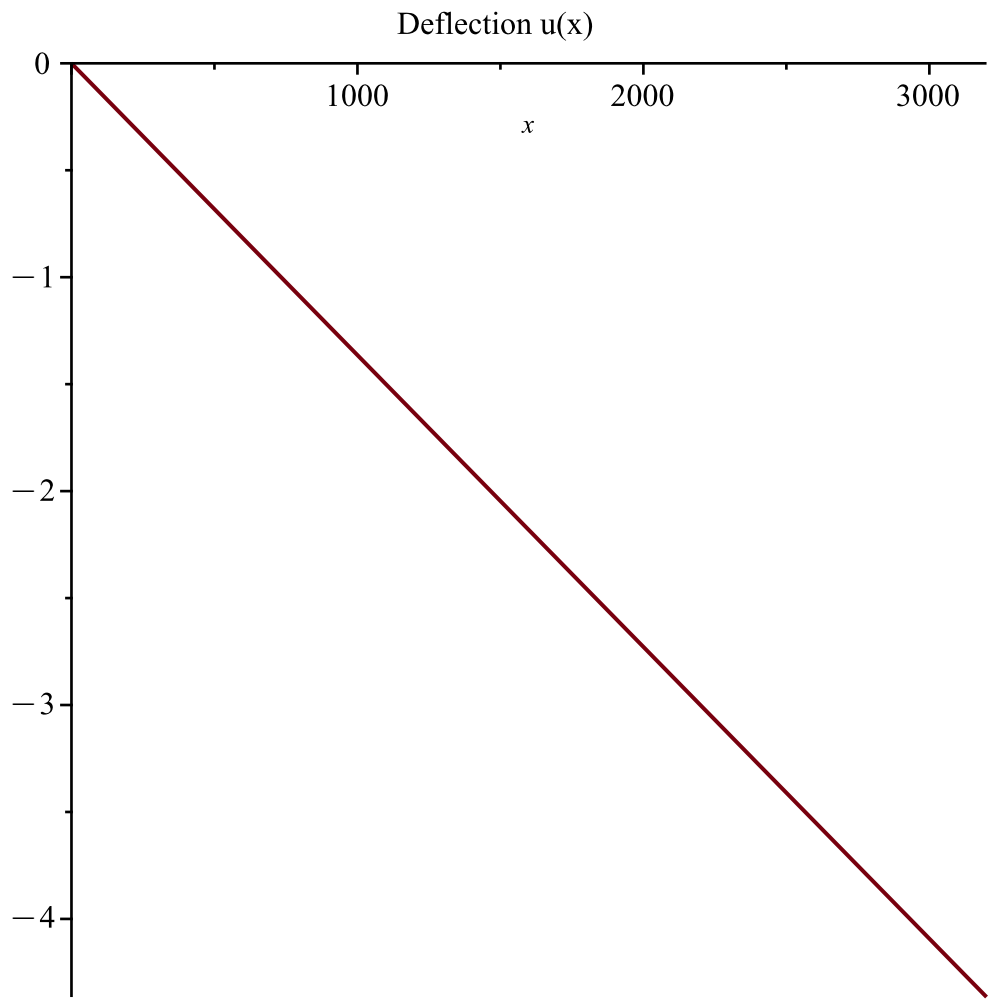


```
>
>
> plot(N, x = 0 ..L, title = "Shear force distribution V(x)");
```

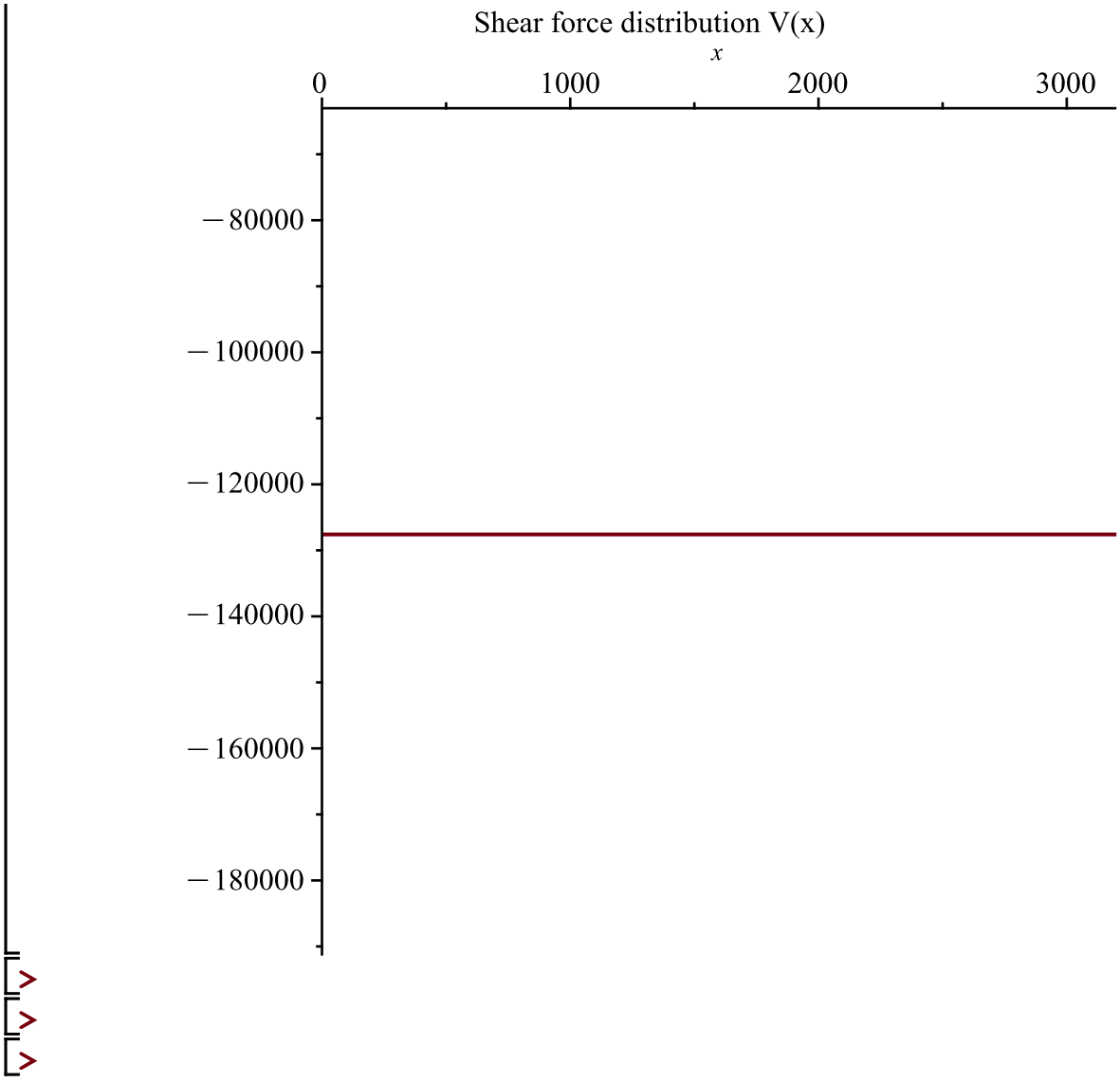
Shear force distribution V(x)
x
0
1000
2000
3000
−80000
−100000
−120000
−140000
−160000
−180000

F

Additional experiment results

This chapter has all of the experimental results visualised. It starts with overall graphs for 6 kN on the inner and outer face deflections and strain results, and 6 kN on the inner face deflections and strains. After that, results starting from experiment 2 have been brought out in the same principle as for the analysis of the experimental results. Some of the graph info has been used in concluding graphs under panel analysis chapter.

The inner and outer face loaded with 6 kN seen in figure F.1 gives very similar trends as to already analysed loading case where 12 kN in on the inner face and 6 kN on the outer face. The deflection curve leans towards the top half of the panel suggesting a possible local failure point. The Karamba3D model encompasses the main experimental results.

The strain results in figure F.2 suggest that RFEM is not capable of predicting the strain results since the support conditions are different to the Karamba3D model. However, the difference is not that significant to experimental set up, but most likely the shell-element layered material definition plays the biggest role in the strain results.

The inner face loaded with 6 kN seen in figure F.3 was compared with experimental results, Karamba3D and RFEM model results. This load case showed a similar case with the model results as for previously, where RFEM deflections are not as big as for experimental or Karamba3D results, but does show a peak towards the top of the panel. This trend is not shown by the Karamba3D model, but the Karamba3D model does surpass most of the deflection results except for test 1 results.

The strain results seen in figure F.4 are this time very similar to the experimental measurements, showing some agreement between the results. However, the Karamba3D model shows a linear distribution of strains meaning a full composite action, but the experiments suggest a separate action from the faces.

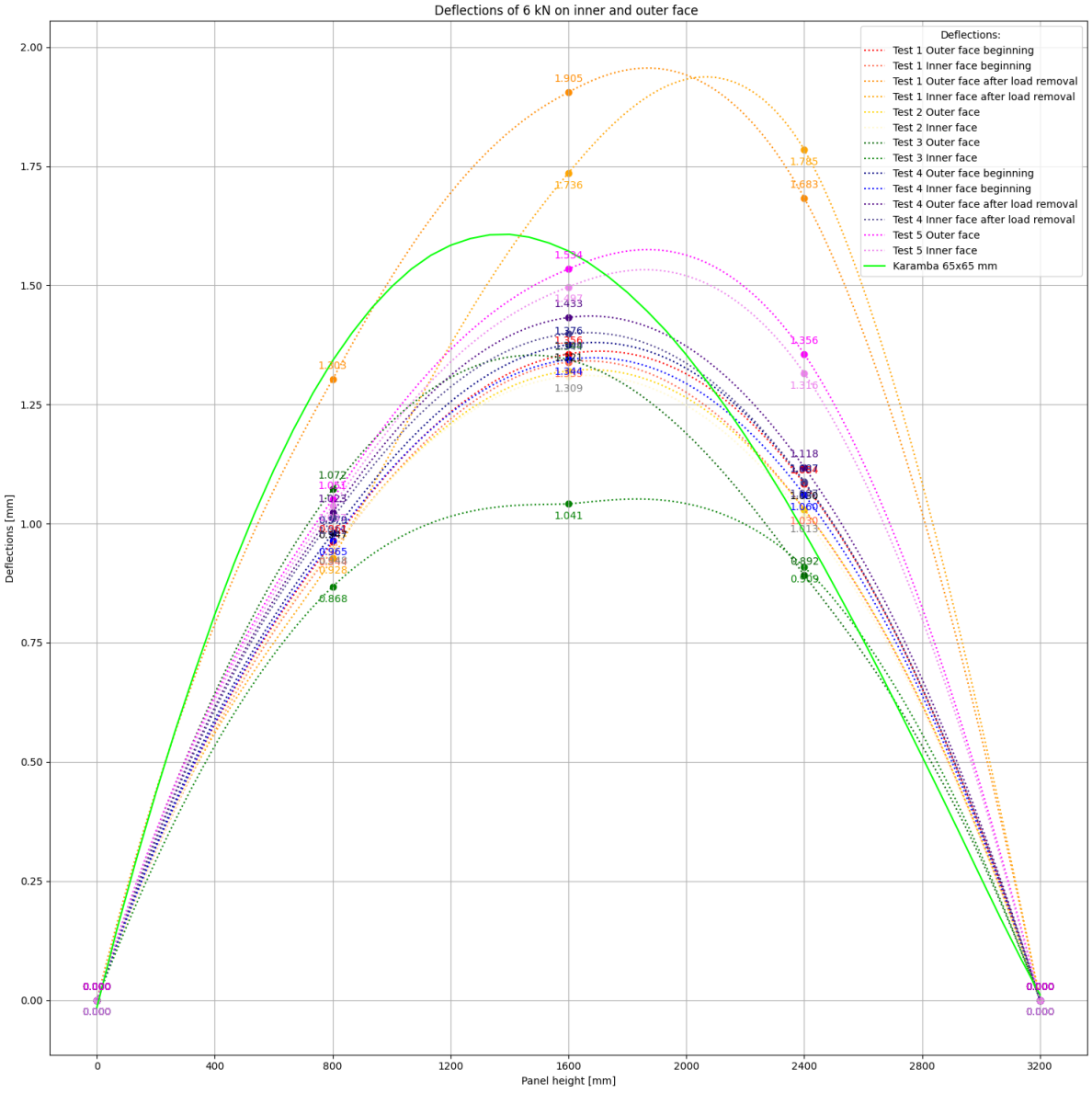

Figure F.1: 6 kN on inner and outer face deflections

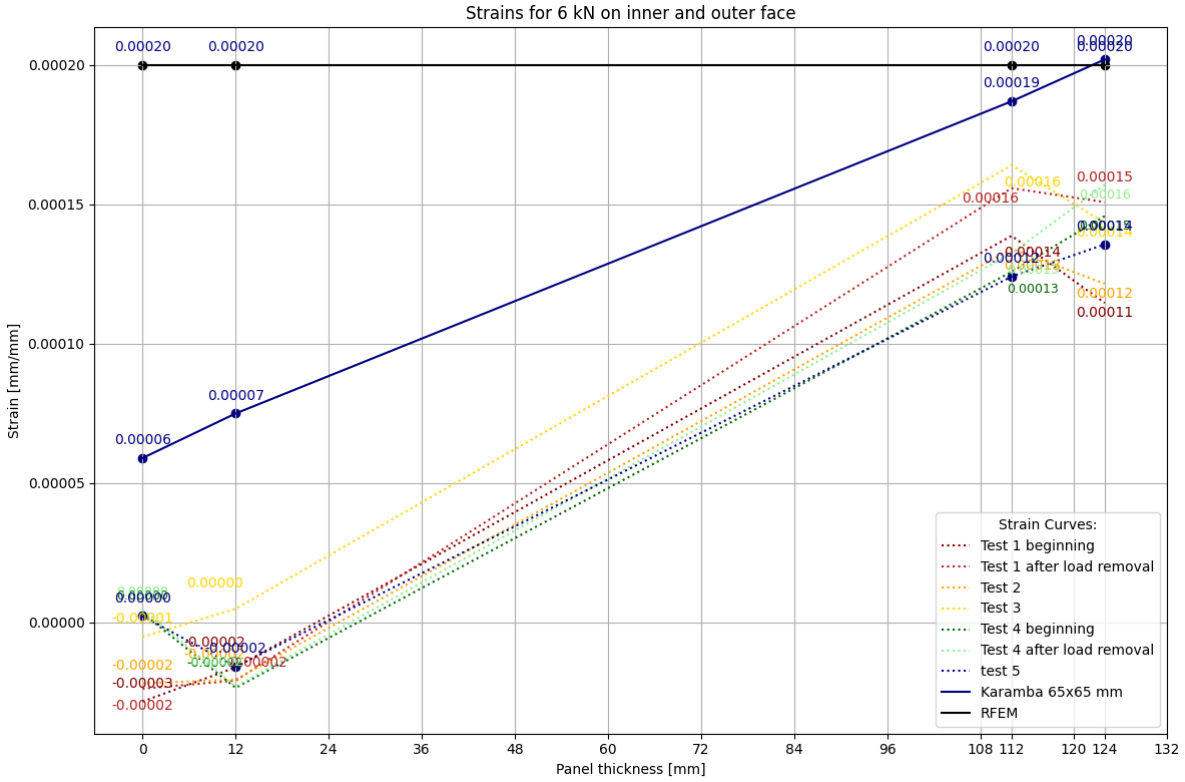

Figure F.2: 6 kN on inner and outer face strains

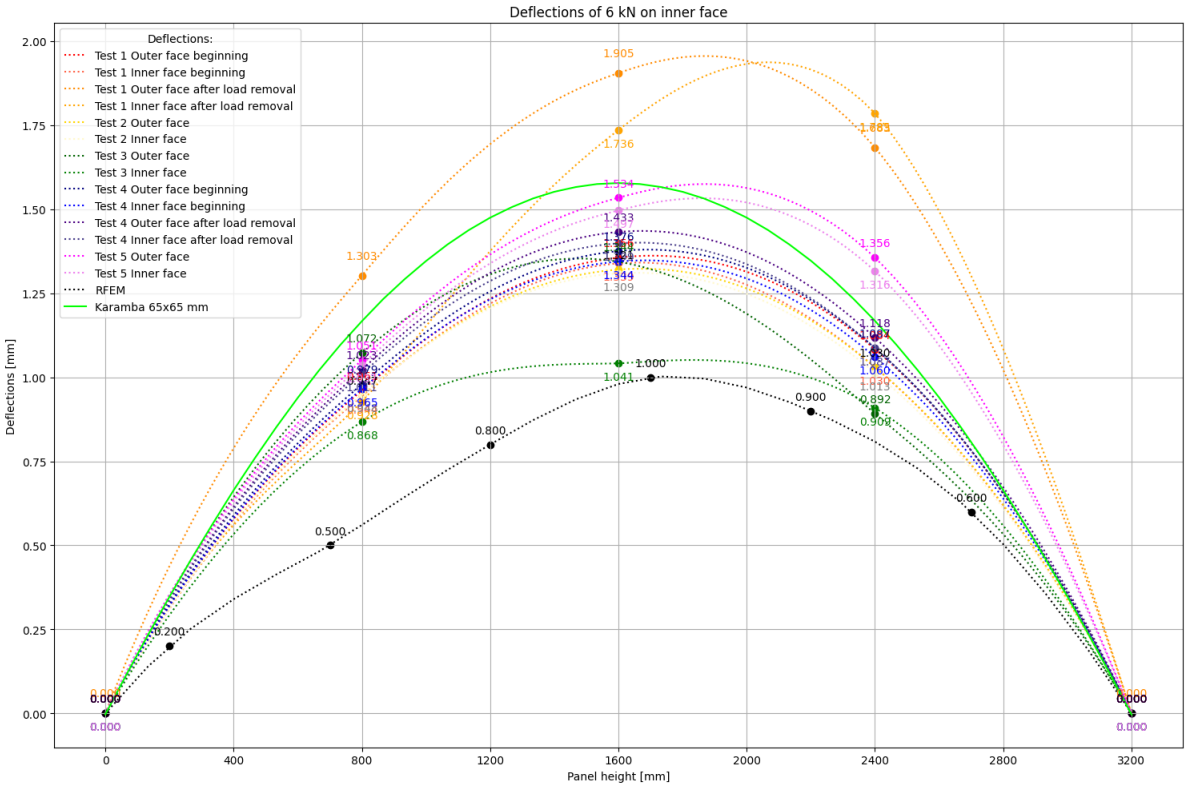

Figure F.3: 6 kN on inner face deflections

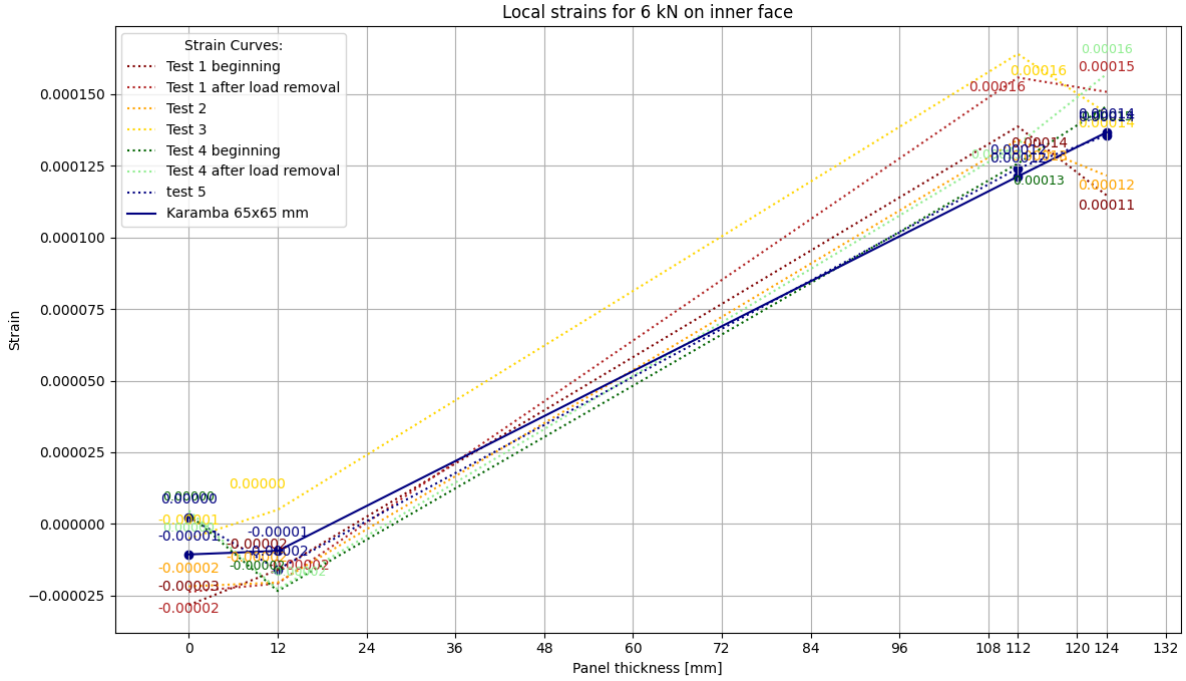

Figure F.4: 6 kN on inner face strains

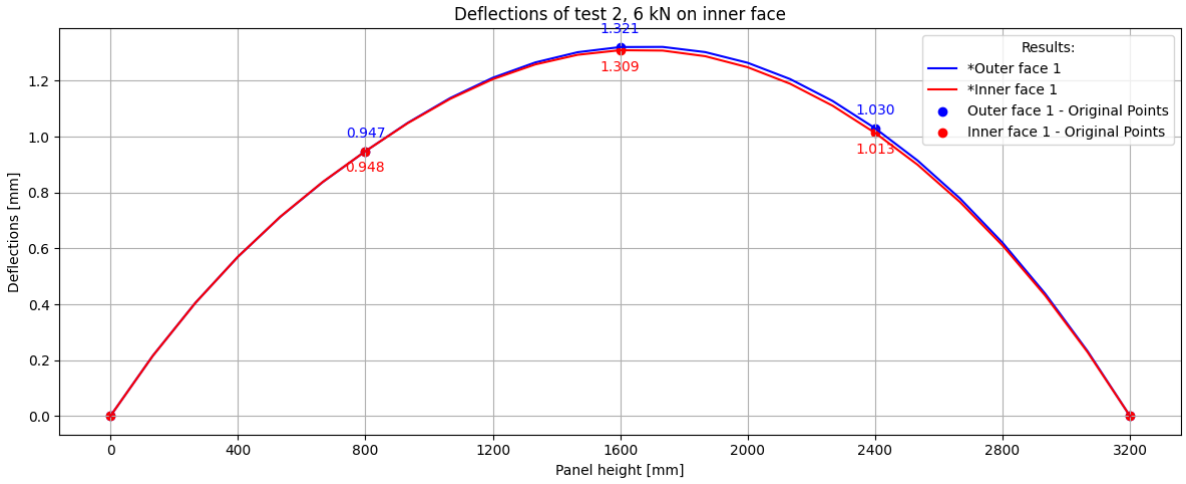

Figure F.5: Test 2 6 kN in defl

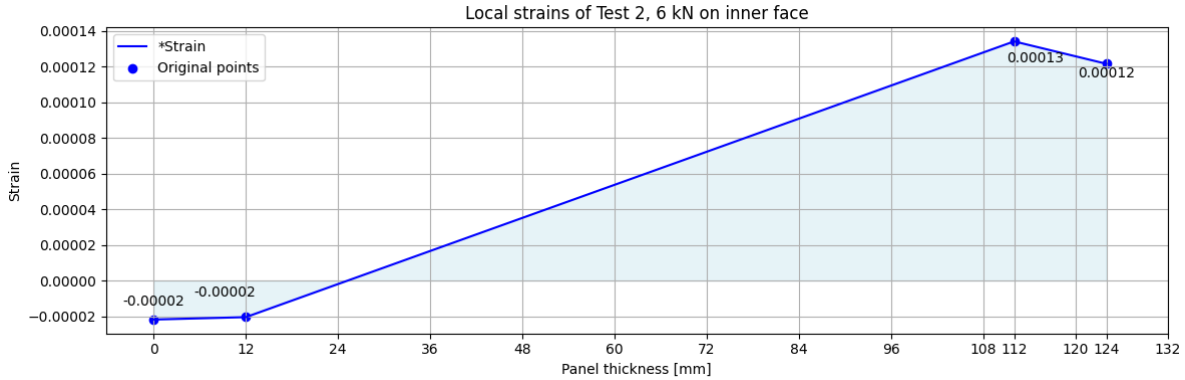

Figure F.6: Test 2 6 kN in strain

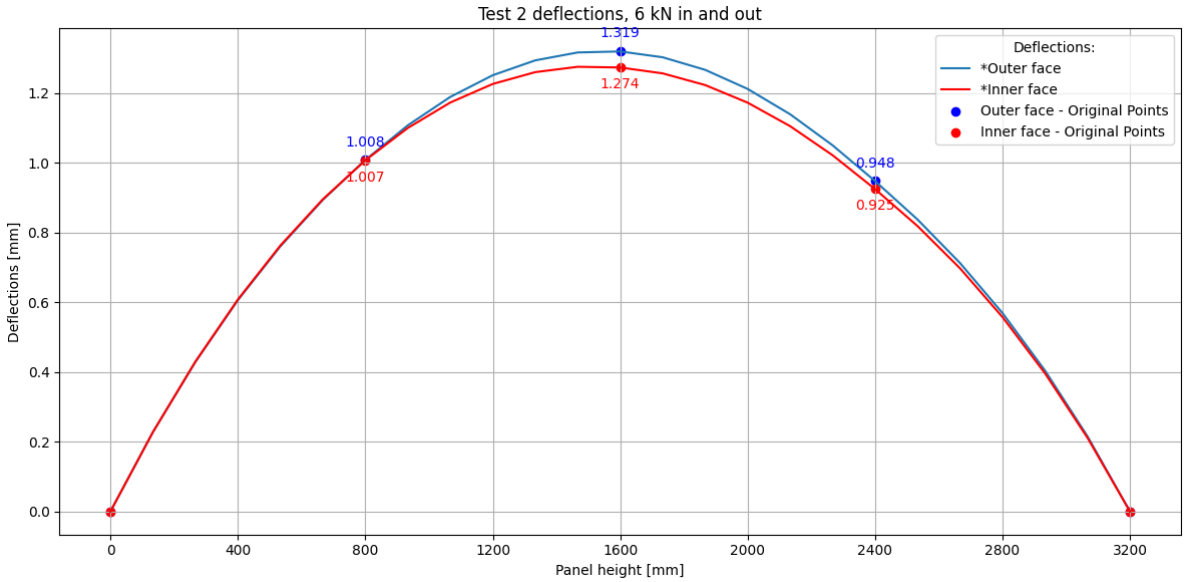

Figure F.7: Test 2 6 kN in and out defl

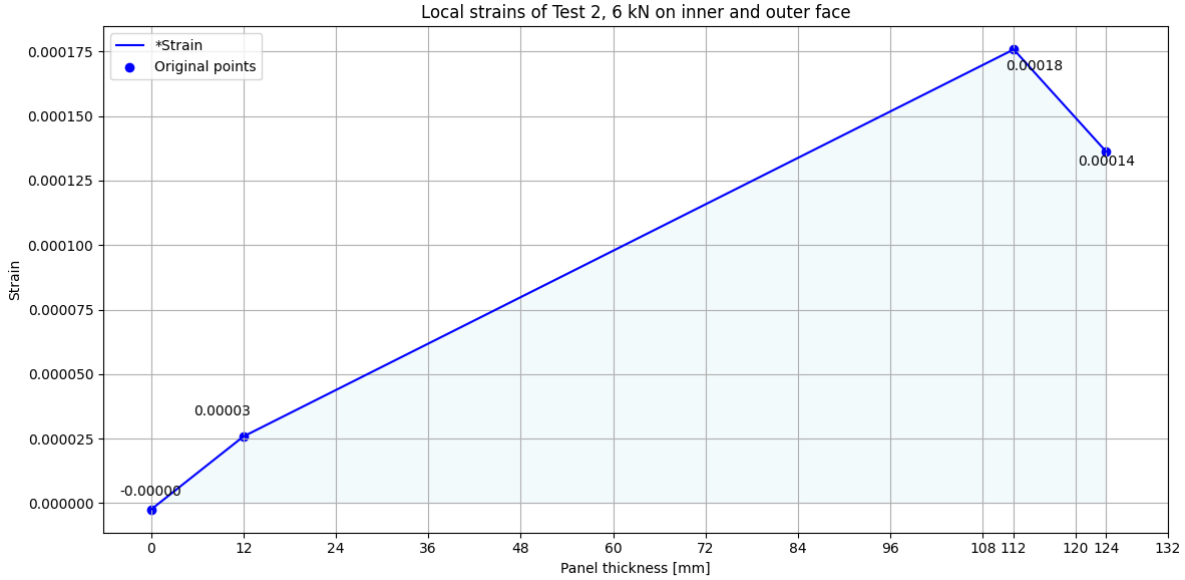

Figure F.8: Test 2 6 kN in and out strain

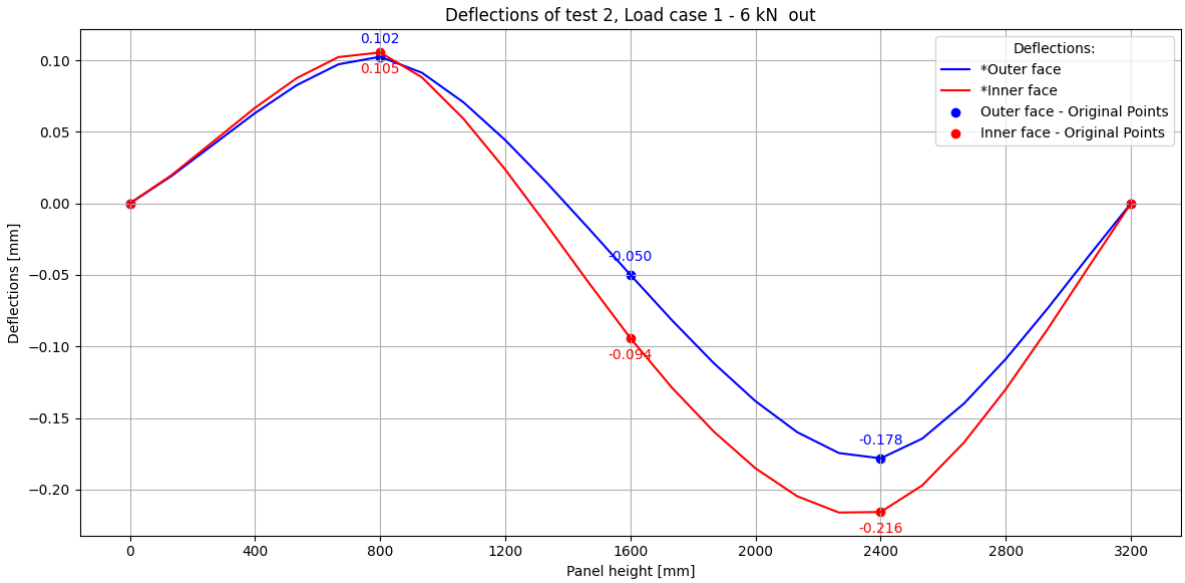

Figure F.9: Test 2 6 kN out defl - load case 1

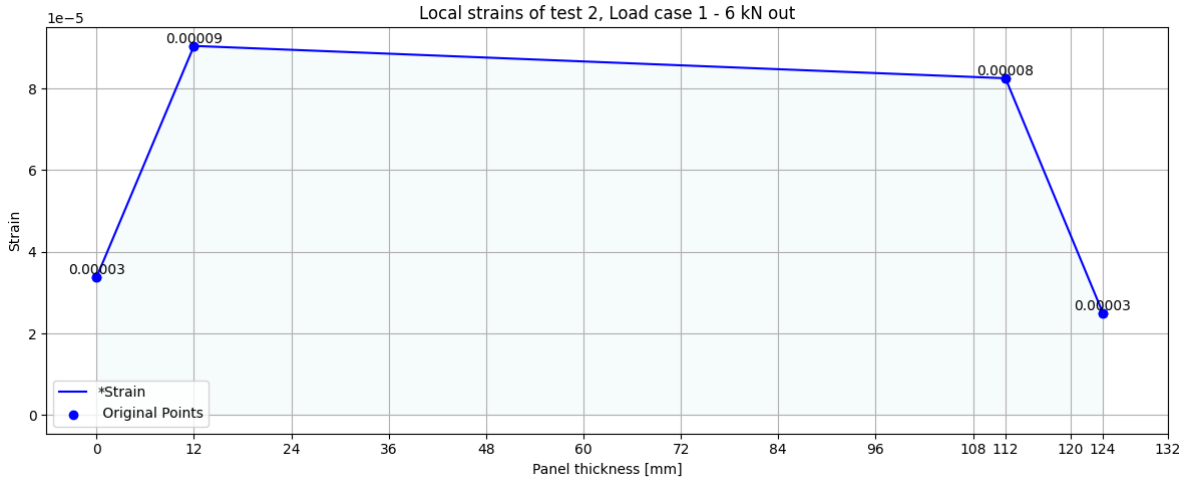

Figure F.10: Test 2 6 kN out strain - load case 1

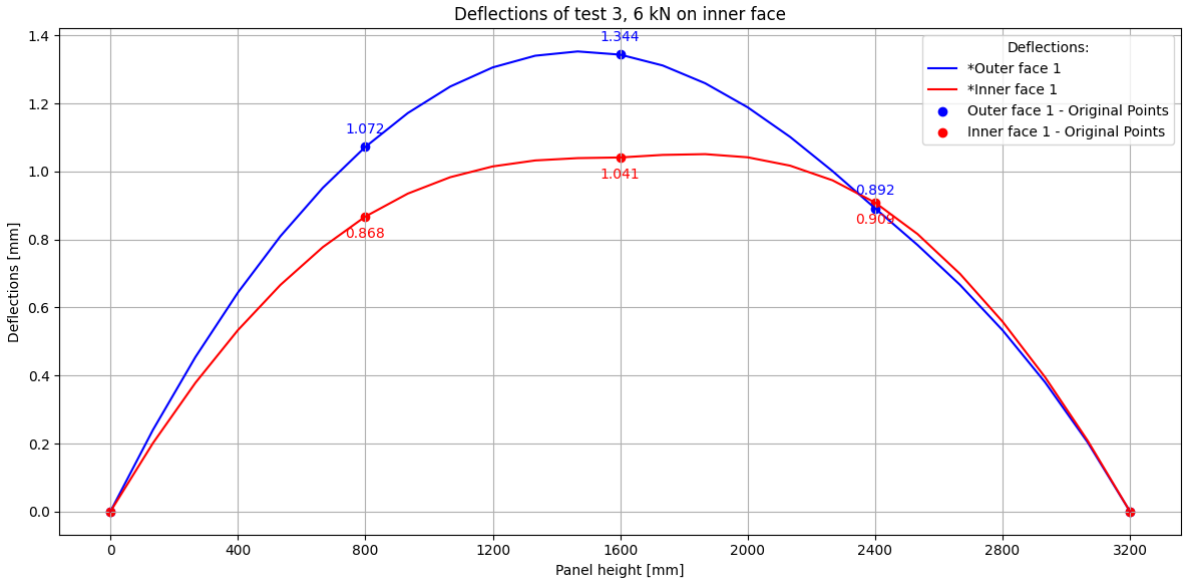

Figure F.11: Test 3 6 kN in defl

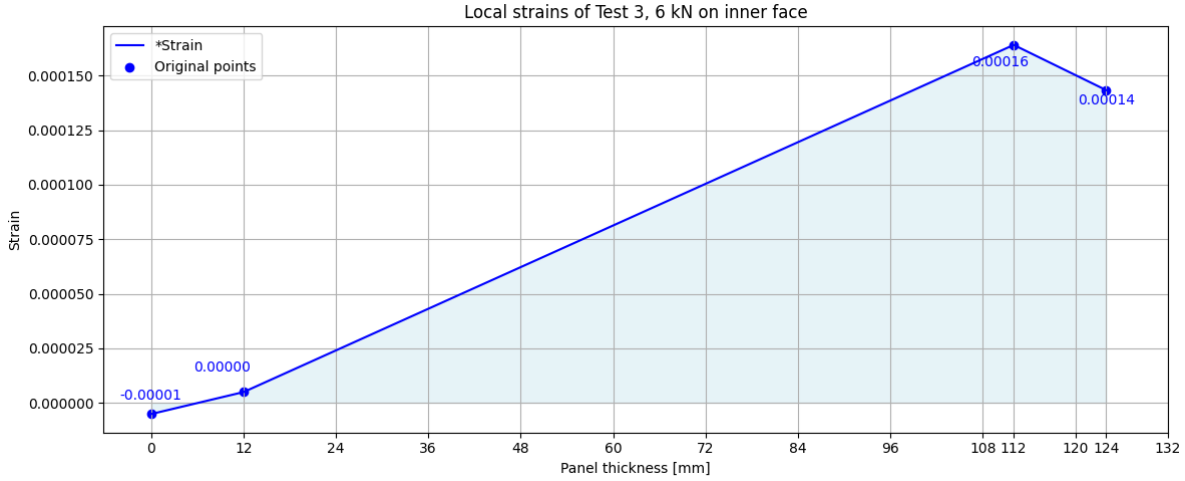

Figure F.12: Test 3 6 kN in strain

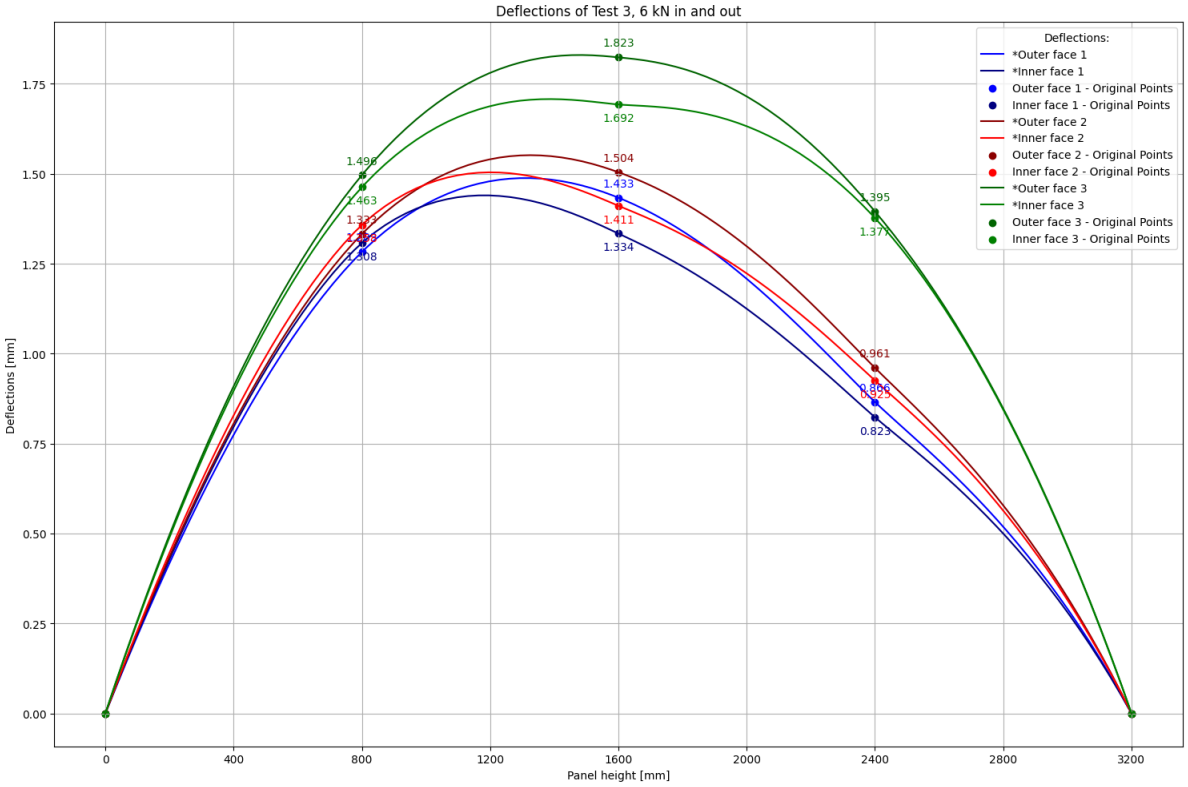

Figure F.13: Test 3 6 kN in and out defl

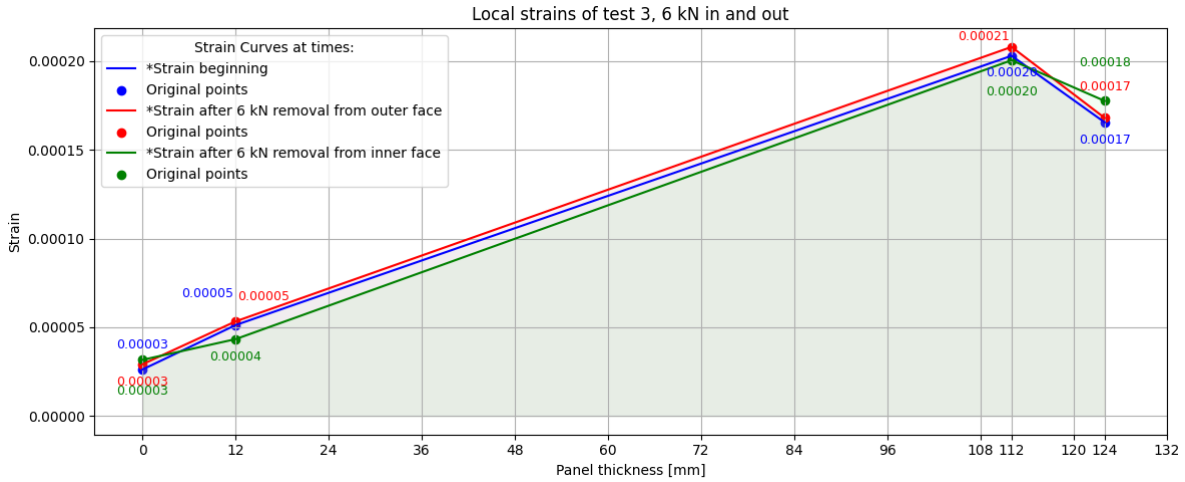

Figure F.14: Test 3 6 kN in and out strain

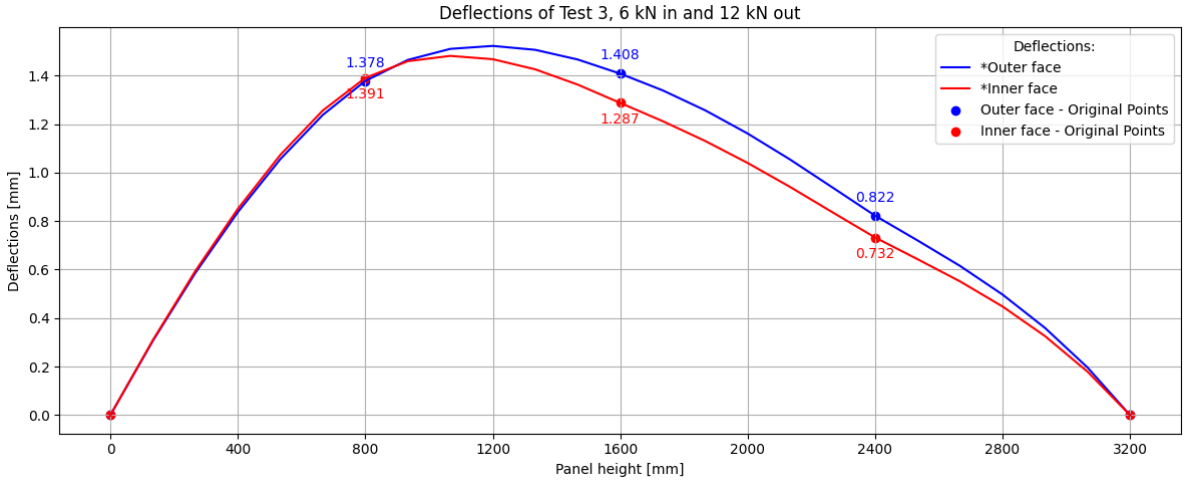

Figure F.15: Test 3 6 kN in and 12 kN out defl

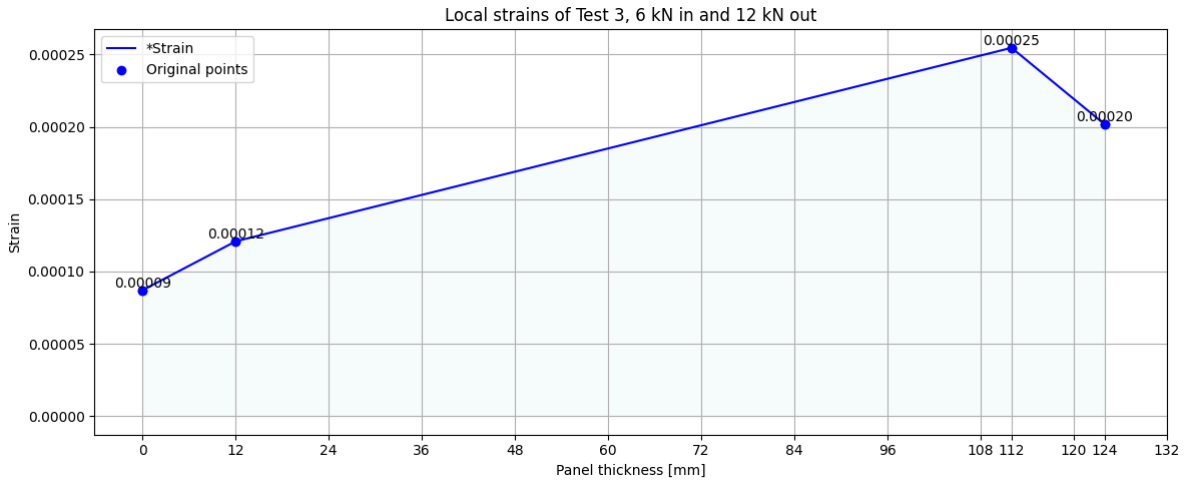

Figure F.16: Test 3 6 kN in and 12 kN out strain

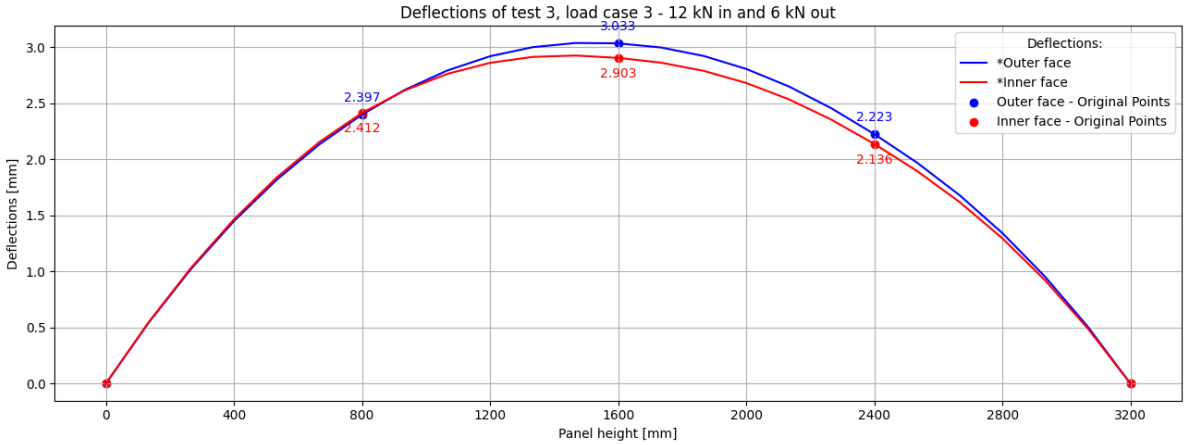

Figure F.17: Test 3 12 kN in and 6 kN out defl - load case 3

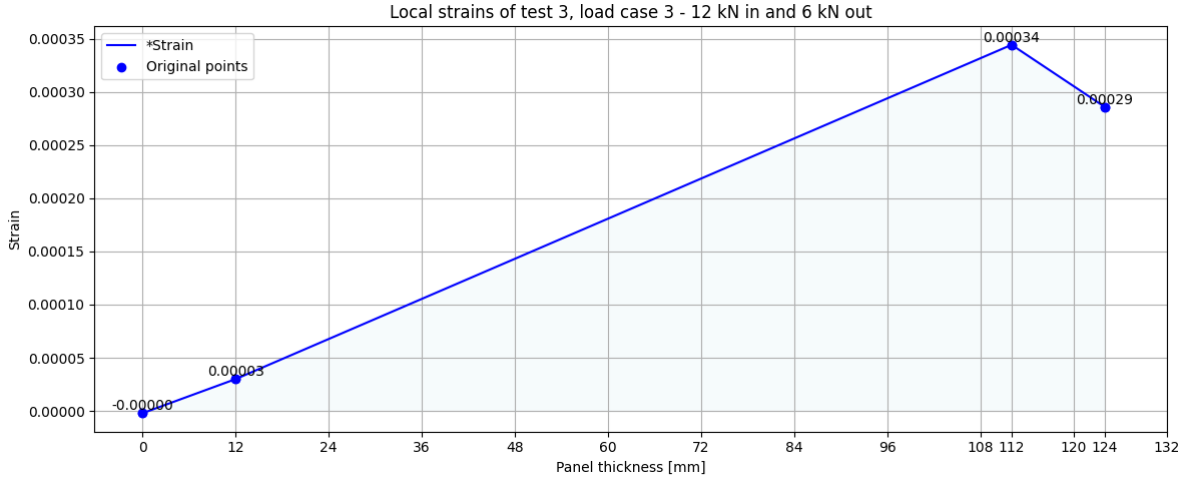

Figure F.18: Test 3 12 kN in and 6 kN out strain - load case 3

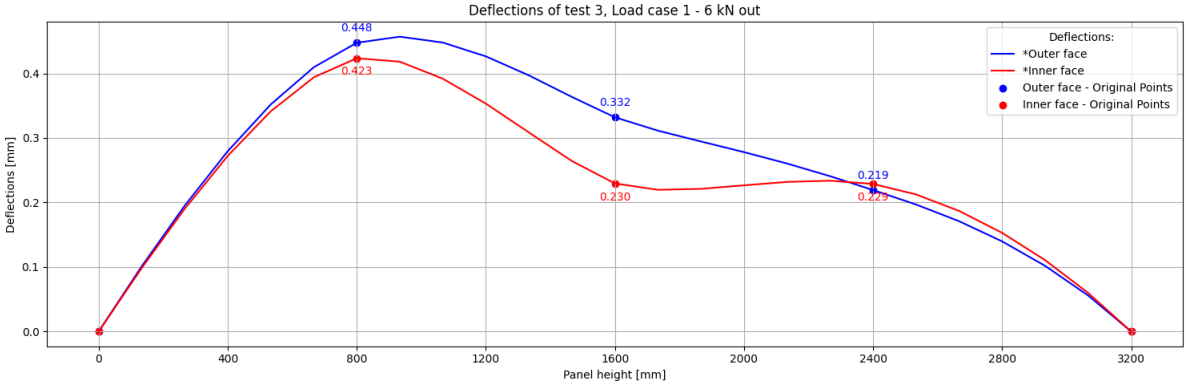

Figure F.19: Test 3 6 kN out defl - load case 1

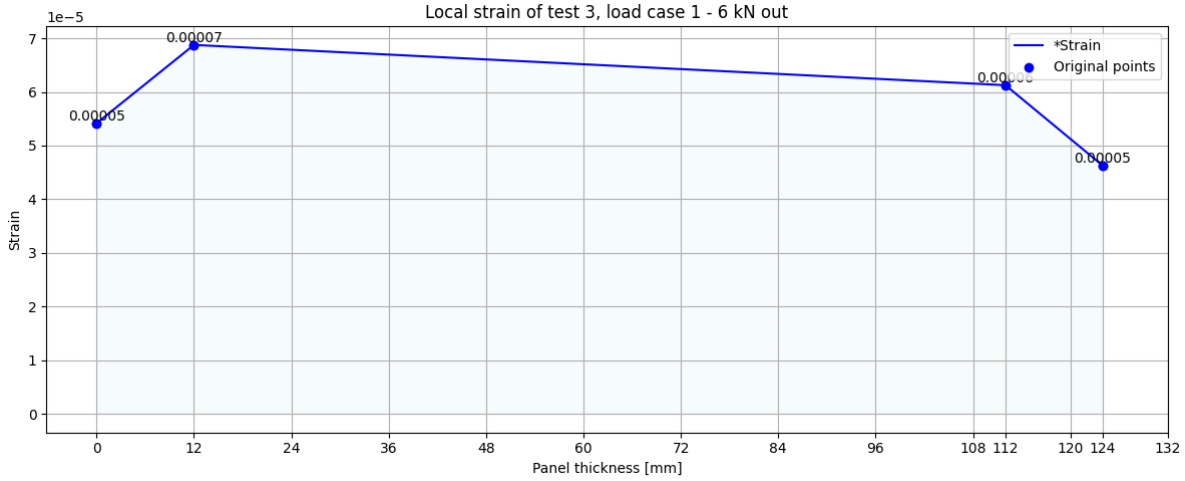

Figure F.20: Test 3 6 kN out strain - load case 1

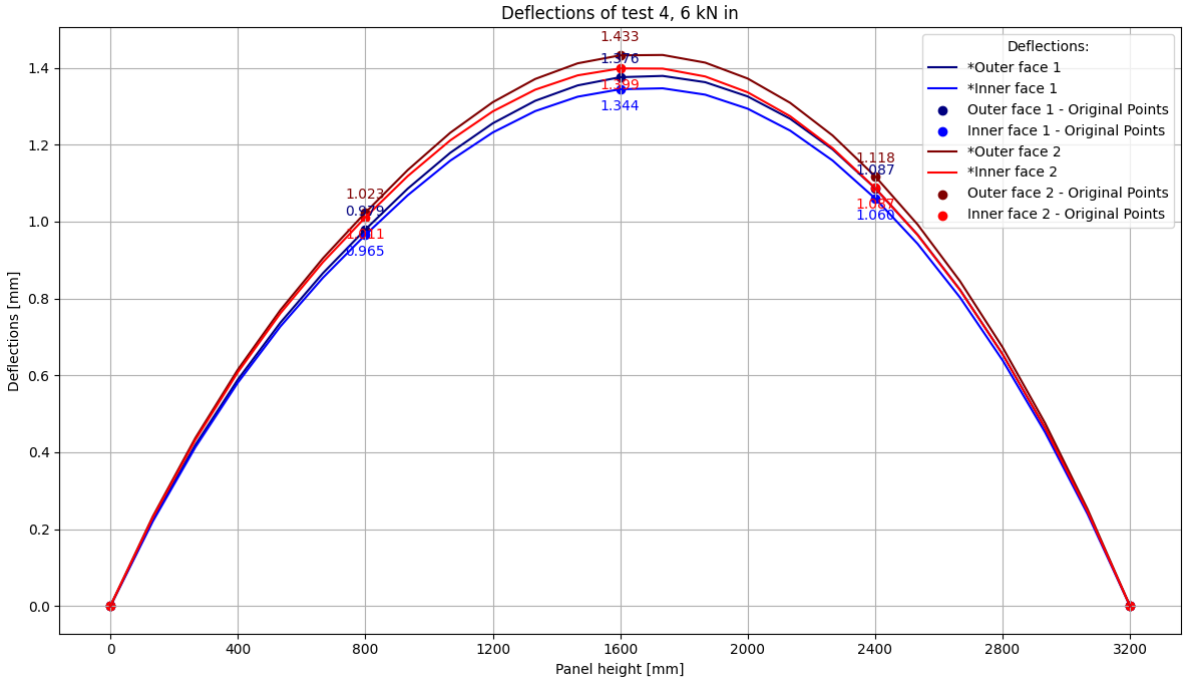

Figure F.21: Test 4 6 kN in defl

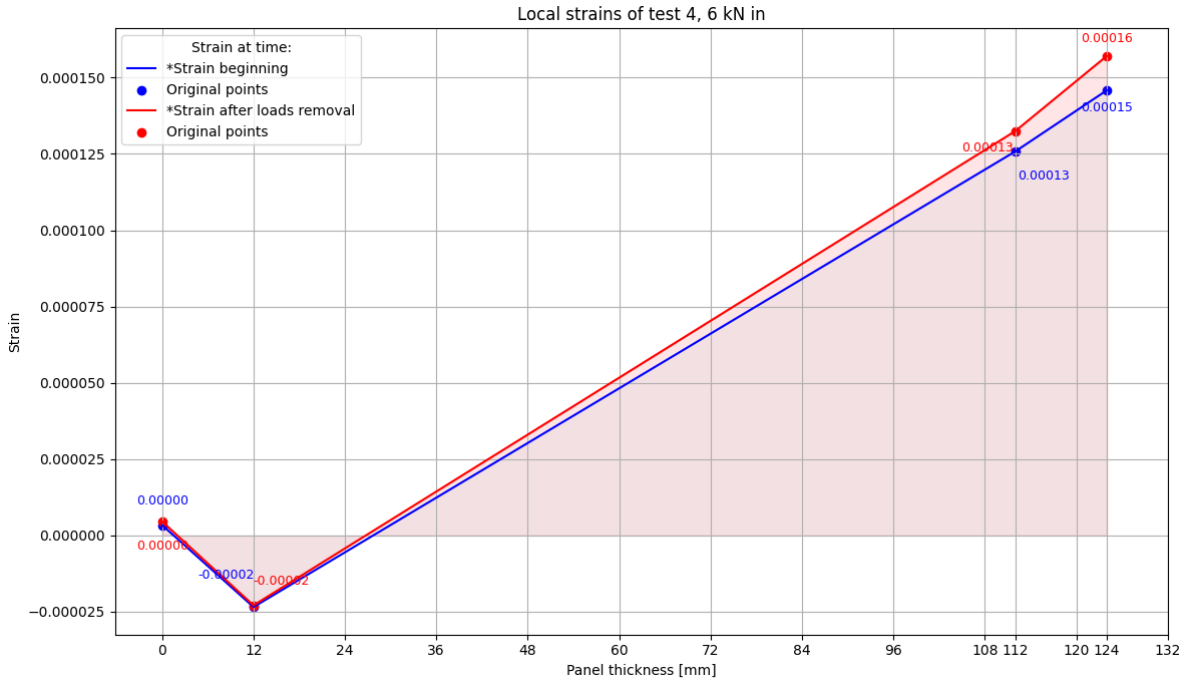

Figure F.22: Test 4 6 kN in strain

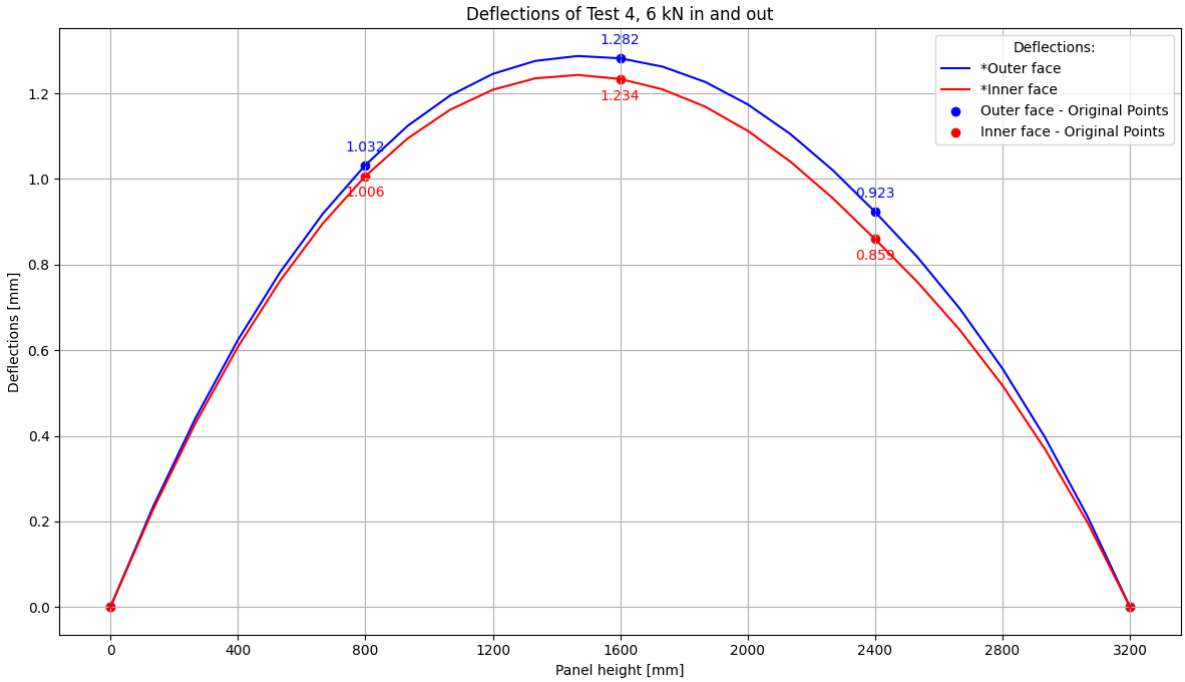

Figure F.23: Test 4 6 kN in and out defl

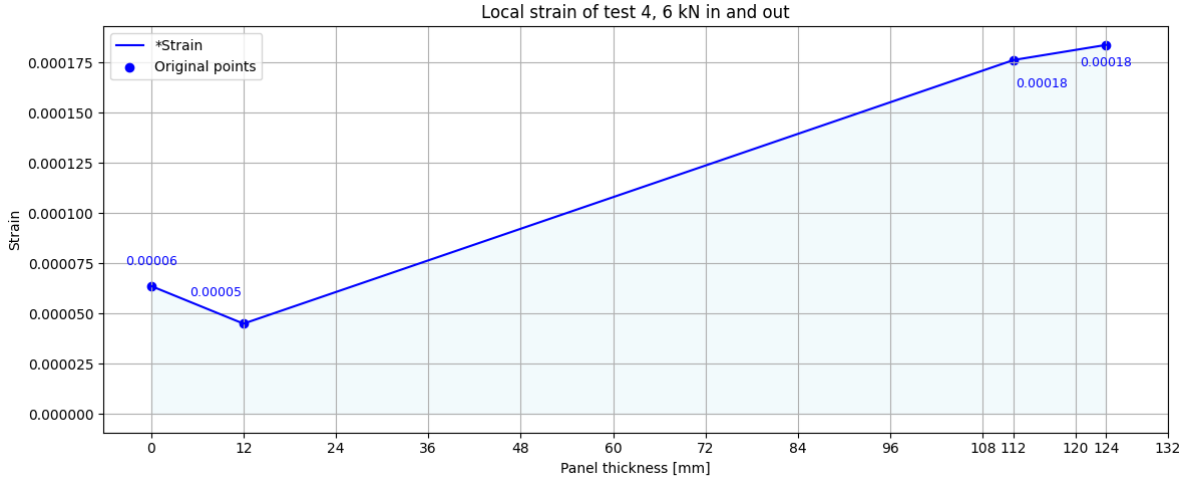

Figure F.24: Test 4 6 kN in and out strain

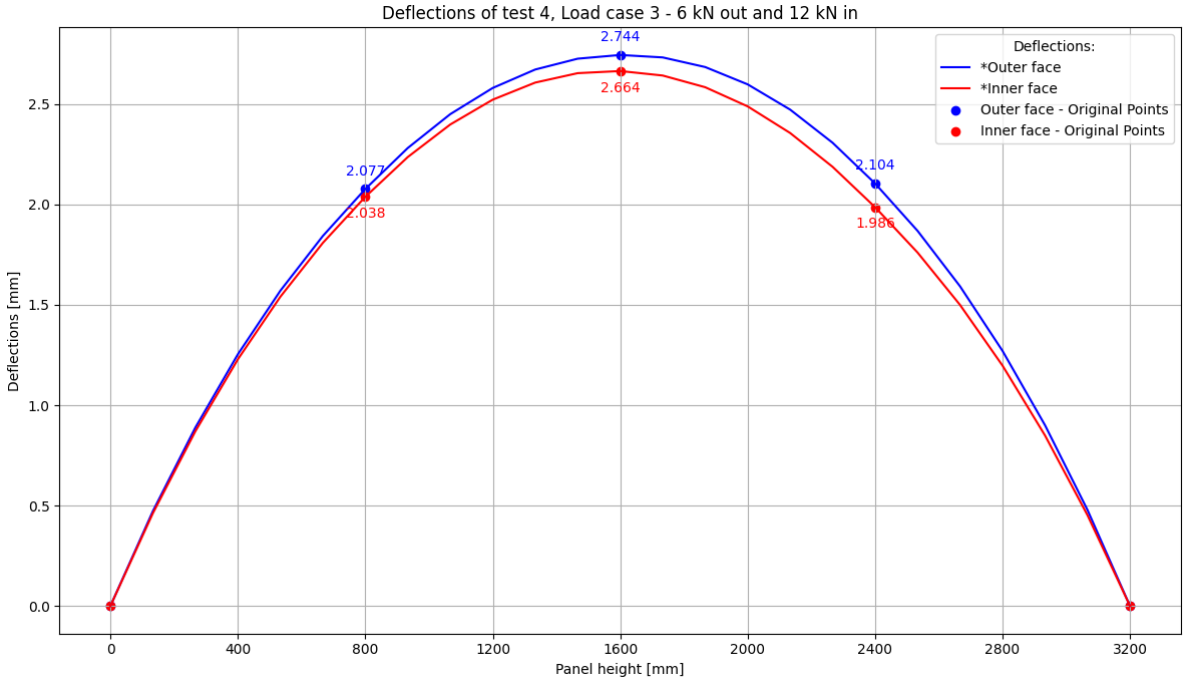

Figure F.25: Test 4 12 kN in and 6 kN out defl - load case 3

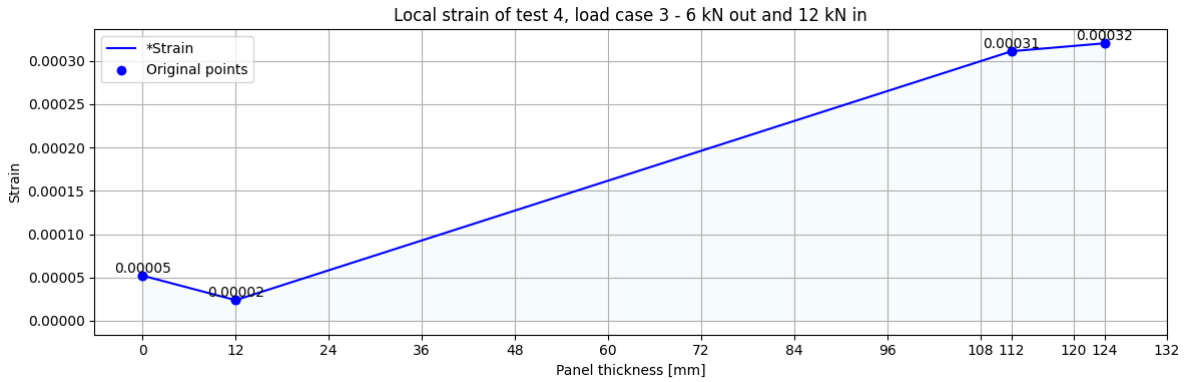

Figure F.26: Test 4 12 kN in and 6 kN out strain - load case 3

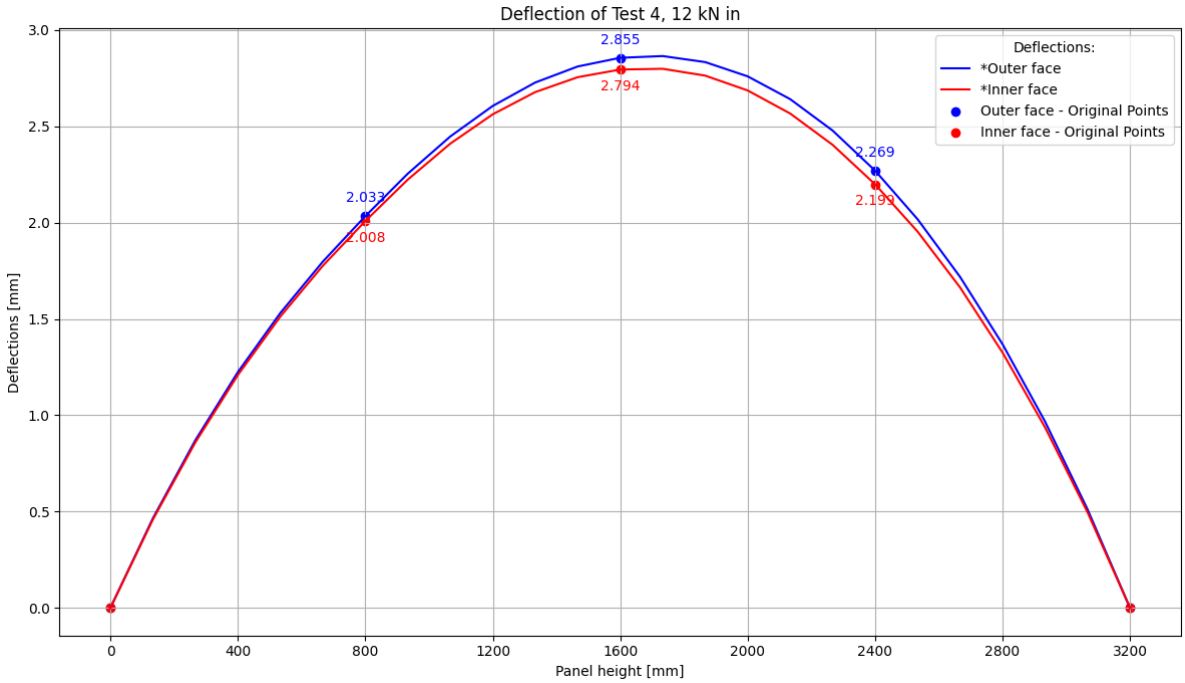

Figure F.27: Test 4 12 kN in defl

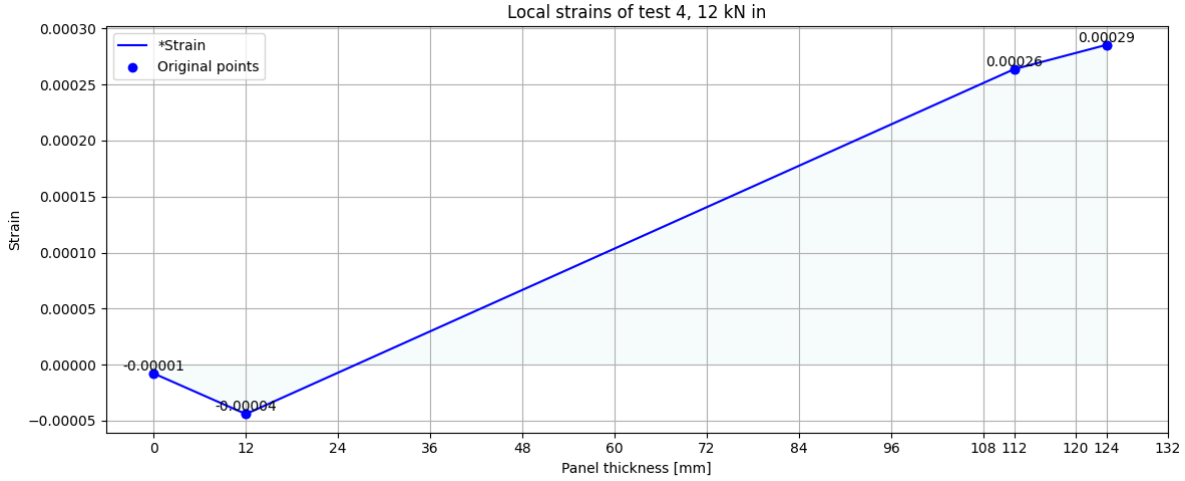

Figure F.28: Test 4 12 kN in strain

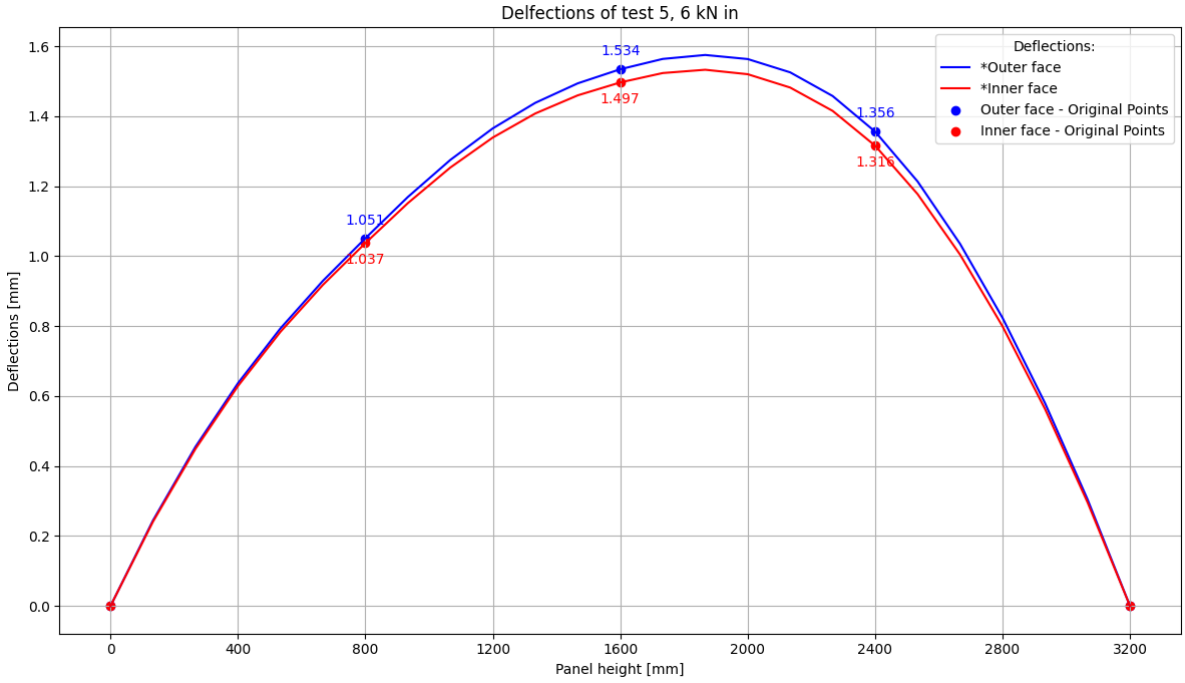

Figure F.29: Test 5 6 kN in defl

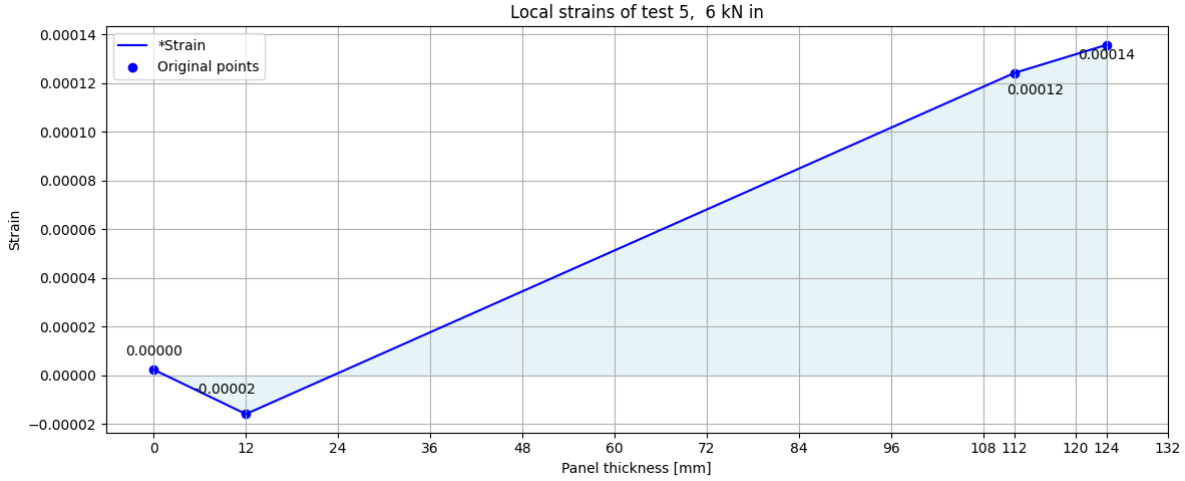

Figure F.30: Test 5 6 kN in strain

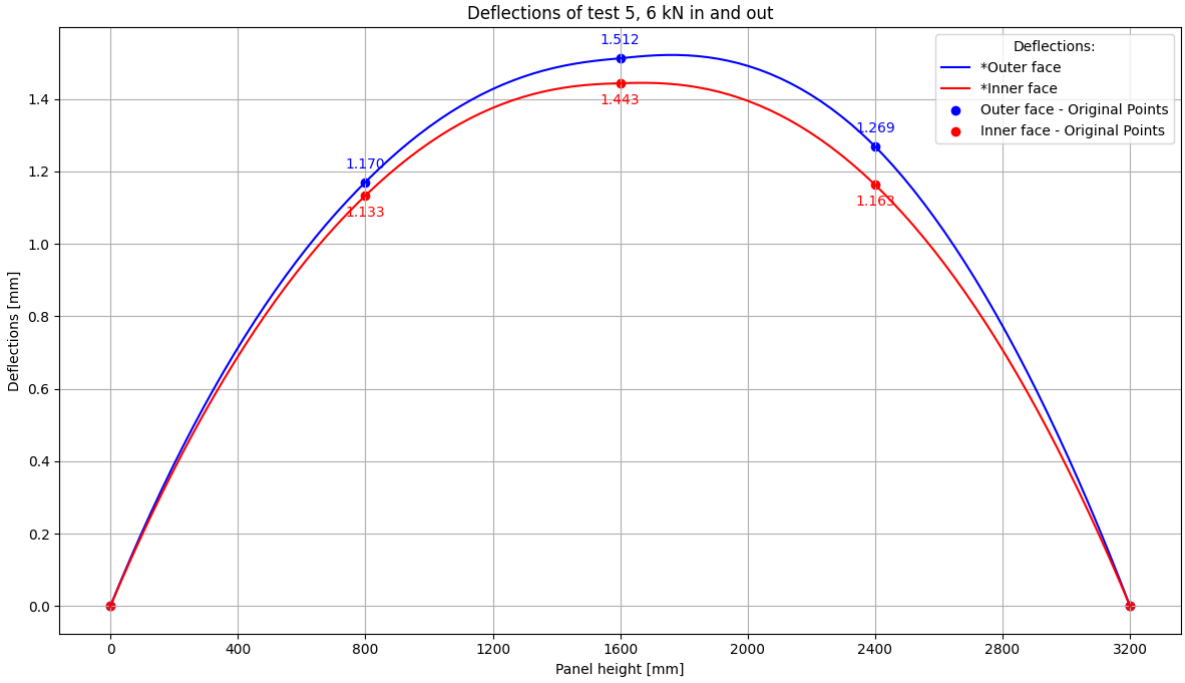

Figure F.31: Test 5 6 kN in and out defl

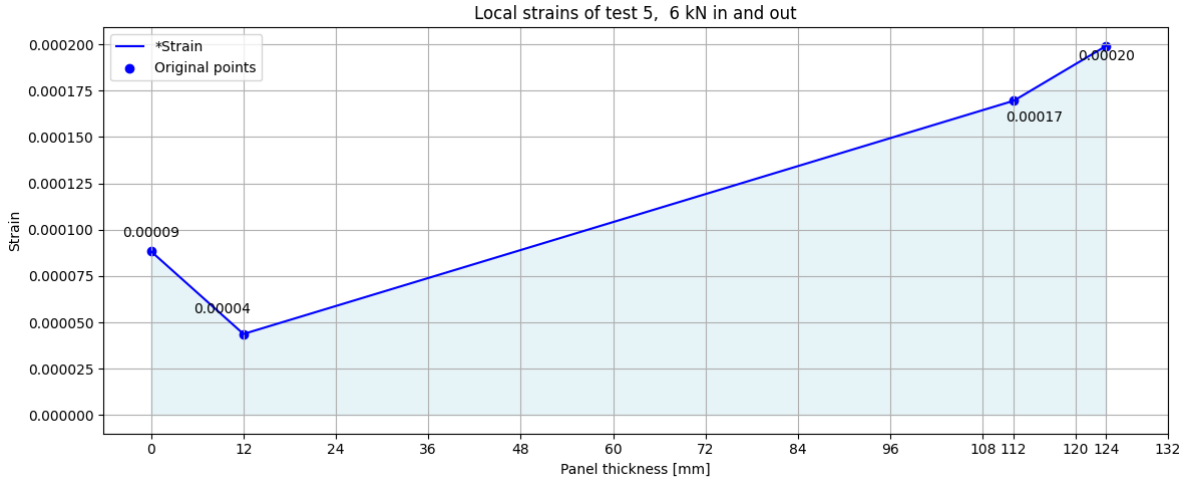

Figure F.32: Test 5 6 kN in and out strain

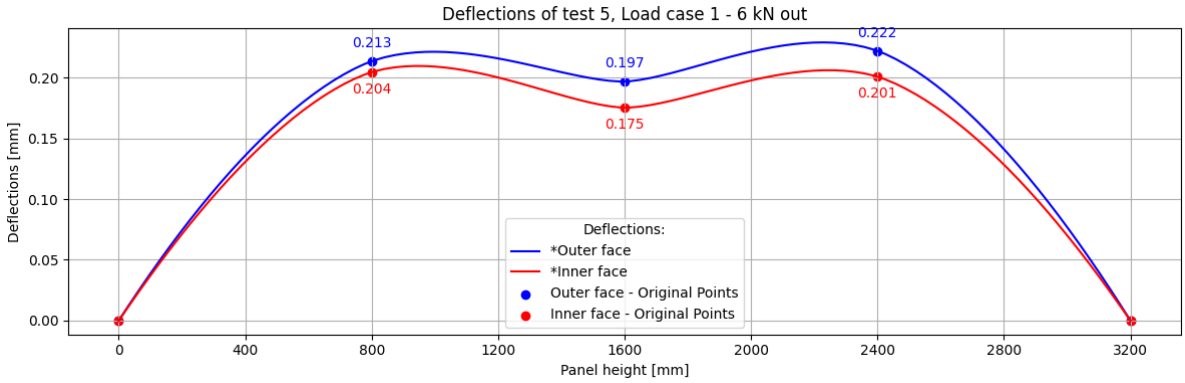

Figure F.33: Test 5 6 kN out defl - load case 1

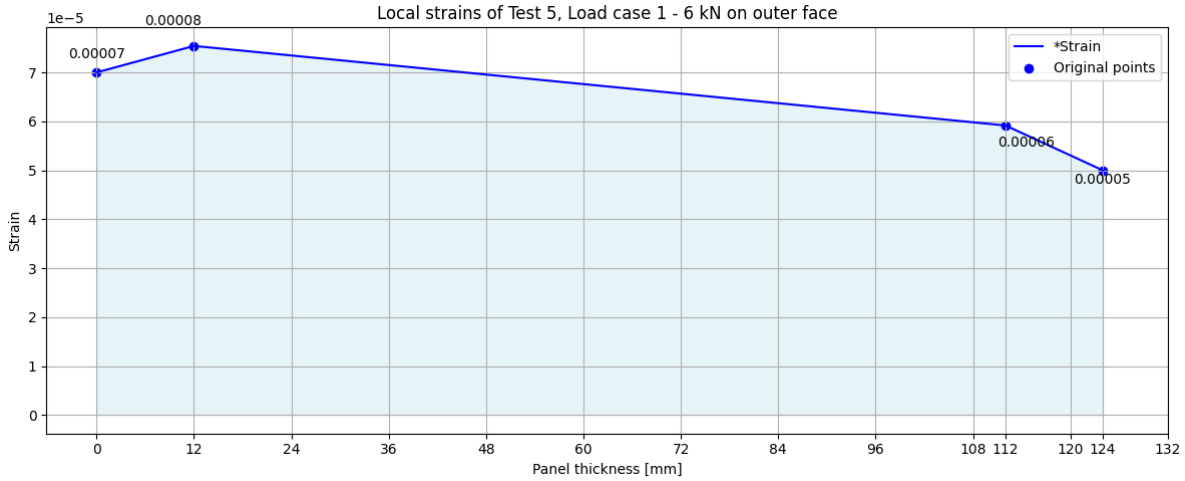

Figure F.34: Test 5 6 kN out strain - load case 1

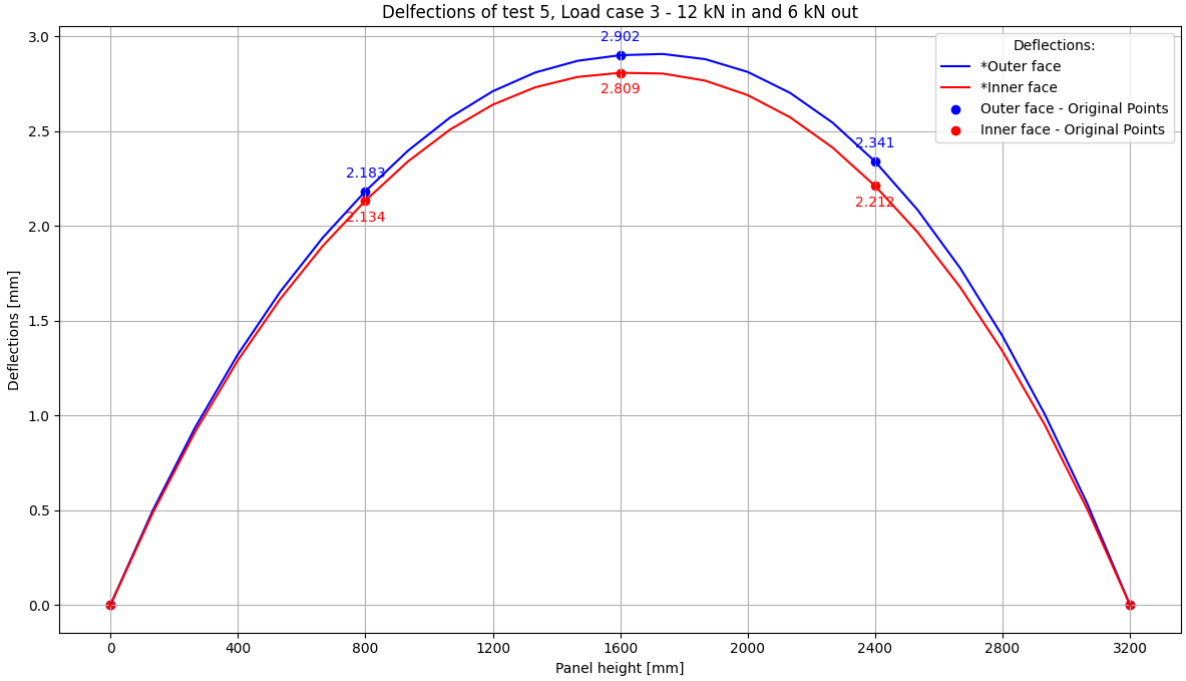

Figure F.35: Test 5 12 kN in and 6 kN out defl - load case 3

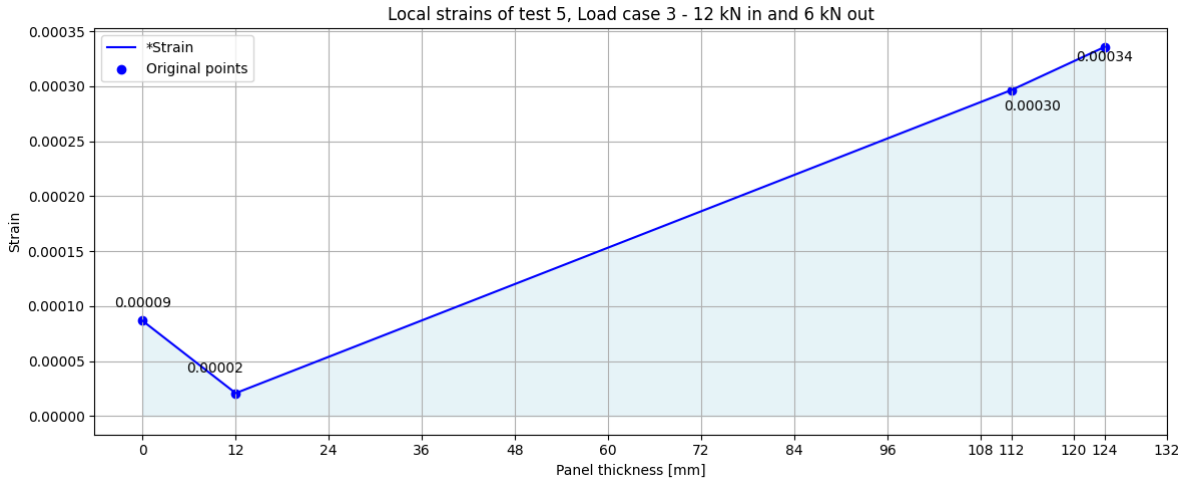

Figure F.36: Test 5 12 kN in and 6 kN out strain - load case 3

G

Additional connection type figures

Additional connection types have been brought out here to have a better understanding of the applications of SIPs.

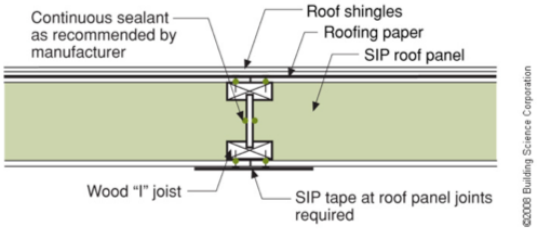

Figure G.1: Wall continuous connection 3. [44]

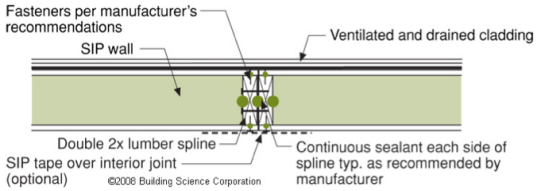

Figure G.2: Wall continuous connection 2. [44]

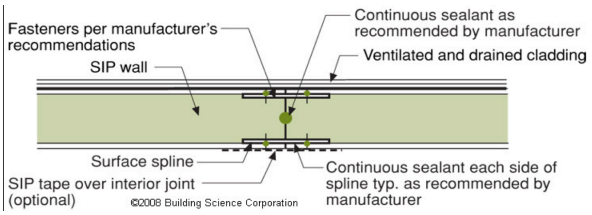

Figure G.3: Wall continuous connection 4. [44]

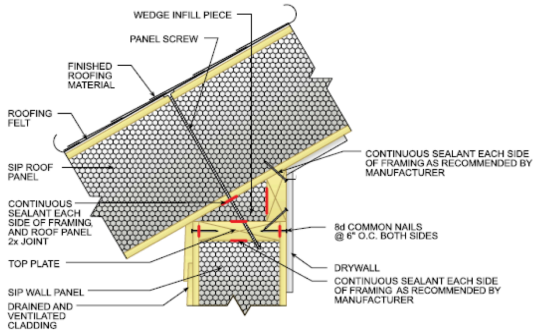

Figure G.4: Roof wall connection 2. [44]

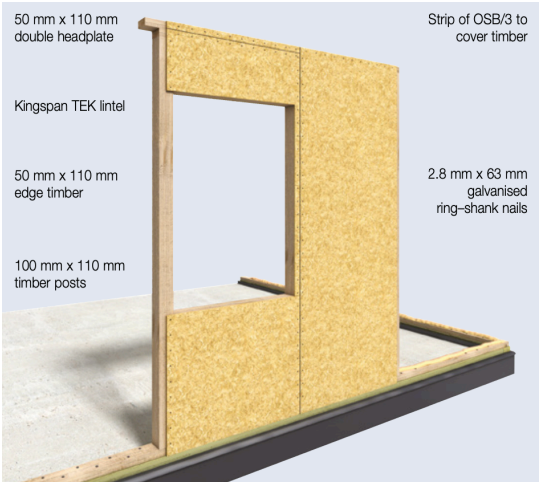

Figure G.5: Opening detail TEK system. [43]

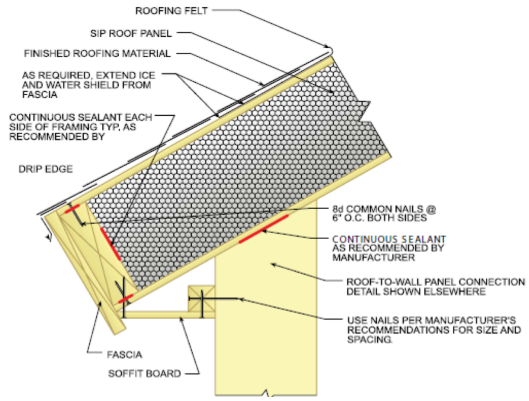

Figure G.6: Roof wall connection 3. [44]

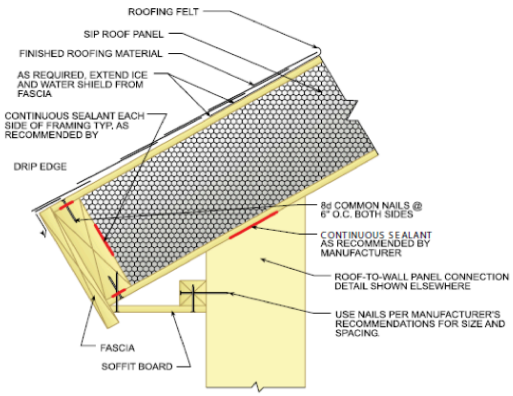

Figure G.7: Roof edge detail 1. [44]

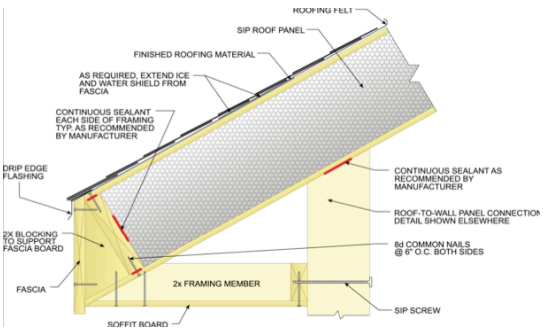

Figure G.8: Roof edge detail 2. [44]

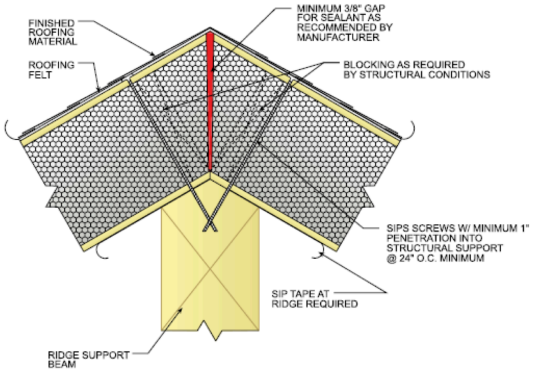

Figure G.9: Roof top connection. [44]

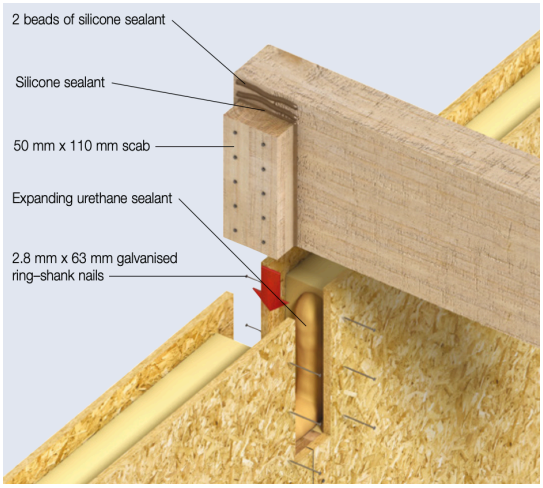

Figure G.10: Roof purlin connection TEK system. [43]

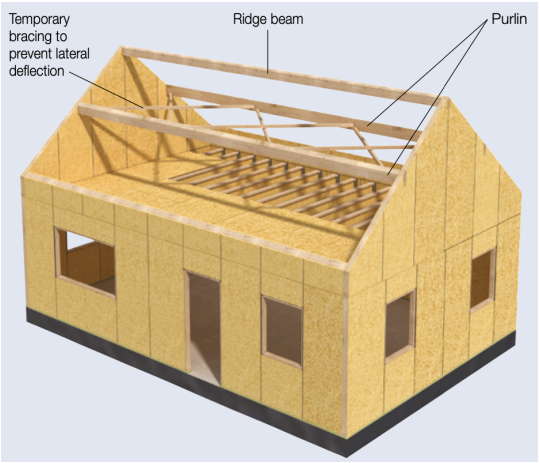

Figure G.11: Roof beams TEK system. [43]

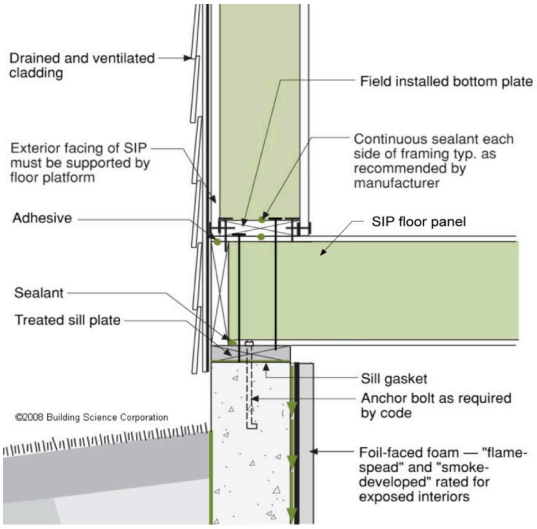

Figure G.12: Foundation connection with a floor beam in between. [44]

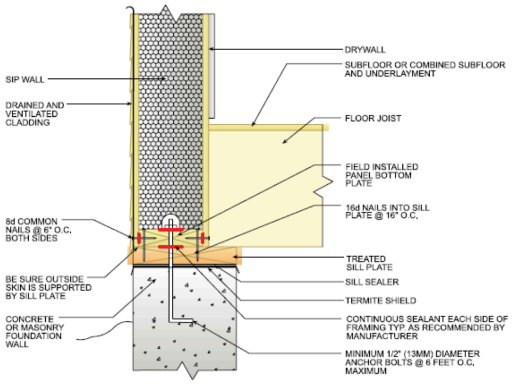

Figure G.13: Foundation connection directly on the foundation. [44]

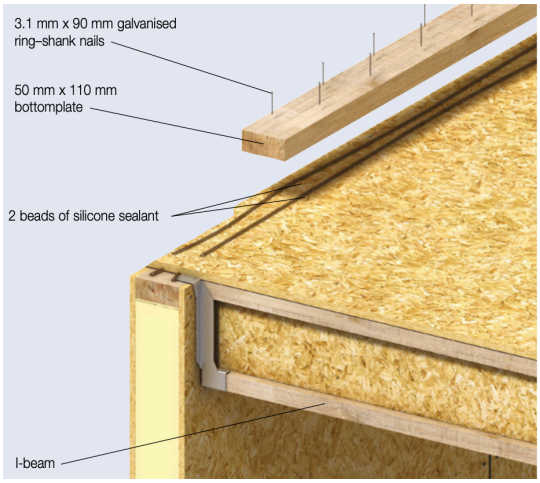

Figure G.14: Joist hanger floor connection TEK system 2. [43]

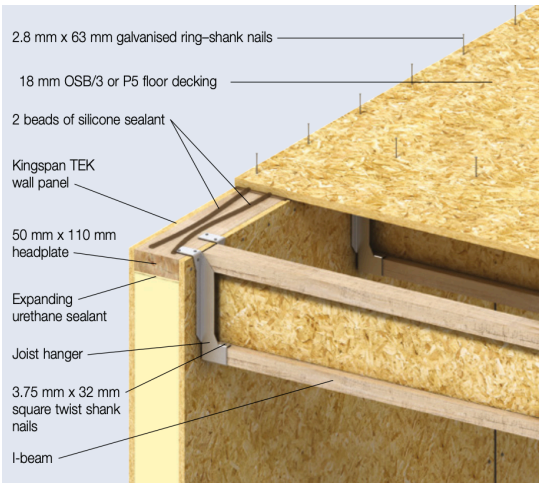

Figure G.15: Joist hanger floor connection TEK system 1. [43]

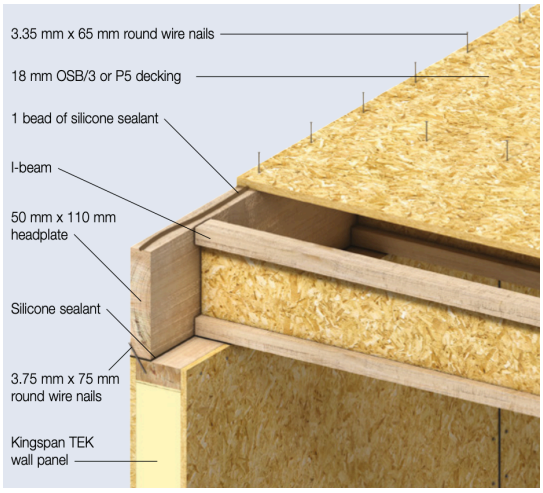

Figure G.16: Rim board floor connection TEK system 1. [43]

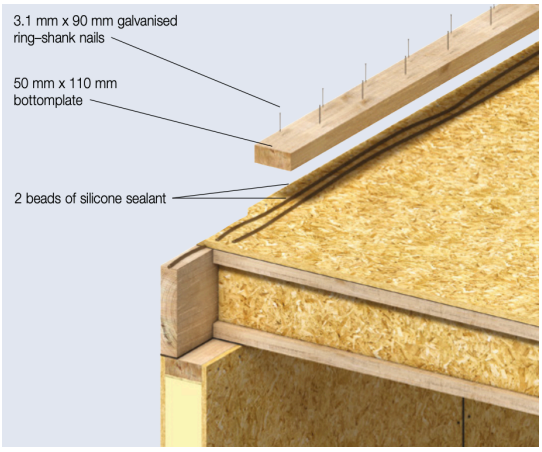

Figure G.17: Rim board floor connection TEK system 2. [43]

H

Model of a Residential Building

The preliminary goal of this thesis was to explore the possibility to have a parametric residential building model for structural insulated panels. This goal was changed due to the behaviour of the structural insulated panel. Therefore, two methods of creating a parametric building model were explored without further analysis. The two methods explored were on Grasshopper karamba3D and Grasshopper Dlubal with a connection to RFEM. To limit the complexity, the models consist of walls, roof/floor beams and openings.

The first option, Karamba3D, will be explored as a simple building model with a square geometry, one storey high with walls, floor/roof beams, and one opening. Example of the build up of a SIP building can be seen in figure 1.7. The second option will be Dlubal plug-in where a more complex model was developed with the same concept. Loads that will be applied are self-weight, another floor weight, and wind loads. The foundation, roof, and facade are out of the scope of this thesis. The research question that was posed is the following:

- How can a residential building out of SIPs be modelled with parametric tools?

Different methods were considered since Karamba3D does not allow a layered material to be used. As seen previously, Karamba3D does predict with a reasonable accuracy the SIP behaviour, however building a model with a panel model which already has hundreds of elements would render the model very slow. Thus, it would be unsuitable for preliminary design choices, and not accurate enough to provide a final design. Therefore, an equivalent panel model was suggested based on the panel bending stiffness.

To have a comparison point, and possibly a better/more accurate modelling option, the Dlubal plug-in is also explored. Since the Dlubal plug-in is connected to RFEM a layered material selection is possible, however as seen for the panel design, it does not give reliable results under axial loading.

This chapter will explore two methods on how to create a SIP building model with parametric tools. The methods to model the material will be discussed and the models will be shown. First, will be a model created in Karamba3D, and second, will be a model created with Dlubal plug-in with a connection to RFEM. However, there will be no analysis since the panel that was investigated is most likely not suitable for load bearing applications according to the analysis conducted within this thesis.

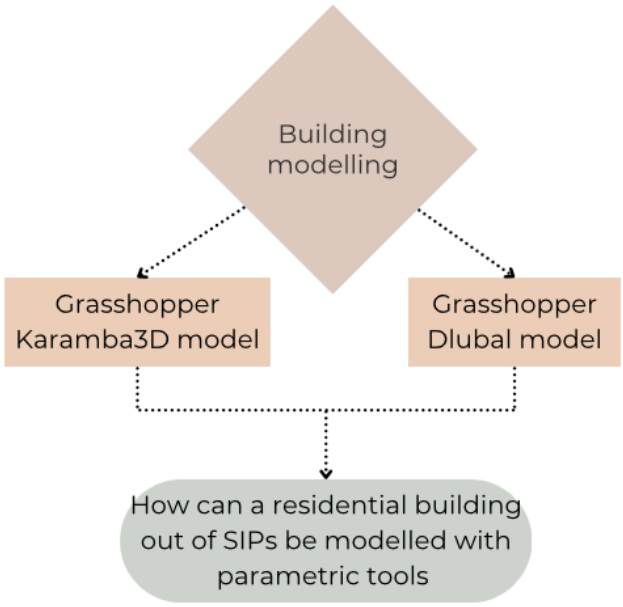

Figure H.1: Theoretical framework for the building model.

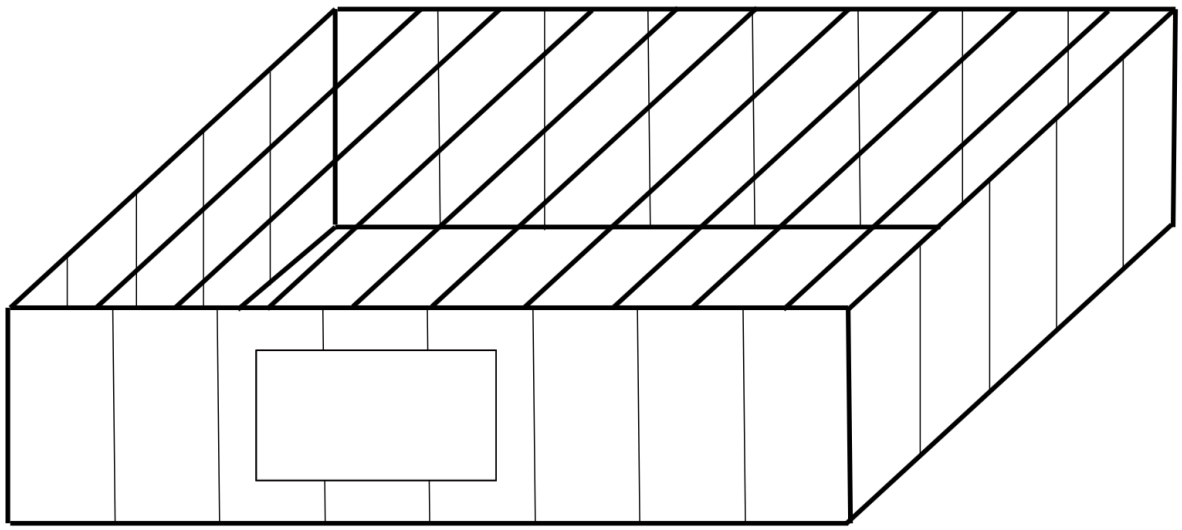

Figure H.2: Simple building concept.

H.1. Karamba3D Model

The Karamba3D model has been created by modelling the panels as one single shell-element to limit the number of elements within the model, and to not cause too long calculation times. The material has been defined as a user-defined material according to the OSB/3 material. This is not a real scenario but is an option to explore if this way of modelling could give preliminary results that could be used in preliminary design choices. The panel has been defined with an equivalent stiffness through the moment of inertia to match with the bending stiffness of the

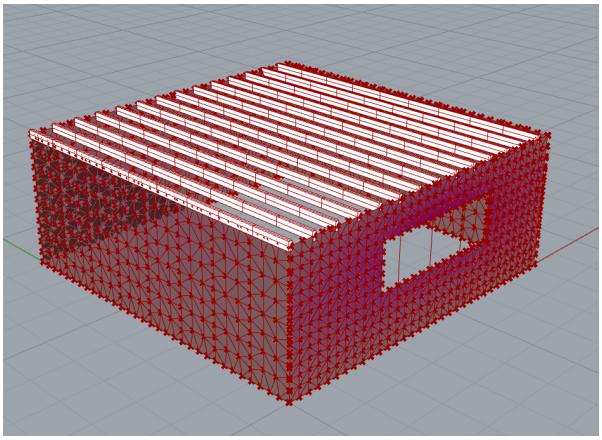

Figure H.3: Karamba simple building geometry.

sandwich panel. The material's E modulus was defined as 3800 MPa and therefore, a panel thickness of 97 mm was assumed. This is not a realistic case, but it is to see whether this could already be a sufficient way of designing with SIPs through a very big simplification and to limit the number of elements in the model.

$$I = \frac{D}{E} \tag{H.1}$$

$$t = \sqrt[3]{\frac{t_f \cdot I}{B}} \tag{H.2}$$

The model consists of panels, one opening, and roof beams. Between each panel, joints have been defined. It is expected that this could transfer the loads, but most probably the deflection results will not be close to what would occur in reality. The panel defined here would be much stiffer. Additionally, the supports that are defined here are not defined with an eccentricity, although this should mimic the real life situation. The top roof beams are connected through nodes which have been defined without a bending stiffness in the connection, but with all the transverse movements restricted. The connections are directly connected to nodes which are not defined with an eccentricity. This method of modelling is worth looking into, depending on what is the goal for modelling. Assumingly, failure could not be predicted due to big simplifications, but it might be that this simplification is enough to make preliminary, very robust design choices if the defined shell-element behaves similarly to the SIP. The modelled structure can be seen in figures H.3 to H.7.

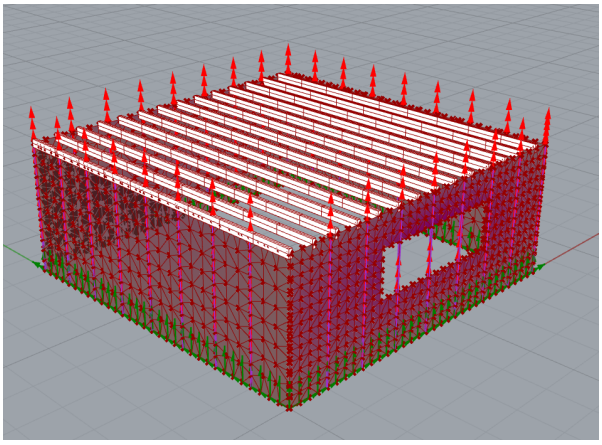

Figure H.4: Karamba simple building with joints and support conditions 1.

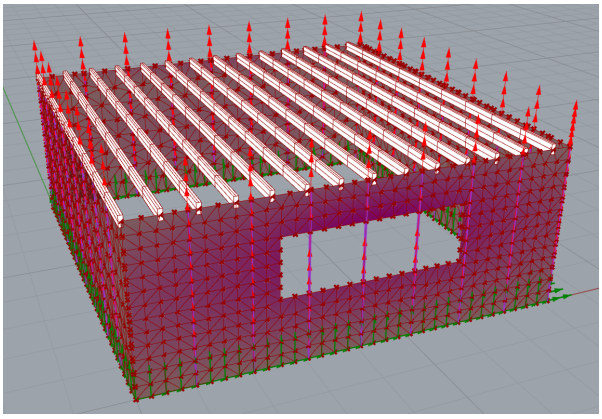

Figure H.5: Karamba simple building with joints and support conditions 2.

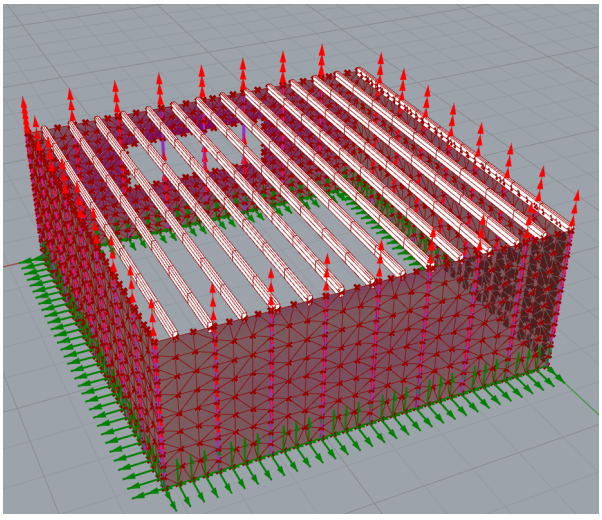

Figure H.6: Karamba simple building with joints and support conditions 3.

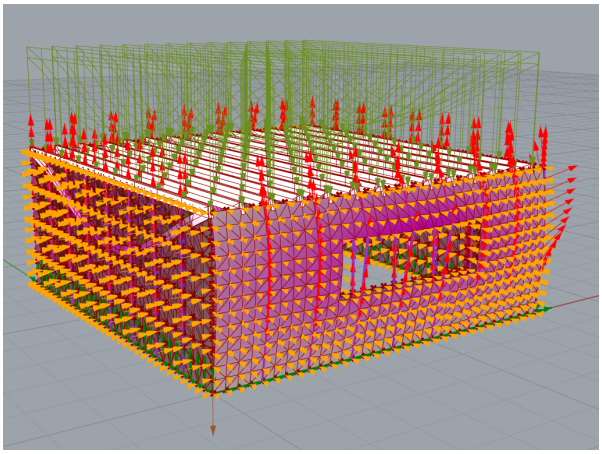

Figure H.7: Karamba simple building with all the loads.

H.2. Dlubal Model

The Dlubal model creation is slightly less user friendly. It follows a very clear pathway to the RFEM interface. It requires the user to number each element and define each elements' material according to those numbers which makes it significantly more complicated than the Karamba3D input. The connection between Dlubal and RFEM works well when everything has been defined correctly. The material can be defined as for the RFEM panel model – in one single shell-element the materials are defined. This would result in presumably good results when transverse loads like wind loads are applied. However, the accuracy of axial load transfer would still need to be further investigated. The suitability for preliminary design options should be evaluated. The model is seen in figure H.8.

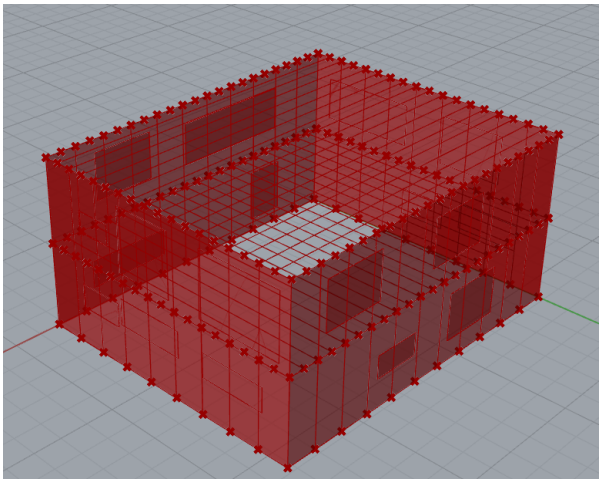

Figure H.8: Grasshopper/Dlubal plug in detailed building for RFEM.

H.3. Additional modelling suggestions

The most accurate method would probably be by applying the developed Karamba3D panel model for the whole building model. The panel model could be scaled for all different kinds of SIP material combinations and would be a useful tool. However, the biggest drawback would be the number of elements created in the model which would slow down the calculation time

of the whole model, and thus not serving the purpose of having a preliminary design tool.

H.4. How can a residential building out of SIPs be modelled in Grasshopper?

Grasshopper has many plug-ins which all allow a different range of structural analysis. Karamba3D and Dlubal connection to RFEM were used to model a building to analyse the feasibility of making a model with Grasshopper for a residential building with structural insulated panels. Dlubal connection to RFEM is a reliable method since the material can be defined within one layer, but does not show the behaviour of the faces separtely. However, it is expected to be an easy method for analysing a building made of SIPs. As previously mentioned, Karamba does not allow the definition of a layered material, hence an equivalent panel was defined as one layer to limit the number of elements, but this is expected to show a big error margin in terms of the real behaviour of a building made of SIPs, because it does not have a deformable layer in the middle. Third method which was not modelled, but would be the most accurate method of the three is the application of the panel developed for the analysis of this thesis. However, the limitation is the number of elements which would be multiplied every time a new panel is added. This would cause the calculation time to be multiple hours if not days, since the panel model with 10x10 mm beams needed sometimes around an hour to calculate. Therefore, if the number of elements gets too large, the whole interface becomes slow, and calculation takes time.